FLUX ASSOCIATIONS AND THEIR RELATIONSHIP TO THE UNDERLYING HETEROGENEOUS SURFACE CHARACTERISTICS

Constance Maria Brown Mitic

Department of Natural Resource Sciences, McGill University

Montreal, Canada, June 1999

A Thesis submitted to

the Faculty of Graduate Studies and Research

in partial fulfilment of the requirements

for the Degree of Doctor of Philosophy

0-612-55307-8

Suggested short title:

Flux Associations and Surface Characteristics

ABSTRACT

This thesis consists of analysis of three different data sets: (i) Aircraft-based eddy correlation data collected above irrigated and non-irrigated agricultural land in Southern California during the California Ozone Deposition Experiment (CODE) summer 1991; (ii) micrometeorological tower data, collected over grape and cotton canopies as part of CODE; (iii) aircraft-based eddy correlation flux data above two grid sites in the Canadian boreal forest during the Boreal Ecosystem-Atmosphere Study (BOREAS), spring and summer of 1994 and 1996.

Results from the CODE aircraft data document composition and size of the dominant structures, which transport heat and gases (H_2O, CO_2 and ozone) over water stressed and non-water stressed surfaces, and the relative frequency with which structures carrying only a single scalar, or given combinations of scalars, were encountered along the flight paths. Interpretation of results provides further evidence for the existence of a second (non-physiological) sink for ozone. The relative preponderance of structures that carry moisture, carbon dioxide and ozone simultaneously, particularly in the gradient-up mode, reflects the importance of vegetation as co-located source/sink for these scalars. The detrending procedures described in this study may help to define a more effective separation between local and mesoscale events in biosphere-atmosphere interaction.

Results from the CODE tower data indicates a single vegetated ozone sink for the grape site, but a vegetated as well as a non-vegetated sink for the cotton site. For both sites, structures simultaneously transporting significant flux

contributions of CO_2, H_2O, heat and ozone dominate during unstable conditions. During stable conditions, unmixed single flux structures dominated over cotton but not over grape. The results of this study contribute empirical evidence about the relationship between ozone uptake and the physical and physiological state of vegetation, as well as the limitations placed on eddy scales in simulation models.

Results from the BOREAS aircraft data shows a decoupling between the surface and the atmosphere, where the patterns of vegetation, greenness and surface temperature may be quite dissimilar to those of the fluxes of sensible heat, latent heat and - to a lesser degree - CO_2. Reasons for this lie in the extraordinary boundary layer conditions, high vapour pressure deficit, moist soil and hot canopies, and the response of the vegetation to these conditions. Analysis of the coherent structure compositions to some extent permits the characterization of the different sources and sinks. Overall, this study shows the importance of understanding the various interacting components of soil, vegetation and atmosphere when attempting to design process-based models for predictions in 'micrometeorologiacally' complex ecosystems.

RÉSUMÉ

Cette thèse porte sur l'analyse de trois bases de données suivantes, obtenues par la méthode des fluctuations ("eddy covariance"):

(1) Les mesures aéroportées de flux de chaleurs sensible et latente, du CO_2 et de l'ozone, recueillies en été 1991 au-dessus de terres agricoles irriguées et non-irriguées du sud de la Californie, lors de l'expérience CODE (California Ozone Deposition Experiment):

(ii) Des flux obtenus à partir de mâts micrométéorologiques, situés au-dessus de cultures de vignes et de coton, lors de l'expérience CODE;

(iii) Finalement, des données aéroportées provenant de vols 'en quadrillage', effectués au printemps et en été 1994 et 1996 au-dessus de la forêt boréale canadienne, lors du projet de BOREAS (Boreal Ecosystem-Atmosphere Study).

Les données aéroportées de l'expérience CODE nous ont permis de documenter la composition et les dimensions des structures dominantes qui transportent la chaleur et les gaz (H_2O, CO_2 et O_3) au-dessus de la végétation soumise ou non à un stress hydrique. Ils montrent, également, la distribution spatiale de ces structures qui transportent soit une seule quantité scalaire (chaleur, gaz), soit une combinaison de telles quantités. L'interprétation de ces données supporte l'hypothèse d'un deuxième puits (non-physiologique) pour l'absorption de l'ozone. La prépondérance des structures transportant simultanément la vapeur d'eau, le CO_2 et l'ozone, particulièrement sous conditions de mouvement ascendent de l'air, souligne l'importance de la végétation comme sources et puits co-localisés

pour l'échange de ces gaz. Les méthodes développées pour l'élimination des tendences spatiales dans les données aéroportées pourraient aider à démarquer plus précisément les phénomènes locaux d'interaction biosphère-atmosphère qui s'opèrent à méso-échelle.

Les résultats provenant des mâts micrométéorologiques de l'expérience CODE suggèrent un seul puits (végétatif) pour l'absorption de l'ozone par les vignes, mais deux puits (végétatif et non-végétatif) pour le coton. Pour ces deux sites, les structures transportant simultanément la chaleur, le H_2O, le CO_2 et l'ozone dominent dans les cas d'instabilité atmosphérique, mais dans les cas de stabilité, les structures non-mélangées dominent, au moins pour le coton. Ces résultats s'ajoutent à l'information empirique déjà acquise sur les relations entre l'absorption de l'ozone et l'état physique et physiologique de la végétation. Ils devraient aussi servir pour mieux définir la gamme d'échelles de structures turbulentes à inclure dans les modèles de simulation.

L'analyse des données aéroportées de BOREAS met en évidence un découplage entre surface et atmosphère, tel que la distribution spatiale de la végétation et celle de la température de surface peuvent se révéler différentes de la distribution des flux de la chaleur sensible et latente et, à un moindre degré, du flux du CO_2. Ceci est attribué aux conditions extraordinaires de la couche limite, à un déficit élevé de la tension de vapeur d'eau dans l'air, à un sol humide couplé à un panache végétal chaud, et à la réponse de la végétation à ces conditions. L'analyse de la composition de ces structures 'cohérentes' permet, en principe, de caracteriser les divers sources et puits. En général, cette étude documente la nécessité d'améliorer nos connaissances sur les diverses composantes en interaction entre le sol, la végétation et l'atmosphère, si on vise le développement de modèles de prévision biosphère-atmosphère pour les écosystèmes complexes.

PREFACE

This thesis focuses on the links between land surface properties and fluxes of heat, moisture, carbon dioxide and ozone exchanged between the surface and the atmosphere. It is hoped that this work will give a deeper understanding of the expected surface boundary layer dynamics under a variety of ecophysiological conditions.

The thesis is presented in manuscript format. It is divided into six chapters. Chapters 1 and 2 give a general introduction and literature review, while Chapter 6 gives the thesis summary and conclusions. Chapters 3, 4 and 5 are independent manuscripts with connecting statements between each chapter. Chapters 3 and 4 have been published in referred scientific journals while Chapter 5 is being prepared for submission. Chapters 3 and 4 are essentially identical to the published paper, with modifications only to the equation, figure and table numbers to give continuity to the thesis.

References are given at the end of the thesis, and incorporate the individual references from each chapter to eliminate redundancy.

CONTRIBUTION TO SCIENCE

1. Contribution to Knowledge

The following aspects of the thesis are considered by the author to be original contributions to knowledge.

(1) The algorithm for the separation of local flux from mesoscale flux and the selection of optimum degree of filtering to achieve this separation.

(2) The characterization of the flux composition of coherent structures, the reconstruction of their size (in one dimension), and the intensities of the individual component fluxes.

(3) Linking flux distribution characteristics via coherent structures to surface conditions derived from remote sensing.

(4) Modelling sources, sinks and their predicted relative strengths, based on the link between observed coherent structures distribution and surface eco-physiological characteristics

2. Research Papers in Refereed Journals

(1) Viau, A., C.M. Mitic, 1992: Potential impacts of CO_2-induced climate change using the GISS, GFDL AND CCC scenarios on corn yields in the Essex county region of Ontario, *Climatological Bulletin, 26, (3), 79-105.*

(2) Mitic, C., A. Viau, 1993: Evaluation de l'impact d'un changement climatique sur les besoins en irrigation et les taux de rendements au champs du mais dans le sud-ouest de l'Ontario. *Le Climat, 11(1), (25pp)*

(3) Mitic, C.M., Schuepp, P.H., Desjardins, R.L., and J.I. MacPherson, 1995: Spatial distribution and co-occurrence of surface - atmosphere energy and gas exchange processes over the CODE grid site, *Atmospheric Environment, 29, (21), 3169-3180.*

(4) Mitic, C.M., Schuepp, P.H., Desjardins, R.L., and J.I. MacPherson, 1997: Flux association in coherent structures transporting CO_2, H_2O, heat and ozone over the CODE grid site, *J. Agri. and Forest Meteorol., 87, 27-39.*

(5) Mitic, C.M., Massman, W.J., Schuepp, P.H., and J.L. Collett (Jr), 1998: Structural Analysis and flux associations of CO_2, H_2O, heat and ozone over cotton and grape canopies, *Atmospheric Environment.*

CONTRIBUTION OF CO-AUTHORS TO PAPERS

The author, who is the second author in papers 1 and the first author in papers 2, 3, 4 and 5, was responsible for all design of analytical procedures, numerical formulations, data analysis, manuscript preparation for publication and the response to reviewers comments, with the exception of papers 1 and 2 where the Dr Alain Viau made the response to the reviewers comments.

Dr Alain Viau contributed to the editing and response to the reviewers comments. Papers co-authored by Dr Viau are not included as part of this thesis.

Dr Peter H. Schuepp, the graduate studies supervisor of this thesis, was responsible for the administration of the research projects, and contributed through his continuous supervision of all aspects of the research, with editorial contributions and guidance on all manuscript preparation.

Dr Raymond L. Desjardins and Mr. Ian J. MacPherson provided aircraft data used in paper (3), paper (4) (Chapter 3) and Chapter 5.

Dr William Massman co-ordinated the data acquisition for paper (5) (Chapter 4) and provided editorial comments.

Dr Jeffery Collett provided editorial comments and assisted in facilitating access to the data for paper (5)(Chapter 4).

ACKNOWLEDGEMENTS

I would like to extend my deepest appreciation to Dr Peter Schuepp, my graduate supervisor, father figure and friend, for his supervision, guidance, support and funding throughout my graduate studies.

I wish to express my thanks to Dr Nigel Roulet of McGill University and Dr. Alain Viau of Université Laval who were on my Ph.D committee, for their guidance in the completion of this thesis, and to Dr William Massman of Rocky Mtn Forest Service (USDA) for his support and editorial comments.

I would also like to extend my gratitude to the members of the Air Quality Research Division of Atmospheric Environment Service ,Canada , in particular, to G. den Hartog, R.E. Mickle, H.H. Neumann, J. Arnold, J. Deary and A. Beavan, for the use of the grape data (Chapter 4). Thanks also to Tony Delany, Steve Semmer, Tom Horst, Steve Oncley and Charlie Martin from the ASTER Facility at the National Centre for Atmospheric Research (NCAR) for the use of the cotton data(Chapter 4). I especially want to thank Jim Pederson and the California Air Research Board, and the Natural Science and Engineering Research Council of Canada for their contribution towards the funding of this study.

My warmest thanks goes out to Joan Schuepp for her motherly concern and care of my daughter, without which life throughout graduate school would have been much more difficult. Thanks Joan.

Finally, thanks to my husband Behzad, my daughter Melissa and all my friends for their patience, support and many entertaining and enjoyable times.

TABLE OF CONTENTS

LIST OF TABLES

LIST OF FIGURES

Figure 5.27. Spatial distribution of coherent structures across the surface types. Grids 26 and 30 from IFC2 southern site.

Figure 5.28. Partitioning of the driving force at the surface derived fro the compositions of the coherent structures. Combined grids 26 and 30 from IFC4 southern site.

LIST OF SYMBOLS

z	measurement height
L	Monin Obukov Length
c	scalar concentration
w	vertical wind
F	flux estimate
FA	flux association
ss	structure size
U	horizontal wind
ℓ	mixing length
ϕ_M	momentum gradient
ϕ_H	temperature gradient
k	Von karman constant
u_*	friction velocity
Θ	mean potential temperature
θ_*	temperature scale in the surface layer
λ	ratio of shear to heat & water vapour forcing
ξ	% driving force
VPD	vapour pressure deficit
RH	relative humidity
β	regression coefficient
r	correlation coefficient
se	standard error

CHAPTER 1.

GENERAL INTRODUCTION

Improvements in our understanding of the interactions between the land surface and the atmosphere have been a focal point for research in land-surface climatology. This is of particular importance because of the implications for model predictions of such phenomenon as climate change. In order to investigate the various phenomena surrounding interactions between the surface and the atmosphere, observations as well as modelling at a variety of spatial and temporal scales are required. One of the most frequent problems of the earth-atmosphere system, relevant to empirical as well as modelling studies, is the degree to which land surface heterogeneity influences atmospheric processes. In the parameterization of atmospheric models, a number of questions have to be addressed, such as: what are the scales of influences for vertical fluxes? does spatial variability in the surface conditions matter? how and at what scales should surface heterogeneity be described? These questions directly involve the spatial distribution of sources and sinks for heat and other scalar fluxes.

The growing interest in land surface climatology, and increasingly routine use of remotely sensed observation of the biosphere-atmosphere dynamics, resulted in the more frequent use of aircraft for regional observation of fluxes of heat, moisture and trace gases (e.g. Lenschow, 1986; Desjardins and MacPherson, 1989). The majority of these studies relate flux estimates to physiological and physical processes at the surface (Austin et al., 1987; Schuepp et al., 1987; Mack et al., 1990; Desjardins et al., 1992; Mahrt et al., 1994; Desjardins et al., 1995; Guo et al., 1995). However, over complex, heterogeneous terrain the interacting conditions and processes that are responsible for the spatial distributions of flux transport are not easily differentiated. Only a few studies have specifically related the distinct coherent motions of turbulence (as opposed to incoherent noise) in the surface layer, hereafter referred to as coherent structures, to surface characteristics (Caramori et al., 1994; Mitic et al., 1995; Mitic et al., 1997; Mitic et al., 1999). These coherent structures are responsible for the bulk of turbulent transport in the surface layer and have been examined from various other perspectives (e.g. Wyngaard, 1983; Eloranta and Forrest, 1992; Paw U et al., 1992; Mahrt and Ek, 1993a & 1993b; Paw U et al., 1995). The combination of regional atmospheric data sampling by aircraft, the ability to discern ecosystem characteristics and variability from remotely sensed satellite data, and the link between coherent structures and the underlying surface suggests the potential of improving our prediction of source and sink distribution over heterogenous landscapes. Such relationships allow for insight into the differential impact of the scales of surface variability on such aspects as surface parameterization of large scale atmospheric models (ie the effective scales at which the various surface parameters impact the atmosphere).

This thesis was motivated by the need to address some of the challenges outlined above. Aircraft and tower data were utilized in order to examine the links between surface properties and the characteristics of the corresponding fluxes and coherent structures. Two different ecosystems are examined: an agricultural site in southern California, with organized heterogeneous surface conditions in the form of surface wetness, and a boreal ecosystem with complex surface heterogeneity in the form of land cover type, surface moisture conditions and topography. These two ecosystems provide very contrasting meteorological and surface-atmosphere exchange dynamics.

OBJECTIVES

The general objective of my research is to increase our understanding of biosphere-atmosphere exchange processes, of how they are tied to the characteristics of the underlying surface and of the degree to which we can predict the ratios of combined fluxes for heterogeneous surfaces. This involves examining the distribution patterns of fluxes of CO_2, water vapour, heat and ozone and the coherent structures which are responsible for the bulk of their transport; and a reconstruction (within the constraints of currently available techniques) of the actual physical structures (in one dimension) as they occurred during the observation period. This will be accomplished by a coincidence analysis, which results in a statistical description of the characteristics of these structures (size, flux composition, flux intensities). This procedure also generates information about how the different scalars (including heat) are linked to each other, to the surface, and the scales involved in these couplings.

I propose to address the relationships discussed above through the following specific objectives:

(1) To develop a method of objectively separating the larger mesoscale flux from the local flux, and thereby identify the categories of scales affecting surface -

atmosphere exchange process. This should be done while achieving a physically meaningful definition of the means used in the calculation of the flux estimates.

(2) To examine, at the landscape scale (10 - 15 km), the spatial distribution, size, and flux composition of coherent structures, their link to each other and to the surface characteristics, under highly unstable conditions and for a relatively 'well behaved', 'organised' heterogenous ecosystem, such as large scale agriculture.

(3) To examine, at the patch (tower measurement) scale, the temporal evolution and characteristics of coherent structures for both stable (night) and unstable (day) conditions, over different crops.

(4) To examine the scales and characteristics of coherent structures over a more 'micrometeorologically complex' ecosystem, such as the boreal forest. Using tower, aircraft and satellite data in a geographic information system, to develop a spatial model to predict the distribution pattern and relative intensities of sources and sinks of scalars (including heat) based on the spatial mix of the surface characteristics.

CHAPTER 2.

GENERAL LITERATURE REVIEW

2.1 SURFACE-ATMOSPHERE INTERACTIONS

The need to better understand the dynamic interrelationships between the surface and the atmosphere has become one of the more prominent objectives in the area of atmospheric and ecosystem studies. For example, improvements in numerical weather simulations from mesoscale to general circulation models require a more accurate representation of the interactions occurring at the land surface, and the scales involved in them. Over the last two decades, several large scale multi-disciplinary projects have been designed to acquire a wide cross-section of information using a combination of measurement techniques, at several different scales. Such projects included HAPEX MOBILHY over a temperate forest (André et al., 1986), the First International Satellite Land Surface Climatological Project Field Experiment [FIFE] over prairie grassland (Sellers et al., 1988), the Northern Wetlands Study [NOWES] over northern wetlands (Glooshchenko et al., 1994), the California Ozone Deposition Experiment [CODE] over agricultural lands (Pederson et al., 1995) and the Boreal Ecosystem Atmosphere Study [BOREAS] over the boreal forest (Sellers et al., 1997). These experiments have progressed from simple homogeneous systems to more complex heterogeneity in the attempt to understand the dynamics underlying the physiological, physical and chemical interrelationships within the biosphere.

These large scale ecosystem studies have yielded invaluable information about the relationships between the ecophysiological properties of the surface and the corresponding atmospheric response. During FIFE, for example, the boundary layer height on a warm sunny day reached 1.2 km (Gal-Chen et al., 1992). For CODE, the boundary layer height extended only up to 550 m (Mitic et al., 1995), while in BOREAS on a clear day in late spring it extended up to 3 km in the late afternoon (Betts et al., 1996), which is similar to springtime boundary layer depth of 3 km in the Saudi Arabian desert (Blake et al., 1983). These differences may be related to the characteristics at the surface. The FIFE grassland had an evaporative fraction (latent heat flux divided by the sum of sensible and latent heat flux) of ~0.73 (Margolis and Ryan, 1997), the CODE fields approximated 0.85 (Mitic et al., 1999; Desjardins et al., 1995), while the BOREAS ecosystem had only 0.32 (Margolis and Ryan, 1997). While the FIFE and CODE ecosystem were rapidly transpiring, the BOREAS ecosystem's vegetation and surface properties retarded the movement of water between the land surface and the atmosphere, even though the surface was very wet. This in turn led to the development of the very deep dry boundary layers observed.

The most common and perhaps most valuable means of studying the interaction between the surface and the atmosphere is through the surface fluxes such as carbon dioxide, latent heat , sensible heat, ozone, and methane, to name the most important ones. Meteorological towers have been and remain the dominant means by which surface fluxes are observed. Such observations have been made over various time scales, under varying meteorological and climatic conditions and over many different canopies (e.g. Verma et al., 1986 &1992;

Laubach et al., 1994; Valentini et al., 1996; Lee et al., 1996; Black et al., 1996; Pattey et al., 1997; Baldocchi et al., 1997; Blanken et al., 1997;) to name only a few. While tower observations are essential to catalogue the relationships between different landscape patches (eg. tree species) and the atmosphere, they lack the spatial dimension necessary to extrapolate to the larger surrounding region. It therefore becomes difficult to translate the point measurements taken at the tower sites to the landscape, regional and global scale. These scales consist of a mosaic of sites, from very productive vegetation, young growth, burnt areas, mature forest, water bodies etc., as well as differences in terrain and soil characteristics. All these differences affect the representativeness of fluxes measured at a tower site (Baldocchi et al., 1996).

Remotely sensed satellite observations on the other hand are fast becoming standard in the estimation and evaluation of the regional surface characteristics and progressively used in the assessment of large scale relationships between the surface and the atmosphere. Studies such as Potter et al. (1993) looked at ecosystem production based on satellite and surface data, and Running et al. (1989), mapped regional forest evapotranspiration from coupling satellite data and an ecosystem model, while others infer fluxes of latent heat, sensible heat and CO_2 directly from satellite observations (Price 1982; Pierce and Conglaton 1988; Gao 1994). The success of satellite observations in effectively and accurately estimating surface processes is essential to their incorporation into the various ecosystem and climate models. However, as studies such as Running et al. (1989), Hall et al. (1992), Copper et al. (1997) and Vidale et al. (1997) have shown, variabilities at the landscape scale are important considerations in regional estimates. Tower observations should not, therefore, be simply aggregated upwards, and satellite estimates cannot simply generalize based on spatially averaged observations. A mosaic approach, with careful consideration of the scales of its constituent elements, is most desirable (Cooper et al., 1997).

Observations made by low flying aircraft have demonstrated their potential and ability to bridge the gap between observations made at the tower and estimates derived from satellite data. These observations capture the spatial distributions of surface characteristics as well as surface fluxes at the landscape scale (15 km x 15 km). Aircraft observed fluxes and satellite observations of surface vegetation parameters during FIFE were well correlated (Desjardins et al., 1992; Cihlar et al., 1992; Gao et al., 1992). Comparisons between the tower fluxes and those obtained by the aircraft were not as impressive. Over the years, however, our understanding of these intercomparisons between aircraft and tower fluxes has vastly improved. Errors may be attributed primarily to variabilities such as footprint area (Kaharabata et al., 1997), the logistic placement of meteorological towers within complex terrain and its impact on the representativeness of the tower observations for the region (Desjardin et al., 1997), vertical flux divergence and mesoscale motions (Betts et al., 1992). During CODE, there was good agreement between both the aircraft and tower fluxes (Desjardins et al., 1995), and between aircraft fluxes and satellite vegetation parameters (Mitic et al., 1995). Comparison between aircraft and tower during BOREAS showed discrepancies that were attributed to aircraft run lengths and different sampling heights as well as the surface wetness detected by the aircraft vs that at the location of the tower (Desjardins et al., 1997).

2.2 SURFACE FLUX ESTIMATES

A variety of ways exist for the calculation of localized surface fluxes. These include aerodynamic techniques, such as the K theory gradient method, eddy correlation and eddy accumulation techniques, based on direct sampling of the near-surface turbulence field, as well as more recent empirical variations, such as surface renewal (Paw U et al., 1995). Methods such as the gradient theory are not suitable for canopies such as over forest due to the presence of counter gradient fluxes. The most widely used direct technique for flux estimation is the eddy correlation method. The main advantage lies in its physical interpretation, where fluctuations in the vertical wind resulting from updrafts and downdrafts near the surface are correlated with fluctuations in the transported scalar fields. This means that the eddy correlation technique derives the flux estimate from a time- (space) average of the fluctuations from the mean values. The definition of the mean is therefore important to the accurate estimation of fluxes. The question of convergence of the mean over heterogeneous surfaces for aircraft data has been addressed by Schuepp et al. (1987). Spatial heterogeneity causes trends or discontinuities in the traces of scalars.

Spatial heterogeneity is usually addressed through some form of detrending procedure, such as non-linear high pass filtering (Caramori et al., 1994; Mitic et al., 1995, 1997, 1999; Ogunjemiyo et al., 1997) or surface related sectional averaging (Mahrt and Ek, 1993). These filtering procedures also allow for the identification of fluxes resulting from mesoscale variations associated with surface heterogeneity, as opposed to flux from transient mesoscale motion .

2.3 COHERENT STRUCTURES

The eddy correlation technique not only allows for the identification of surface based mesoscale fluxes from non-linear detrending, but also for the definition of the turbulent coherent structures involved in flux transport between the surface and the atmosphere. A coherent structure is defined as a "connected turbulent fluid mass with instantaneous phase-correlated vorticity over its spatial extent" (Hussain, 1986). Coherent structures have been recognised as the dominant means of exchange between the surface and the atmosphere (Antonia, 1981; Shaw, 1985; Lenschow and Stephens, 1980; Grant et al., 1986;) and are of particular importance within vegetation canopies (Raupach et al., 1996).

The definition of the coherent structures depends on the operational technique used. Coherent structures may be defined from the decomposition of the eddy correlation fluxes into quadrants or modes of transport (Mitic et al., 1997). Alternately they may be identified using a wavelet transform (Liandrat and Moret-Bailly, 1990; Meneveau, 1991; Collineau and Brunet 1993).

CHAPTER 3.

FLUX ASSOCIATION IN COHERENT STRUCTURES TRANSPORTING CO_2, H_2O, HEAT AND OZONE OVER THE CODE GRID SITE

3.1 INTRODUCTION

Growing interest in land surface climatology, and in particular the potential assessment of biosphere-atmosphere exchange processes from remote sensing observations of the surface, led to increased use of aircraft for regional observation of fluxes of heat, moisture and trace gases (e.g. Lenschow, 1986; Desjardins and MacPherson, 1989). Such studies usually try to relate flux estimates to characteristics of - and processes at - the underlying surface (Austin et al., 1987; Schuepp et al., 1987; Mack et al., 1990; Desjardins et al., 1992b; Mahrt et al., 1994; Desjardins et al., 1995; Guo et al., 1995a). However, the various driving forces responsible for the transport of scalars are not easily distinguishable over heterogeneous terrain. Only a few studies have specifically related the coherent structures, which are responsible for the bulk of turbulent transport, to surface characteristics (Caramori et al., 1994; Mitic et al., 1995), although they have been examined from various other perspectives (e.g. Wyngaard, 1983; Eloranta and Forrest, 1992; Mahrt and Ek, 1993a, b). A study of coherent turbulent structures allows for the improvement of our understanding of the processes operating on surface fluxes, and of the degree to which various fluxes are associated with each other and with the underlying sources and sinks at the surface (Mitic et al., 1995). Identifying the physical extent of structures and their composition, will give some indication of the driving forces (defined as the primary factors or processes initiating transport) operating on flux transport as well as of how they are partitioned between the surface and the atmosphere. In our study, flux associations of CO_2, H_2O, heat and ozone are examined for the two gradient modes of transport, where the surface acts as a sink for CO_2 and ozone, and as a source for H_2O and sensible heat.

3.2 DATA COLLECTION AND SITE DESCRIPTION

The data used in this study were collected by the Twin Otter research aircraft of the National Research Council of Canada during the California Ozone Deposition Experiment (CODE) in 1991. The primary objective of CODE was to make observations that will improve our understanding of ozone uptake at the surface and therefore improve estimates made by regional photochemical models of ozone deposition. A detailed account of CODE is given in Pederson et al. (1995). There were an extensive number of data sampling flights during the field campaign. Two of these were grid patterns (flight number 16 on July 26 and flight number 21 on August 2) and form the data base for our study. The grid areas covered 15 km by 15 km of agricultural fields, consisting primarily of irrigated cotton, non-irrigated fields and senescent safflower. The diagonal corners of the grids are defined at 36.083° N / 119.696° W and 35.940° N / 119.869° W, located in Kings County of the San Joaquin Valley of Southern California. Each grid flight consisted of 22 parallel runs, flown 30 m above the surface in an E-W direction, with an offset of 0.75 km in the N-S direction. Given the overall offset of 0.375 km in the N-S direction between the two grids, the 'combined grid' (incorporating both flights) represents a set of 44 evenly spaced, parallel flight trajectories, with a spacing of 0.375 km between the lines. Wind direction was from the North, perpendicular to the grid lines (345° and 23° for flights 16 and 21, respectively). Recorded flight times for the grids are from 1136 to 1457 hours PDT (Flt 16) and 1239 to 1553 hours PDT (Flt 21). Using an eddy correlation system, flux data were digitized at 16 Hz, with an effective data point separation of 3.75 m at an average flying speed of 60 m s^{-1}.

On both days of observation the sky was clear, with average incident short-wave radiation of 892 W m^{-2} (Flt 16) and 863 W m^{-2} (Flt 21). Thermal stratification was unstable for both days, with median $z/L \approx -4.9$ and -4.1 (where z=30 m), and CBL tops at 549 m and 701 m, respectively, as determined from aircraft-based soundings of temperature and moisture to above the capping inversion layer. A detailed description of the aircraft instrumentation and the flight summary of operations during CODE are given in MacPherson (1992) and MacPherson et al. (1995).

3.3 DATA ANALYSIS

The eddy correlation technique derives flux estimates from the covariance between fluctuations of vertical wind (w') and scalar admixtures (c'). Implicit in the procedure is the need for a realistic definition of the mean, that does not artificially cluster the resulting modes of flux transport and removes trends that may be present in the data. A linear trend over the grid site might represent mesoscale transports with spatial scales far exceeding the dimensions of the site, which would not be directly linked to characteristics of the immediate underlying surface. A nonlinear trend of single or multiple cycles over the grid site may represent smaller mesoscale flux related to the heterogeneous nature and scales of the surface characteristics. It is therefore necessary to select a detrending technique which not only accurately defines the mean but also achieves the most effective filtering of mesoscale events from the local flux.

In an attempt to satisfy the conditions stated above, both linear and nonlinear detrending were applied to heat, the scalar admixtures (CO_2, H_2O and O_3) and the vertical wind component. The linear detrending was in the form of a simple linear regression, and a truncated Fourier series was used to remove nonlinear trends. Quadrant analysis (e.g. Antonia, 1981; Shaw, 1985; Grant et al., 1986) coupled with the eddy correlation technique was used to determine the different modes of transport, defined as excess/deficit up and excess/deficit down. The procedure used to determine the mean of the data vector for optimum separation of local and mesoscale flux is described below.

3.3.1 Definition of Mean and Separation of Local Events

The net local flux estimate was calculated using fluctuations against a mean defined from linear detrending as well as from running means defined by Fourier series truncated at the second, third, and consecutively higher terms. In the case of nonlinear detrending, mesoscale flux estimates were derived from the low-frequency oscillations filtered from the scalar concentration and vertical wind fields. The procedure, illustrated in Figure 3.1 for actual data of vertical wind (w) and CO_2 (c), is based on the decomposition of the flux into large area averages, represented

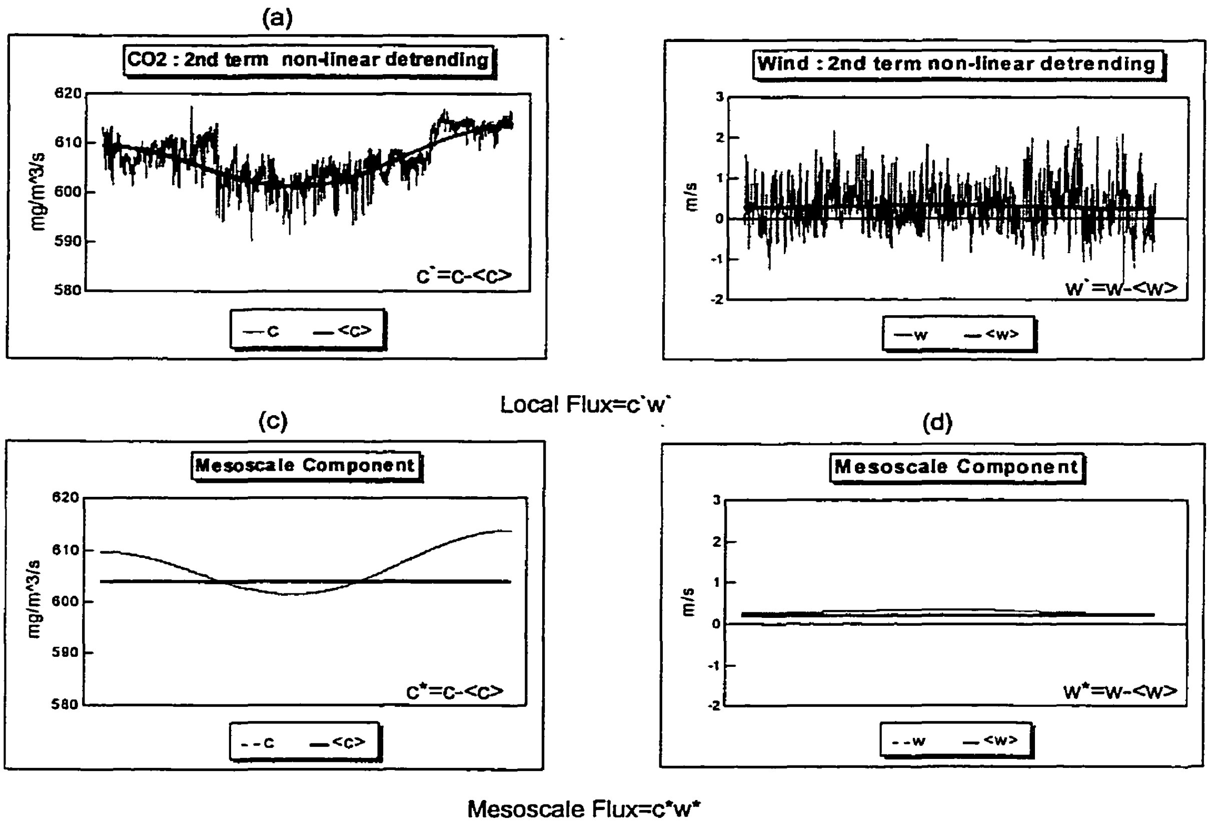

Fig. 3.1. Illustration of the definition of local flux (a,b) and mesoscale flux (c,d) by nonlinear detrending

by the means in Figure 3.1 (c) and (d), as opposed to the running (local) means represented by c^* and w^*. Instantaneous fluctuations (w' and c') are defined against the local means (Figure 3.1 (a) and (b)), which may be variable due to mesoscale 'events'. Considering this Reynolds type expansion into means and fluctuations, and the fact that $\langle c' \rangle$ and $\langle c^* \rangle$ (or $\langle w' \rangle$ and $\langle w^* \rangle$) vanish by definition, the instantaneous area-averaged vertical flux F_A, observed at height h over area A at time t, is then given, in principle, by

$$F_A = \frac{1}{A}\int_A w(x,y,h,t)\,c(x,y,h,t)\,dxdy$$
$$= \langle w\rangle\langle c\rangle + \langle c^*w^*\rangle + \langle c'w'\rangle \qquad (1)$$

where area averaging $\langle\rangle$ is approximated by time-averaging in the moving frame of reference of the aircraft. In practice, this integration can, of course, only be approximated by discrete sampling over the area, with the expression reduced to $F_A = \langle c^*w^*\rangle + \langle c'w'\rangle$ in the case of $\langle w\rangle = 0$, which is a reasonable assumption for large, flat terrain such as the San Joaquin Valley, i.e. into the sum of 'mesoscale flux' ($\langle c^*w^*\rangle$) and 'local flux' ($\langle c'w'\rangle$).

The mode of transport of the net mesoscale flux at each truncation level in the Fourier series is identified as either gradient or counter gradient. As commonly defined in quadrant analysis (Antonia, 1981), gradient modes for upward transport of scalars from the surface, such as heat or moisture under daytime conditions, associate upward (positive) excursions of vertical wind with positive excursions of scalar concentration, and downward gusts with negative scalar fluctuations ('deficit down'). Conversely, gradient modes for flux of scalars towards the surface, such as CO_2 or ozone, would be associated with deficit up or excess down. In other words, a contribution in the gradient mode increases the flux estimate in the direction expected on the basis of the scalar gradient, so that elimination (filtering) of net gradient mesoscale components by non-linear detrending should reduce the local flux estimate, while filtering of net counter gradient mesoscale flux should enhance it. The change in the net local flux (NLF) estimate with consecutively higher levels of filtering should, therefore, be consistent with the net transport mode of the filtered net mesoscale flux (NMF), and reflected in the magnitude of the NMF estimate. We selected detrending levels on the basis of 'accountability', defined as the percent change in the net local flux accounted for by the filtered mesoscale flux, as described below.

3.3.2 Selection of detrending technique

Several criteria were used for the selection of the Fourier series truncation level in the presence of mesoscale flux contributions. **Linear detrending** was used where: (a) The change in the net local flux (NLF) estimate derived from nonlinear detrending was negligible (<4%) and mesoscale accountability for this small change either approximates 0 or exceeds 150%; (b) The change in the NLF estimate was non-negligible (>4%), but mesoscale flux remained approximately 0 for increasing Fourier terms; (c) The direction of change (increase or reduction) in the net local flux estimate was inconsistent with the net transport mode of the mesoscale flux estimate, and where this inconsistency persisted or was exaggerated at consecutively higher levels of the Fourier series. The definition of negligible change (4%), represents one fifth of the maximum observed change in the NLF estimate, which was 20%.

For **nonlinear detrending**, the Fourier series truncation level was selected as follows: (a) A two-term truncation was selected if the direction of change in the local flux estimate was consistent with the transport mode of the mesoscale flux; the mesoscale accountability was between 50% and 150%, and inclusion of two consecutively higher terms in the series did not alter these results. (b) Higher level truncation of the Fourier series was selected, if the direction of change in the net local flux was inconsistent with the transport mode of the mesoscale flux at one level, but the inconsistency was corrected by inclusion of a higher Fourier term, with mesoscale accountability between 50% and 150%. (c) Higher level truncation of the Fourier series was also selected if the direction of change in the net local flux estimate was consistent with the transport mode of the mesoscale flux, but mesoscale accountability (while maintaining directional consistency with inclusion of higher terms) moved closer to the 100% ideal. Graphs (a), (c) and (e) of Figure 3.2 show the change in the NLF estimate and the corresponding net mesoscale flux (NMF) estimate of CO_2 for six different runs from grid 16, with gradient flux for CO_2 resulting in negative flux. Graphs (b), (d) and (f) of Figure 3.2 indicate the degree to which the mesoscale flux accounts for the changes in the local flux estimates. In the cases shown, a two-term truncation level of non-linear detrending was selected for runs 5, 6, 8, 9 and 10, where the transport mode as well as the magnitudes of the mesoscale flux account for the changes in the local flux estimates as a result of filtering. Linear detrending was used for run 7.

3.3.3 Structural Analysis

Following a similar procedure used by Mitic et al. (1995), based on Duncan and Schuepp (1992) and Caramori et al. (1994), a series of analytical steps were taken to identify the structures that dominate turbulent transport. These 'coherent' structures are defined as a set of correlated flux signals (w and c excursions) in time

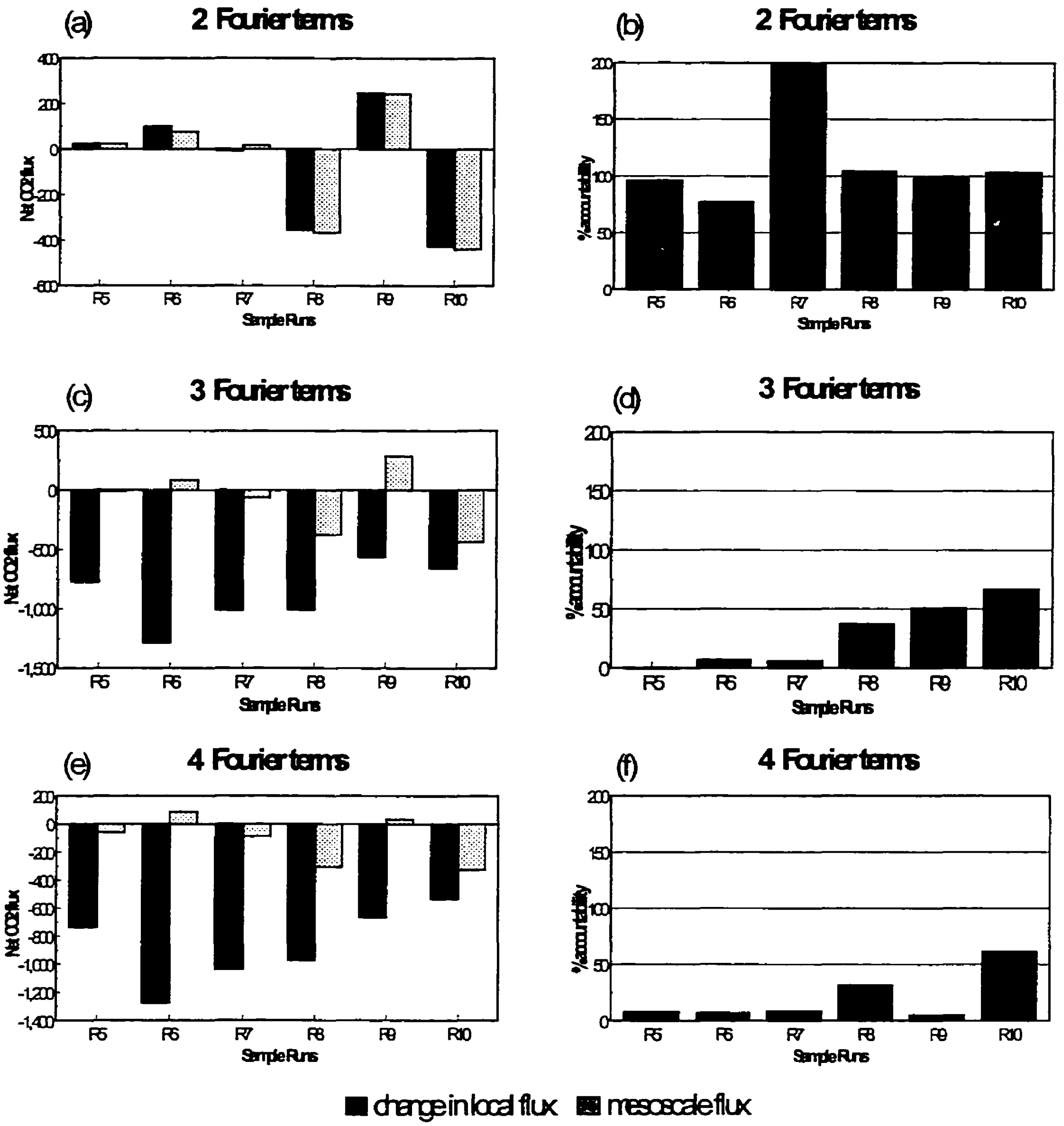

Fig. 3.2. (a,c,e) Changes in the net local flux and the corresponding net mesoscale flux for CO_2 along six sample runs from grid 16. (b,d,f) The mesoscale accountability for the changes in the local flux as a result of higher-order filtering. Flux estimates are cumulative contributions along the run as a measure of the net flux (in cumulative units of mg m^{-2} s^{-1}).

and space which are distinctly different and interspersed between less coherent components.

In order to separate these structures from incoherent noise, a hyperbolic hole corresponding to 0.2 rms was imposed on the scatter plot of c' vs. w' excursions, prior to structure definition. This is consistent with similar methods used by Antonia, (1981); Shaw, (1985); Grant et al., (1986); Caramori et al, (1994) and Mitic et al., (1995) to remove weak signals that may be positioned at the tails of structures.

Structures are identified by a series of eight or more consecutive pairs of w' and c' excursions (corresponding to ≈ 30 m in spatial extent) within the same mode of transport (excess-up/down, deficit-up/down). This minimum spatial scale is consistent with cospectral analysis of Twin Otter data at the flight level, which suggest that scales less than 30 m do not contribute significantly to the flux (Saucier et al., 1991; Desjardins et al., 1992a, b). The potential fragmentation resulting from inclusion of unmixed parcels of air was corrected by a defragmentation procedure as used by Mitic et al. (1995). A threshold based on a quadratic measure of the flux contribution from each structure (for details see Duncan and Schuepp, 1992; Caramori et al., 1994; Mitic et al., 1995), was then imposed to eliminate the weak structures and retain only the extreme events which generally occupy 20% of the time domain of the run but contribute about 80% of the overall flux. These may be expected to present the clearest picture of interactions among flux variables and the surface.

3.3.4 Coincidence Analysis

Structural analysis defines the physical locations (positions along the flight track) of structures separately for each scalar. These separately defined structures, termed *substructures* for the purpose of discussion, may physically overlap. Coincidence analysis attempts to reconstruct the size (along the flight line) of these structures and define their composition in terms of what scalars they are simultaneously transporting.

According to our concept, overlapping substructures were considered part of a main structure whose dimensions are defined by the outer limits of the overlapping substructures, from the beginning of the first substructure to the end of the last substructure within the overlap, and whose composition is given by the combined composition of the substructures. If one or more substructure were embedded in a larger one, the same rule for composition applied, with the size of the resulting structure defined by the extent of the larger substructure. It was expected that linking these reconstructed structures to the underlying surface would give insight into the co-location of sources and sinks, the degree to which driving forces are partitioned between the surface and the atmosphere, and a qualitative appreciation of the degree of mixing that occurs within coherent structures.

Association between fluxes was defined in two ways: (a) as a ratio (or percentage) of the number of structures with a particular composition to the total number of structures transporting a particular scalar and (b) as a ratio of the number of structures with a particular composition to the total number of structures defined across the grid site. This is an adaptation to the Jaccard coefficient used by Mitic et al. (1995), which defined flux associations based only on the coincidence of two scalars. The modifications applied in this study eliminate ambiguity of flux associations in cases where structures simultaneously transport more than two scalars. The flux associations for the various combination of scalars are mutually exclusive and expressed as:

$$FA=\frac{C_{i,j,k,l}}{N_x-\sum mp} \tag{2}$$

where $C_{i,j,k,l}$ is the number of coherent structures with the composition of scalars i, j, k, l, either exclusively or in combination of one, two or three of the other scalars; N_x is the total number of substructures for the scalar x (either i, j, k or l), or the total number of substructures for all scalars; mp is the number of sub-structures for x in excess of one, that is incorporated in any one coherent structure, so that $N_x-\sum mp$ is the total number of reconstructed structures.

3.4 RESULTS AND DISCUSSION

In the combined grids (44 grid lines for each scalar), linear detrending was selected in 19% of the cases, based on the criteria outlined in section 3.3.2. A second-term Fourier series truncation level accounted for 53%, third-order truncation for 24%, and fourth-order for 3% of the cases. Only in four cases (2.2%) were there unresolved inconsistencies in the direction of change of the net local flux and the net transport mode of the mesoscale flux. The thresholding procedures outlined in section 3.3.3 resulted in an average reduction of approximately 20 % in the flux estimates, as expected, indicating that 80% of the flux is transported by the dominant coherent structures, comparable to earlier observations over grassland (Duncan and Schuepp, 1992).

3.4.1 Flux Association in the Gradient Modes

Flux associations for both gradient modes are shown in Figures 3.3, 3.4 and 3.5. Figures 3.3 and 3.4 show the flux association calculated as a function of the total number of structures transporting the individual scalars (CO_2, H_2O, heat and O_3 - denoted by C,H,T and O, respectively, in the designation of combined structures) for grid flights 16 and 21. Figure 3.5 shows flux association as a function of the total number of structures identified within the grid. The following observations are apparent in Figure 3.3 (Flt 16): Among structures transporting CO_2, the dominant associations for structures moving toward the surface (gradient down) are with H_2O and with structures carrying both H_2O and ozone (H-O). For the gradient up mode, flux association of CO_2 with H-O dominates. In both gradient modes the majority of structures transporting heat are not associated with other fluxes. H_2O shows a similar pattern of flux association as CO_2, with dominant flux association to CO_2 as well as to the C-O combination, as expected. In the gradient down mode, the dominant proportion of ozone structures is not associated with other fluxes (41%)[1] with a 29% association to CO_2 and H_2O, while in the gradient up mode O_3 association to CO_2 and H_2O dominates (38%). The flux associations in Figure 3.4

---

1) Percentage figures are rounded to the nearest integer in this and the following discussion.

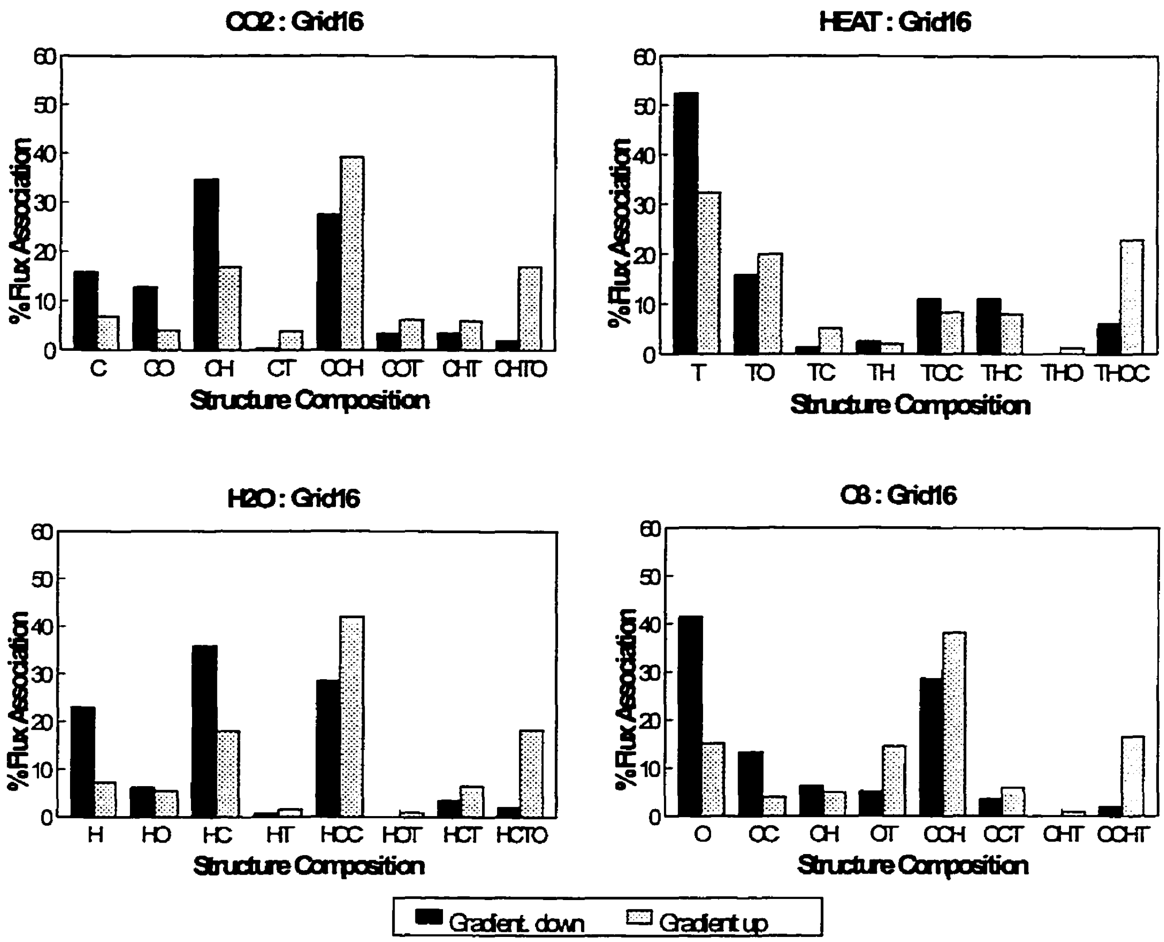

Fig. 3.3. Flux associations for grid 16, calculated as a function of the number of structures that transport each variable. C, T, H and O denote CO_2, heat (temperature), H_2O and O_3 respectively. The combination of these represent structures that transport the associated scalars.

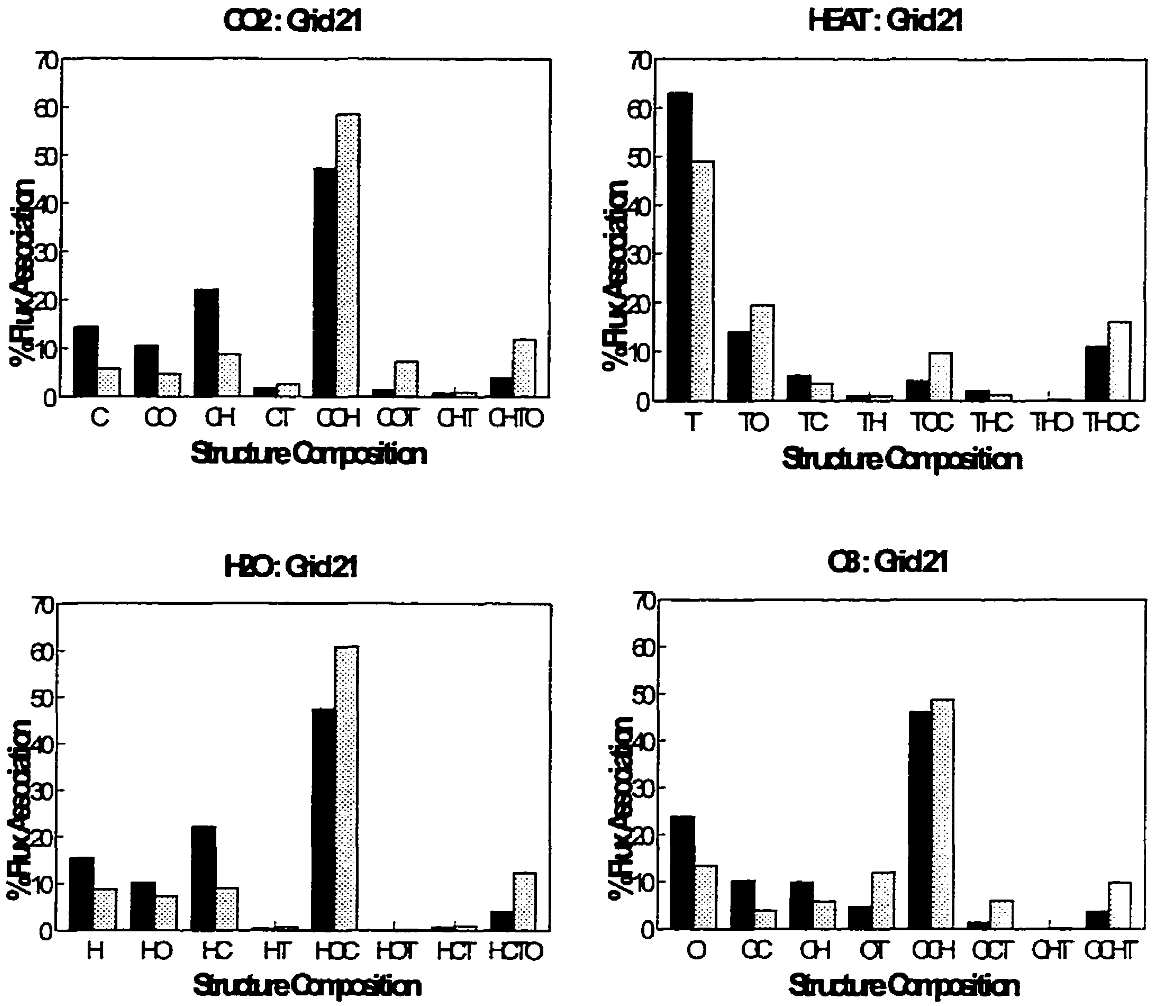

Fig. 3.4 Flux associations for grid 21, calculated as a function of the number of structures that transport each variable. C, T, H and O denote CO_2, heat (temperature), H_2O and O_3 respectively. The combination of these represent structures that transport the associated scalars. (Legend is similar to Fig 3.3)

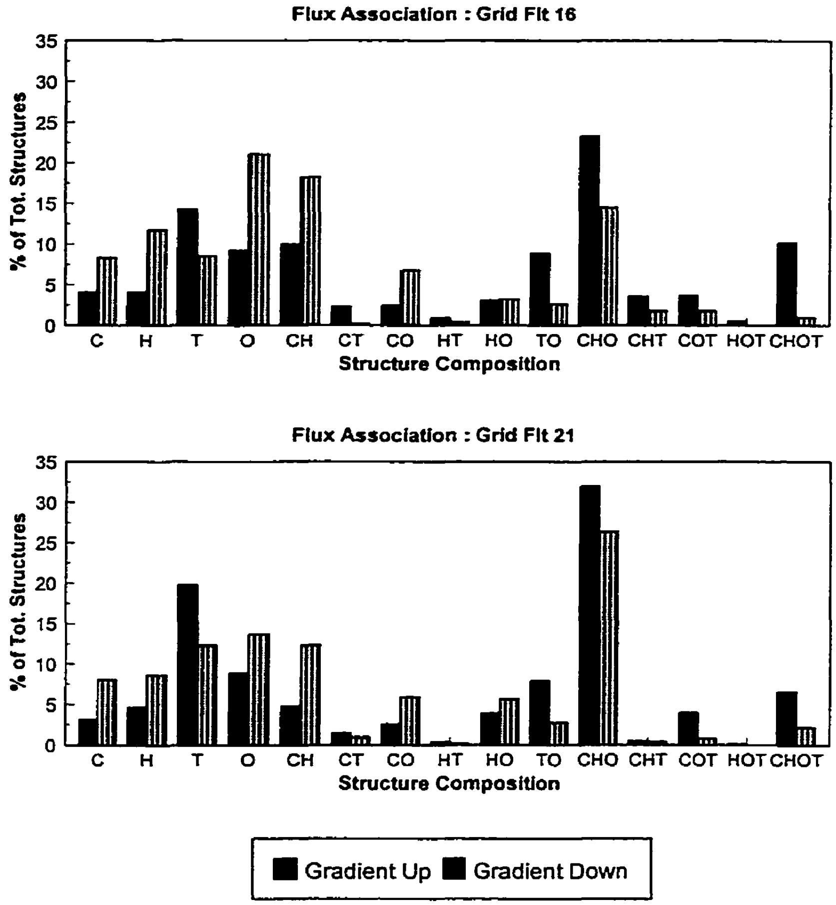

Fig. 3.5. Flux associations, calculated as a function of the total number of structures identified for each grid.

(Flt 21, flown two days after Flt 16), show similar relationships for both gradient down and gradient up modes, but the dominance of co-occurrence of CO_2, O_3 and H_2O in the same structure (C-O-H), and of single thermal structures, is more pronounced.

The relationships indicated for the individual fluxes are reflected in the flux associations calculated as a function of the total number of structures for each grid, as shown in Figure 3.5. For grid 16, structures transporting only ozone, and associations of C-H-O and C-H, dominate in the gradient down mode, while the C-

H-O combination dominates in the gradient up mode. For grid 21, flux association in the gradient down mode is dominated by C-H-O, with single-component structures and C-H combinations also relatively frequent. For the gradient up mode, the dominant flux associations are with structures transporting only heat, and those transporting C-H-O. The percentage of the total number of structures without heat in its composition tends to be larger for the gradient down mode than for the gradient up mode, with the notable exception of C-H-O. This indicates that heat is more important as a driving force for transport away from the surface than towards the surface. The relative importance of structures with C-H-O composition in the gradient up mode reflects the significant role of stomatal exchange processes in vegetation for the net transport of all these scalars.

The total number of structures (by composition) for the two gradient modes for both grids is given in Table 3.1. The overall ratio of structures in the gradient up mode to those in the gradient down mode is 1.34 and 1.41 for flights 16 and 21, respectively, for all scalars and combination of scalars across the grid. This indicates the importance of the surface in generating these structures. The important role of surface-generated buoyancy is shown by the fact that this ratio increases to around 2.7 for the heat structures alone, and to 5.4 for all structures associated with heat. The number of structures transporting exclusively H_2O, CO_2 and O_3 (the latter in the case of Flt 16), and the number transporting C-O and C-H combinations, are larger for the gradient down mode than the gradient up mode. Structures with other compositions are larger in number for the gradient up mode.

A closer examination of the structures in the gradient up mode, i.e. away from the surface, may help to interpret the observed flux associations. Assuming that uptake of CO_2 by vegetation is the only daytime surface sink for CO_2 across the grid site, we may try to classify the surface in terms of vegetated and non-vegetated areas based on the presence or absence of CO_2 in the structure composition. We may then subdivide the vegetated areas into water-stressed and non-water stressed sub-categories based on the presence or absence of H_2O. The hierarchical classification of structures according to this scheme is shown in Figure 3.6, and will be the focus of discussion in the next two paragraphs.

CO_2 flux is transported by 59% and 55% (Flts 16 and 21, respectively) of all structures in the gradient up mode. This figure is roughly comparable to the 60% land cover attributed to growing cotton within the grid area on the basis of remote sensing observations (Mitic et al., 1995). Of these CO_2 transporting structures, about 45% include either C-H or C-O combinations, while 36% include both C-O combinations and single H_2O structures. Structures with O_3 and H_2O account for 39%. Of the total CO_2 transporting structures, 21% are related to water stressed vegetation for flight 16, and 20% for flight 21. This results in an approximate 4:1 ratio of unstressed to stressed vegetation for the overall grid. For flight 16, 49% of structures transporting CO_2 over the water stressed portion of the canopy are associated with ozone and 71% over the unstressed portions, while the corresponding figures for flight 21 are 59% and 88%.

Grid areas that do not transport CO_2 may be classified as non-vegetated (no active photosynthesis). These areas account for an average of 43% of all structures

Structure Composition	Gradient Down		Gradient Up	
	Grid 16	Grid 21	Grid 16	Grid 21
Heat	43	63	113	171
O_3	106	70	73	76
CO_2	42	41	32	27
H_2O	59	44	32	40
O_3-Heat	13	14	70	68
O_3-CO_2	34	30	19	22
O_3-H_2O	16	29	24	33
O_3-CO_2-H_2O	73	135	184	276
O_3-CO_2-H_2O-Heat	5	11	80	56
Heat-CO_2	1	5	18	12
Heat-H_2O	2	1	7	3
Heat-H_2O-CO_2	9	2	28	4
Heat-H_2O-O_3	0	0	4	1
Heat-CO_2-O_3	9	4	29	34
CO_2-H_2O	92	63	79	41
TOTAL	504	512	792	864

Table 3.1. Structures identified in the gradient up and gradient down mode, categorised by the fluxes they transport, for grid 16 and grid 21.

in the gradient up mode, of which 65% are associated with heat and 49% with ozone. As seen in Figure 3.6, ozone is primarily associated with structures not transporting heat over these areas. For both grid flights, the vegetated areas account for the bulk of ozone uptake (43% of structures). One quarter of structures, however, have ozone in their composition in the absence of CO_2, indicating an additional non-vegetated sink for ozone.

In the estimation of ozone uptake by vegetation, the degree of error associated with directly linking ozone uptake to stomatal conductance of moisture varies across the canopy (Massman et al., 1993). The flux associations given above, suggest variations across canopies in the simultaneous uptake of CO_2 and ozone, and the release of water vapour, and that such differences vary with variations of moisture within the canopy. This could have implications for the estimation of ozone deposition if the degree of differential water stressed conditions of the canopy, and therefore the degree of association between ozone and H_2O or ozone and CO_2 is not considered. Using stomatal conductances acquired over water stressed portions of the canopy could underestimate ozone uptake for a canopy that is not uniformly water stressed. Ozone uptake is therefore not linearly related to stomatal conductance of H_2O and changes with surface moisture variability. Our results indicate that it would be desirable to attach differential weights both to the relationship between ozone and CO_2 and ozone and H_2O in order to make more accurate estimates of ozone uptake by vegetation.

A tentative classification and interpretation of the driving forces affecting flux transport may be based on the presence/absence of H_2O and heat, i.e. on the relative importance of water vapour density gradients and thermal buoyancy. As shown in Figure 3.7, water vapour as a driving force (defined as the presence of H_2O in the absence of heat) accounts for an average of 43% of the structures, which is about the same proportion (42%) as structures that contain heat. Structures

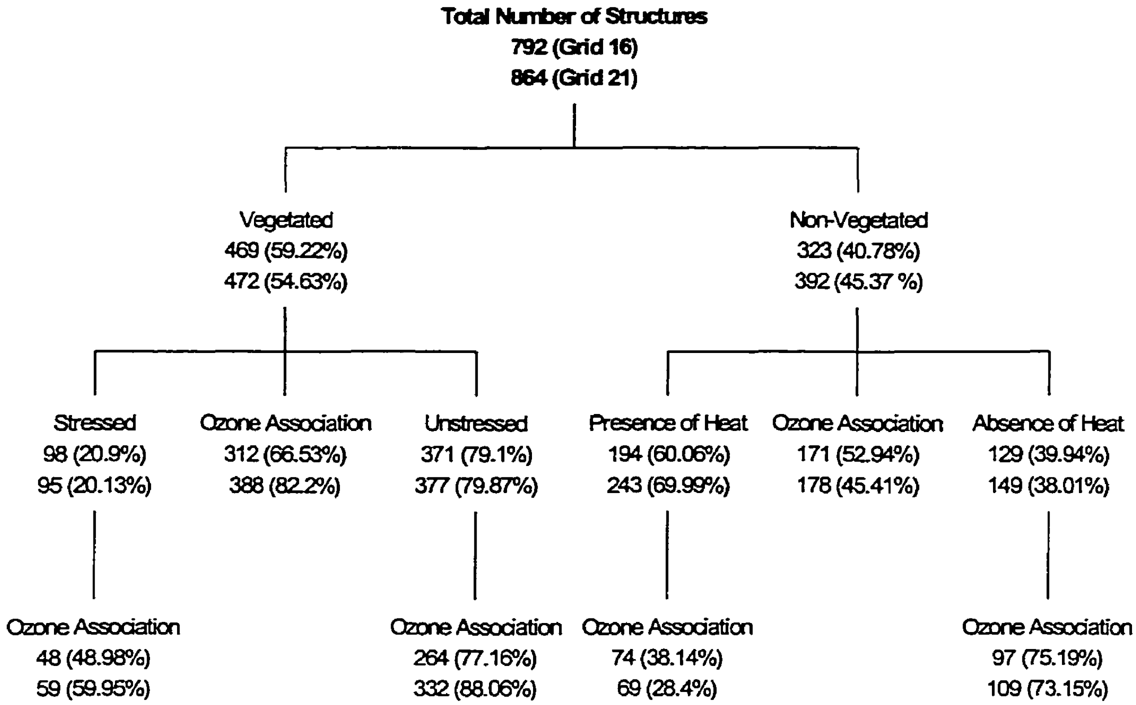

Fig. 3.6. Hierarchical breakdown of the surface conditions based on the flux composition of structures: presence of CO_2 (vegetated); absence of H_2O in the structure composition (stressed); presence of O_3 in structure composition (ozone association).

transporting only ozone, CO_2, or both in association, for which shear may be assumed to be the dominant driving force, account for the remaining 15%. This distribution of the driving forces underlines the importance of the surface as the source for driving forces of vertical exchange at a height of 30 m.

3.4.2 Structure Sizes and Mean Intensities

The average diameter of the structures defined by their flux composition, as determined from horizontal, one-dimensional transects, is given in Figure 3.8. Not

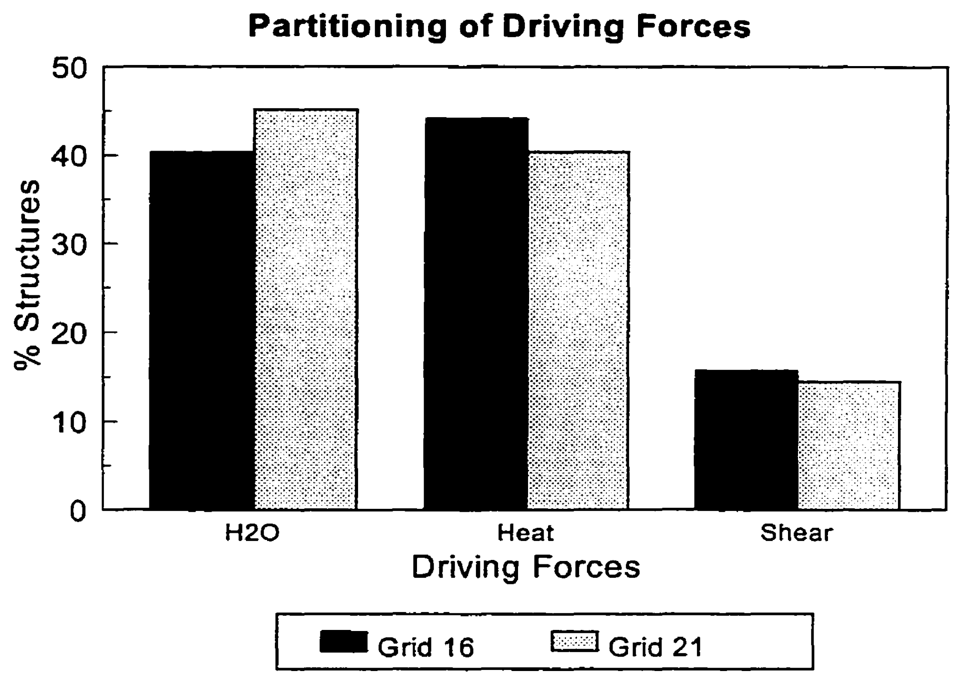

Fig. 3.7. Partitioning of the driving forces operating on the surface fluxes, as deduced from the composition of the transporting structures.

surprisingly, structures moving towards the surface (gradient down) are significantly larger than structures moving away from the surface, structures transporting a single flux variable are generally smaller than composite structures with multiple fluxes, and structures which contain heat are consistently bigger than those that do not.

An examination of the flux densities carried by structures with associations of O-C-H, O-C and O-H from flight 16 is summarized in Figure 3.9. For O-C-H structures, the fluxes of O_3 and CO_2 are correlated, with a low CO_2 flux corresponding to a low ozone flux and vice versa. The same holds true for the relationship between flux densities of H_2O and O_3 in those structures, with inverse

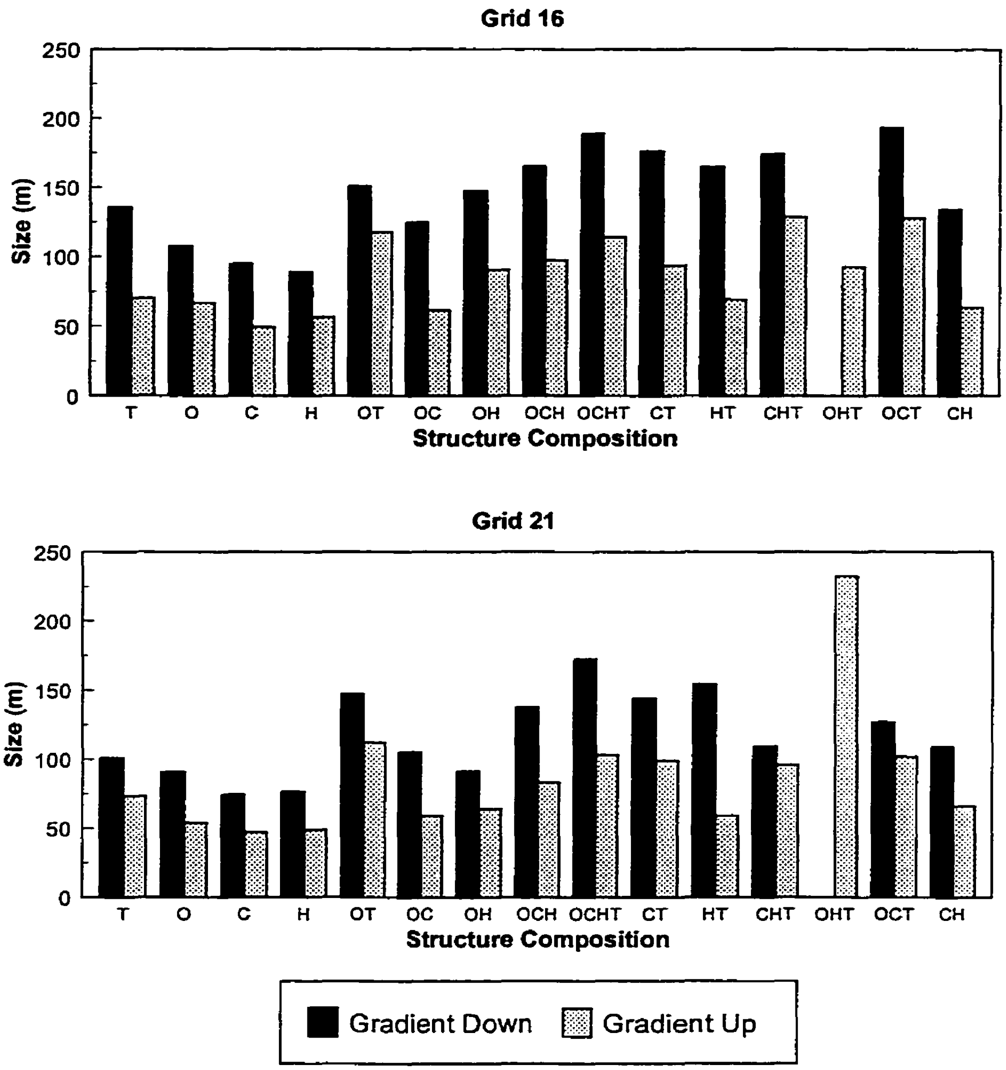

Fig. 3.8. Sampled horizontal dimensions, as a measure of the size of the structures moving towards the surface (gradient down) and away from the surface (gradient up).

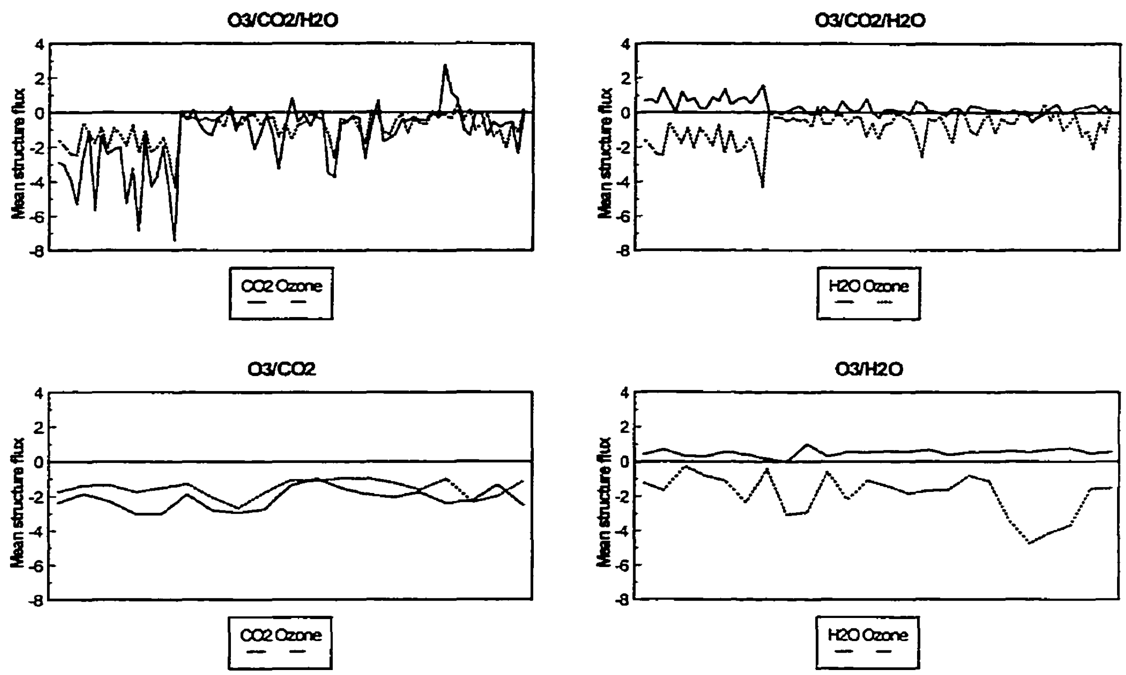

Fig. 3.9. Variations in the mean fluxes carried by structures with the exclusive compositions of $O_3/CO_2/H_2O$, O_3/CO_2 and O_3/H_2O. The *x*-axis represents the sequence of structures with that particular composition throughout the grid. Units of measurements are: CO_2 (mg m^{-2} s^{-1}), H_2O (g m^{-2} s^{-1}), O_3 (μg m^{-2} s^{-1}).

sign in the correlation, as expected. The corresponding R^2 values are 0.62 for O_3 and CO_2, 0.54 for O_3 and H_2O, and 0.89 for CO_2 and H_2O. For structures transporting only O_3 and CO_2, the relationship degrades, with an R^2 value of 0.21. Structures transporting only O_3 and H_2O have an even smaller R^2 value of 0.14. These results support the flux associations discussed earlier, where ozone, although highly associated to H_2O, has a higher association to CO_2.

3.4 CONCLUSION

The flux association of coherent structures has been shown to generate a large amount of information about the characteristics of these structures which dominate transport. Some findings from an earlier, more limited study (Mitic et al., 1995) have been confirmed, where ozone show differential degree of association to CO_2 and H_2O, indicating variations in the spatial distribution of sources and sinks within the vegetated portion of the site. The examination of the flux composition of the structures indicates that ozone is still taken up by the vegetation even under water stressed conditions. This was shown not only by the flux association values but also by the R squared values calculated for the mean fluxes within each structure. The partitioning of ozone uptake between the vegetated and non-vegetated surface was also apparent, suggesting a second, non-physiological sink for ozone, possibly associated with destruction of ozone by NO emission from soil (Guo et al., 1995b).

The study also showed that the driving forces for fluxes in the gradient up mode are dominated by surface forcing, through water vapour density gradients and thermal buoyancy, with a relatively much smaller percentage attributable only to shear forces. Transport in the gradient down mode is dominated by atmospheric driving forces, and structures are larger and fewer.

Although the magnitude of the mesoscale flux across the grids was quite small, the analytical scheme used to partition the local flux events from mesoscale flux was very effective. This procedure may be useful in cases where there are much larger and more dominant mesoscale motions contributing significantly to flux transport.

Further extension of this analysis, currently underway, includes ground-based tower data, both under stable and unstable conditions, over canopies with different characteristics. These studies are intended to add to our understanding of the degree of mixing that occurs as the turbulent transport structures move away from the surface, in terms of composition and size. Our analysis should be seen in the context of current attempts to define smaller-scale climate, energy and gas exchange models to be nested within boundary layer models, with increasingly realistic description of surface features, including vegetation. This raises questions as to the scales at which surface features should be parameterized, and the height above the surface where vertical transport loses its 'signature' of distinct surface source and sink distributions. We hope that the study of flux associations at different heights help to link structure composition to spatial distribution patterns of surface source and sink distributions and the spectral and thematic characteristics of the surface. In this way, this study and those currently in progress may be useful to validate models of biosphere-atmosphere exchange processes, and of the mixing among scalars within near-surface structures, at increasingly finer scales.

CONNECTING STATEMENT BETWEEN CHAPTERS 3 AND 4

Over a spatially organised but heterogeneous agricultural surface, aircraft data was able to successfully link the characteristics of fluxes and their corresponding coherent structures to the underlying surface conditions. The results in Chapter 3 are a continuation of a paper published in Atmospheric Environment, 29, 3169-3180,1995, which does not form part of this thesis. However for a more complete understanding of the findings of the spatial analysis for the CODE grid, this paper may be consulted.

The majority of surface observations are made from meteorological towers. The following chapter uses tower data collected over two different crop canopies in the same agricultural region as part of CODE, to examine the characteristics of fluxes and coherent structures. This chapter gives some temporal dimension to the overall study and allows some general comparisons with results from Chapter 3.

The material in Chapter 3 has been published in the Journal of Agricultural and Forest Meteorology, 87, 27-39, 1997, and Chapter 4 has been published in Atmospheric Environment, 33, 1159-1173, 1999. Since they were written independently of each other, some duplication in analytical expression and methodologies is unavoidable.

CHAPTER 4.

STRUCTURAL ANALYSIS AND FLUX ASSOCIATIONS OF CO_2, H_2O, HEAT AND OZONE OVER COTTON AND GRAPE CANOPIES

4.1 INTRODUCTION

The use of models for simulation and prediction of surface-atmosphere dynamics has become an integral part of research in the atmospheric/environmental sciences. Almost all forms of these models have to incorporate some form of parameterization of the surface characteristics (McGuire et al., 1991; Koster and Suarez, 1992; Sellers et al., 1992; Melillo et al., 1993; Bonan, 1993; Massman et al., 1994; Goetz and Prince, 1996; Ruimy et al., 1996). The fact that these models are sensitive to spatial variability of physical surface characteristics (Wollenweber, 1995; Klaassen and Claussen, 1995; Sud et al 1988), and the uncertainty surrounding the relative influence of the various scales of such variability (Moore et al., 1993), highlight the need to improve our understanding of the atmosphere-ecosystem exchange processes. This need is reflected in the increasing number of studies that focus on the parameterization of surface characteristics (Hanan et al., 1995; Hall et al., 1995; Lee et al., 1996) and, in particular, the transport dynamics of various fluxes and their coupling to the underlying surface (Schuepp et al., 1987; Mack et al., 1990; Hollinger et al., 1994; Massman et al., 1993; Rochette et al., 1995; Baldocchi, 1994; Guo et al., 1995a; Mitic et al., 1997).

Some studies have specifically related the coherent motions of turbulence (as opposed to incoherent noise) in the surface layer to surface characteristics

(Caramori et al., 1994; Mitic et al., 1995; Mitic et al., 1997). These coherent "structures" are responsible for the bulk of turbulent transport in the surface layer and have been examined from various other perspectives (Wyngaard, 1983; Eloranta and Forrest, 1992; Mahrt and Ek, 1993a & 1993b; Paw U et al., 1995). A study of coherent turbulent structures allows for the improvement of our understanding of the processes operating on surface fluxes, and the associations of the various fluxes with each other and with the underlying surface. Identifying the physical extent of structures and their composition, will give some indication of the driving forces operating on flux transport as well as their partitioning between the surface and the atmosphere. This is of particular importance in the assessment of the potential for predicting fluxes from surface characteristics in cases where some fluxes, like those of water vapour and CO_2, are more readily inferred from surface observation than others, such as ozone flux.

Our study uses tower data collected at the cotton and grape sites during the California Ozone Deposition Experiment (CODE) in the summer of 1991, to examine flux associations of CO_2, H_2O, heat and ozone. This is done for the two gradient modes of transport, where the surface acts as a sink for CO_2 and ozone and a source of moisture and heat during the day, and a source of CO_2 and a sink for heat at night. The focus is on exchange processes at the "patch" scale (1 km^2), and the objective is to characterize the temporal evolution and characteristics of coherent structures during unstable (day) and stable (night) conditions over these two different crop canopies. Due to the importance of ozone deposition in the study area and the primary objective of CODE (part of the San Joaquin Valley Air Quality

Study, Pederson et al., 1995), and given the fact that regional models for ozone deposition are based on a variety of physical and physiological surface characteristics at different scales (e.g. Massman et al., 1994), the emphasis is on the associations of ozone to the other flux variables. Such associations and the spatial scales involved are of interest as bases of reference for soil-vegetation-atmosphere transport (SVAT) models and as validation data sets for scaled-down large eddy simulation models, which are increasingly being used to describe canopy-atmosphere exchange.

4.2 SITE AND DATA DESCRIPTION

The data were collected at two meteorological tower sites over a cotton and grape canopy located in the central valley of southern California at approximately 100 m above sea level (Pederson et al., 1995). The field observation period lasted from early July to early August, 1991. Five days were selected for study from each of the two data sets. For each of these days, two 20 min time segments were used for analysis, one during stable nighttime conditions and the other during unstable daytime conditions. The daytime segments were selected from periods between midday and mid-afternoon when the boundary layer was considered to be fully developed, with unstable thermal stratification (z/L significantly negative). The nighttime segments had zero solar radiation and stable stratification (positive z/L). The selection of days for analysis depended on data quality as well as on similarity in conditions such as mean wind speed and atmospheric stability. The data sets include eddy correlation observations, based on fast response sampling of the vertical wind component, air temperature, and the concentrations of CO_2, H_2O, and ozone. A detailed description of sites and sampling procedures is given below.

4.2.1 Cotton site

The tower at the cotton site was operated by the ASTER group from the U.S. National Centre for Atmospheric Research (NCAR). The site was located at 36° 48' 50" N and 120° 40' 38" W, 80 km west of Fresno. The crop was planted in an E-W row orientation spaced 1 m apart. During the observation period, the average height of the cotton crop increased from 0.4 m to 0.9 m, and the leaf area index from 1.8 to 2.5. Eddy correlation systems were located at 5 m above the surface to sample the three wind components, water vapour, CO_2 and air temperature at a frequency of 20 Hz. Data were collected continuously from July 11 to August 7. The selected days and time segments used in this study are listed in Table 4.1. The mean wind direction was perpendicular to the rows. For the selected nighttime segments, the mean wind speed ranged from 1.7 m s^{-1} to 2.2 m s^{-1}, z/L between 0.11 and 0.65, the mean surface temperature between 22 °C and 24.5 °C, and dew was present in all cases. The daytime segments are characterized by mean wind speeds between 1.2 m s^{-1} and 2.3 m s^{-1}, z/L between -0.19 and -2.0, mean surface temperature between 30 °C and 38.8 °C and half hourly averaged incident solar radiation between 946 W m^{-2} and 987 W m^{-2} with the exception of one day (Aug. 5) where it was 750 W m^{-2}. The cotton fields were irrigated.

		Cotton		Grape	
Date (1991)	*DOY*	*night*	*day*	*night*	*day*
July 21	202			4:00 *am*	1:30 *pm*
July 22	203	1:00 *am*	12:00 *pm*	1:00 *am*	12:00 *pm*
July 23	204	4:00 *am*	1:30 *pm*		
July 24	205	4:00 *am*	12:30 *pm*		
July 30	211			1:00 *am*	12:00 *pm*
July 31	212			4:00 *am*	2:30 *pm*
August 01	213	3:30 *am*	1:00 *pm*		
August 03	215			12:30 *am*	1:00 *pm*
August 05	217	9:30 *pm*	3:30 *pm*		

Table 4.1. Selected dates and start time of the 20 minute segments used as case studies for the cotton and grape sites. Times are in Pacific local time, and night refers to conditions of zero solar radiation.

4.2.2 Grape site

The tower at the grape site was operated by the Air Quality Processes Research Division of the Atmospheric Environment Service of Canada. The site was located 40 km northwest of Fresno, California, at 36° 51' 36" N and 120° 6' 7" W. The grape crop was planted in E-W rows spaced 3 m apart. The grass growing between the rows was mowed about a week prior to the start of field measurements and grew to about 30 cm by the end of the study. The average height of the vines was 1.7 m, and the LAI remained unchanged at 3.4 for the duration of the experiment. Data were collected continuously from July 11 to August 8, at a height of 9.4 m above the surface, at a frequency of 20 Hz. Table 4.1 shows the days and time segments used in this study. The mean wind direction was diagonal to the rows. The nighttime series are characterized by mean wind speeds between 1.68 m s^{-1} and 2.46 m s^{-1}, z/L between 0.22 and 1.0 and mean surface temperatures from 15.6°C to 20.7 °C. During the daytime segments, the mean wind speed ranged from 1.05 m s^{-1} to 3.76 m s^{-1}, z/L from -0.19 to -3.07, mean surface temperature from 28.9 °C to 37.6 °C, and mean incident solar radiation from 837 W m^{-2} to 967 W m^{-2}. The grape site was irrigated twice during the observation period.

Details of the instrumentation and site characteristics for both sites may be found in Massman et al. (1994).

4.3 DATA ANALYSIS

The analytical procedures used to define the flux estimates for CO_2, H_2O, heat and ozone, which identify the coherent structures and examine the relationships and associations between the various scalars transported by these structures, are similar to those of Mitic et al. (1997) on aircraft data. However, while Mitic et al. (1997) provided a spatial analysis of flux and the corresponding coherent structures, this paper is concerned with their temporal distribution and characteristics at the stationary observation point. The mean used to estimate the flux in the eddy correlation technique is therefore defined across time, and the removal of trends from the data filters out low frequency ('mesoscale' or 'mesocycle') oscillations that either represent organized large scale cycles within the selected time segment or span a time frame larger than that being studied. By contrast, we define the instantaneous flux contributions within the 20 min time segment as 'local flux events'.

The accurate definition of the mean is an important aspect of the eddy correlation technique, and varying approaches may be found in the literature (Mahrt and Ek, 1993a; Caramori et al., 1994; Mitic et al., 1995 and 1997; Ogunjemiyo et al., 1997). Flux estimates are calculated as the covariance between the deviations of the vertical wind (w') and scalar admixtures (c') from their means. Implicit in this definition of a physically meaningful mean is the removal of any trends that might be present in the time series, as well as the separation of any large scale temporal cycles from the local instantaneous flux events which are directly tied to the underlying surface and the time segment under study.

The local flux estimates were calculated using the fluctuations from the local means derived from linear detrending, in the form of a simple regression, and nonlinear detrending in the form of a truncated Fourier series (see Mitic et al., 1997, for details). In cases where a nonlinear trend is present within the time series, the larger scale (mesocycle) flux is derived from the low frequency oscillations filtered from the scalar concentration and the vertical wind field. The procedure is based on the decomposition of the flux into large scale time averages, represented by the mesoscale means (<w> and <c>), and running (local) means (w* and c*) represented by the linear or nonlinear series fitted to the data. Instantaneous fluctuations (w' and c') are defined against the local means, which may be non-stationary due to 'mesocycle events'. Considering this expansion into means and fluctuations (w = <w> + w* + w', etc.), applying Reynolds averaging under consideration of the fact that <w'> and <w*> (or <c'> and <c*>) vanish by definition, the time-averaged vertical flux F_T, over time T, at height h, is then given by

$$F_T = \frac{1}{T}\int_T w(h,t)\,c(h,t)\,dt$$
$$= \langle w\rangle\langle c\rangle + \langle c{*}w{*}\rangle + \langle c'w'\rangle \qquad (3)$$

The conditions for Reynolds averaging may not be perfectly satisfied when a running mean is expressed by the truncated Fourier series, but any terms excluded from equation 3, such as <c*w'>, are bound to be negligible. In the case of <w> = 0, which is a reasonable assumption for large, flat terrain such as the San Joaquin Valley, equation (3) is reduced to F_T = <c*w*> + <c'w'>, which is the sum of the mesocycle flux and the local flux, respectively.

Using quadrant analysis and an imposed hyperbolic hole of 0.2 rms of the flux, the modes of flux transport are defined for each local flux event (w'c') (Antonia, 1981; Grant et al., 1986). Each of these instantaneous contribution to the flux, resulting from a correlation between the vertical wind fluctuation and the scalar fluctuation, may be characterized according to the four modes of the eddy covariant transport as 'excess up' ($w'^{(+)}$ $c'^{(+)}$), 'excess down' ($w'^{(-)}$ $c'^{(+)}$), 'deficit up' ($w'^{(+)}$ $c'^{(-)}$) and 'deficit down' ($w'^{(-)}$ $c'^{(-)}$), i.e. the four quadrants of a (c'w') plot. Our paper focuses on the gradient modes, which describe the dominant direction of flux, such as an upward transport of an excess of heat and moisture and a deficit of CO_2 and O_3 during daytime conditions. Downward gradient transport during the day is characterized by an excess of CO_2 and O_3 and a deficit of heat and moisture. For nighttime conditions, upward gradient transport of heat and CO_2 is effected by an excess of CO_2 and deficit of heat. The nighttime transport modes for moisture and O_3, cannot be generalized and must be determined from the empirical data.

The separation of local flux from larger scale motions was followed by *structural analysis*, the process of identifying the coherent structures that transport each scalar, and *coincidence analysis,* which determines to what extent the structures for the various scalars overlap, and examines size and composition of these 'combined structures' (Mitic et al., 1997). The horizontal extent of structures is based on Taylor's frozen hypothesis (Taylor, 1938), assuming that the timescale for an eddy to evolve is longer than the time it takes to be advected past the sensor (Powell and Elderkin, 1974). Structural analysis identifies coherent (turbulent) structures within a time series or along a spatial transect, as a series of consecutive instantaneous flux events above the given threshold, within the same transport mode (quadrant). The structure size (ss) in one dimension is then given by the product of the duration of flux events within a certain transport mode and the corresponding wind speed.

$$ss=(N^{i}*\frac{1}{f})*\bar{U} \qquad (4)$$

N^i is the number of consecutive flux events in quadrant i, f is the sampling frequency, and $\bar{U}$ is the mean wind speed. We arbitrarily defined the minimum size of a structure (s_{min}) to be resolved in our analysis at twice the spatial resolution of the sensor array (0.4 m), i.e. at 0.8 m. The minimum number of consecutive flux events (N^i_{min}) required to yield s_{min}, as given by equation 4, depends on mean wind speed $\bar{U}$. For the purpose of this study, $\bar{U}$ was classified into high ($\bar{U} > 1.5$ m s^{-1}) and low ($\bar{U} \leq 1.5$ m s^{-1}), with thresholds N_{min} fixed at 10 and 16, respectively, to yield a threshold for the definition of structure size. Record segments with $N^i < N^i_{min}$ are then disregarded as incoherent noise.

Our process of structural analysis initially defines coherent structures separately for the various scalars (CO_2, H_2O, heat and ozone). These are termed 'substructures' (Mitic et al., 1997) since their size and composition are determined in isolation from the other fluxes. In reality, scalars are not transported exclusively of each other, so that coincidence analysis is used to examine the overlap of these substructures into 'combined' structures, which transport more than one scalar simultaneously, and to provide a description in terms of their size, composition and spatial distribution. It overlays the location of the substructures along the time series for all four scalar fluxes and combines those that are co-located in so far as there is some overlap in their spatial extent. The size of the combined ('reconstructed') structures is defined by the outer limits of its overlapping substructures, such that if substructure A (located between time vectors t_1 and t_3) overlaps substructure B (located between t_2 and t_4), where $t_1 < t_2 < t_3 < t_4$, the resulting two-component structure is considered to be located between t_1 and t_4. Analysis of the composition of these reconstituted structures permits us then to define the extent to which different scalars are associated in transport. The absence of a particular flux from the composition of a reconstituted structure indicates that, for the duration of time over which that structure was observed, there was no consistent coherent contribution of that flux, in the sense that the minimum requirement for significant flux contribution (N_{min}) was not met along that particular segment of the time series.

The frequency of association between fluxes, FA, is defined as a ratio (or percentage) of the number of structures with a particular composition, to the total number of structures defined for the 20 minute time series. Flux association for the four variables examined may be defined for 15 categories based on the mutually exclusive combinations of CO_2, H_2O, heat and O_3. These combinations represent the presence of sustained coherent flux contribution within the structure. Using the above definition, a structure with a composition of H_2O and O_3 (HO) indicates that, for the duration of the structure, only H_2O and O_3 had a sustained coherent flux contribution while the flux events of heat and CO_2 within that structure have been classified as incoherent noise. This technique is an improvement to the Jaccard coefficient used by Mitic et al. (1995), which defined flux associations (FA) based only on the coincidence of two scalars, and similar to Mitic et al. (1997) for aircraft grid data sampled during CODE. The resulting definitions of flux associations eliminate ambiguity and are mutually exclusive for the various combination of scalars. The expression takes the form:

$$FA=\frac{C_{i,j,k,l}}{N-mp} \tag{5}$$

$C_{i,j,k,l}$ is the number of coherent structures with the exclusive composition of scalars i, j, k, l (heat, H_2O, CO_2,O_3), or any combination of these ; N is the total number of structures (before reconstruction) for the overall time series; mp ("multiple pockets") is the reduction in the number of structures as a result of overlap, so that N-mp is the total number of reconstructed structures.

During the process of defining the flux compositions of the structures, the mean flux of the individual scalars that make up that composition is also defined. Correlation analysis of the flux intensities within the dominant FA categories is used to complement the flux association analysis. Correlation between fluxes such as CO_2 and H_2O within the FA category CHOT (representing CO_2, H_2O, ozone and heat) represents the correlation of the mean magnitudes of these scalars within all the structures defined as having the composition CHOT.

It may be of interest to compare structure sizes generated by the above analysis against expected length scales in the surface boundary layer. We may use mixing length in surface scaling as a parameter that should be comparable to the observed one-dimensional structure size. The mixing length (ℓ) under unstable conditions is defined as

$$\ell_{M,H} = \frac{kz}{\phi_{M,H}} \qquad (6)$$

for shear driven (M) and buoyancy driven (H) eddies, respectively, where k is the Von Karman constant (taken as 0.4) and z is the measurement height. ϕ_M and ϕ_H are the dimensionless wind shear and potential temperature gradient in the surface layer expressed for non-zero surface stress (Stull, 1988) and defined as

$$\Phi_M = \frac{kz}{u_*}\frac{\partial \overline{U}}{\partial z} = (1-15\frac{z}{L})^{-1/4} \tag{7}$$

$$\Phi_H = \frac{kz}{\Theta_*}\frac{\partial \Theta}{\partial z} = 0.74(1-9\frac{z}{L})^{-1/2} \tag{8}$$

where $\bar{U}$ is the mean wind speed, Θ is mean potential temperature, u_* is friction velocity, θ_* is the temperature scale for the surface layer based on u_* and L is the Obukhov Length. In cases where buoyancy dominates, the dimensionless moisture gradient ϕ_E may be equated to ϕ_H. Decomposition of the forces responsible for flux transport at the surface, (discussed later) into shear, heat and water vapour, may serve as a weighting factor for ℓ_M and ℓ_H, and the ratio of shear forces to heat and water vapour forces defined as

$$\lambda = \frac{\xi_M}{\xi_H + \xi_E} \tag{9}$$

where ξ_M, ξ_H, ξ_E are the percentages of the driving forces attributes to shear, heat and water vapour respectively. The mean mixing length as a function of ℓ_M and ℓ_H is then defined as

$$\ell = \lambda \ell_M + [(1-\lambda)\ell_H] \tag{10}$$

4.4 RESULTS AND DISCUSSION

No consistent trends were observed in the wind and scalar data for both grape and cotton, for the night and day time series. For the majority of cases nonlinear detrending was most appropriate. Only in 5 of the 50 cases were linear detrending appropriate for the grape data and in 17 of 50 cases for the cotton data. In these cases there were no significant low frequency variation other than the linear trend. Since linear detrending only extracts low frequency signals at a scale larger than the sample length (vector), the resulting local flux estimate is a combination of low and high frequency contributions. The non-linear high-pass filtering inherent in isolation of the low frequency signals, at a scale which is smaller than the sample length, will result in local flux estimate which is different from the linear estimate and is defined only by high frequency contributions. In the case of nonlinear detrending, the filtered low frequency mesoscale flux accounted for 95% - 110% of the difference in flux estimate when linear was replaced by non-linear detrending for the grape data and 84% - 111% for cotton, indicating successful isolation of the local fluxes from the larger mesocycles or mesoscale fluxes. The filtered mesoscale flux was negligible and is not considered in the subsequent analyses, which only examine the local instantaneous flux. For a more elaborate illustration of this procedure see Mitic et al. (1997).

The mean flux densities for all cotton and grape data show the surface acting as a sink for CO_2 (C), and ozone (O) and a source of heat (T) and H_2O (H) during the day. During the night, it becomes a source of CO_2, and a sink for heat, but remains a sink for ozone and a source of H_2O. This is seen in Figure 4.1, which also shows consistent dominance of latent heat flux over sensible heat flux during the day. The sensible heat fluxes from both grape and cotton are significantly lower around day of year (DOY) 211 to 215, due to irrigation, a situation which is not reflected in the other variables. The observations shown in Figure 4.1 allow for the definition of the gradient modes of transport of each flux during the day as well as - particularly - during the night.

4.4.1 Cotton Site Results

4.4.1.1 *Flux Associations*

The flux associations (FA) for all ten case studies are shown in Figure 4.2. The pattern of flux associations is similar for structures in both the gradient down and gradient up modes. Under **stable nighttime conditions**, structures associated with transporting only one flux component (CO_2 (C), H_2O (H), O_3 (O) or heat (T), exclusively) dominate, cumulatively accounting for 35% to as high as 70% of the total number of structures. This may indicate the relative lack of mixing within the nighttime collapsed boundary layer as well as some decoupling of nocturnal surface processes. The association of ozone with non-CO_2 transporting structures (no sustained presence of coherent CO_2 flux) during the night indicates the existence of a non-vegetated sink for ozone. The non-vegetated ozone sink is indicated by the relative prominence of structures transporting H_2O-O_3-heat (HOT), which are also present during the day.

During **unstable day time conditions,** structures simultaneously transporting CO_2-H_2O-O_3-heat (CHOT) dominate, with FA (in the gradient up mode) between 26% and 57%, associated with the dominant vegetated sink. This indicates not only a higher degree of mixing, compared to the nighttime cases, as would be expected, but presumably reflects also the co-located vegetated daytime source-sink for these variables. The association among structures transporting H_2O, O_3 and heat is the second consistently significant flux association. On DOY 213, however, structures transporting only CO_2, H_2O and ozone figure prominently at 19%. This corresponds to the low sensible heat flux during this time (Figure 4.1) and is a direct result of the irrigation of the field. Coherent structures transport approximately 80% of the total flux in about 20% of the averaging time. The association between the flux components of structures simultaneously transporting CHOT and HOT, indicating vegetated and non-vegetated source/sinks, respectively, was therefore further documented by correlation analysis of the mean flux magnitudes within these structures, as shown in Figures 4.3 and 4.4 The following discussion therefore deals with the correlation of the flux

intensities within the dominant structure categories. For the **CHOT** structures, there is a consistent high correlation between H_2O and ozone flux intensities, ranging from 0.68 to 0.91. The correlation between CO_2 and ozone is more variable and reflects the correlation pattern between CO_2 and H_2O which ranges from 0.5 to 0.8. There is also a consistent moderate to high correlation between heat and ozone within these structures. The correlation plots for the combined CHOT structures from all five days (Figure 4.4) show a positive relationship among all the flux components. The corresponding correlation coefficients show the highest overall

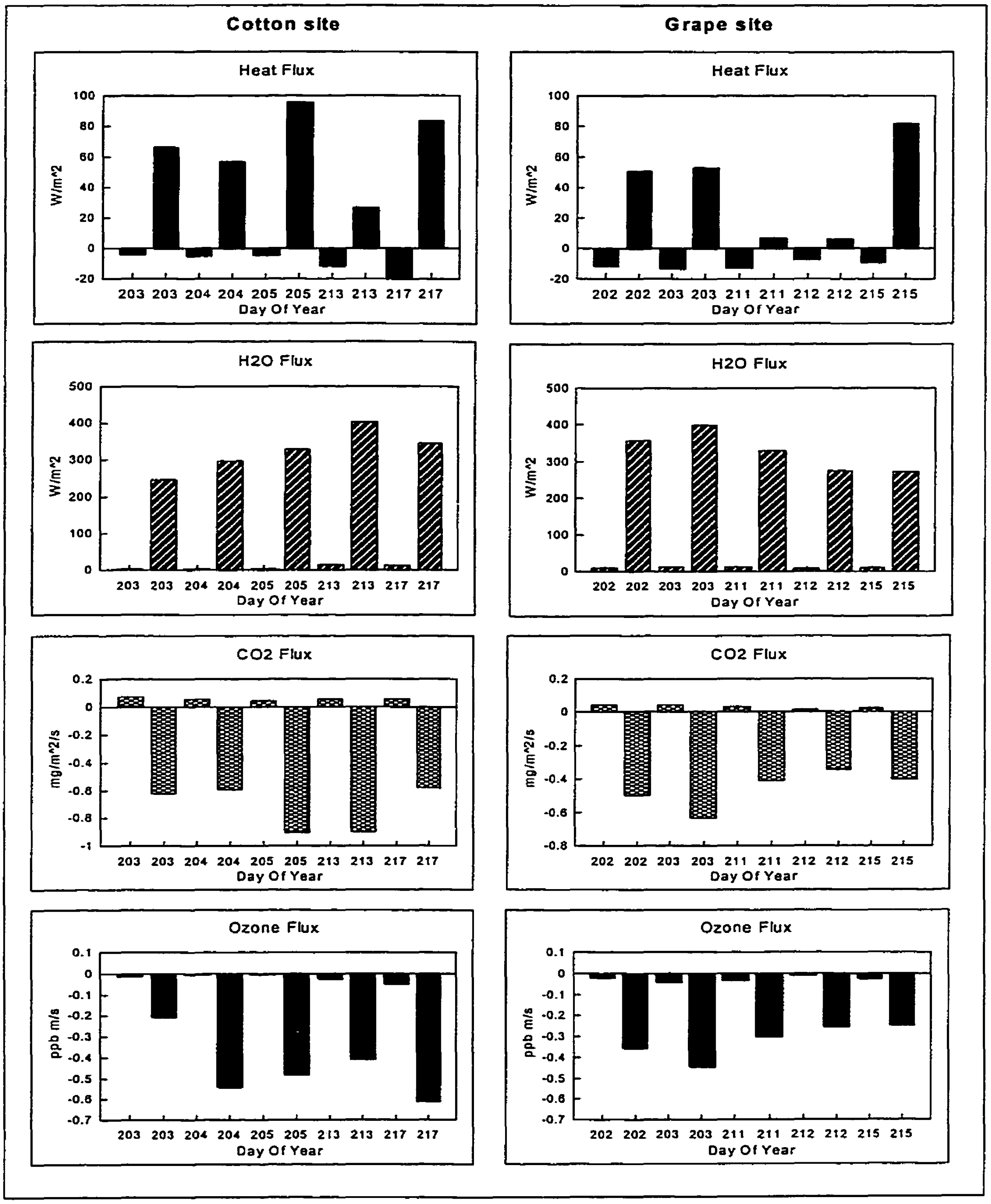

Fig. 4.1. Mean fluxes for 20 min. time segments over the cotton and grape sites. Bars are in the order of night-day.

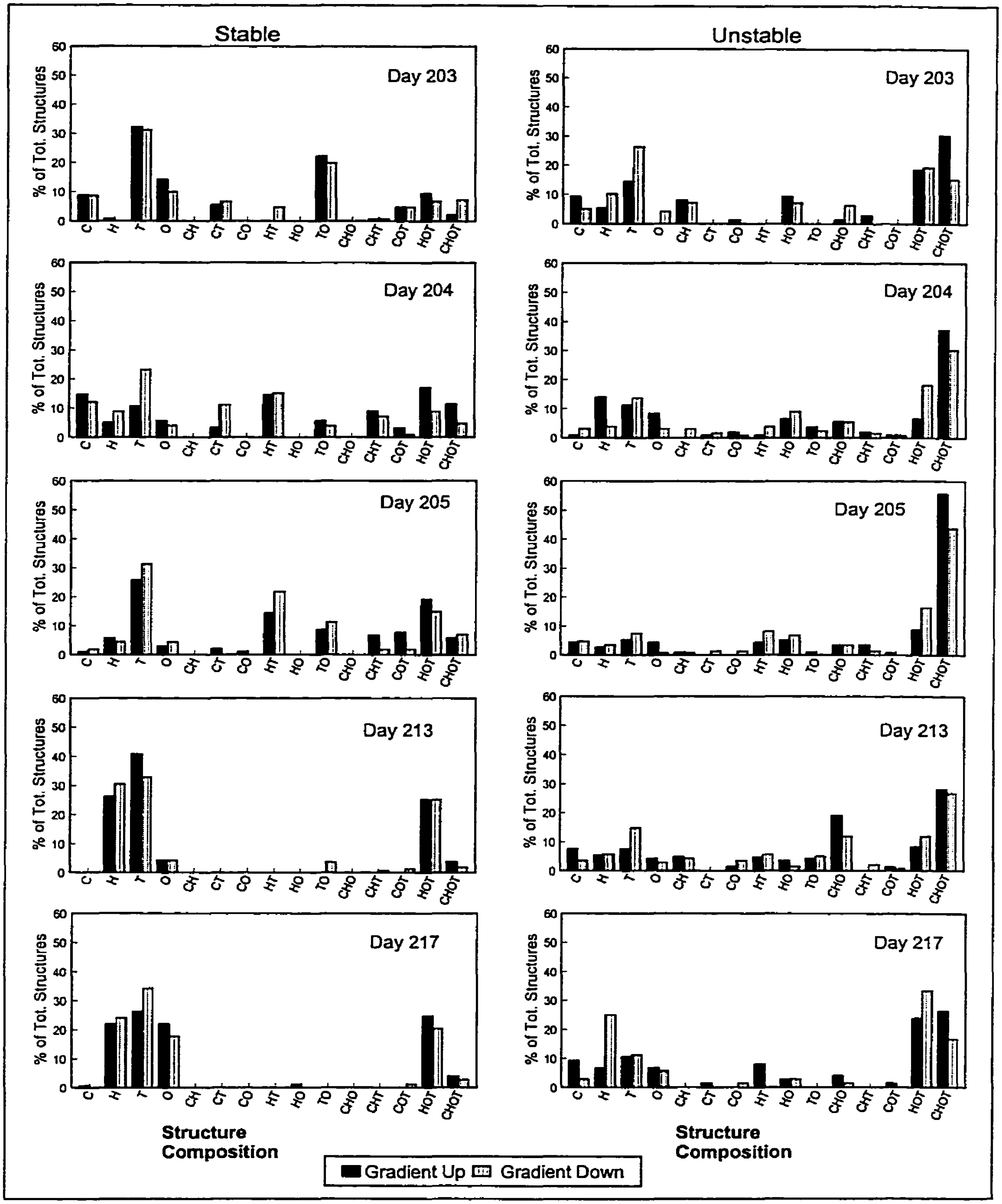

Fig. 4.2. Flux association at the cotton site for both stable and unstable conditions

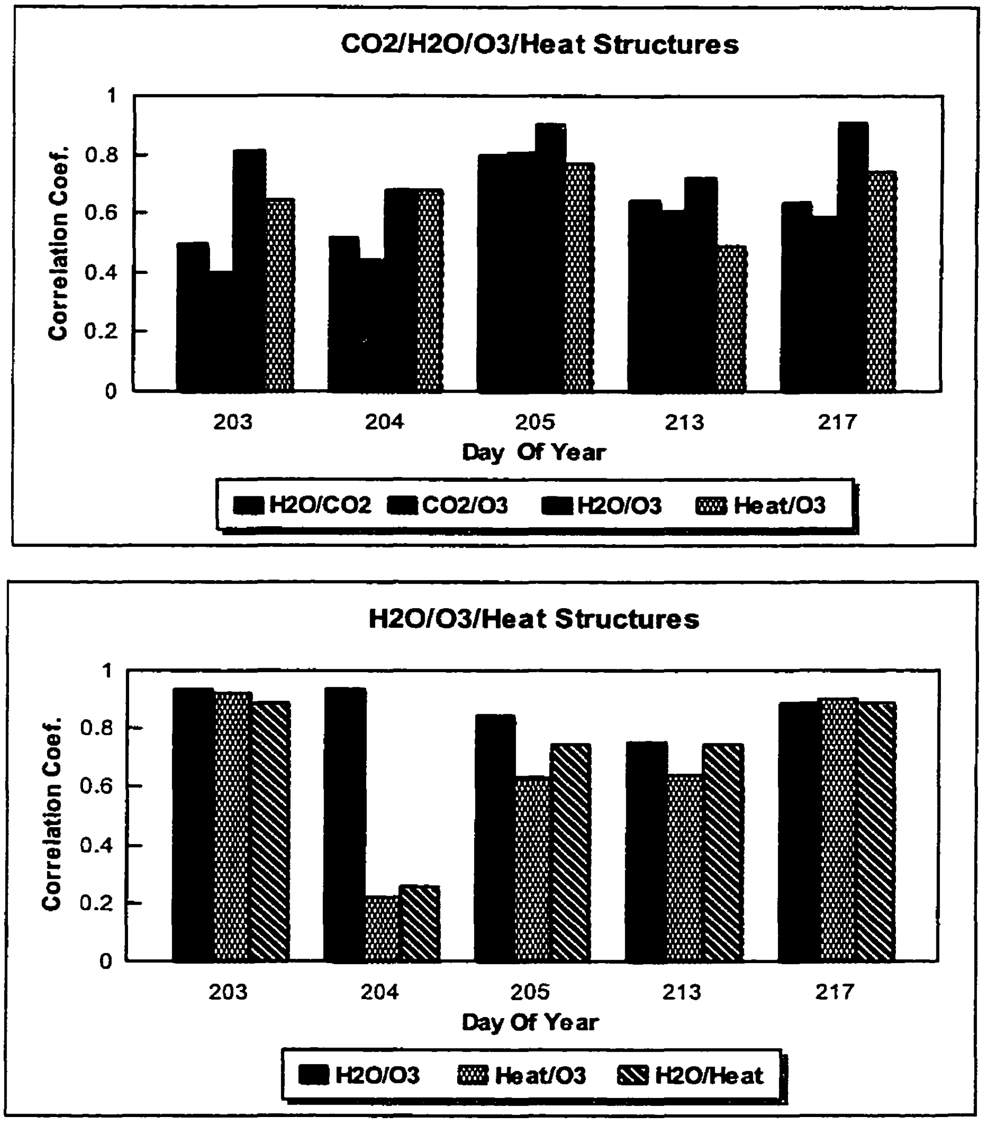

Figure 4.3. Correlation analysis within the dominant gradient up structures for the cotton site during unstable conditions. All sample days shown

correlation between H_2O and ozone, at 0.725. The mean structure flux intensities for the components of the CHOT structures may also be seen in Figure 4.4, with approximate maximum values of -6.5 mg m^{-2} s^{-1} for CO_2, -4.5 ppb m s^{-1} for ozone (where the negative sign indicates the surface as a sink), 2750 W m^{-2} for water vapour, and 750 W m^{-2} for heat. For structures transporting H_2O, O_3 and heat

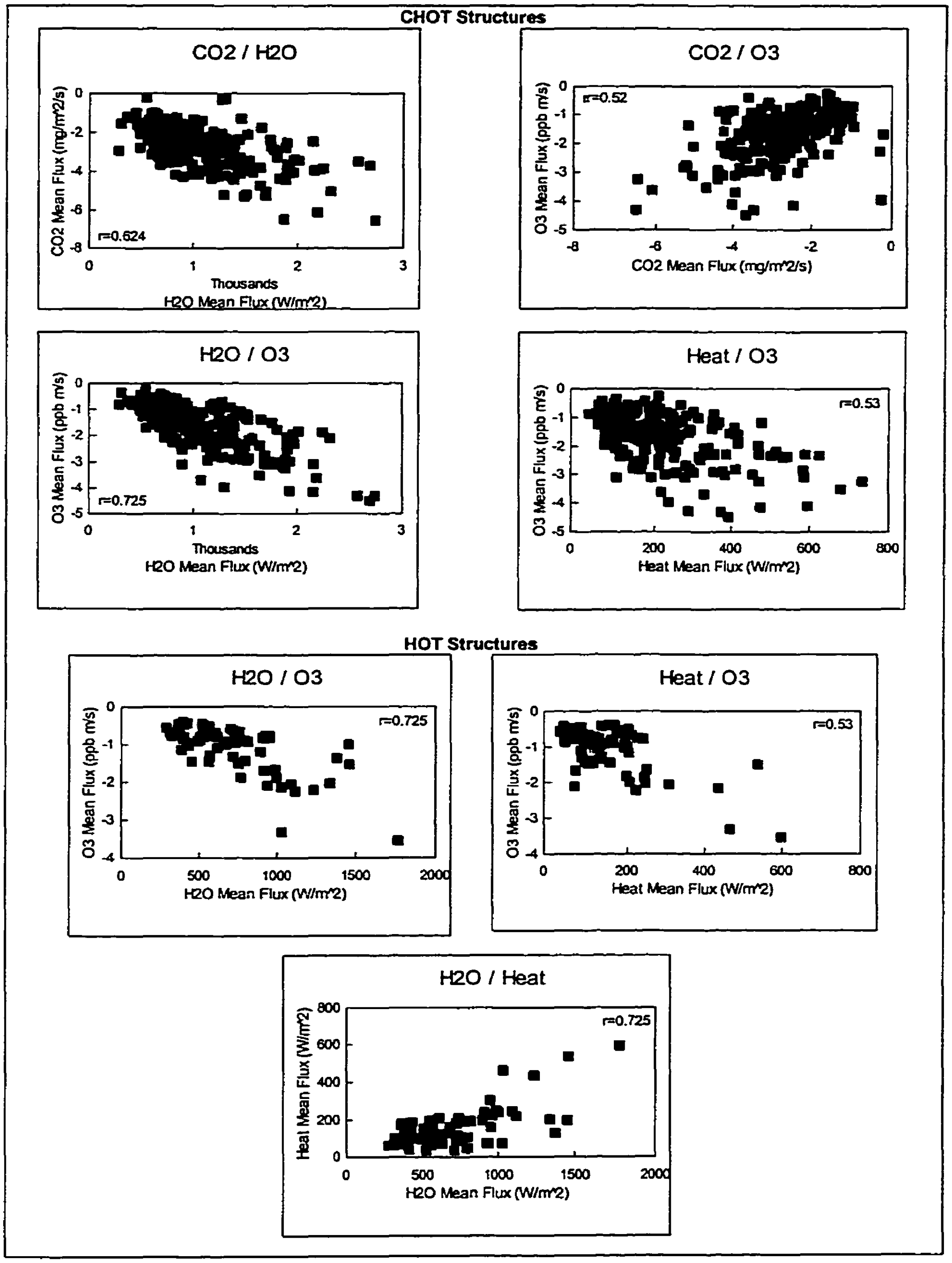

Fig. 4.4. Scatter diagram of the correlation analysis for the dominant structures over cotton during unstable conditions. Results from the five sample days are combined

exclusively (**HOT** structures), the relationship between H_2O and ozone is even more pronounced with a correlation coefficient greater that 0.8 in all cases. The correlation between ozone and heat is more variable, but in all cases less than that of H_2O and ozone. The relationship for the individual DOY is also reflected in the correlation coefficient for the combined cases shown in Figure 4.4, where the highest correlation is between H_2O and ozone at 0.7. In general, the correlation for all three fluxes is greater than 0.5. The above results suggest that under the well mixed daytime conditions over the cotton site, moisture and heat flux exert control over ozone flux with H_2O flux dominating in all cases.

4.4.1.2 *Driving Forces*

The presence/absence of heat and H_2O in the structure composition is directly related to the buoyancy flux which incorporates terms corresponding to both the heat flux and the water vapour flux. The buoyancy flux ($w'\theta'_v$), i.e. the virtual temperature flux associated with the moisture content of the air, was not explicitly calculated, but in the absence of liquid water in the air it can be approximated by

$$\overline{w'\theta'_v} \cong (\overline{w'\theta'})[1+0.61\overline{r}]+0.61\overline{\theta}(\overline{w'r'}) \qquad (11)$$

where r is the water vapour mixing ratio (Stull, 1988). When $w'\theta'$ is negligible, the water vapour-related density effects dominate in buoyancy but even in the presence of significant heat flux the latter contribute to buoyancy, as shown by the ratios of

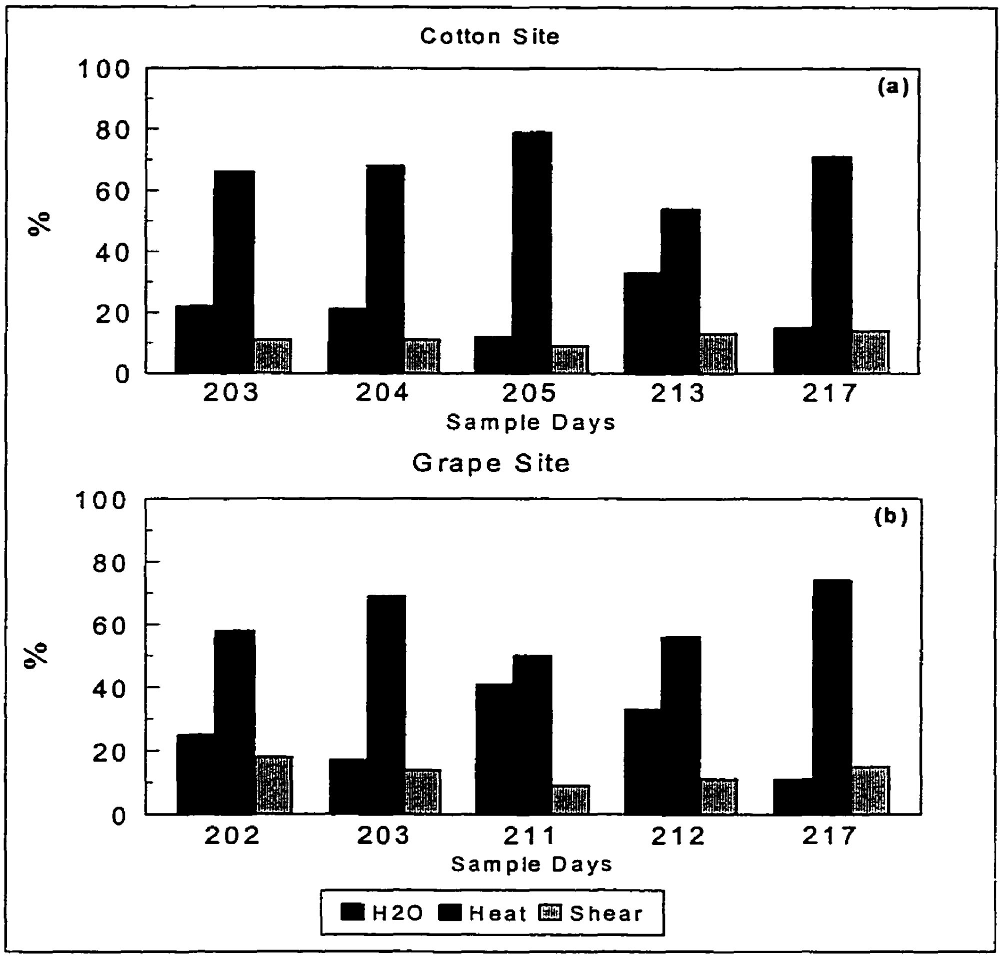

Fig. 4.5. Partitioning of the driving forces over cotton (a) and grape (b) sites during unstable conditions.

virtual density flux to sensible heat flux which ranged from 1.1 to 1.4, representing considerable enhancement of total buoyancy over that associated with sensible heat flux only (1.0). In our analysis we differentiate between structures that have sensible heat and virtual temperature buoyancy effects from those that do not contain sensible heat flux, with a further category defined by the absence of buoyancy, presumably associated with shear forces. This partitioning of the driving forces operating at the cotton site during daytime conditions is shown in Figure

4.5(a). Heat is the dominant driving force in so far as 50% to 79% of the structures have coherent heat flux in their composition.

4.4.1.3 *Structure sizes*

Structure size refers to the one dimensional horizontal extent (diameter) of the structure as intercepted by the tower and defined in section 4.3. During stable nighttime conditions the majority of the structures are less than 10 m in diameter. During the day, the CHOT structure sizes range from 3 m to 40 m, with a mean of 10.1 m. The sizes for HOT structures range from 2 m to 32 m, with a mean size of 6.1 m. Using equations 4 to 8 in section 3, with a λ range of 0.1 to 0.22 (from Figure 4.5(a)), and the values for z and z/L from sections 2.1, ℓ_M ranges from 2.8 m to 4.8 m and ℓ_H between 4.4 m and 11.8 m. The mean mixing length (ℓ) then ranges from 4.2 m to 10.2 m. The mean CHOT structure sizes, correspond closely to ℓ_H, and fall within the range of the expected mean mixing length (ℓ).

4.4.2 Grape Site Results

4.4.2.1 *Flux Associations*

The results from the FA analysis on the grape data are shown in Figure 4.6. The distribution of FA during **nighttime stable conditions** is very different from that of cotton. Here single component fluxes do not dominate, and ozone transport appears predominantly in the presence of CO_2 in CHOT structures. The distinctly low occurrence of HOT structures in Figure 4.6 suggests that a non-vegetated sink for ozone is not present. The consistently dominant structure compositions are

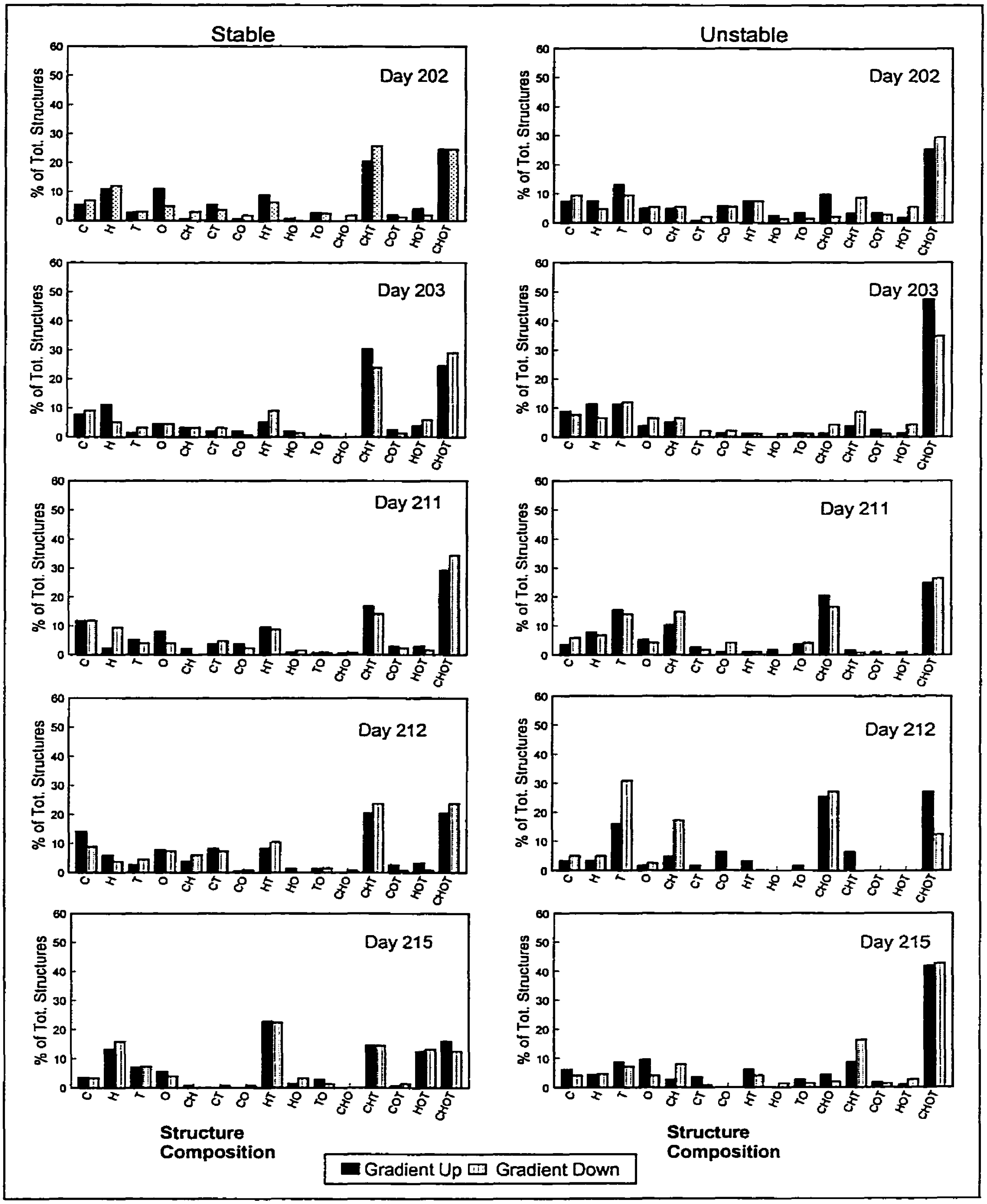

Fig. 4.6. Flux association at the grape site for both stable and unstable conditions

CHOT with FA ranging from 16% to 29% and CHT with FA between 14% and 30%. This may reflect the much greater level of mixing during nighttime stable conditions over grape, linked to the greater measurement height (almost twice that of cotton), and possibly differences in the level of nocturnal metabolic activities such as respiration levels. The FA during the **daytime unstable conditions** is similar to that of cotton with the majority of structures transporting CO_2, H_2O, ozone and heat (CHOT) simultaneously, and FA between 25% and 48%. Structures with fluxes of CO_2, H_2O and ozone (CHO) are also prominent during two sample periods, with FA of 21% and 25%.

The indication of a single dominant ozone sink for grape, that is, the one associated with vegetation, represents a significant difference between the FA for grape and cotton. The non-vegetated ozone sink at the cotton site may be the result of deposition to the soil and photochemical reactions with NO, as suggested by Massman et al., (1995) from examining ozone flux divergence between tower and aircraft flux.

The correlations of flux intensities within the dominant CHOT structures for unstable daytime conditions (Figure 4.7) are similar to those for cotton. There is a consistently high correlation between CO_2 and ozone (0.57 to 0.97), H_2O and ozone (0.64 to 0.96), and CO_2 and H_2O (0.67 to 0.96). The CO_2-ozone relationship, however, does not indicate a dependence on the correlation between the flux intensities of CO_2 and H_2O as appear to be the case over the cotton canopy. This difference may be due to the presence of the single ozone sink for the grape site. The flux intensity correlation for the combined CHOT structures for all five days are

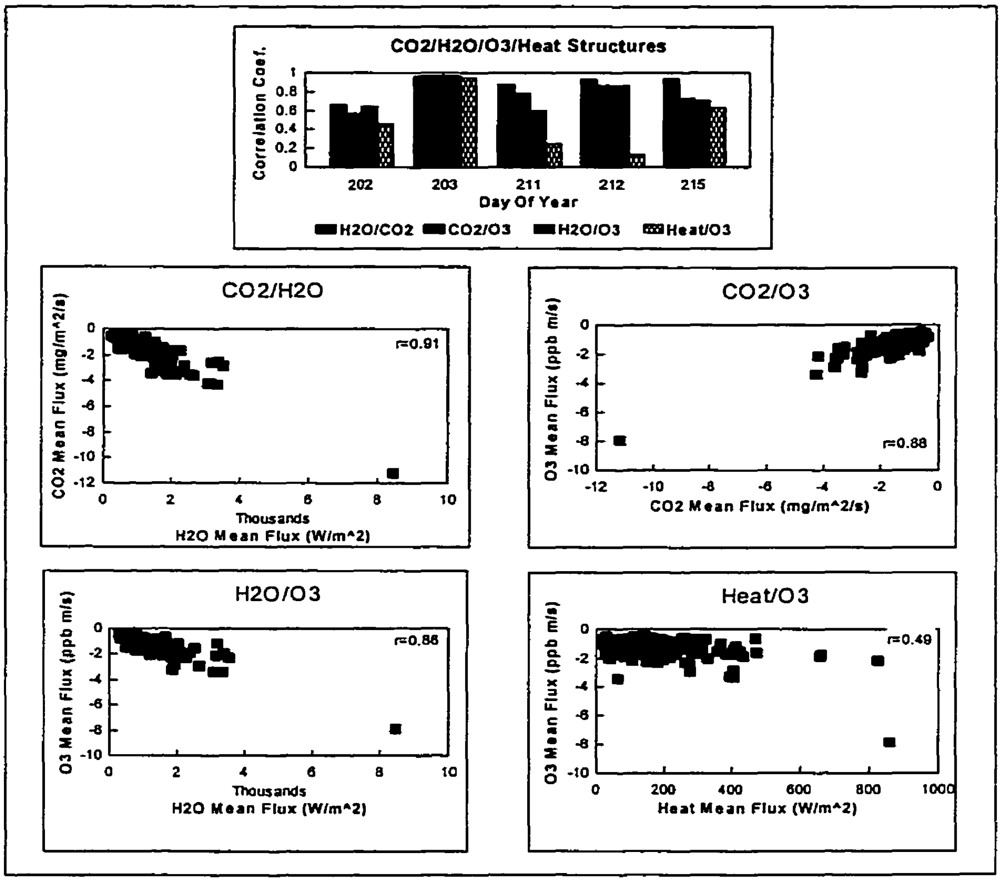

Fig. 4.7. Correlation analysis within the dominant gradient up structures for the grape site during unstable conditions.

all very high with CO_2 and ozone at 0.88, H_2O and ozone at 0.86 and CO_2 and H_2O at 0.91. The correlation between heat and ozone, by contrast, is much lower at 0.49.

The scatter plot in Figure 4.7 shows a positive relationship among all four fluxes within the CHOT structures. The mean flux intensities for the components of the CHOT structures (also shown in Figure 4.7) indicate approximate maximum values (excluding a few outlier) of -4.5 mg m^{-2} s^{-1} for CO_2, -3.5 ppb m s^{-1} for ozone, 3750 W m^{-2} for water vapour and 450 W m^{-2} for heat flux. Comparing the mean structure flux between grape and cotton, CHOT structures for cotton have a higher CO_2 flux, as may be expected given the actively growing stage of the cotton crop, as well as higher ozone and heat flux and lower H_2O flux. However, it should be considered that the partitioning of the energy fluxes at both sites depends on the dynamics of the rotating irrigation scheme. The findings on ozone flux correlate well with those of Massman et al. (1994, 1995), who found ozone flux to be higher at the cotton site than at the grape site. As suggested by Guo et al. (1995), the higher degree of wetness indicated by the higher H_2O flux and lower heat flux at the grape site would reduce the production of NO, accounting for the lower ozone flux as well as the absence of a dominant non-vegetated ozone sink.

4.4.2.2 *Driving Forces*

The breakdown of the driving forces during unstable conditions, shown in Figure 4.5(b), indicates that although heat remains a principal driving force for the surface fluxes (>50%), water vapour density gradients plays a more prominent role than was observed over cotton. This results in somewhat higher ratios of buoyancy flux to sensible heat flux (ranging up to 1.7 instead of 1.4), especially for days with significantly lower heat flux around the time of irrigation (211 and 212).

4.4.2.3 *Structure sizes*

The sizes for the dominant daytime CHOT structures are larger than those over cotton, ranging from 3 m to 69 m with a mean of 15.7 m. Using equations 4 to 8 in section 4.3, with a λ range of 0.1 to 0.15 (Figure 4.5(b)), and the values for z and z/L from sections 4.2.2, ℓ_M ranges from 5.3 m to 9.9 m and ℓ_H between 8.4 m and 26.9 m. The mean mixing length (ℓ) then ranges from 8.1 m to 24.3 m with the mean CHOT structure size falling comfortable within this range. The structure sizes for grape fall between those from the cotton site and those reported by Mitic et al. (1997) for aircraft data at 30 m over a partly irrigated grid area with cotton as the dominant crop. This indicates the increased mixing and subsequent coalescing of structures with increasing height (Caramori et. al., 1994) and verifies to some degree, the empirical definition of the physical extent of the coherent structures.

4.5 CONCLUSION

The association between fluxes of ozone and those of CO_2 and H_2O, within the turbulent structures that dominate exchange processes between cotton and grape canopies and the atmosphere under daytime conditions, is not affected by variations in the heat flux. Under unstable conditions, structures simultaneously transporting CO_2, H_2O, ozone and heat (CHOT) dominate for both the grape and cotton canopy. During stable conditions, the flux association differs between cotton and grape, with the cotton canopy having more dominant single component structures. The results for the stable conditions, however, must be interpreted with caution in light of the very small magnitude of the fluxes and the difficulties associated with sampling under nighttime stable conditions.

The separation of ozone deposition into vegetative and non-vegetative sinks may be inferred from the proportion of structures transporting ozone in the presence and absence of CO_2. For the cotton site, a vegetated ozone sink associated with CHOT structures and a non-vegetated sink associated with HOT structures were observed. The grape site indicated only a vegetated sink for ozone associated with the dominant CHOT structures. These results not only illustrate differences in the types of sinks for different vegetation types, but should help to quantify the link between ozone uptake by crops and their physical and physiological status. They may be compared with those of Mitic et al., (1997) for CODE aircraft data, where the dominant flux association was between CO_2, H_2O and ozone, without significant difference between the correlation of CO_2 and Ozone, and H_2O and ozone. The aircraft data, however, were obtained at a height of 30 m above a 15 x 15 km grid with varying crop and surface conditions, i.e. at a height where considerable coalescence of structures has already occurred.

The structure sizes indicate that on average the dominant structures at the grape site are larger than those at the cotton site but considerably smaller than those reported by Mitic et al., (1997) for aircraft data from CODE. These structures sizes fall within range of the expected mean surface layer eddy scales and may be helpful as an empirical verification of eddy scale limitations within simulation models.

CONNECTING STATEMENT BETWEEN CHAPTERS 4 AND 5

The results from Chapters 3 and 4 were not entirely surprising; the meterological and surface conditions were such that the results conform to general expectations. Modelling the links between the surface and the atmosphere for the CODE ecosystem would, as a consequence, be a straightforward quasi-linear relationship. Chapter 5 presents a similar study but for a far more complex boreal ecosystem.

This chapter is also self contained, and is being prepared as a manuscript for submission.

CHAPTER 5.

SURFACE ATMOSPHERE INTERACTIONS IN THE BOREAL FOREST

5.1 INTRODUCTION

Over the past several decades much research in the environmental sciences has focused on global climate change (D'Arrigo et al., 1987; Mooney et al., 1991; Field et al., 1992; Harris and Frolking, 1992; Viau and Mitic, 1992; Melillo et al., 1993; Chapman and Thurlow, 1996). Global change research uses large scale atmospheric models for climate and/or weather forecasting, and has to incorporate some form of parameterization of the surface characteristics (Koster and Suarez, 1992) for the estimation of the surface fluxes. This is especially significant and sensitive in cases where the surface heterogeneity is such that it creates a patchwork of sources and sinks for heat and scalar quantities. A large percentage of the errors in the surface parameters of these model is due to the misrepresentation of important biophysical processes (Sellers et al., 1997). The need to develop ways to empirically validate the lower boundary conditions of these models has led to the widespread use of remotely sensed data. Flux observations by low flying aircraft, used in conjunction with satellite observation, promise to provide a more accurate spatial picture of the surface-atmosphere exchange dynamics.

Remotely sensed surface observations from satellites have been recognised as a useful way to characterize surface characteristics. Their advantages over other data sources for regional studies include their frequent repeat cycles, large area samples, wide spectral range, and suitability for automated classification. They also provide a spatially explicit way of monitoring short term variations in vegetation, and can be used in relatively simple modelling frameworks. Apart from the classification of surface cover, and in particular the classification of deciduous and boreal forest from Landsat Thematic Mapper (TM) and SPOT satellites (Nelson et al., 1984; Buchheim et al., 1985; Shen et al., 1985; Horler and Ahern, 1986; Vogelmann and Rock, 1986; Hopkins et al., 1988; Moore and Bauer, 1990; Bolstad and Lillesand, 1992; Beaubien, 1994), satellite images have proven their usefulness in the derivation of a variety of indices related to the ecophysiological characteristics of the surface, and in particular those of vegetation. Such variable descriptors include the Normalised Difference Vegetation Index (NDVI) (Hanan et al., 1995; Wollenweber, 1995; Hall et al., 1995), Photosynthetically Active Radiation (PAR), Net Primary Productivity (NPP) and Leaf Area Index (LAI) (Lee et al., 1996; Hanan et al., 1995; Goetz and Prince, 1996). These descriptors have been applied extensively to forest ecosystems.

This study uses data collected by the Canadian Twin Otter aircraft, and some meteorological towers and satellite systems during the Boreal Ecosystem-Atmosphere Study (BOREAS) intensive field campaigns of 1994 and 1996. BOREAS was a large scale multi-disciplinary international investigation in the Canadian boreal forest, designed to improve our understanding of the exchange processes between the boreal forest and the lower atmosphere. Similar to such studies as the First International Satellite Land Surface Climatology Project Field

Experiment (FIFE) (Hall and Sellers, 1995), Hydrological Atmospheric Pilot Experiment (HAPEX) Goutorbe et al., 1994) and California Ozone Deposition Experiment (CODE) (Pederson et al., 1995), BOREAS had a nested multiscale measurement strategy, designed to capture and integrate observations from the process scale at $1 m^2$ - $(100\ m)^2$ to the regional scale at $(1000\ km)^2$ (Figure 5.1).

The objective of this paper is to examine the spatial scales and characteristics of fluxes of CO_2, H_2O, and heat and their corresponding coherent structures for two sites in the Canadian boreal forest. Satellite and aircraft data are used to develop a spatial model to predict the distribution patterns and relative intensities of sources and sinks of heat, water vapour and CO_2 based on the spatial mix of the surface characteristics.

5.2 DATA COLLECTION AND SITE DESCRIPTION

The BOREAS site is located in the Canadian boreal forest of northern Saskatchewan and Manitoba. It is dominated by black spruce, jack pine, aspen, birch, larch, in various stages of regeneration, along with numerous lakes, bogs and fens. The climate is characterized by strong seasonal variations with short, moderately warm and moist summers and long, extremely dry and cold winters. The BOREAS site extends 1000 km x 1000 km from the southern edge to the northern regions of the boreal forest. Within this region there are two localized sites. The Southern Study Site (SSA) is located at the southern edge of the boreal zone, in the

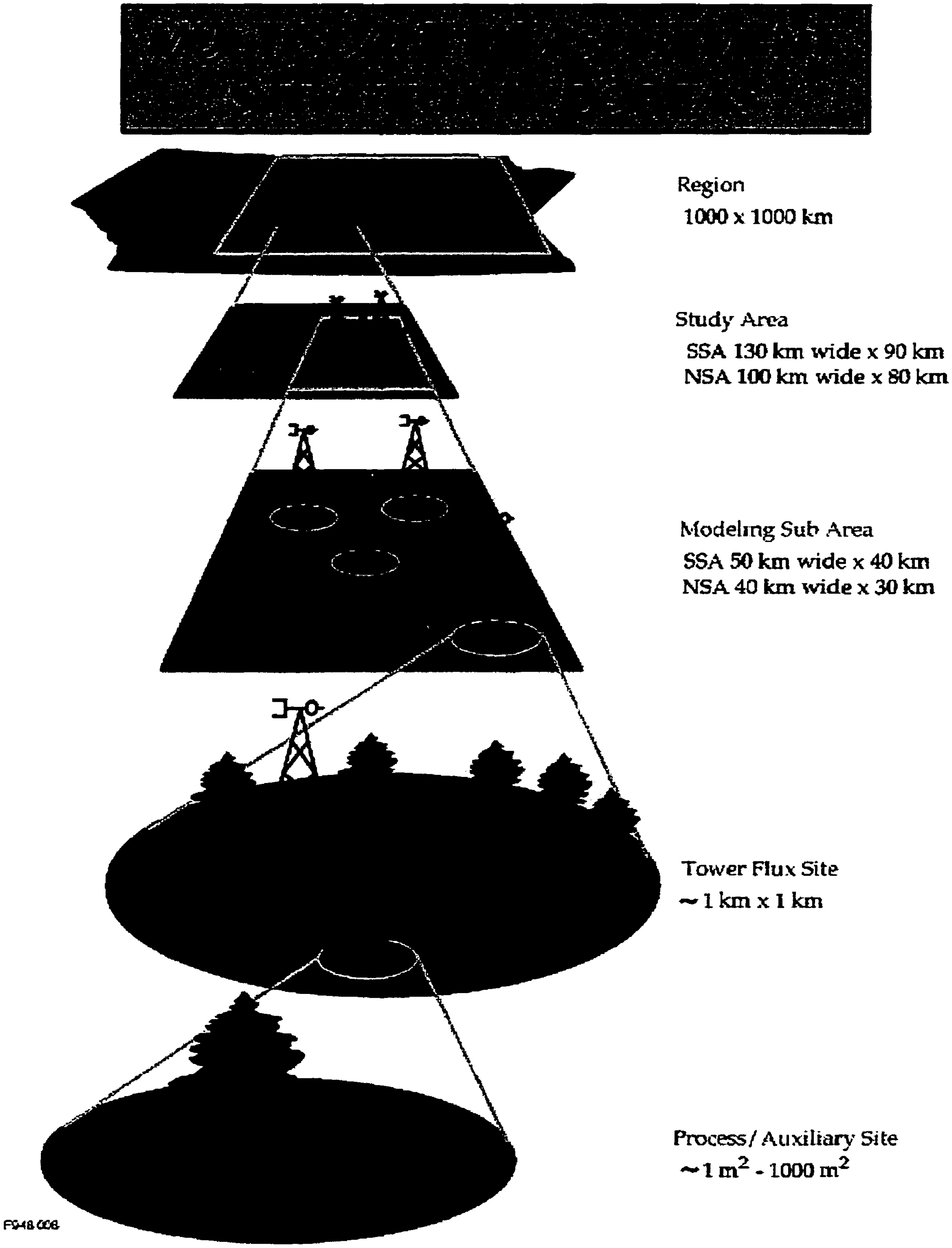

Figure 5.1. Multiscale measurement strategy. Source BOREAS Information System.

vicinity of Prince Albert, Saskatchewan. It covers 11,170 km^2 and is expected to be water limiting during the growing season. The Northern Study Area (NSA) is located 500km northeast of the SSA and 40 km west of Thompson, Manitoba, with a size of 8000 km^2. It is near the northern limit of the boreal forest where the ecosystem is expected to be temperature limiting during the summer. Figure 5.2 shows the location of these sites.

The NSA is flat with gentle rolling hills. This relief, along with the predominantly clay soil, results in poor drainage with abundant wetlands. The area contains a few lakes, mainly black spruce with scattered birch and stands of jack pine in the drier areas. The SSA is gentle in relief with soils ranging from gray wooded to degraded black. The vegetation consist of a mixed-wood zone and an aspen grove section. Feather mosses dominate the forest floor in the conifer dominated stands. The deciduous and mixed deciduous stands have an extensive low shrub/herb understory.

The Canadian Twin Otter aircraft team established one grid site for more intensive observation within both the SSA and the NSA. Each grid site is 16 km x 16 km.

The Twin Otter aircraft made grid flight observations during the three BOREAS Intensive Field Campaigns (IFC) in 1994 (May 24 - Sept. 19) and one in 1996 (July8 - Aug.8), at both the southern and northern sites. Each grid flight consisted of nine parallel lines, separated by 2 km, flown twice in opposite direction in a time-centred mode such that each line was sampled at the same average time (Ogunjemiyo et al., 1997). A total of 32 grids were flown. Among other parameters, eddy correlation

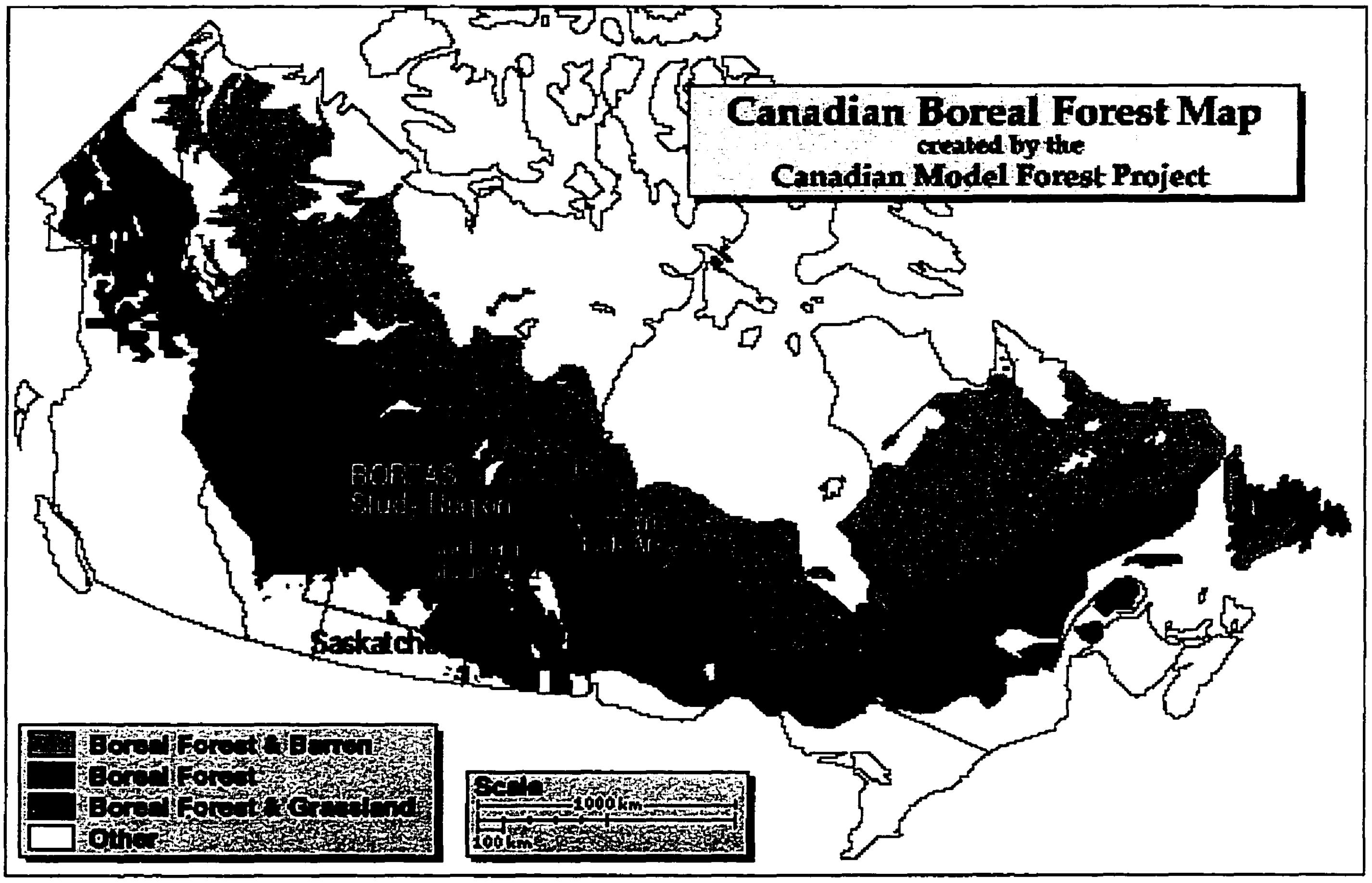

Figure 5.2. Location of the BOREAS study site,the Northern Study Area (NSA) and the Southern Study Area (SSA).

data on water vapour, air temperature, CO_2, the three components of wind, as well as radiometric surface temperature and a simple ratio vegetation index were collected at a frequency of 16 Hz, 30 - 45 m (100 - 150 feet) above the surface. All data were geographically referenced to latitude and longitude coordinates.

Six grid flights were selected for study from three different IFCs, selected for optimum radiation conditions. Two grid flights each from IFC 1 and IFC4 were analysed for the northern site, and two grid flights from IFC 2 for the southern site. Grid 13 flown on June 7, 1994 in an E-W direction and grid 15 flown on June 8, 1994 in a N-S direction represent IFC1. Grid 26 flown on July 24, 1994 in an E-W direction and grid 30 flown on July 26, 1994 in a N-S direction represent IFC 2. Grid 76 flown on July31, 1996 in an E-W direction and grid 79 flown on August in a N-S direction represent IFC4.

5.2.1 Northern Grid Site

The northern grid is located in the west-central section of the NSA at 55.80° - 55.94° N and 98.39° - 98.65° W. Figure 5.3 shows the surface Landsat TM surface classification (provided by the BOREAS Terrestrial Ecology 18 team). This site has a distinct north south characteristics. The northern section consists of fen (14%), characterized by areas with a water table very near the surface, deciduous species (18%) primarily aspen/birch, and wet conifers (4%), primarily black spruce and jack pine, with understory of feather moss and sphagnum. The southern section of the site is dominated by regenerating conifers (20%) (black spruce and jack pine) and deciduous (33%) (aspen) regrowing up to 10 years after a burn. The canopy height in the northern section averages 20 m with a predominantly wet to saturated moss understory.

During IFC 1, gird 13 flight had a mean vapour pressure deficit (VPD) of 1.41 kPa, representing a relative humidity (RH) of 28%, mean air temperature of 17.3°C, average Bowen ratio (ratio of sensible to latent heat flux H/LE) of 1.9, with an evaporative fraction (LE/(H+LE)) of 0.34. Conditions were clear with southerly winds at 4 mps. Grid 15 flight had a mean VPD of 2.6 kPa, representing a RH of 17%, mean air temperature of 24.7 °C, average Bowen ratio of 1.35, and evaporative fraction of 0.42, with clear conditions and WSW winds at 5 mps.

During IFC 4, grid 76 flight had a mean VPD of 1.56 kPa, representing a RH of 47%, mean air temperature of 23.7 °C, average Bowen ratio of 0.67, an evaporative fraction of 0.60, with mostly clear skies and a south wind at 3.1 mps. Grid 79 flight had a mean VPD of 1.8 kPa, representing an RH of 40%, mean air temperature of 24.1 °C, average Bowen ratio of 0.51, evaporative fraction of 0.67, mostly clear skies with SW winds at 5.1 mps.

5.2.2 Southern Grid Site

The southern grid site is located in the east-central section of the SSA at 53.78° - 53.93° N and 104.56° - 104.80° W. Figure 5.4 shows the surface Landsat TM surface classification (provided by the BOREAS Terrestrial Ecology 18 team). This site shows variation of surface cover in a diagonal NE to SW direction. The SW section is characterised by a mixture of fen (11.5%), medium-aged regenerating conifers (14.49%) and some mixed deciduous and conifers (9.04%). The NE section

Landsat TM Classification (1995) Northern Grid

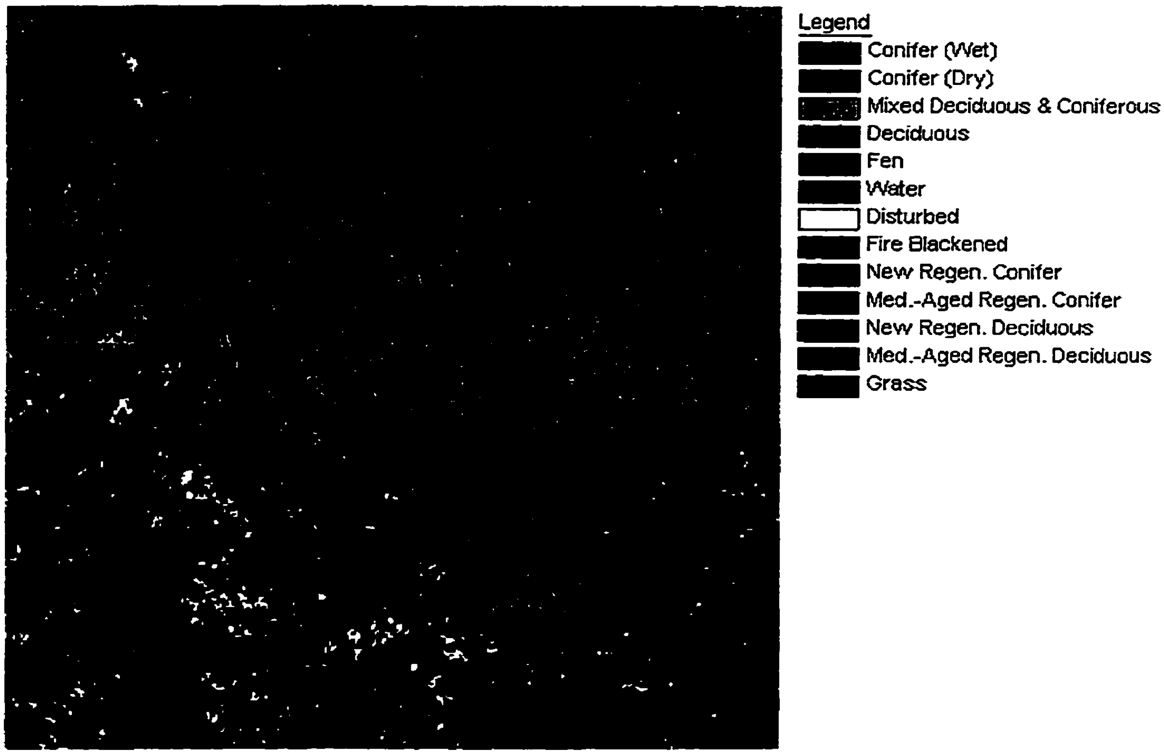

Figure 5.3 Surface Classification of the Northern Grid from June 21 1995 Landsat-5 TM image. Scenes Provided by BOREAS TE-18 group.

Landsat TM Classification (1994) Southern Grid

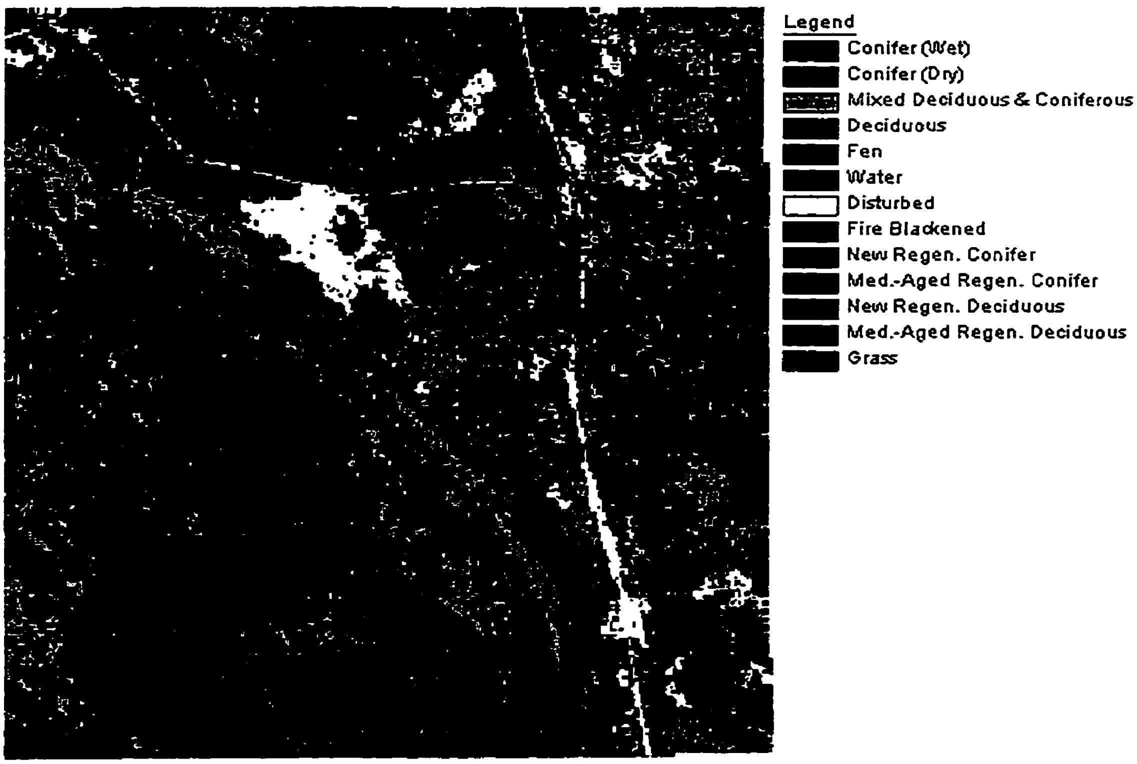

Figure 5.4 Surface Classification of the Southern Grid from September 02, 1994 Landsat-5 TM image. Scenes Provided by BOREAS TE-18 group.

has patches of conifers on dry soil (8.85%), and conifers on wet soil (38.38%) as well as some new regenerating conifers (4.09%), new regenerating deciduous (3.62%) and disturbed, recently cleared patches (4.29%). There is also a large SE - NW strip of wet conifers across the middle of the site.

During IFC 2, grid flight 26 had a mean VPD of 1.5 kPa, representing a RH of 31%, mean air temperature of 19.9 °C, average Bowen ratio of 0.89, an evaporative fraction of 0.52, with clear skies and a north wind at 5 mps. Grid flight 30 had a mean VPD of 1.7 kPa, representing an RH of 39%, mean air temperature of 22.9 °C, average Bowen ratio of 0.78, evaporative fraction of 0.56, with mostly clear skies with light SW to NW winds.

5.3 DATA ANALYSIS

The analytical procedures used to define the flux estimates, identify the coherent structures and examine the relationships of flux associations, are similar to those used by Mitic et al. (1997 & 1999) in Chapters 3 and 4. The area averaged flux F_A is estimated by the eddy correlation technique, as the covariance between the deviations of the vertical wind (w') and scalar admixtures (c') from their means at a height h, as a factor of time t, integrated over interval A as

$$\begin{aligned} F_A &= \frac{1}{A}\int_A w(x,y,h,t)\, c(x,y,h,t)\, dxdy \\ &= \langle w\rangle\langle c\rangle + \langle c^* w^*\rangle + \langle c' w'\rangle \end{aligned} \tag{12}$$

This is similar to Equation (1) where F_A is separated into the domain average <w><c>, the running mean <c*w*> and the instantaneous flux <c'w'> as described in Chapter 3 section 3.3.1.

A combination of linear (simple regression) and non linear (truncated Fourier series) detrending techniques, is used to separate the *local* instantaneous fluxes relating directly to the underlying surface from the larger scale low frequency oscillations (termed *mesoscale flux*). Selection of a particular detrending technique is according to the criteria used in Mitic et al. (1997), given in Chapter 3.

Quadrant analysis is used to identify the modes of transport (excess up/down and deficit up/down), and coherent structures are identified as a series of 8 or more consecutive pairs of w'c' excursions (equivalent to a spatial dimension of ≥ 30 m) within the same quadrant, where the one-dimensional structure size *ss* (in time units) is given by

$$ss=N^{i}*\frac{\overline{U}}{f} \tag{13}$$

N^i is the number of consecutive flux events in quadrant i, $\bar{U}$ is the mean horizontal wind and f is the sampling frequency. Only the gradient modes of flux towards the surface (gradient down) and away from the surface (gradient up) are used in this study. During daytime conditions this represents an excess of moisture and heat and a deficit of CO_2 transported away from the surface, and a deficit of heat and moisture and an excess of CO_2 transported towards the surface. The degree of association between the fluxes is determined by coincidence analysis, which basically redefines the composition and locations of structures which overlap in their physical extent. It is then defined as a ratio of the number of coherent structures with a particular composition to the total number of structures identified across the grid. This *flux association* is given by

$$FA=\frac{C_{i,j,k}}{N-mp} \tag{14}$$

$C_{i,j,k}$ is the number of coherent structures with the exclusive composition of scalars i, j, k (heat, H_2O, CO_2) or any combination of these, N is the total number of structures (before reconstruction) for the overall time series, mp ("multiple pockets") is the reduction in the number of structures as a result of overlap, so that N-mp is the total number of reconstructed structures. A more elaborate definition of the coincidence analytical procedure may be found in Mitic et al. (1999), given in Chapter 4.

In order to investigate the degree to which the spatial distribution of surface fluxes may be predicted from the surface characteristics, simple and multiple correlation/regression analyses are performed. The simple correlation/regression takes the form of Pearson linear regression, and looks at pairs of fluxes, as well as fluxes and surface parameters (greenness, radiative surface temperature). The step-wise multiple regression uses greenness index and the fractional influence of the surface type (eg. conifer), adjusted by surface temperature excess, to predict the distribution of CO_2, H_2O and heat fluxes. The footprint corrections for one of the multiple regression models is based on solutions from Kaharabata et al. (1997). This *footprint model* uses the fractional contribution of each cover type contained in the upwind area of the sampled data points (which represents the correlation grid points), according to the footprint estimates. The footprint adjusted model is done only for IFC1 grid 13. An alternate *variable scale model* does not use the footprint adjustments because its pixel size overlaps the calculated upwind footprint distance. The variable scale model is used for the combined grids 13 and 15 from IFC1, combined grids 26 and 30 from IFC2 and combined grids 76 and 79 from IFC4. These models are created for two spatial scales which represents the correlation pixel size. The land cover type independent variables are calculated over a 240 m x 240 m area (pixel) and over a 560 m x 560 m area (pixel). The land cover variables then represent the frequency of the various land cover classes within these areas.

5.4 RESULTS AND DISCUSSION

5.4.1 IFC 1 Northern Grid Site

5.4.1.1 *Flux Magnitudes*

IFC 1 is represented by grids 13 and 15 flown on June 7 and 8, 1994, respectively. The detrending and flux separation procedure resulted in the mesoscale:local flux ratios shown in Figure 5.5. For both Grid 13 and grid 15 a significant portion of the flux (> 10%) of water vapour and CO_2 is represented by the larger scale low frequency oscillations (mesoscale flux), while only a very small percentage of the heat flux (< 4%) is accounted for by the mesoscale flux. This suggests that while heat flux is primarily generated by local sources at local spatial scales, the latent and sensible heat fluxes have a wider range of spatial scales associated with significant transport, representing both local as well as more

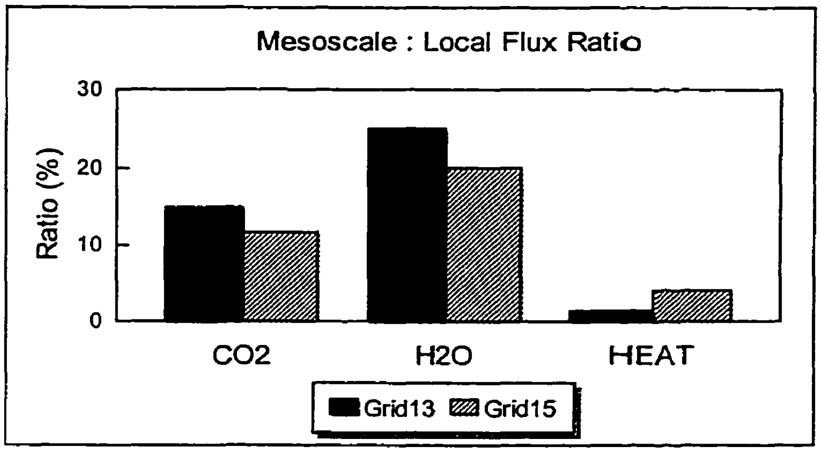

Figure 5.5. Ratio of mesoscale flux to local flux for grid 13 and grid 15 from IFC1 northern site.

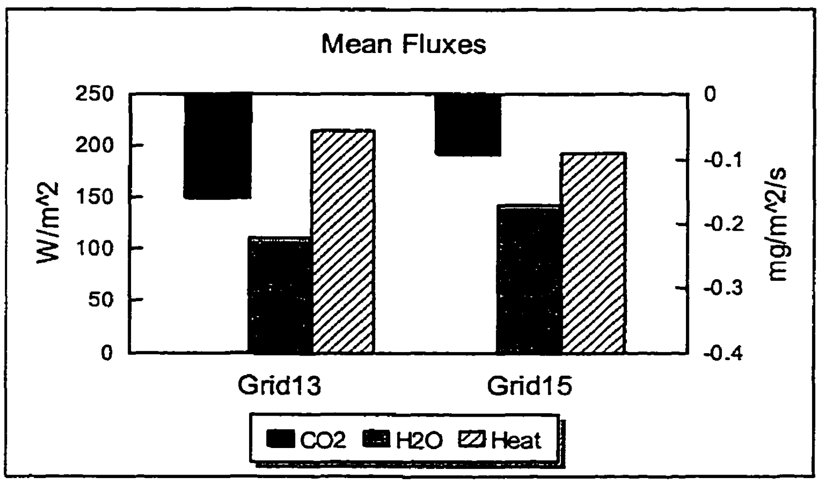

Figure 5.6. Local flux estimates for grids 13 and 15 from IFC1 northern site. Sensible and latent heat fluxes are in W m^{-2}

wide-spread sources and sinks. The mean fluxes for both grids shown in Figure 5.6 indicate the dominance of sensible heat flux in the energy balance, giving rise to a Bowen ratio for grids 13 and 15 of 1.9 and 1.35, respectively. Grid 13 has mean fluxes of -1.6 mg m^{-2} s^{-1}, 111 W m^{-2} and 213 W m^{-2} for CO_2, latent and sensible heat flux, respectively. Grid 15 has mean fluxes of -0.9 mg m^{-2} s^{-1}, 142 W m^{-2} and 192 W m^{-2} for CO_2, latent and sensible heat fluxes, respectively. The flux estimates for CO_2 are quite low, reflecting a significantly lower overall photosynthetic rate compared to levels observed over the CODE sites. The relatively low latent heat flux, compared to the sensible heat flux, over this predominantly wet surface, may be partly attributed to the fact that the air is very dry, as indicated by vapour pressure deficits above 1 kPa. This causes stress on the vegetation which, due to physiological characteristics, is not able to take up moisture from the partly frozen soil at an adequate compensating rate. This is further demonstrated in the next section.

5.4.1.2 *Fluxes and Surface Characteristics*

One kilometre averages were used to create spatial flux and surface maps with a Geographic Information System (GIS), using a potential mapping procedure with a search radius of 2 km. The E-W runs from grid 13 and the N-S runs from grid 15 were combined to yield a higher spatial resolution and a higher confidence in the resulting spatial patterns. Figure 5.7 shows the spatial distribution pattern for surface temperature excess (surface temperature minus air temperature)and greenness index (infrared : red ratio), Figure 5.8 shows the leaf area

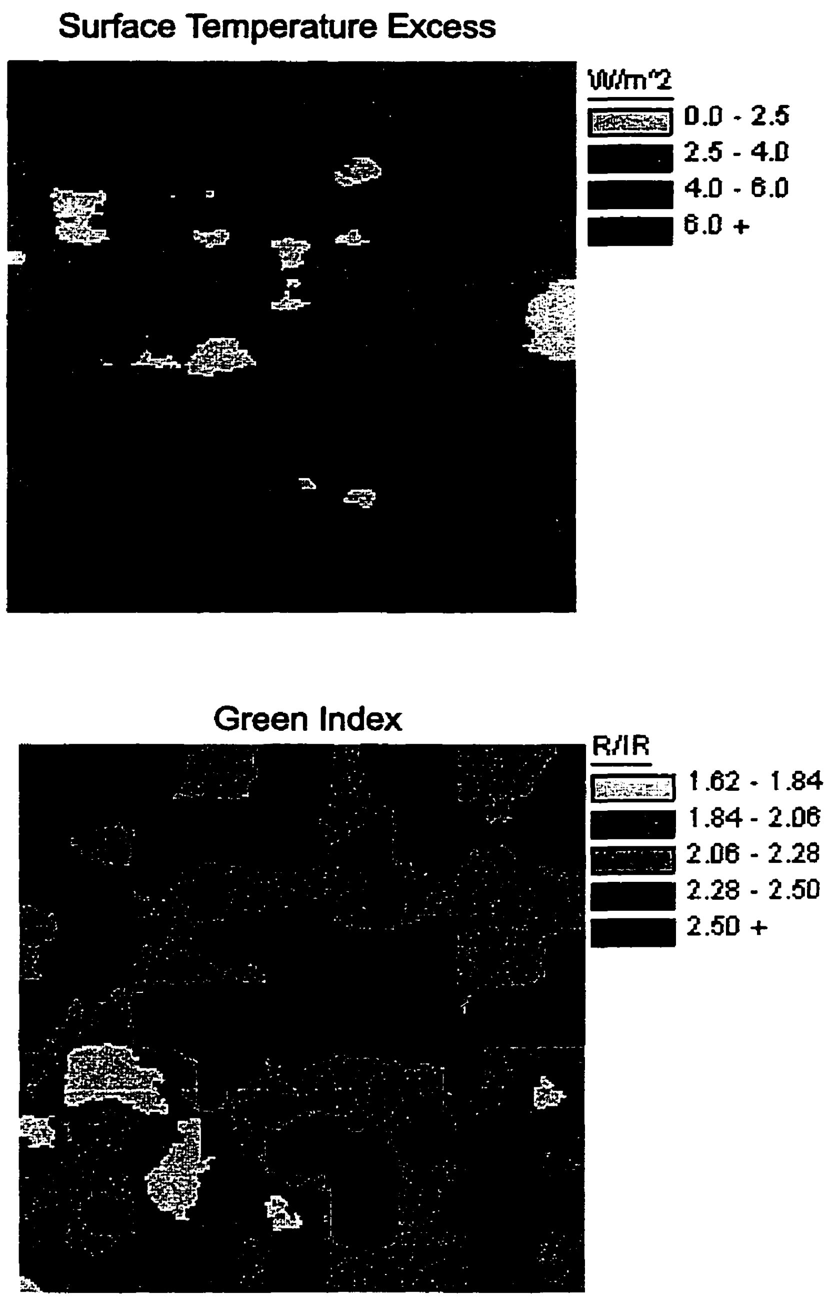

Figure 5.7 Twin Otter Surface Temperature Excess and Greenness index for the northern grid IFC1

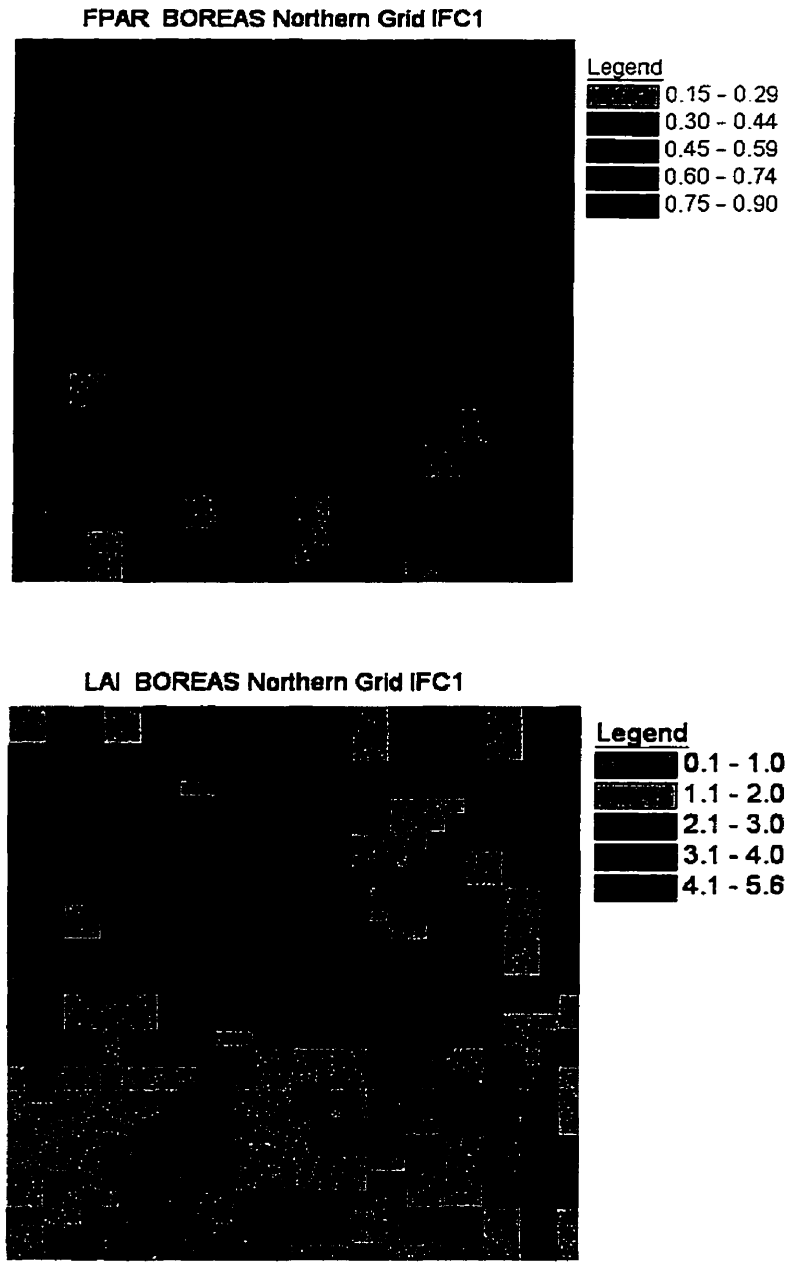

Figure 5.8. NOAA AVHRR FPAR and LAI for the northern grid from IFC1. Source: CCRS

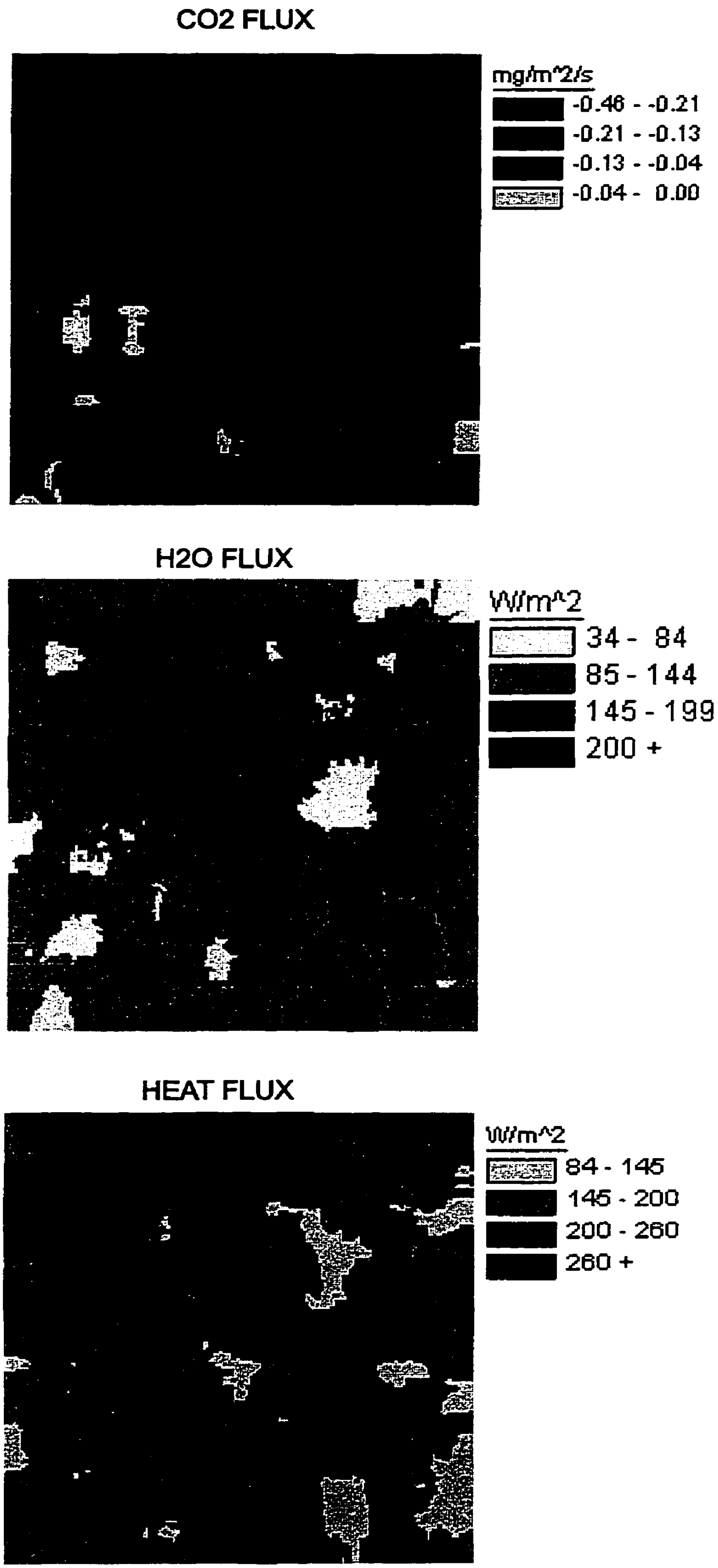

Figure 5.9. Spatial flux maps, combined grids 13 & 15, IFC1 northern site.

index (LAI) and the fraction of the photosynthetically active radiation (FPAR) and Figure 5.9 shows the spatial flux pattern for CO_2, latent and sensible heat fluxes.

The spatial patterns of the surface temperature excess and the greenness index reflect the vegetation pattern shown in Figure 5.3. High surface temperatures and low greenness are located in the southern section of the site which is an area undergoing regeneration. The lower surface temperatures and higher greenness are in the northern section of the site which is dominated by fen, deciduous and wet conifers. These patterns are similarly reflected in LAI and the FPAR. The surface characteristics are not as clearly reflected in the spatial distribution patterns of the fluxes. The CO_2 flux pattern reflects that of the greenness, LAI and FPAR. This indicates that the higher levels of photosynthesis occurs in the northern section of the site. It would, therefore, be conventionally expected that this area should exhibit a low sensible heat flux. This, however, is not the case, as seen from the map of sensible heat flux. In contrast to the distribution pattern of surface temperature excess, the higher sensible heat flux is concentrated in the northern section of the site. This means that there is a high level of decoupling between the surface and the atmosphere and that the heat flux is not generated by the surface but predominantly by the tree canopy.

As has been previously noted and described (e.g. Ogunjemiyo et al., 1997), the inconsistencies between the surface temperature, the sensible heat flux and CO_2 may be explained by the complex combination of characteristics at the surface. While the northern section has tall thin mature trees, its understory has a moss and sphagnum layer on very wet to saturated soil conditions. The downward looking IR thermometer responds to moist cooler surface between the often sparse trees, while the contrast between mature trees and understory vegetation is much less pronounced for the properties recorded by the optical sensors for greenness, LAI and FPAR. The much shorter vegetation in the southern section gives a more complete picture of both the canopy and the surface. The high VPD and the varying response of the different species to environmental conditions may also explain the decoupling of the heat flux from the surface temperature and differences in the response of photosynthetic levels. Dang et al. (1996) showed that the magnitude of vapour deficit limitation varies with tree species, with deciduous species such as aspen (dominant as new regeneration in the southern section of the site) having a much higher stomatal sensitivity than conifer species, such as black spruce found in the northern section of the site. This causes the aspen species to restrict stomatal opening and consequently CO_2 uptake under high VPD. The conifer species are able to fix CO_2 to some extent under these conditions. Species such as black spruce, growing in an environment of organic soil, moss-covered, with low thermal conductivity and lower oxygen concentration, are adapted to a more rigorous extraction of soil moisture, and can tolerate a much lower shoot water potential (Dang et al., 1996). On the other hand, the conifer needles have a lower leaf boundary layer resistance than the deciduous species.

These atmospheric, surface, and physiological conditions may explain why the canopy in the northern section of the site would heat up and generate a higher sensible heat flux but also maintain the higher levels of photosynthetic activity as indicated by the greenness and CO_2 maps, while the southern section of the site would have the higher surface temperature but lower sensible and CO_2 fluxes.

The distribution pattern of the latent heat flux is probably more indicative of surface evaporation than transpiration, and illustrates the overall wetness of the site. Oncley et al. (1997) found that the contrast between aspen dominated and conifer dominated forest is not as great in the CO_2 exchange as in the latent heat exchange, indicating that evaporation probably contributed significantly to the latent heat flux. Similarly, Baldocchi and Vogel (1996) and Moore et al. (1996) observed that evaporation from the soil surface accounted for a large percentage of the latent heat flux from the jack pine forest during BOREAS

5.4.1.3 *Coherent Structures and Sources and Sinks*

The association of fluxes within the coherent structures responsible for the bulk of flux transport, and the spatial distribution of these structures, give some indication of the distribution of the sources and sinks for the fluxes at the surface. Figures 5.10 and 5.11 gives the flux association for grids 13, 15 and the combined grids. The exclusion of a particular flux from the composition of a structure means that there was no sustained significant contribution of that flux over the duration for which the structure was observed. For both grids, four distinct, dominant structure compositions are evident, as indicated in Figure 5.11: structures simultaneously transporting CO_2, H_2O and heat (CHT), or H_2O and heat (HT), and those transporting exclusively heat or H_2O. This distribution may indicate the two distinct source/sink characteristics of the surface and the canopy. The difference in

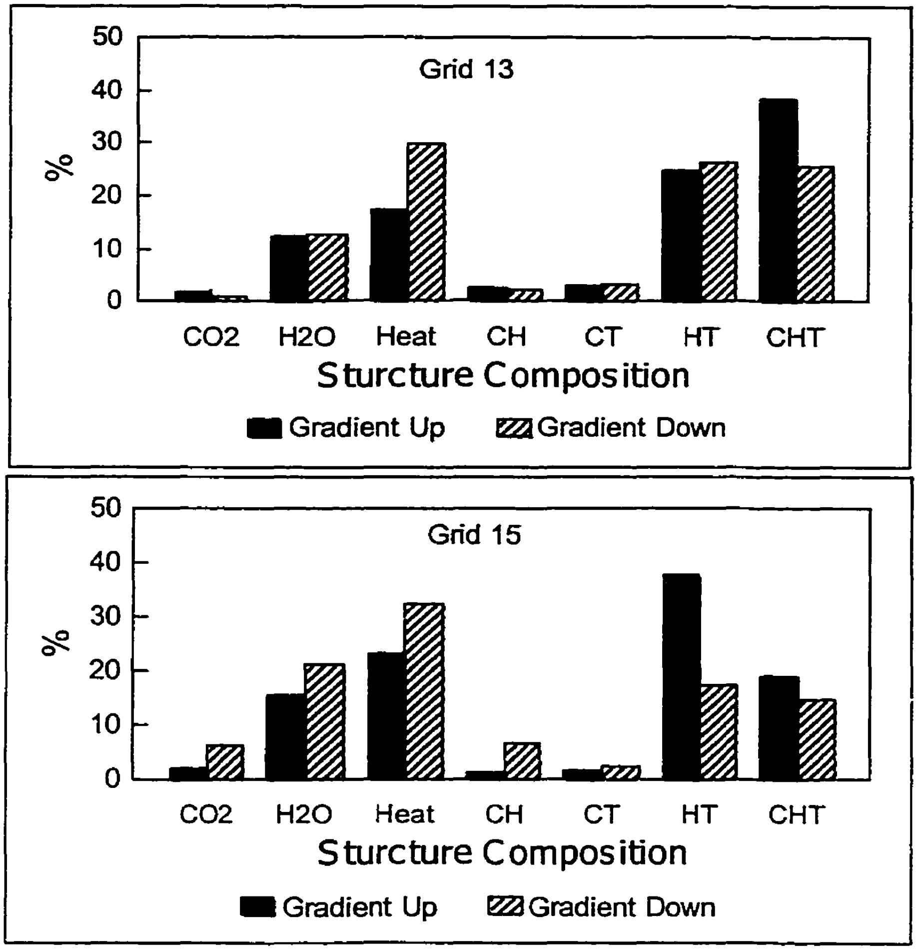

Figure 5.10. Flux associations in the gradient modes for grid 13 and grid 15 from IFC1 northern site.

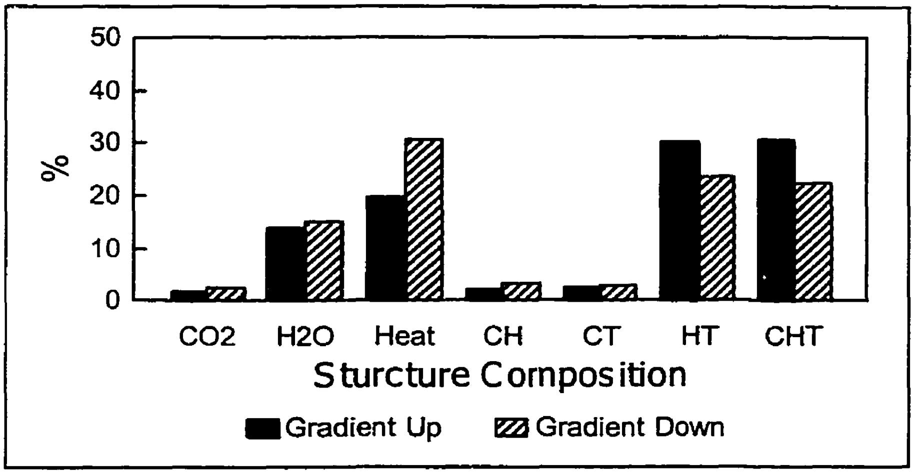

Figure 5.11. Flux association for the combined grids (13 & 15), IFC 1 northern site.

dominant structures compositions between grids 13 and 15 (Figure 5.10) may be a reflection of the difference in the VPD between the two days (1.9 kPa vs 2.6 kPa). The assumption can be made that the H_2O structures represent unmixed evaporation from the surface, the heat structures represent unmixed sensible heat plumes from the canopy, the HT structures represent a mixture of surface H_2O flux and canopy sensible heat flux, and the CHT structures represent the transpiring portion of the canopy. The difference in the structure compositions for the two grid could then be interpreted as a result of the higher VPD stress exerted on the vegetation resulting in higher stomata conservation. This would be expected to lower the CHT structures and increase the HT and heat structures.

The spatial distribution of the dominant structures across the TM classes of surface vegetation is shown in Figure 5.12. Unlike the results obtained in CODE, the distribution of the structures is relatively constant for the dominant surface types, both in the northern and southern sections. Possible reasons for the lack of distinction in the spatial distribution of the structures is similar to that of the spatial fluxes: the decoupling of the fluxes from the surface, as well as the fine scale of the surface heterogeneity, which exhibits no extended, contiguous areas within any given surface classification.

The composition of the coherent structures is used to determine the partitioning of the driving forces at the surface. As shown in Figure 5.13, the dominant driving force at the surface is heat, accounting for > 80% of the forcing. This is confirmed by the correlation of 99% between sensible heat flux and buoyancy flux.

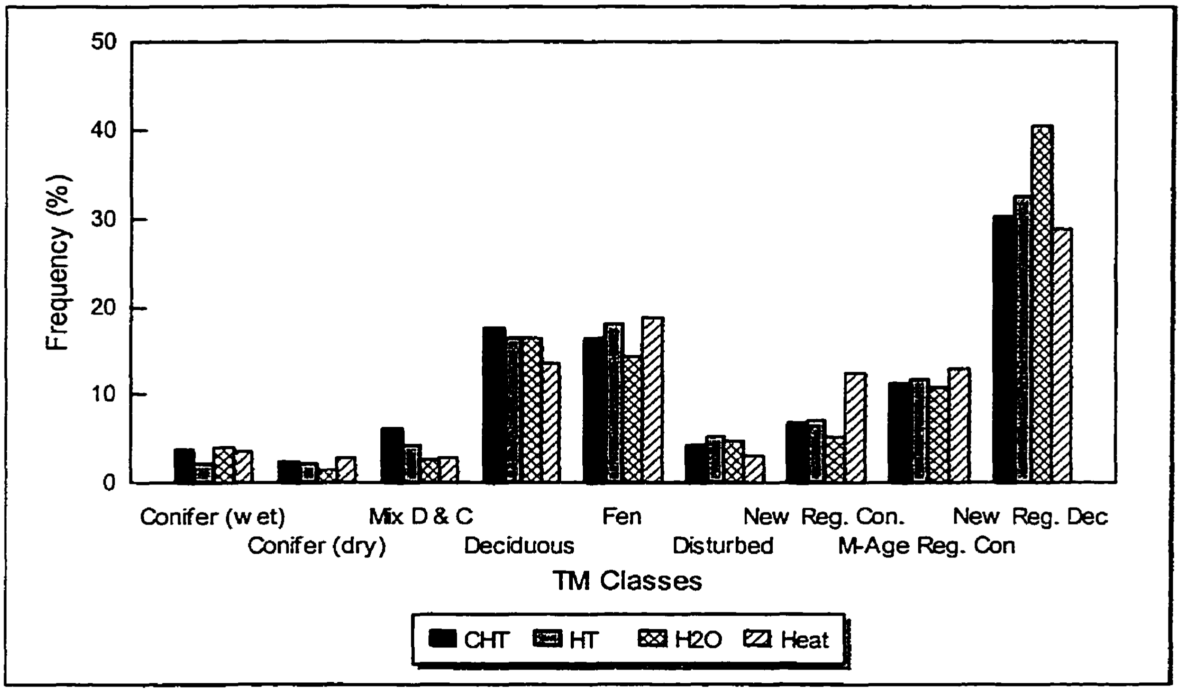

Figure 5.12. Spatial distribution of the coherent structures across the surface types. Grids 13 and 15, IFC1 northern site.

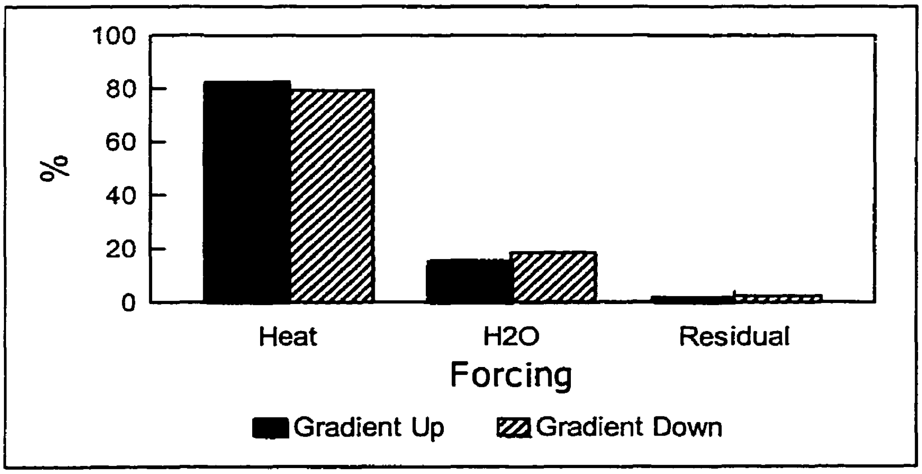

Figure 5.13. Partitioning of the driving force at the surface derived from the composition of the coherent structures. Grid 13 and 15 IFC1 northern site.

The one-dimensional cross-sections of the dominant mixed structures are much larger than those of the unmixed single component structures. The CHT and HT structures have mean sizes of 122 m and 95 m, and maxima of 555 m and 664 m, respectively. The H_2O and sensible heat structures have means of 66 m and 68 m and maxima of 304 m and 276 m, respectively.

5.4.1.4. *Correlation and Regression*

A simple correlation and regression analysis ($y = a \pm \beta x$) was done for the fluxes and surface characteristics to enhance the interpretation of the spatial flux distributions. Table 5.1 gives the correlation and regression parameters for the combined grids13 and 15. The degree to which the surface is decoupled from the fluxes is evident in the correlation parameter r. The highest correlations are among the fluxes of CO_2, H_2O, heat and buoyancy. CO_2 has a moderate positive correlation with greenness as was evident in the flux maps, and the surface characteristics all have a moderate to high correlation with each other. The almost perfect correlation between sensible heat flux and buoyancy indicates that buoyancy is almost completely driven by heat, as is evident in the driving force partitioning in Fig. 5.13.

5.4.2 IFC 4 Northern Grid Site

5.4.2.1 *Flux Magnitudes*

IFC 4 is represented by grids 76 and 79 flown on July 31 and August 02, 1996, respectively. Unlike IFC 1, the detrending procedure indicates that the bulk of the flux has a local source areas, with the exception of the CO_2 flux from grid 79

y	x	r	a	β	se
H_2O	CO_2	-0.51	71.06	-441.27	62.26
H_2O	Heat	0.45	47.895	0.3881	64.4
H_2O	STExcess	-0.08	136.84	-2.127	72.09
H_2O	Greenness	0.02	112.76	6.23	72.28
CO_2	Heat	0.55	-0.016	0	0.07
CO_2	STExcess	0.02	-0.129	0.001	0.08
CO_2	Greenness	0.35	0.104	-0.1034	0.08
Heat	STExcess	0.02	199.51	0.696	84.67
Heat	Greenness	0.17	91.05	50.25	83.5
Buoyancy	Heat	0.996	0.0039	0.001	0.007
Buoyancy	H_2O	0.52	0.115	0.001	0.06
STExcess	Greenness	0.48	14.52	-4.366	2.27

Table 5.1 Regression analysis for the combined IFC 1 Northern grids 13 and 15

which has 14% of its total flux contribution from larger low frequency structures. The mesoscale:local flux ratios for grids 76 and 79 are shown in Figure 5.14. Also unlike IFC 1, sensible heat flux does not dominate the energy budget. Figure 5.15 shows the mean fluxes for both grids. Grid 76 has a mean CO_2 flux of -0.2 mg m^{-2} s^{-1}, a mean sensible heat flux of 103 W m^{-2} and a mean latent heat flux (H_2O) of 153 W m^{-2} . Grid 79 has mean fluxes of -0.17 mg m^{-2} s^{-1}, 77 W m^{-2} and 152 W m^{-2} for CO_2, sensible heat and latent heat fluxes, respectively. This gives a Bowen ratio of 0.67 for grid 76, and 0.51 for grid 79. These data indicate changes in the 'behaviour' of the surface, compared to IFC 1. The lower CO_2 flux reflects a reduction of

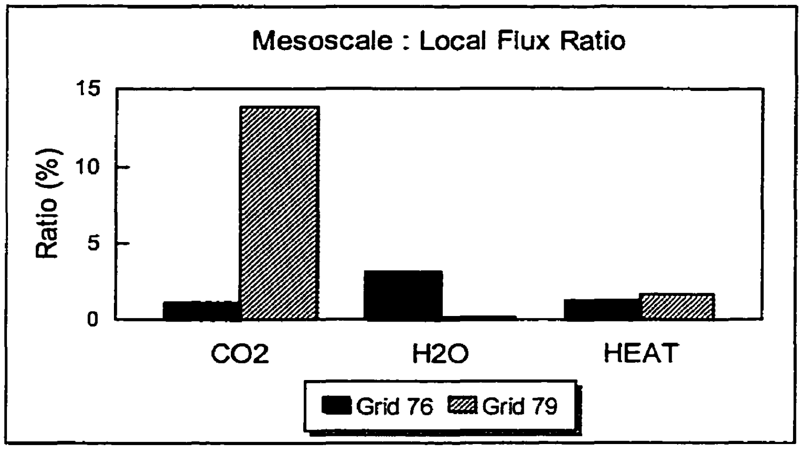

Figure 5.14. Mesoscale flux to local flux ratios for grid 76 and 79 from IFC4 northern site.

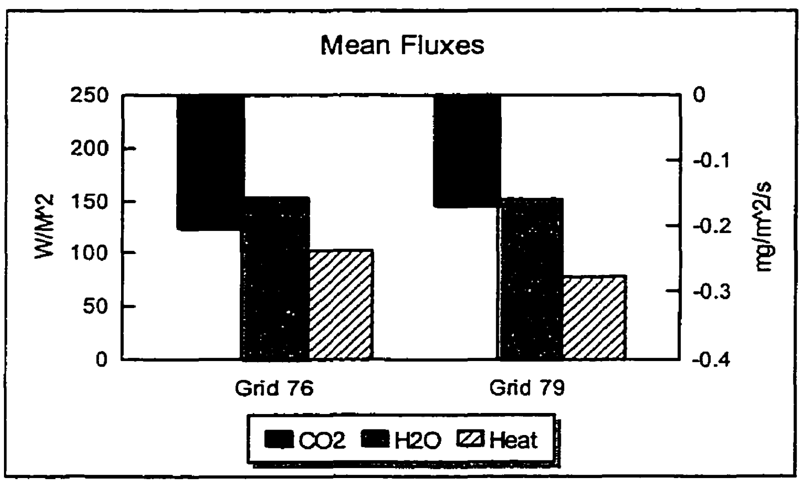

Figure 5.15. Local flux estimates for grids 76 and 79 from IFC4 northern site. Sensible and latent heat fluxes are in W m^{-2}

photosynthesis. There is also an absolute reduction in the energy fluxes, with water vapour dominating the budget. These differences could be the result of the increased heat stress placed on the vegetation as a result of an overall increase in air temperature. The prominence of the moisture flux could be a result of soil moisture being made more available to the regenerating deciduous vegetation as the growing season progresses. This is explored further in the next section.

5.4.2.2 *Fluxes and Surface Characteristics*

The spatial distribution of the surface conditions observed from the aircraft is shown in Figure 5.16. The distribution pattern of the surface temperature excess is similar to that of IFC 1 with low surface temperature excess in the north which has a high percentage of fens and wet to saturated soils, and high surface temperature excess to the south. The greenness index, however, is now higher in the southern section of the site. This area is dominated by regenerating aspen in the former burn area which, by the middle of the growing season, has completed its leaf-out. Overall the level of greenness is higher as would be expected as the growing season progresses. The FPAR and LAI were not available for this period. Figure 5.17 shows the spatial distribution pattern of the surface fluxes. The CO_2 flux pattern does not show the same degree of correspondence to greenness as during IFC 1. Higher values of the moisture flux are seen in the southern section of the site, while the higher sensible heat fluxes are concentrated towards the northern section. Similar to IFC 1, there is a decoupling of the surface from the atmosphere in terms of the heat flux, moisture flux and surface temperature excess, although the

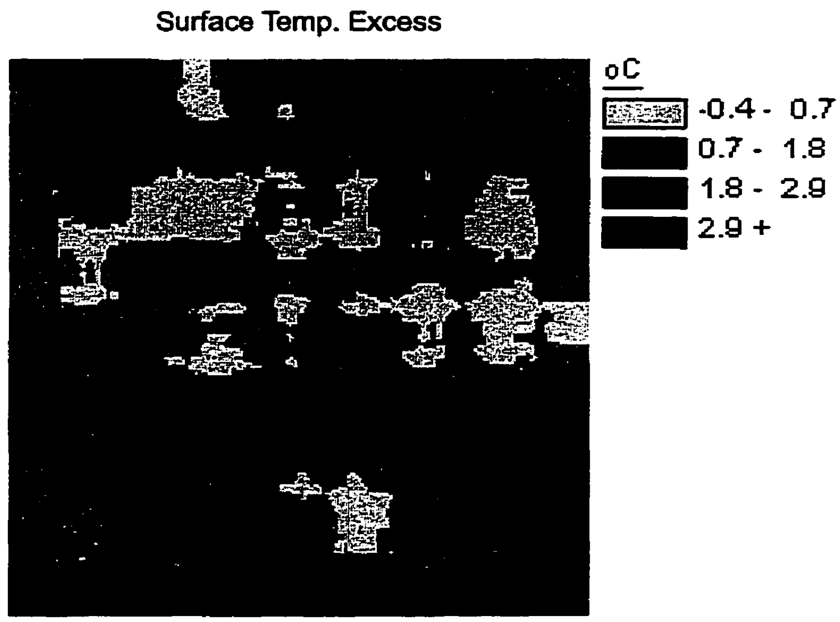

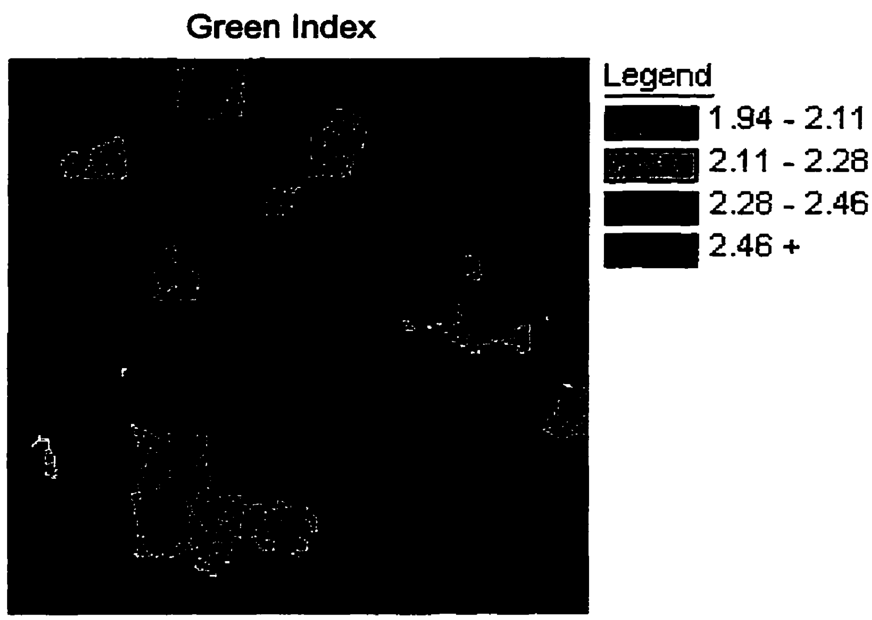

Figure 5.16 Twin Otter Surface Temperature Excess and Greenness index for the northern grid IFC4

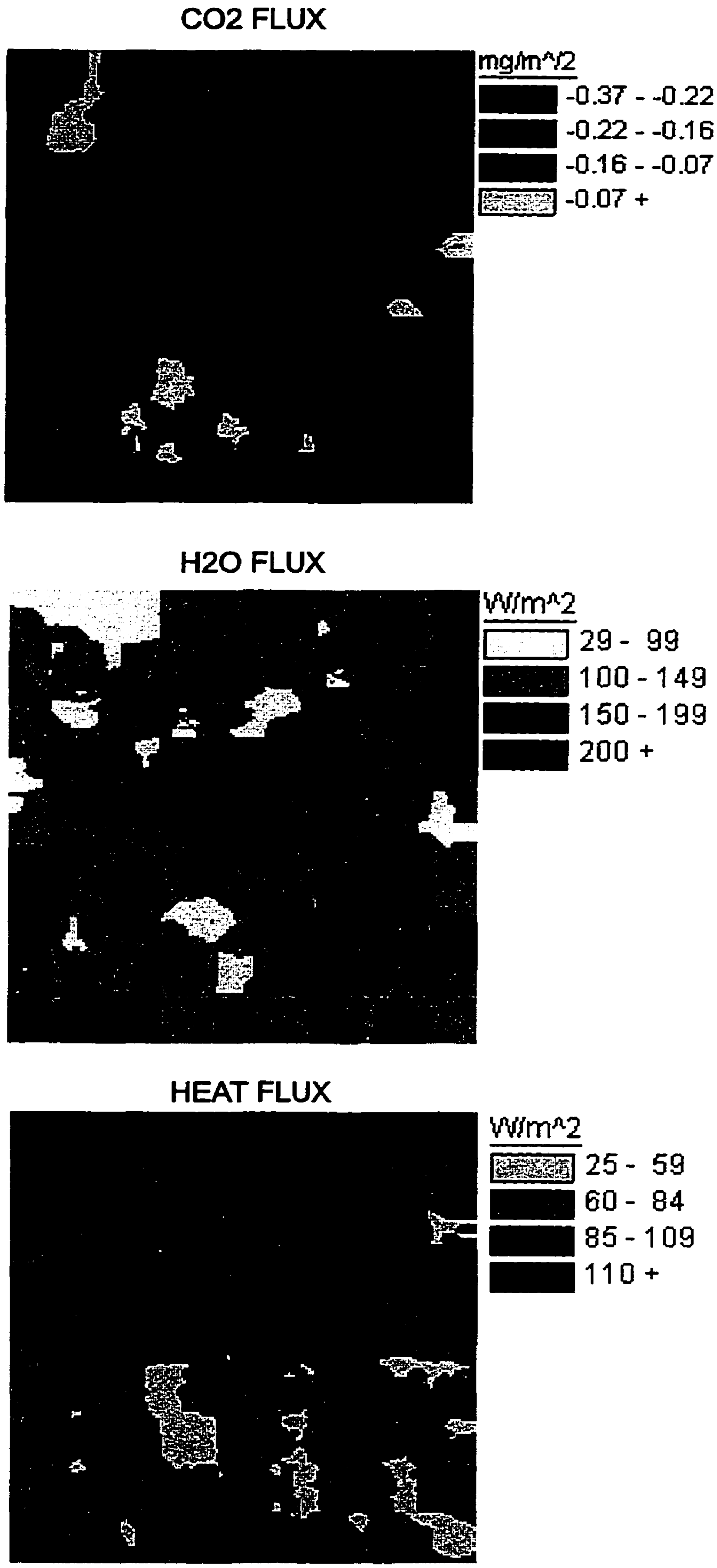

Figure 5.17 Spatial flux maps, combined grids 76 & 79, IFC4 northern site.

distribution patterns of the moisture flux to some extent reflects the surface greenness. These patterns indicate the complex set of micrometeorological dynamics operating at this site, and so far suggest that the distribution patterns of fluxes may not be accurately determined from the patterns of greenness and surface temperature alone.

5.4.2.3 *Coherent Structures and Sources and Sinks*

Figure 5.18 gives the flux association (FA) for grids 76, 79 and the combined grids. As in IFC 1, the four dominant categories of coherent structures in the gradient up mode are those which simultaneously transport CO_2, H_2O and heat (CHT) or H_2O and heat (HT), and those transporting only heat or H_2O. These categories are more prominent for grid 76. The large FA for single component structures of heat and H_2O again suggests the significant presence of heat and moisture plumes off the surface in the absence of sustained photosynthesis.

The FA for grid 79 are lower for the single component structures, and the significant percentage of combined moisture and heat plumes suggest that vegetation was more active in evapotranspiration. However, the FA results also indicate that many of the sources for water vapour flux and sensible heat flux are not co-located, as was seen in the Figure 5.17 flux maps.

Figure 5.19 gives the spatial distribution of the coherent structures for the different surface classifications. Similar to IFC1 the spatial distribution of all four dominant categories are fairly evenly distributed on the three dominant surface classifications. There is, however a 10% shift (compared to IFC1) in the number of

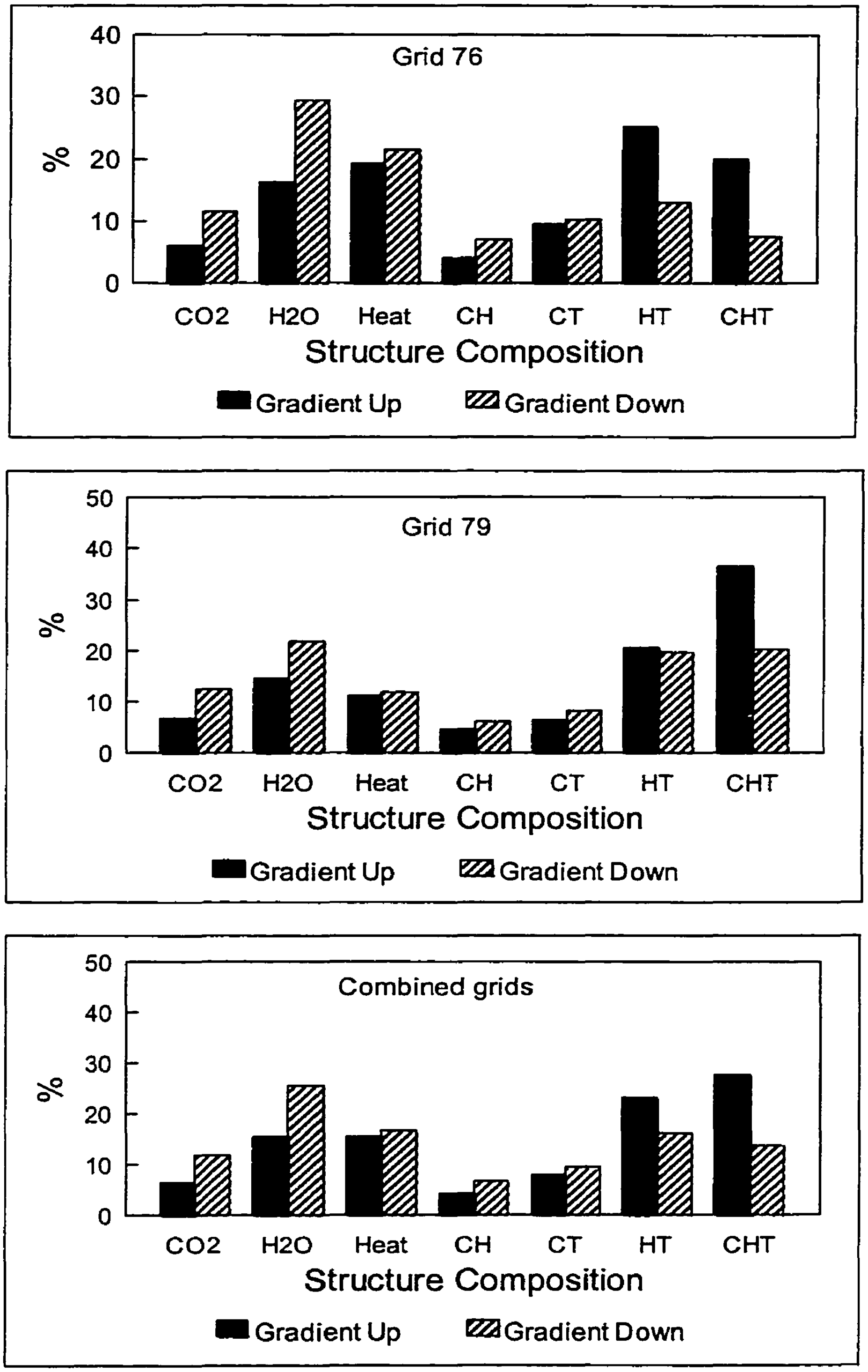

Figure 5.18. Flux Associations for grids 76, 79 and the combined grids from IFC4 northern site.

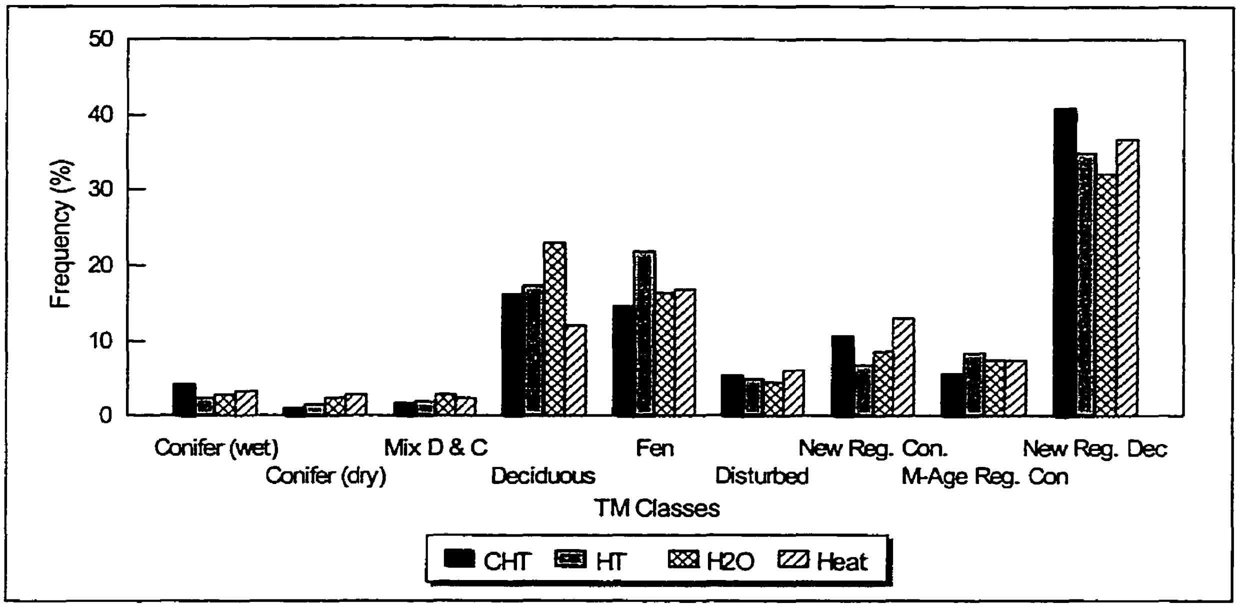

Figure 5.19. Spatial distribution of the coherent structures across the surface classification types. Grids 76 and 79 from IFC4, northern site.

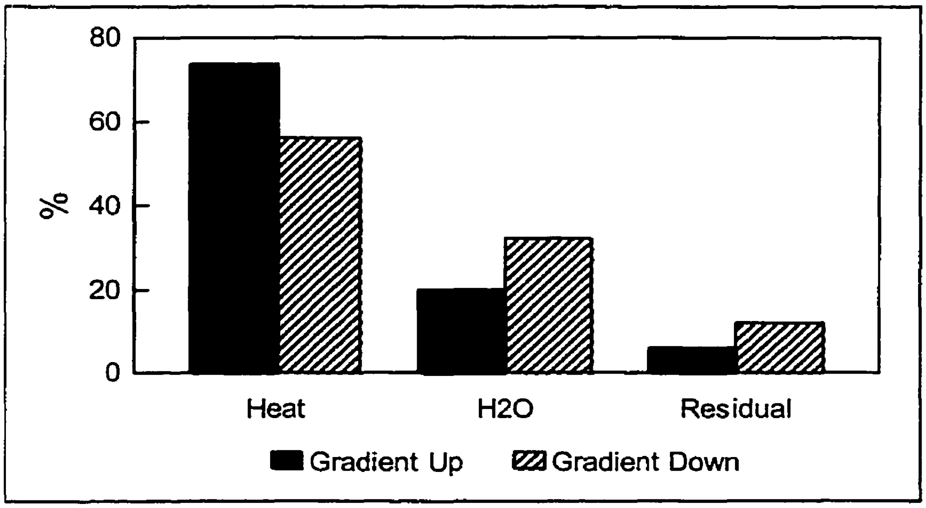

Figure 5.20. Partitioning of the driving forces at the surface derived from the coherent structure compositions. Grids 76 and 79 from IFC4 northern site.

CHT structures from medium aged regenerating conifers to the new regenerating deciduous surface class. This may reflect changes in the environmental conditions for the new regenerating deciduous as a more active source/sink.

The mean one-dimensional size for the CHT and HT structures were 112 m and 84 m, and the maxima 300 m and 244 m, respectively. The heat and H_2O structures had means of 56 m and 60 m, and maxima of 180 m and 229 m, respectively. These sizes are smaller than those observed in IFC 1, and may be an indication of the more localized source/sink areas.

The driving force partitioning derived from the coherent structure compositions is shown in Figure 5.20. Similar to IFC 1 heat is the dominant driving force at the surface. This dominance of heat as a driving force is further corroborated in the almost perfect correlation of 99% between heat and buoyancy flux (Table 5.2).

5.4.2.4 *Correlation and Regression*

The degree to which the surface is decoupled from the fluxes is evident in the correlation parameter r given in Table 5.2. The highest correlations are among the fluxes of CO_2, H_2O, heat and buoyancy which all have a direct (positive) relationship to each other. CO_2 has a low correlation with greenness as was indicated by the flux maps, and the surface characteristics of greenness and surface temperature excess have a low correlation with each other. Unlike the results from IFC 1, all the correlations are below 0.5 (50%) with the exception of buoyancy and heat.

y	x	r	a	β	se
H_2O	CO_2	0.31	111.88	-219.96	83.49
H_2O	Heat	0.25	111.65	0.45	85
H_2O	STExcess	0.09	144.57	4.42	87.54
H_2O	Greenness	0.079	77.73	30.3	87.61
CO_2	Heat	0.29	-0.12	0	0.12
CO_2	STExcess	0.15	-0.18	-0.001	0.12
CO_2	Greenness	0.19	0.07	-0.1	0.12
Heat	STExcess	0.37	71.52	10.18	45.3
Heat	Greenness	-0.047	114.8	-10.12	48.72
Buoyancy	Heat	0.99	0.008	0.001	0.006
Buoyancy	H_2O	0.38	0.06	0	0.041
STExcess	Greenness	-0.11	3.86	-0.84	1.77

Table 5.2 Regression analysis for the combined IFC 4 Northern grids 76 and 79

5.4.3 IFC 2 Southern Grid Site

5.4.3.1 *Flux Magnitudes*

The detrending procedure resulted in the mesoscale:local flux ratios shown in Figure 5.21. The relative importance of the mesoscale component is not as consistent between grids as in IFC 1, and its contribution is not as significant as for IFC 1 and IFC 4 in the northern grids. For grid 26, less that 2% of the flux is accounted for by larger scale transport and less than 10% for grid 30. In this case, however, CO_2 flux has the largest mesoscale contribution. Considering the generally small mesoscale contributions, we may conclude that the fluxes for the southern

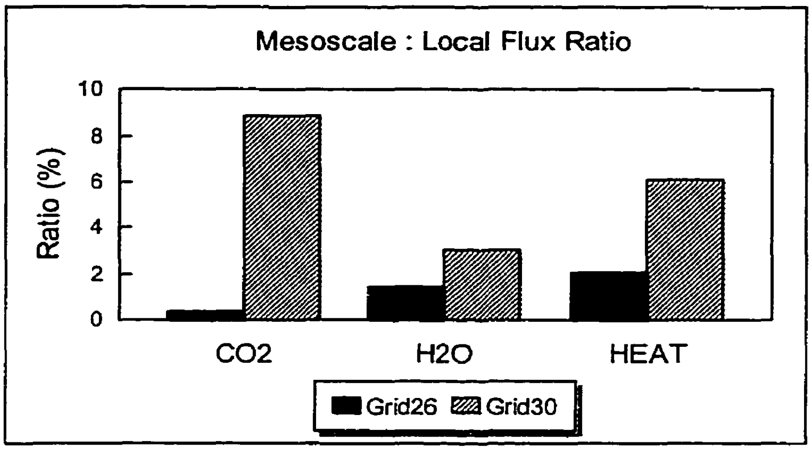

Figure 5.21. Ratios of mesoscale flux to local flux estimates for grids 26 and 30 from IFC2 southern site.

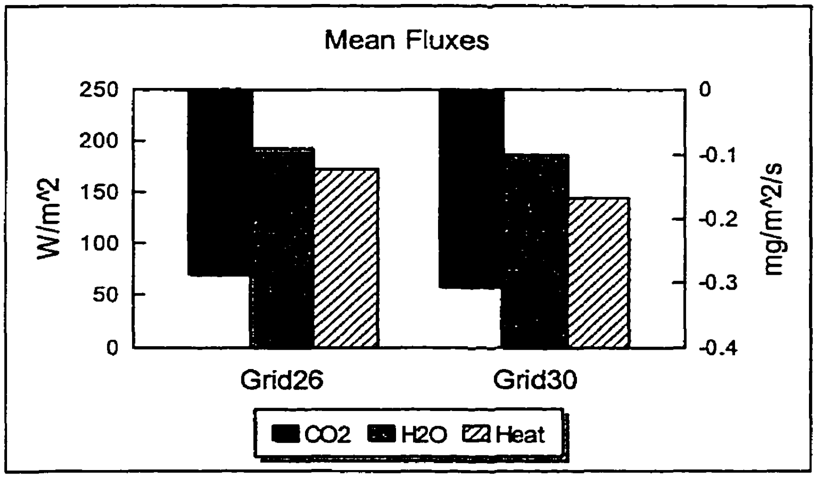

Figure 5.22. Mean local flux estimates for grids 26 and 30 from IFC2 southern site. Sensible and latent heat fluxes are in W m^{-2}

grid are generated primarily at the local scale. The mean fluxes for both grids are shown in Figure 5.22. The difference between the sensible and latent heat flux is not as large as at the northern grid, while the CO_2 flux is considerably larger. The sensible heat flux, in this case, does not dominate and is in fact less than the latent heat flux, with a Bowen ratio for grids 26 and 30 of 0.89 and 0.75, respectively. This partitioning is indicative of the surface, where a larger percentage of vegetation is at maturity than at the northern site. Grid 26 has mean fluxes of -0.29 mg m^{-2} s^{-1}, 193 W m^{-2} and 172 W m^{-2} for CO_2, latent and sensible heat flux, respectively, and grid 30 has -0.31 mg m^{-2} s^{-1}, 187 W m^{-2} and 146 W m^{-2} for CO_2, latent and sensible heat flux, respectively.

5.4.3.2 *Fluxes and Surface Characteristics*

The spatial distribution of the surface temperature excess and the greenness index shown in Figure 5.23 reflects the distribution pattern of the surface classes shown in Figure 5.4. The higher surface temperatures and the lower greenness are found in the northeastern section of the grid which has disturbed areas from recent logging, some bare soil as well as conifers on dry soil (jack pine). The southwestern section, which has low surface temperature and high greenness, reflects a surface cover dominated by fen and conifers (black spruce on wet soil) and mixed deciduous/conifer vegetation. The LAI and FPAR (Figure 5.24), although showing similar patterns, do not readily reflect the dominant characteristics of the surface. The flux maps for CO_2, H_2O and heat are shown in Figure 5.25. The distribution patterns for CO_2 and H_2O fluxes reflect the diagonal surface feature and the

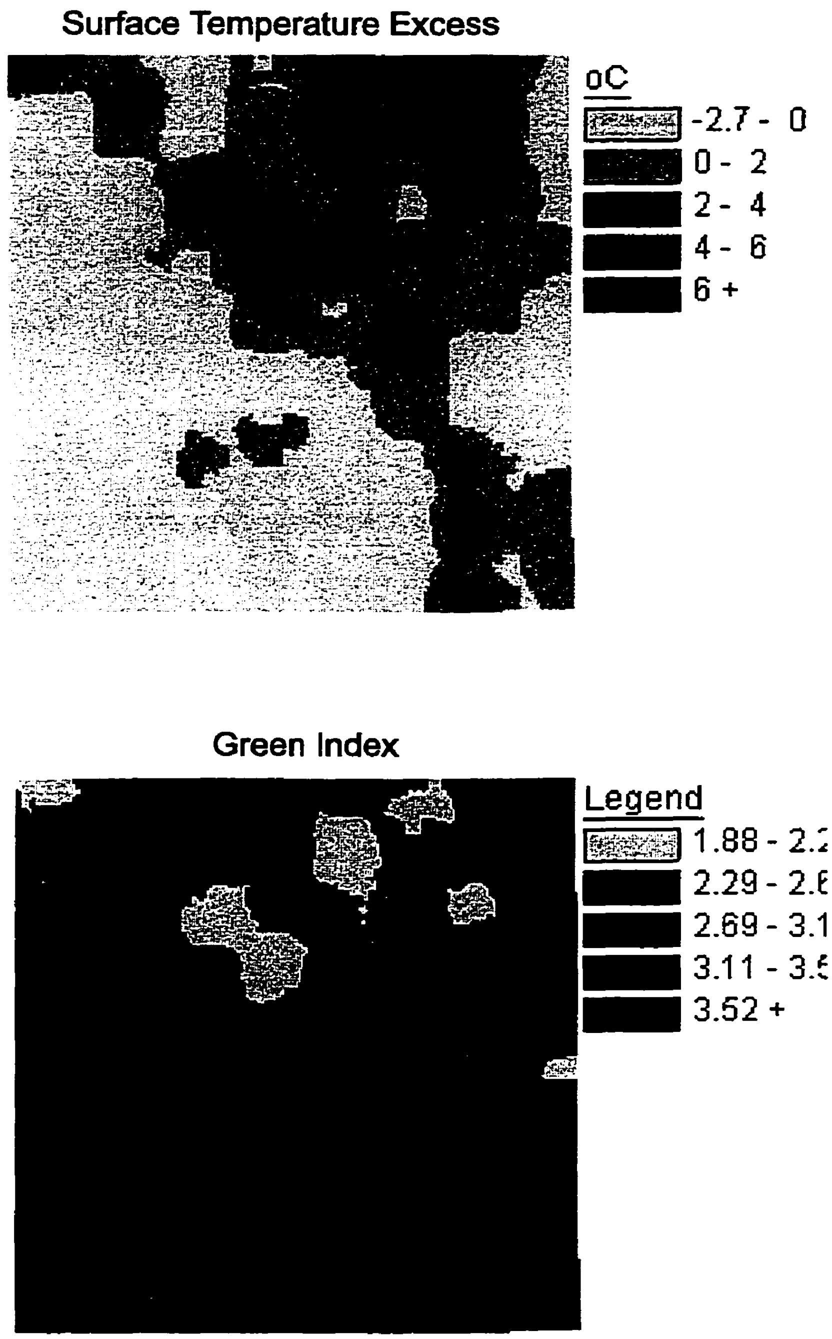

Figure 5.23 Twin Otter Surface Temperature Excess and Greenness index for the southern grid IFC2

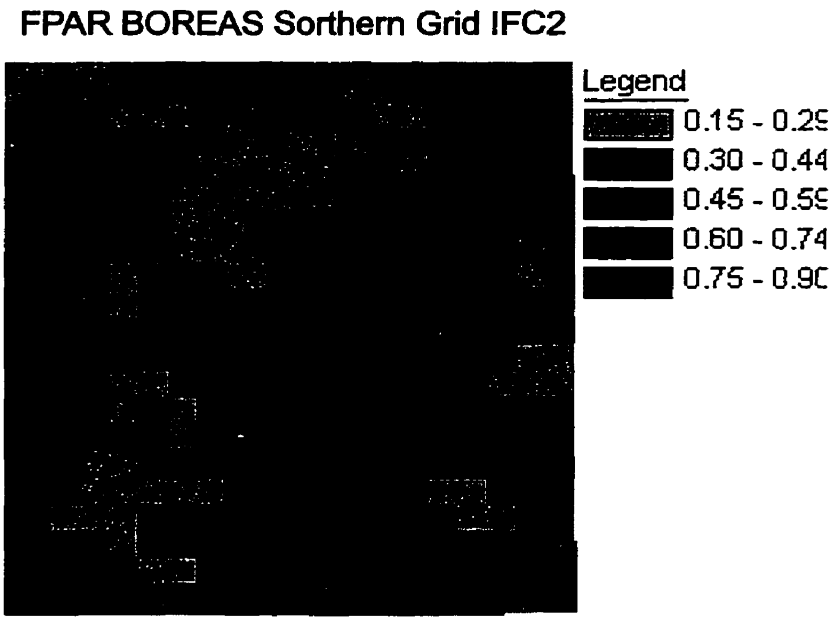

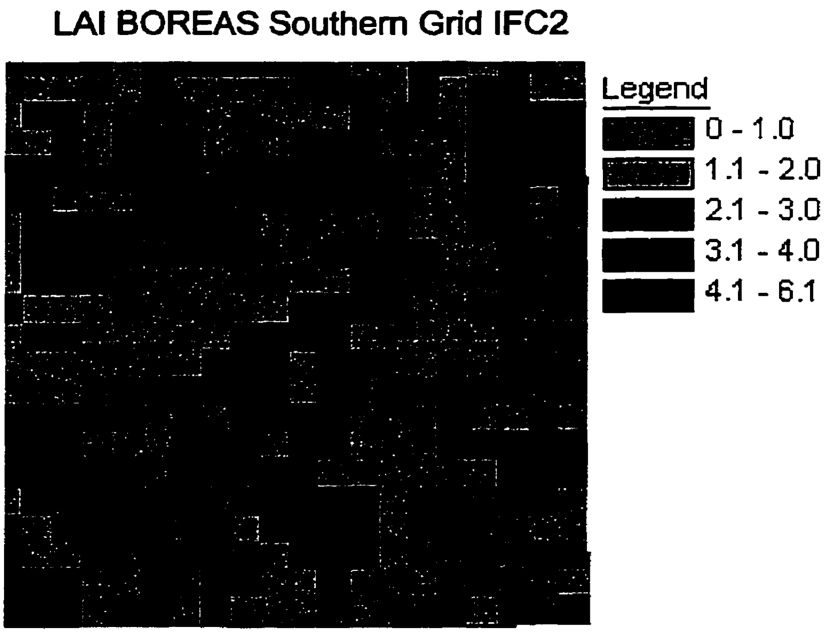

Figure 5.24 NOAA AVHRR FPAR and LAI for the southern grid from IFC2. Source: CCRS.

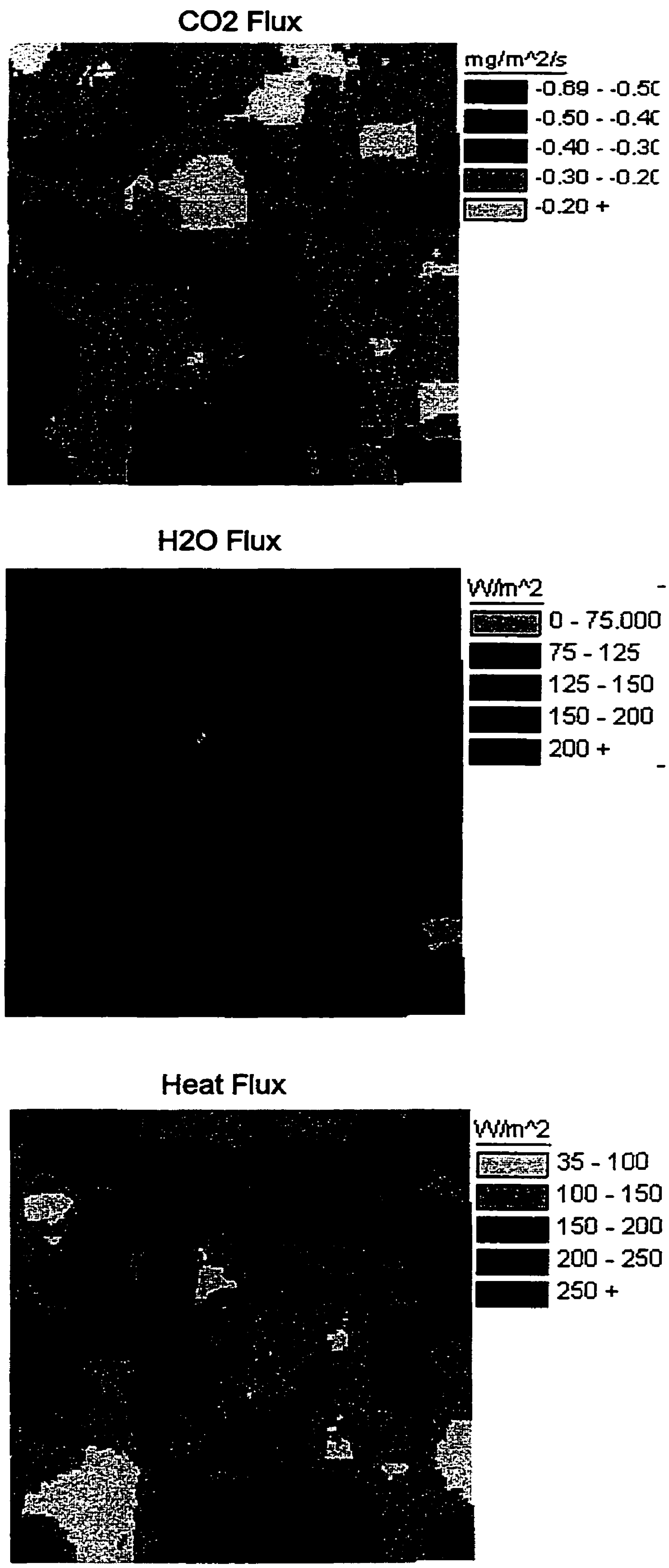

Figure 5.25 Spatial flux maps, combined grids 26 & 30, IFC2 southern site.

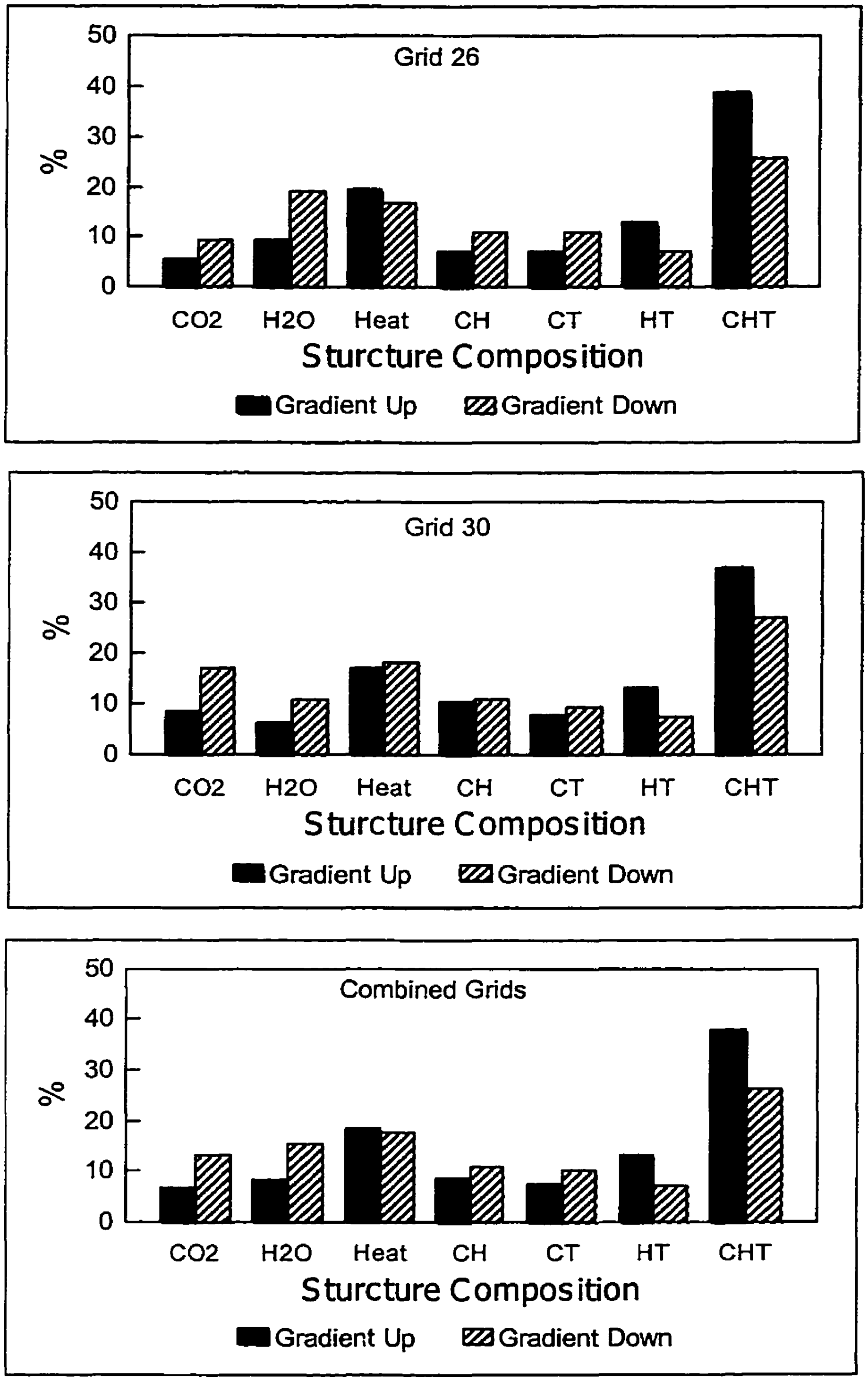

Figure 5.26. Flux associations for grid 26, grid 30 and the combined grids from IFC2 southern site.

distribution pattern of the greenness index. Similar to the northern site, the heat flux is decoupled from the surface and shows no distinct similarity to the pattern of surface temperature excess.

5.4.3.3 *Coherent Structures and Sources and Sinks*

The flux associations for the coherent structures for grid 26, grid 30 and the combined grids are shown in Figure 5.26. It is readily obvious that structures transporting CO_2, H_2O and heat (CHT) simultaneously dominate (37%), seconded by heat structures (18%), with structures transporting H_2O and heat at about 12% for grids 26 and 30. This, again, documents the existence and relative importance of the two major source/sink areas (vegetation-based and non-vegetated) across the grid.

The distribution of the coherent structures over the different surface classes is shown in Figure 5.27. The majority of the structures are located on the areas of wet conifer (black spruce), the dominant surface class, which consequently acts as the dominant source/sink across the site for all three fluxes. Given the fact that all four types of dominant structures are significantly represented in this classification, it is difficult to distinguish the separate sources and sinks as indicated by these structures, except for the obvious importance of heat (both in exclusive thermal plumes and mixed plumes with heat), also over the dry conifers. There is some indication of characteristic differences in structure distribution for some of the other surface classification (such as the relative dominance of CH over the new regenerating class), but in view of the small areas involved, such differences cannot be distinguished with assurance.

The driving forces at the surface determined from the composition of the coherent structures are shown in Figure 5.28. Similar to the northern site, the dominant driving force is heat, accounting for >75% in the gradient up mode. Similar also to the northern site, the correlation between the heat flux and the buoyancy flux is almost perfect at 99%.

The mean one-dimensional sizes for the CHT and CH structures were 110 m and 83 m, and the maxima 442 m and 277 m, respectively. The heat and H_2O structures both had means of 63 m, and maxima of 330 m and 225 m, respectively.

5.4.3.4 *Correlation and Regression*

The simple correlations and regressions given in Table 5.3 show much higher values than those observed at the northern site. The higher correlations are not only between the fluxes but also with the surface, as was evident from the flux maps. Fluxes of CO_2, H_2O and heat all have a moderate to high correlation with each other, and the sensible heat flux for this site is still essentially decoupled from the surface, with a 0.09 correlation to surface temperature excess.

5.4.4 Model Prediction of Surface Fluxes

5.4.4.1 *Footprint Adjusted Model*

The footprint adjusted step-wise regression model uses the upwind area generating up to 80% of the flux, and a width of 500 m as correlation sample cells.

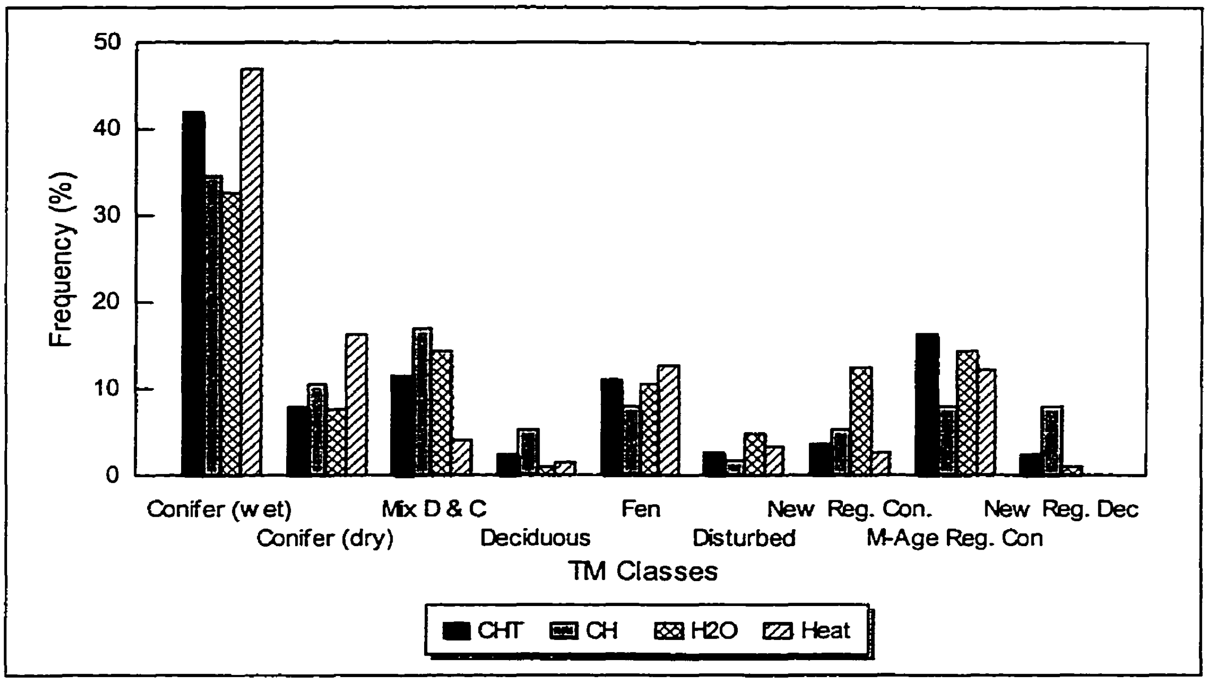

Figure 5.27. Spatial distribution of coherent structures across the surface types. Grids 26 and 30 from IFC2 southern site.

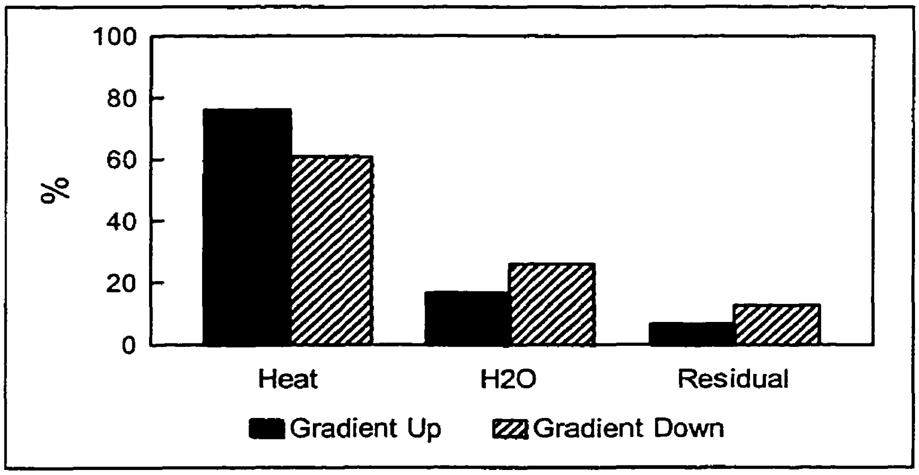

Figure 5.28. Partitioning of the driving force at the surface derived fro the compositions of the coherent structures. Combined grids 26 and 30 from IFC4 southern site.

y	x	r	a	β	se
H_2O	CO_2	0.75	35.32	-523.34	63.89
H_2O	Heat	0.52	81.9	0.68	81.73
H_2O	STExcess	-0.13	191.6	-4.56	94.9
H_2O	Greenness	0.25	30.31	56.95	92.87
CO_2	Heat	0.43	-0.17	0	0.12
CO_2	STExcess	-0.34	-0.3	0.02	0.13
CO_2	Greenness	0.42	0.096	-0.14	0.124
Heat	STExcess	0.09	157.9	2.26	73.3
Heat	Greenness	-0.08	197.92	-13.96	73.38
Buoyancy	Heat	0.9957	0.0058	0.001	0.006
Buoyancy	H_2O	0.59	0.073	0	0.055
STExcess	Greenness	-0.62	12.81	-4.43	2.3

Table 5.3 Regression analysis for the combined IFC 2 Southern grids 26 and 30.

The frequency of the cover types within these cells are used as indices for independent variables. The model input of independent variables therefore consist of indices of all the relevant cover types present in Figure 5.3 as well as greenness index and incident radiation.

The step-wise regression for CO_2 flux yielded an r^2 of 0.3032, significant at the 0.1500 level, and includes the following independent variables: greenness, incident radiation, and disturbed, medium-aged regenerating conifers, and new regenerating deciduous cover types. The model for H_2O flux had an r^2 of 0.0482, significant at 0.1500 level, and consist of incident radiation, conifer (wet), mixed deciduous, disturbed and medium-aged regenerating conifer cover types. The model for heat flux had an r^2 of 0.0835, with independent variables greenness, incident radiation, disturbed, conifer (dry), conifer (wet) and new regenerating conifers.

The model equations are not given due to the low predictive results. The use of a linear step-wise multi regression is unable to significantly predict the surface flux estimates in this case. The moderate r^2 value for the CO_2 flux is a result of the greenness index, as seen from the simple regression in Table 5.3.

5.4.4.2 *Variable Scale Model*

The same independent variables used in the footprint adjusted model in section 5.4.4.1 were used in this model. Both the TM image and the aircraft derived maps were gridded to the same spatial resolution. The land cover types class frequency was then calculated over a 240 m x 240 m (*scale one*) and 560 m x 560 m (*scale two*) area.

The variable spatial scales used to calculate the class frequencies did not make any significant difference in the r^2 values, although they are all slightly higher for scale two model. Possible reasons may be that the change in scale was not large enough or significant enough to have an impact on the relationships, or introduce any underlying influence that may have been missing. Similar to the footprint adjusted model, the model for CO_2 had the best results with an r^2 of 0.3366 and 0.3645 for IFC1, 0.4076 and 0.4148 for IFC2 and 0.1533 and 0.1734 for IFC4, for scale one and scale two, respectively. The relatively poor performance for IFC4 may be the result of the more dominant effects of midsummer atmospheric conditions such as higher air temperature and vapour pressure deficit. The r^2 values for H_2O and heat flux were much lower and are listed in Table 5.4.

	IFC1 NSA . Grid		IFC4 NSA . Grid		IFC2 SSA. Grid	
	scale 1	scale 2	scale 1	scale 2	scale 1	scale 2
CO_2	0.3366	0.3645	0.1533	0.1734	0.4076	0.4148
H_2O	0.0302	0.0526	0.1029	0.1158	0.1736	0.182
Heat	0.1307	0.1858	0.221	0.2664	0.1299	0.1733

Table 5.4 Values for r^2 from the variable scale regression models. Scale one represents a 240 m x 240 m area and scale two represents a 560 m x 560 m area.

The best model for CO_2 flux prediction is the IFC2 southern grid larger scale two model with an r^2 value explaining 42% of the variability in the CO_2 flux. The larger scale two model for IFC4 northern grid was the best predictor for the heat flux, explaining 22% variability. The larger scale two model from IFC2 southern grid was the best predictor for the H_2O flux, explaining 18% of the variability.

An important variable missing in the models was the vapour pressure deficit or relative humidity. The extremely high VPD is a significant forcing on the various vegetation types. Hog and Hurdle (1996), and Dang et al. (1996), showed a strong nonlinear response between both boreal conifer and deciduous conductance and VPD. There was, however, very little spatial variability of VPD across the grid sites as well as between the different IFCs examined, so that VPD was not included in the models. It may not be possible to make an accurate prediction of spatially averaged surface fluxes at the landscape scale with a straightforward linear model

At this scale, the surface variability is very small in comparison to the variabilities in such parameters as soil moisture, soil temperatures and soil type. Vegetation influence, although noticeable at this scale, is difficult to translate into fluxes, particularly in view of the nonlinear relationship between the vegetation and the fluxes . Baldocchi et al. (1997) showed a nonlinear relationship between latent heat and canopy resistance, and between canopy CO_2 uptake and transpiration for old jack pine and deciduous forest. These vegetation parameters were unavailable for incorporation into the models.

5.5 CONCLUSIONS

One of the most obvious conclusions to emerge from this study is that the boreal ecosystem is very complex, without straightforward inter-relationships between structure and composition of the soil and vegetation, and characteristics of the atmospheric boundary layer and its transport processes. The vegetation patterns seen in the classification maps are reflected in the spatial distribution of the surface temperature and the greenness index for both the northern and southern grids. This does not, however, translate into corresponding spatial distributions for the fluxes as would be expected from micrometeorological convention. Both the flux maps and the correlation/regression analyses indicate that only the CO_2 flux may be predicted with limited accuracy from vegetation indices such as greenness or NDVI.

The coincidence analysis for the southern grid from IFC2 indicates that the dominant source/sink area for heat, H_2O and CO_2 is the vegetation canopy under condition of active photosynthesis, with a small portion generating only sensible heat plumes. The coincidence analysis from both IFC1 and IFC4 for the northern grid suggests that there are four distinct source/sink areas at the northern grid site: the part of the surface which is actively photosynthesizing; sources of thermally driven evaporation; sources where shear eddies transport moisture; sources with only sensible heat plumes. This breakdown of the sources and sinks again points to the complex nature of the micrometeorology at this scale. The inability of the distribution of the coherent structures to show the location of these various sources and sinks, may be attributed to a large extent to the difference in scales between the aircraft grid run spatial resolution of 2 km and the scale of the heterogeneity, of the order of metres, of the surface features.

While this study was able to identify the inconsistencies between the fluxes and the underlying surface characteristics, it was unable to quantitatively determine the interacting relationships which may have generated these conditions. Some evidence, however, was presented to explain the unusual micrometeorological conditions at the sites. Overall, the emerging picture presents an enormous challenge to modellers intending to produce process-based descriptions of the energy and scalar fluxes in complex ecosystems such as the boreal forest. Such an approach would require a full understanding of the major structural (e.g., surface/canopy patchiness), physiological (e.g., vegetation makeup and response to stresses) and meteorological (e.g., relative humidity and boundary layer structure) factors within the given climatological context. The challenge is particularly acute because these parameters also vary with scale. To a large extent, this could only have been realized through large scale, multi-disciplinary studies such as BOREAS.

CHAPTER 6.

GENERAL SUMMARY AND CONCLUSIONS

This thesis contributes to our understanding of the degree to which assumptions can be made about the relationship between the atmosphere and the underlying surface. The California Ozone Deposition Studies (CODE) demonstrated that for large scale agricultural system, the relationships can be simple and straightforward, with the exception of trace gases such as ozone, which is of particular interest in this area. The boreal ecosystem, however, is much more complex, and requires knowledge of a wider range of parameters in order to understand the surface-atmosphere flux relationships.

Procedures introduced in the CODE aircraft study for the separation of the larger scale flux event from more local small scale events were shown to be successful, and useful also in cases such as in BOREAS, where large mesoscale flux contributions were sometimes present. The CODE studies showed that the flux association of coherent structures can generate a large amount of information on the characteristics of these structures which dominate transport. Findings of the differential degree of associations of ozone to CO_2 and H_2O were confirmed, along with the continued uptake of ozone even under stressful conditions. The identification of the different sinks for ozone was established through the characteristics of the coherent structures. Over the cotton canopy there were two separate sinks, a vegetated and a non-vegetated one, while over the grape canopy there appeared to be only a vegetated sink for ozone. These findings can help to clarify the link between ozone uptake by crops and their physical and physiological status.

Studies of the one-dimensional size of the structures show some dependence of structure size on underlying crop structure, and the structures sizes from the tower data fall within range of the expected mean surface layer eddy scales. This may be helpful as an empirical verification of eddy scale limitations within simulation models.

For a long time in the past, and to some extent at present, models and simulations of surface-atmosphere processes, such as fluxes for remote ecosystems, were based on limited micrometeorological understanding of these systems. As a result, extrapolations were made from more widely studied but homogeneous and simple ecosystems such as large scale agriculture, and grassland. Such studies as CODE, the Northern Wetlands Study and BOREAS made it obvious that the surface heterogeneity, not only in terms of vegetation cover but also in terms of the scale of the heterogeneity, the surface moisture availability, the soil type, etc., in combination with prevailing atmospheric conditions, create a very complex set of micrometeorological conditions. This might not have been foreseen based on our conventional understanding of the relationships between micrometeorological parameters. Studies such as those contained in this thesis are expected to contribute to the understanding of the relationships that are apparent at the various scales at which the surface interacts with the atmosphere.

The results from the BOREAS studies, in conjunction with similar studies, allow disciplines such as atmospheric science, eco logy, remote sensing, hydrology, plant physiology and modelling to move closer together. What can we determine about the surface-atmosphere link at the various scales? Can the relationships observed, but not explained, at one scale be explained at another? And if so, can it be scaled up? Do we have to understand interactions at the scale used in this flux association study to be able to scale up successfully in heterogeneous ecosystems? These are relevant questions, and studies such as this one and others that came out of BOREAS, while not yet able to give conclusive answers, hopefully contribute to such answers. We may not yet be able to successfully scale up all the relevant relationships to have a realistic, process-based model for these complex ecosystems, but through these studies we have come a long way in understanding the inter-relationships between soil, vegetation and the atmosphere, and are hopefully able to address them in more refined simulation and prediction models.

REFERENCES

Antonia, R.A., 1981. Conditional sampling in turbulence measurement. *Ann. Rev. Fluid Mech., 13*: 131-156.

Austin, L.B., Schuepp, P.H., and R.L. Desjardins, 1987. The feasibility of using airborne flux measurements for the imaging of the rate of biomass production. *Agri. and Forest Meteorol., 39*: 13-23.

Baldocchi, D.D. (1994) A comparison study of mass and energy exchange over a closed (wheat) and an open (corn) canopy. II: CO_2 exchange and water use efficiency, *Agri. and Forest Meteorol., 67*, 291-321.

Baldocchi, D.D and C. Vogel, 1996: Energy and CO_2, flux densities above and below a temperate broadleaf forest and a boreal pine forest, *Tree Physiology, 16*, 5-16.

Baldocchi, D., Valentini, R., Running, S., Oechels, W., and R. Dahlman, 1996: Strategies for measuring and modelling carbon dioxide and water vapour fluxes over terrestrial ecosystems, *Global Change Biology, 2*, 159-168.

Baldocchi, D.D., Vogel, C.A., and B. Hall, 1997: Seasonal variation of energy and water vapour exchange rates above and below a boreal jack pine canopy, *J. Geophys. Res., 102, (D24), 28*, 939-28, 951.

Betts, A.K., Ball, J.H., Beljaars, A.C.M., Miller, M.J., and P.A. Viterbo, 1996: The land surface-Atmosphere interaction: a review based on observational and global modelling perspectives, *J. Geophys. Res., 101, (D3)*, 7,209-7,225.

Betts, A.K., Desjardins, R.L., and J.I. MacPherson, 1992: Budget analysis if the boundary layer grid flights during FIFE 1987, *J. Geophys. Res., 97, (D17)*, 18,533-18,547.

Black, T.A., Den Hartog, G., Neumann, H.H., Blanken, P.D., Yang., P.C., Russell, C., Nesic, Z., Lee, X., Chen, S.G., Staebler, R., and M.D. Novak, 1996: Annual cycles of water vapour and carbon dioxide fluxes in and above a boreal aspen canopy, *Global Change Biology, 2*, 219-229.

Blanken, P.D., Black, T.A., Yang, P.C., Neumann, H.H., Nesic, Z., Staebler, R., den Hartog, G., Novak, M.D., and X. Lee, 1997: Energy balance and canopy conductance of a boreal aspen forest: Partitioning overstory and understory components, *J. Geophys. Res., 102, (D24)*, 28,915-28,927.

Blake, D.W., Krishnamurti, T.N., Low-Nam, S.V., and J.S. Fein, 1983: Heat low over the Saudi Arabian desert during May 1979, *Monthly Weather Rev., 111*, 1759-1775.

Bonan, G.D., 1993: Importance of leaf area index and forest type when estimating photosynthesis in boreal forest, *Remote Sens. Environ., 43,* 303-314.

Caramori, P., Schuepp, P.H., Desjardins, R.L., and J.I. MacPherson, 1994: Structural analysis of airborne flux measurements over a region, *J. Climate, 7*, 627-640.

Chapman, S.J., and M. Thurlow, 1996: The influence of climate on CO_2 and CH_4 emissions from organic soils, *Agri. and Forest Meteorol. 79*, 205-217.

Cihlar J., Caramori, P.H., Schuepp, P.H., Desjardins, R.L., and J.I. MacPherson, 1992: Relationship between satellite-derived vegetation indices and aircraft based CO_2 measurements, *J. Geophys. Res., 97, (D17)*, 18,515-18,521.

Collineau, S., and Y. Brunet 1993: Detection of turbulent coherent motions in a forest canopy. Part 1: Wavelet analysis, *Boundary-Layer Meteorol., 61,* 398-405.

Cooper, H.J., Smith, E.A., and J. Gu, 1997: Modelling the impact of averaging on aggregation of surface fluxes over BOREAS, *J. Goephys. Res., 102, (D24)*, 29,235-29, 253.

Dang, L-Q, Margolis, H.A., Coyea,M.R., Sy, M., and G.J. Collatz, 1996: Regulation of branch-level gas exchange of boreal trees: roles of shoot water potential and vapour pressure difference, *Tree Physiology, 17*, 521-535.

Desjardins, R.L. and J.I. MacPherson, 1989: Aircraft-based measurements of trace gas fluxes. In: Andreae, M.O. and Schimel, D.S. (eds), Exchange of Trace Gases between Terrestrial Ecosystems and the Atmosphere. *J.Wiley & Sons, New York*, pp. 135-172.

Desjardins, R.L., Hart, R.L., MacPherson, J.I., Schuepp, P.H., and Verma, S.B., 1992a. Aircraft and tower-based fluxes of carbon dioxide, latent, and sensible heat, *J. Geophys. Res. 97, (D17),* 18,477-18,485.

Desjardins, R.L., Schuepp, P.H., and J.I. MacPherson, 1992b. Spatial and temporal variations of the fluxes of carbon dioxide and sensible and latent heat over the FIFE site. *J. Geophys. Res., 97, (D17),* 18,467-18,475.

Desjardins, R.L., MacPherson, J.I., Neumann, H., den Hartog, G., and P.H. Schuepp, 1995: Flux estimates of latent and sensible heat, carbon dioxide, and ozone using an aircraft-tower combination. *Atmos. Environ., 29, (21)*, 3147-3158.

Desjardins, R.L., MacPherson, J.I., Mahrt, L., Schuepp, P., Pattey, E., Neumann, H., Baldocchi, D., Wofsy, S., Fitzjarrald, D., McCaughey, H., and D.W. Joiner, 1997: Scaling up flux measurements for the boreal forest using aircraft-tower combinations, *J. Geophys. Res. 102, (D24)*, 29,125-29,133.

Duncan, M.R., and P.H Schuepp, 1992: A method to delineate extreme structures within airborne flux traces over the FIFE site. *J. Geophys. Res., 97, (D17)*, 18,487-18,498.

Eloranta, E.W., and D.K. Forrest, 1992: Volume imaging lidar observations of the convective structure surrounding the flight path of a flux-measuring aircraft, *J. Geophys. Res., 97, (D17),* 18,383-18,498.

Gao, W., Wesely, M.L., Cook, D.R., and R.L. Hart, 1992: Air-surface exchange of H_2O, CO_2, and O_3 at a tall grass prairie in relationship to remotely sensed vegetation indices, *J. Geophys. Res., 97, (D17),* 18,663-18,671.

Gal-Chen, T., Xu, T., and W.L. Eberhard, 1992: Estimations of atmospheric boundary layer fluxes and other turbulent parameters from Doppler lidar data, *J. Geophys. Res., 97, (D17)*, 18,409-18,423

Goetz, S.J., and S.D. Prince, 1996: Remote Sensing of net primary production in boreal forest stands, *Agri. and Forest Meteorol., 78*, 149-179

Grant, R.H., Bertolin, G.E., and L.P. Herrington, 1986: The intermittent vertical heat flux over a spruce forest canopy. *Boundary-Layer Meteorol., 35,* 317-330.

Guo, Y., Desjardins, R.L., MacPherson, J.I., and P.H. Schuepp, 1995a: The correspondence of aircraft-measured fluxes of sensible heat, latent heat, CO_2, and ozone to the surface characteristics in the San Joaquin Valley of California, *Atmos. Environ., 29, (21),* 3159-3168

Guo, Y., Desjardins, R.L., MacPherson, J.I., and P.H. Schuepp, 1995b: A simple scheme for partitioning aircraft-measured ozone fluxes into surface uptake and chemical transformation, *Atmos. Environ., 29, (21)*, 3199-3207.

Hall, F. G., and P.J. Sellers, 1995: First International Satellite Land Surface Climatology Project (ISLSCP) Field Experiment (FIFE)in 1995, *J. Geophys. Res., 100*, 25,383 - 25,395.

Hall, F.G., Shimabukuro, Y.E., and K.F. Huemmrich, 1995: Remote sensing of forest biophysical structure using mixture decomposition and geometric reflectance model, *Ecological Applications, 5, (4),* 993-1013.

Hall, F.G., Huemmrich, K.F., Goetz, S.J., Sellers, P.J., and J.E. Nickeson, 1992: Satellite Remote Sensing of Surface Energy Balance : Success, Failures, and Unresolved Issues in FIFE, *J. Geophys. Res., 97, (D17),* 19,061-19,089

Hanan, N.P., Prince, S.D. and A. Begue, 1995: Estimation of absorbed photosynthetically active radiation and vegetation net production efficiency using satellite data, *Agri. and Forest Meteorol., 76,* 259-276

Hog, E.H., and P.A. Hurdle, 1996: Sap flow in trembling aspen: Implications for stomatal responses to vapour pressure deficit, *Tree Physiology., 17*, 501-509

Hollinger, D.Y., Kelliher, FM., Byers, J.N., Hunt, J.E., McSeveny, T.M and P.L. Weir, 1994: Carbon dioxide exchange between an undisturbed old-growth temperate forest and the atmosphere, *Ecology, 75,* 134-150

Kaharabata, S.K., Schuepp, P.H., Ogunjemiyo, S., Shen, S., Leclerc, M.Y., Desjardins, R.L., and J.I. MacPherson, 1997 : Footprint considerations in BOREAS, *J,. Geophys. Res., 102, (D24)*, 29,113-29124.

Klaassen, W., and M. Claussen, 1995: Landscape variability and surface flux parameterization in climate models, *Agri. and Forest Meteorol., 73,* 181-188

Koster, R.D., and M.J. Suarez, 1992: Modelling the land surface boundary in climate models as a composite of independent vegetation stands, *J. Geophys. Res., 97, (D3)*, 2697-2715

Laubach, J., Raschendorfer, M., Kreilien, H., and G. Gravenhorst, 1994: Determination of heat and water vapour fluxes above a spruce forest by eddy correlation, *Agri. and Forest Meteorol., 71*, 373-401.

Lee, X., Black, A.T., den Hartog, G., Nuemann, H.H., Nesic, Z., and J. Olejnik, 1996: Carbon dioxide exchange and nocturnal processes over a mixed deciduous forest, *Agri. and Forest Meteorol., 81,* 13-29.

Lenschow, D.H, 1986. Aircraft measurements in the boundary layer. In: Lenschow, D.H. (ed), Probing the Atmospheric Boundary Layer, *American Meteorol. Soc., Boston*, pp. 29-55.

Liandrat, J and F. Moret-Bailly, 1990: The wavelet transform: some applications to fluid dynamics and turbulence, *Eur. J. of Mech. B/Fluids, 9*, 1-19.

Mack, A.R., Desjardins, R.L., MacPherson, J.I., and P.H. Schuepp, 1990: Relative Photosynthetic Activity of Agricultural Lands from Airborne Carbon Dioxide and Satellite Data, *Int. J. Remote Sens., 11, (2),* 237-2501.

Mahrt, H. and M. Ek, 1993a: Mesoscale (subgrid) variability of turbulent fluxes in HAPEX and CODE, *Proc. Conference on Hydroclimatology*, Amer. Meteorol. Soc., Anaheim, Calif., Jan. 17-22, 1993, 130-131.

Mahrt, H. and M. Ek, 1993b: Spatial variability of Turbulent fluxes and roughness lengths in HAPEX-MOBILHY, *Boundary-Layer Meteorol., 65,* 381-400

Margolis, H.A., and G.M. Ryan, 1997: A physiological basis for biosphere-atmosphere interactions in the boreal forest: an overview, *Tree Physiology, 17*, 491-499.

Massman, W.J., Pederson, J., Delany, A., den Hartog, G., Neumann, H.H., Grantz, D. and R. Pearson Jr., 1993: A Comparison of independent determinations of the canopy conductance for carbon dioxide, water vapour and ozone exchange at selected sites in the San Joaquin Valley of

California, *Proc. Conference on Hydroclimatology*, Amer. Meteorol. Soc., Anaheim, Calif., Jan. 17-22, 1993, 112-117

Massman, W.J., Pederson, J., Delany, A., Grantz, D., den Hartog, G., Neumann, H.H., Oncley, S.P., Pearson Jr., R., and R.H. Shaw, 1994: An evaluation of the regional acid deposition model surface module for ozone uptake at three sites in the San Joaquin Valley of California, *J. Geophys Res., 99 (D4)*, 8281-8294

Massman, W.J., MacPherson, J.I., Delany, A., den Hartog, G., Neumann, H.H., Oncley, S.P., Pearson Jr., R., Pederson, J., and R.H. Shaw, 1995: Surface conductance for ozone uptake derived from aircraft eddy correlation data, *Atmos. Environ., 29, (21)*, 3181-3188

McGuire, A.D., Melillo, J.M., Joyce, L.A., Kicklighter, D.W., Grace, A.L., Moore, B. and C.J. Vorosmarty, 1991: Interactions between carbon and nitrogen dynamics in estimating net primary productivity for potential vegetation in North America, *Global Biogeochem. Cycles, 6,* 101-124.

Melillo, J.M., McGuire, D.A., Kicklighter, D.W., Moore III, B., Vorosmarty C.J., and A.L. Schloss, 1993: Global climate change and terrestrial net primary production, *Nature, 363*, 234-240.

Memeveau, C., 1991: Analysis of turbulence in the orthogonal wavelet representation, *J. Fluid Mech. 232,* 469-520.

Mitic, C.M., Schuepp, P.H., Desjardins, R.L., and I.J. MacPherson, 1995: Spatial distribution and co-occurrence of surface-atmosphere energy and gas exchange processes over the CODE grid site, *Atmos. Environ., 29, (21),* 3169-3180.

Mitic, C.M., Schuepp, P.H., Desjardins, R.L., and J.I. MacPherson, 1997: Flux association in coherent structures transporting CO_2, H_2O, heat and ozone over the CODE grid site, *Agri. and Forest Meteorol, 87*, 27-39.

Mitic, C.M., Massman, W.J., Schuepp, P.H., and J.L. Collett (Jr), 1999: Structural Analysis and flux associations of CO_2, H_2O, heat and ozone over cotton and grape canopies, *Atmos. Environ., 33, 1159-1173.*

Moore, C.E., Fitzjarrald, D.R., and J.A. Ritter, 1993: How well can regional fluxes be derived from smaller scale estimates?, *J. Geophys. Res., 98,* 7177-7198.

Moore, K.E., Fitzjarrald, D.R., Sakai, R.K., and J.M Freedman, 1996: Partitioning latent heat flux between tree and understory components in temperature deciduous and boreal forest, *Proceedings of the 22nd Conference on*

Agricultural and Forest Meteorology, pp 21-23, Amer. Meteorol. Soc., Boston, Mass.

Ogunjemiyo, S.O., Schuepp, P.H., MacPherson,J.I., and R.L. Desjardins, 1997: Analysis of flux maps vs. Surface characteristics from Twin Otter grid flights in BOREAS 1994, *J. Geophys. Res., 102 , (D24)*, 29,135 - 29,145.

Oncley, S.P., Lenchow, D.H., Campos, T.L., Davies, K.J., and J. Mann, 1997: Regional-scale surface flux observations across the boreal forest during BOREAS, *J. Geophys. Res., 102, (D24),* 29,147-29,154.

Pattey, E., Desjardins, R.L., and G. St-Amour, 1997: Mass and energy exchanges over a black spruce forest during key periods od BOREAS 1994, *J. Geophys. Res., 102, (D24),* 28,967-28,975.

Paw U, K.T., Qiu, J., Su, H-B., Watanabe, T., and Y. Brunet, 1995: Surface renewal analysis: a new method to obtain scalar fluxes, *Agri. and Forest Meteorol., 74*, 119-137

Pederson, J.R., Massman, W.J., Mahrt, L., Delany, A., Oncley, S., Den Hartog, G., Neumann, H.H., Mickle, R.E., Shaw, R.H., Paw U, K.T., Grantz, D.A., MacPherson, J.I., Desjardins, R., Schuepp, P.H., Pearson Jr, R., and T.E.

Arcado, 1995: California Ozone Deposition Experiment: Methods, results and opportunities. *Atmos. Environ., 29, (21)*, 3115-3132.

Pierce L.L., and R.G. Conglaton, 1988: A method for mapping forest latent heat flux densities using remote sensing, *Remote Sens. Environ., 24,* 405-418.

Potter, C.S., Randerson, J.T., Field, C.B., Matson, P.M., Vitousek, P.M., Mooney, H.A. and S.A Klooster, 1993: Terrestrial ecosystem production: a process model based on global satellite and surface data, *Global Biogeochem. Cycles, 7*, 811-841.

Powell, D.C., and C.E. Elderkin, 1974: An investigation of the application of Taylor's hypothesis to atmosphere boundary layer turbulence, *J. Atmos. Sc., 31,* 990-1002.

Price, J.C., 1982: On the use of satellite data to infer surface fluxes at meteorological scales, *J. Applied Meteorol., 21, (8)*, 1111-1122.

Raupach, M.R., Finnigan, J.J., and Y. Brunet, 1996: Coherent eddies and turbulence in vegetation canopies: The Mixing-Layer Analogy, *Boundary-Layer Meteorol., 78*, 351-382.

Rochette, P., Desjardins, R.L., Patty, E. and R. Lessard, 1994: Crop net carbon dioxide exchange rate and radiation use efficiency in soybean, *J. Agron., 87, 22-28.*

Ruimy, A., Kergoat, L., Field, C., and B. Saugier, 1996: The use of CO_2 flux measurements in models of the global terrestrial carbon budget, *Global Change Biology, 2,* 287-290.

Running, S.W., Nemani, R.R., Peterson, D.L., Band, L.E., Potts, D.F., Pierce, L., and M.A. Spanner, 1989: Mapping regional forest evapotranspiration and photosynthesis by coupling satellite data with ecosystem models, *Ecology, 70,* 1090-1101.

Saucier, A., Duncan, M.R. and G.L. Austin, 1991. Mean flux estimation and cospectra of airborne carbon dioxide and water vapour eddy flux measurements in the planetary boundary surface layer. *Boundary-Layer Meteorol.*, 55,: 227-254.

Schuepp, P.H., Desjardins, R.L., MacPherson, J.I., Boisvert, J., and L.B. Austin, 1987; Airborne determination of regional water use efficiency and evapotranspiration: present capabilities and initial field tests. *Agri. and Forest Meteorol., 41*, 1-19

Schuepp, P.H., MacPherson, J.I., and R.L. Desjardins, 1992; Adjustment of footprint correction for airborne flux mapping over the FIFE site. *J. Geophys. Res., 97, (D17)*, 18455-18466.

Sellers, P., Hall, F., Margolis, H., Kelly B., Baldocchi, D., den Hartog, G., Cihlar, J., Ryan, M.G., Goodison, B., Crill, P., Ranson, K.J., Lettermaier, D., and D.E. Wickland, 1995: The Boreal Ecosystem-Atmosphere Study (BOREAS): An overview and early results of the 1994 field year, *Bull. Amer. Meteorol. Soc., 76, (9)*, 1549-1577

Sellers, P., Hall, F., Kelly R.D., Black , A., Baldocchi, D., Berry, J., Ryan, M., Ranson, K., Crill, P.M., Lettermaier, D.P., Margolis, H., Cihlar, J., Newcomer, J., Fitzjarrald, D., Jarvis, P.G., Gower, S.T., Halliwell, D., Williams, D., Goodison, B., Wickland, D.E., and F.E. Guertin, 1997: BOREAS in 1997: Experiment overview, scientific results and future directions, *J. Geophys. Res., 102, (D24)*, 28,731-28,769.

Shaw, R.H., 1985. On diffusive and dispersive fluxes in forest canopies In: The Forest Atmosphere Interaction. Reidel Publ., Dordrecht, pp. 407-419.

Stull, Roland B. 1988: *An Introduction to Boundary Layer Meteorology,* Kluwer Academic Press, Dordrecht, The Netherlands, 666 pp.

Sud, Y.C., Shukla, J., and Y. Mintz, 1988: Influence of land surface roughness on atmospheric circulation and rainfall. A simulation with a general circulation model, *J. Applied Meteorol., 27,* 1036-1054

Taylor, G.I., 1938: The Spectrum of Turbulence, *Proc. R. Soc., A164*, 476-490.

Valentini, R., De Angelis, P., Matteucci, G., Monaco, R., Dore, S., and G.E. Scarascia Mugnozza, 1996: Seasonal net carbon dioxide exchange of a beech forest with the atmosphere, *Global Change Biology, 2,* 199-207

Verma, S.B., Baldocchi, D.D., Anderson, D.E., Matt, D.R. and R.E. Clement, 1986: Eddy fluxes of CO_2, water vapour and sensible heat over a deciduous forest, *Boundary-Layer Moteorol., 36*, 71-91.

Verma, S.B., Kim, J., and R.J. Clement, 1992: Momentum, Water Vapour, and Carbon Dioxide Exchange at a Centrally Located Prairie Site during FIFE, *J. Geophys. Res., 97, (D17),* 18,621-18,639.

Vidale, P.L., Pielke Sr., R.A., Steyaert, L.T., and A. Barr, 1997: Case study modelling of turbulent and mesoscale fluxes over BOREAS region, *J. Geophys. Res. 102, (D24)*, 29,167-29,188.

Wollenweber, Gabriel C., 1995: Influence of fine scale vegetation distribution on surface energy partition, *Agri. and Forest Meteorol., 77,* 225-240

Wyngaard, J.C. 1983: Lectures on the planetary boundary layer. In: D.K. Lilly and T. Gal-Chen (eds.) *Mesoscale Meteorology Theories, Observations and Models*. Reidel Publ., Dordrecht, pp. 603-650 and pp. 216-224

APPENDIX 1 : Reprints

Reprinted from

AGRICULTURAL AND FOREST METEOROLOGY

An International Journal

Agricultural and Forest Meteorology 87 (1997) 27–39

Flux association in coherent structures transporting CO_2, H_2O, heat and ozone over the code grid site

Constance M. Mitic [a,*], Peter H. Schuepp [a], Raymond L. Desjardins [b], Ian J. Macpherson [c]

[a] *Department of Natural Resource Sciences, McGill University, Macdonald Campus, Ste-Anne-de-Bellevue, Que., H9X 3V9, Canada*
[b] *Centre for Land and Biological Resources Research, Agriculture Canada, Ottawa, Ont., Canada*
[c] *Institute for Aerospace Research, National Research Council of Canada, Ottawa, Ont., Canada*

Received 27 February 1996; accepted 1 November 1996

ELSEVIER

AGRICULTURAL AND FOREST METEOROLOGY

Scope of the journal
Agricultural and Forest Meteorology is an international journal for the publication of original articles and reviews on the inter-relationship between meteorology and the fields of plant, animal and soil sciences, ecology, and biogeochemistry. Emphasis is on basic and applied scientific research relevant to practical problems in agriculture, forestry, and natural ecosystems. Articles must appeal to an international audience. Theoretical models should be tested against experimental data. Special issues devoted to single topics are also published. Typical topics include canopy micrometeorology (e.g., the characterization of radiative transfer, turbulence, evapotranspiration, and the exchange of trace gases and energy within and above managed and natural ecosystems), aerobiology (e.g., the dispersion of pollen, pathogens, insects, and pesticides), biometeorology (e.g., the effect of weather and climate on plant distribution, crop yield, water-use efficiency, phenology of plant and animal development, and the energy balance of animals), forest-fire/weather interactions and the role of vegetation on climate and weather.

Publication schedule and subscription information
Agricultural and Forest Meteorology (ISSN 0168-1932). For 1997 volumes 83–87 are scheduled for publication. Subscription prices are available upon request from the Publisher. Subscriptions are accepted on a prepaid basis only and are entered on a calendar year basis. Issues are sent by surface mail except to the following countries where air delivery via SAL mail is ensured: Argentina, Australia, Brazil, Canada, Hong Kong, India, Israel, Japan, Malaysia, Mexico, New Zealand, Pakistan, PR China, Singapore, South Africa, South Korea, Taiwan, Thailand, USA. For all other countries airmail rates are available upon request. Claims for missing issues must be made within six months of our publication (mailing) date.
Orders, claims and product enquiries: please contact the Customer Support Department at the Regional Sales Office nearest you:
New York, Elsevier Science, P.O. Box 945, New York, NY 10159-0945, USA. Tel: (+1) 212-633-3730, [Toll free number for North American customers: 1-888-4ES-INFO (437-4636)], Fax: (+1) 212-633-3680, E-mail: usinfo-f@elsevier.com
Amsterdam, Elsevier Science, P.O. Box 211, 1000 AE Amsterdam, The Netherlands. Tel: (+31) 20-485-3757, Fax: (+31) 20-485-3432, E-mail: nlinfo-f@elsevier.nl
Tokyo, Elsevier Science, 9-15, Higashi-Azabu 1-chome, Minato-ku, Tokyo 106, Japan. Tel: (+81) 3-5561-5032, Fax: (+81) 3-5561-5045, E-mail: kyi04035@niftyserve.or.jp
Singapore, Elsevier Science, No. 1 Temasek Avenue, #17-01 Millenia Tower, Singapore 039192. Tel: (+65) 434-3727, Fax: (+65) 337-2230, E-mail: asiainfo@elsevier.com.sg

Back volumes. Orders and information requests should be addressed to Elsevier Science B.V., Journals Department, P.O. Box 211, 1000 AE Amsterdam, Netherlands. Back volumes are available on microfilm. Orders and information requests concerning back volumes on microfilm should be addressed exclusively to: Elsevier Science Inc., Journal Information Center, 655 Avenue of the Americas, New York, NY 10010, USA.
US mailing notice – *Agricultural and Forest Meteorology* (ISSN 0168-1923) is published monthly except August and October by Elsevier Science B.V. (Molenwerf 1, Postbus 211, 1000 AE Amsterdam). Annual subscription price in the USA US$1620.00 (valid in North, Central and South America only), including air speed delivery. Application to mail at second class postage rate is pending at Jamaica, NY 11431.
USA POSTMASTERS: Send address changes to *Agricultural and Forest Meteorology* Publications Expediting, Inc., 200 Meacham Avenue, Elmont, NY 11003. **AIRFREIGHT AND MAILING** in the USA by Publications Expediting Inc., 200 Meacham Avenue, Elmont, NY 11003.

ELSEVIER

Agricultural and Forest Meteorology 87 (1997) 27–39

AGRICULTURAL AND FOREST METEOROLOGY

Flux association in coherent structures transporting CO_2, H_2O, heat and ozone over the code grid site

Constance M. Mitic [a,*], Peter H. Schuepp [a], Raymond L. Desjardins [b], Ian J. Macpherson [c]

[a] *Department of Natural Resource Sciences, McGill University, Macdonald Campus, Ste-Anne-de-Bellevue, Que., H9X 3V9, Canada*
[b] *Centre for Land and Biological Resources Research, Agriculture Canada, Ottawa, Ont., Canada*
[c] *Institute for Aerospace Research, National Research Council of Canada, Ottawa, Ont., Canada*

Received 27 February 1996; accepted 1 November 1996

Abstract

Aircraft-based eddy correlation flux data obtained at a height of 30 m above irrigated and non-irrigated agricultural land in southern California have been analyzed in terms of the coherent structures that dominate the turbulent exchange of energy and gases during daytime conditions. The analysis focused on transport of sensible heat, moisture, carbon dioxide and ozone in the gradient modes, i.e. excess up or deficit down for heat and moisture, and deficit up or excess down for carbon dioxide and ozone. Results are presented for composition and size of the dominant structures, over water-stressed and non-water-stressed surfaces, and on the relative frequency with which structures carrying only a single scalar, or given combinations of scalars, were encountered along the flight paths. Interpretation of results provides further evidence for the existence of a second (non-physiological) sink for ozone. The relative preponderance of structures that carry moisture, carbon dioxide and ozone simultaneously, particularly in the gradient up mode, reflects the importance of vegetation as co-located source/sink for these scalars. Surface characteristics resulting in thermal buoyancy and water vapour density gradients appears to be responsible for about 85% of gradient up transport. Finally, the detrending procedures described here may help to define more effective separation between local and mesoscale events in biosphere–atmosphere interactions. © 1997 Elsevier Science B.V.

Keywords: Coherent structures; Ozone; Sensible heat; Carbon dioxide

1. Introduction

The growing interest in land surface climatology, and in particular the potential assessment of biosphere–atmosphere exchange processes from remote sensing observations of the surface, has led to increased use of aircraft for regional observation of fluxes of heat, moisture and trace gases (e.g. Lenschow, 1986; Desjardins and MacPherson, 1989). Such studies usually try to relate flux estimates to characteristics of — and processes at — the underlying surface (Austin et al., 1987; Schuepp et al., 1987;

* Corresponding author.

PII S0168-1923(97)00004-X

Mack et al., 1990; Desjardins et al., 1992b; Mahrt et al., 1994; Desjardins et al., 1995; Guo et al., 1995a). However, the various driving forces responsible for the transport of scalars are not easily distinguishable over heterogeneous terrain. Only a few studies have specifically related the coherent structures, which are responsible for the bulk of turbulent transport, to surface characteristics (Caramori et al., 1994; Mitic et al., 1995), although they have been examined from various other perspectives (e.g. Wyngaard, 1983; Eloranta and Forrest, 1992; Mahrt and Ek, 1993a,b). A study of coherent turbulent structures allows for the improvement of our understanding of the processes operating on surface fluxes, and of the degree to which various fluxes are associated with each other and with the underlying sources and sinks at the surface (Mitic et al., 1995). Identifying the physical extent of structures and their composition, will give some indication of the driving forces (defined as the primary factors or processes initiating transport) operating on flux transport as well as of how they are partitioned between the surface and the atmosphere. In our study, flux associations of CO_2, H_2O, heat and ozone are examined for the two gradient modes of transport, where the surface acts as a sink for CO_2 and ozone, and as a source for H_2O and sensible heat.

1.1. Data collection and site description

The data used in this study were collected by the Twin Otter research aircraft of the National Research Council of Canada during the California Ozone Deposition Experiment (CODE) in 1991. The primary objective of CODE was to make observations that will improve our understanding of ozone uptake at the surface and therefore improve estimates made by regional photochemical models of ozone deposition. A detailed account of CODE is given in Pederson et al. (1995). There were an extensive number of data sampling flights during the field campaign. Two of these were grid patterns (flight number 16 on 26 July and flight number 21 on 2 August) and form the database for our study. The grid areas covered 15 × 15 km of agricultural fields, consisting primarily of irrigated cotton, non-irrigated fields and senescent safflower. The diagonal corners of the grids are defined at 36.083°N/119.696°W and 35.940°N/119.869°W, located in Kings County of the San Joaquin Valley of southern California. Each grid flight consisted of 22 parallel runs, flown 30 m above the surface in an E–W direction, with an offset of 0.75 km in the N–S direction. Given the overall offset of 0.375 km in the N–S direction between the two grids, the "combined grid" (incorporating both flights) represents a set of 44 evenly spaced, parallel flight trajectories, with a spacing of 0.375 km between the lines. Wind direction was from the north, perpendicular to the grid lines (345° and 23° for flights 16 and 21, respectively). Recorded flight times for the grids are from 1136 to 1457 hours PDT (Flt 16) and 1239 to 1553 hours PDT (Flt 21). Using an eddy correlation system, flux data were digitized at 16 Hz, with an effective data point separation of 3.75 m at an average flying speed of 60 m s^{-1}.

On both days of observation the sky was clear, with average incident short-wave radiation of 892 W m^{-2} (Flt 16) and 863 W m^{-2} (Flt 21). Thermal stratification was unstable for both days, with median $z/L \approx -4.9$ and -4.1 (where $z = 30$ m), and CBL tops at 549 and 701 m, respectively, as determined from aircraft-based soundings of temperature and moisture to above the capping inversion layer. A detailed description of the aircraft instrumentation and the flight summary of operations during CODE are given in MacPherson et al. (1995).

2. Data analysis

The eddy correlation technique derives flux estimates from the covariance between fluctuations of vertical wind (w') and scalar admixtures (c'). Implicit in the procedure is the need for a realistic definition of the mean, that does not artificially cluster the resulting modes of flux transport and removes trends that may be present in the data. A linear trend over the grid site might represent mesoscale transports with spatial scales far exceeding the dimensions of the site, which would not be directly linked to characteristics of the immediate underlying surface. A nonlinear trend of single or multiple cycles over the grid site may represent smaller mesoscale flux related to the heterogeneous nature and scales of the surface characteristics. It is therefore necessary to select a detrending technique that not only accurately defines the mean, but also achieves the most effective filtering of mesoscale events from the local flux.

In an attempt to satisfy the conditions stated above, both linear and nonlinear detrending were applied to heat, the scalar admixtures (CO_2, H_2O and O_3) and the vertical wind component. The linear detrending was in the form of a simple linear regression, and a truncated Fourier series was used to remove nonlinear trends. Quadrant analysis (e.g. Antonia, 1981; Shaw, 1985; Grant et al., 1986) coupled with the eddy correlation technique was used to determine the different modes of transport, defined as excess/deficit up and excess/deficit down. The procedure used to determine the mean of the data vector for optimum separation of local and mesoscale fluxes is described below.

2.1. Definition of mean and separation of local events

The net local flux estimate was calculated using fluctuations against a mean defined from linear detrending as well as from running means defined by Fourier series truncated at the second, third and consecutively higher terms. In the case of nonlinear detrending, mesoscale flux estimates were derived from the low-frequency oscillations filtered from the scalar concentration and vertical wind fields. The procedure, illustrated in Fig. 1 for actual data of vertical wind (w) and CO_2 (c), is based on the decomposition of the flux into large area averages, represented by the means in Fig. 1(c,d), as opposed to the running (local) means represented by c^* and w^*. Instantaneous fluctuations (w' and c') are defined against the local means (Fig. 1a,b), which may

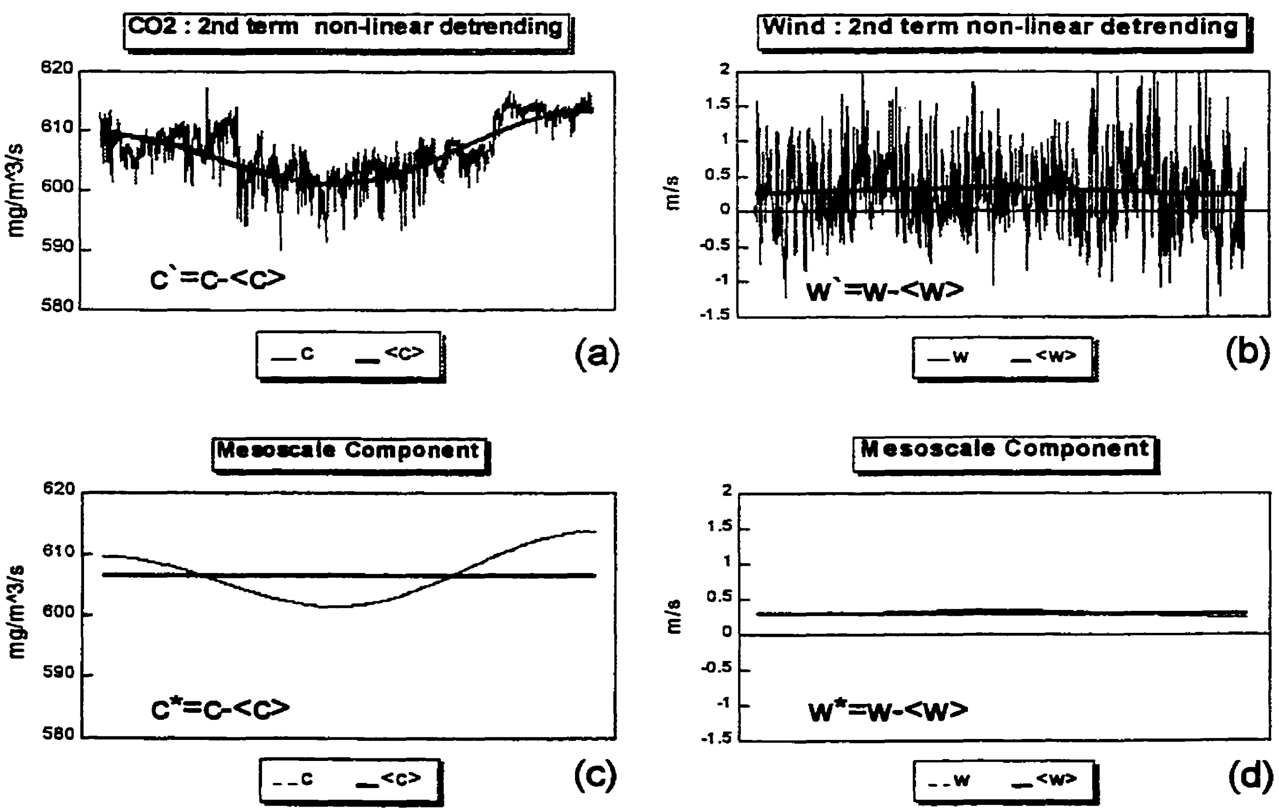

Fig. 1. Illustration of the definition of local flux (a,b) and mesoscale flux (c,d) by nonlinear detrending.

be variable due to mesoscale "events". Considering this Reynolds-type expansion into means and fluctuations, and the fact that $\langle c' \rangle$ and $\langle c^* \rangle$ (or $\langle w' \rangle$ and $\langle w^* \rangle$) vanish by definition, the instantaneous area-averaged vertical flux F_A, observed at height h over area A at time t, is then given by

$$F_A = \frac{1}{A} \int_A w(x,y,h,t)\, c(x,y,h,t)\, \mathrm{d}x\, \mathrm{d}y$$

$$= \langle w \rangle \langle c \rangle + \langle c^* w^* \rangle + \langle c' w' \rangle \qquad (1)$$

where area averaging $\langle\ \rangle$ is approximated by time-averaging in the moving frame of reference of the aircraft. This expression reduces to $F_A = \langle c^* w^* \rangle + \langle c' w' \rangle$ in the case of $\langle w \rangle = 0$, which is a reasonable assumption for large, flat terrain such as the San Joaquin Valley, i.e. into the sum of "mesoscale flux" ($\langle c^* w^* \rangle$) and "local flux" ($\langle c' w' \rangle$).

The mode of transport of the net mesoscale flux at each truncation level in the Fourier series is identified as either gradient or counter gradient. As commonly defined in quadrant analysis (Antonia, 1981), gradient modes for upward transport of scalars from the surface, such as heat or moisture under daytime conditions, associate upward (positive) excursions of vertical wind with positive excursions of scalar concentration, and downward gusts with negative scalar fluctuations ("deficit down"). Conversely, gradient modes for flux of scalars towards the surface, such

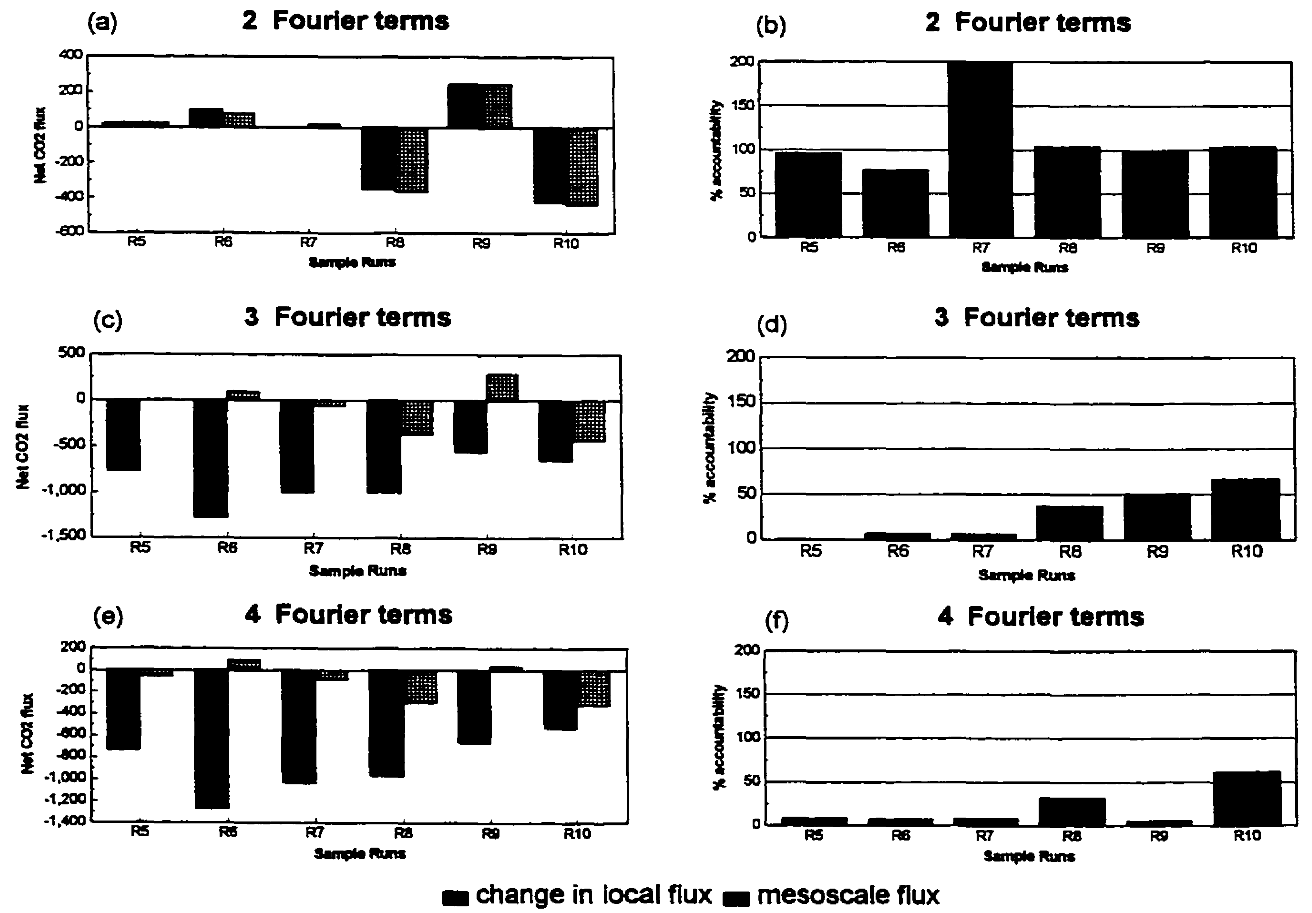

Fig. 2. (a,c,e) Changes in the net local flux and the corresponding net mesoscale flux for CO_2 along six sample runs form grid 16. (b,d,f) the mesoscale accountability for the changes in the local flux as a result of higher-order filtering. Flux estimates are cumulative contributions along the run as a measure of the net flux (in units of mg m^{-2} s^{-1}).

as CO_2 or ozone, would be associated with deficit up or excess down. In other words, a contribution in the gradient mode increases the flux estimate in the direction expected on the basis of the scalar gradient, so that elimination (filtering) of net gradient mesoscale components by nonlinear detrending should reduce the local flux estimate, while filtering of net counter gradient mesoscale flux should enhance it. The change in the net local flux (NLF) estimate with consecutively higher levels of filtering should, therefore, be consistent with the net transport mode of the filtered net mesoscale flux (NMF), and reflected in the magnitude of the NMF estimate. We selected detrending levels on the basis of "accountability", defined as the percent change in the net local flux accounted for by the filtered mesoscale flux, as described below.

2.2. Selection of detrending technique

Several criteria were used for the selection of the Fourier series truncation level in the presence of mesoscale flux contributions.

Linear detrending was used where: (a) the change in the net local flux (NLF) estimate derived from nonlinear detrending was negligible ($< 4\%$) and mesoscale accountability for this small change either approximates 0 or exceeds 150%; (b) the change in the NLF estimate was non-negligible ($> 4\%$), but the mesoscale flux remained approximately 0 for increasing Fourier terms; or (c) the direction of change (increase or reduction) in the net local flux estimate was inconsistent with the net transport mode of the mesoscale flux estimate, and where this inconsistency persisted or was exaggerated at consecutively higher levels of the Fourier series. The definition of negligible change (4%), represents one-fifth of the maximum observed change in the NLF estimate, which was 20%.

For *nonlinear detrending*, the Fourier series truncation level was selected as follows. (a) A two-term truncation was selected if the direction of change in the local flux estimate was consistent with the transport mode of the mesoscale flux; the mesoscale accountability was between 50% and 150%, and inclusion of two consecutively higher terms in the series did not alter these results. (b) Higher-level truncation of the Fourier series was selected if the direction of change in the net local flux was inconsistent with the transport mode of the mesoscale flux at one level, but the inconsistency was corrected by the inclusion of a higher Fourier term, with mesoscale accountability between 50% and 150%. (c) Higher-level truncation of the Fourier series was also selected if the direction of change in the net local flux estimate was consistent with the transport mode of the mesoscale flux, but mesoscale accountability (while maintaining directional consistency with inclusion of higher terms) moved closer to the 100% ideal. Graphs (a), (c) and (e) in Fig. 2 show the changes in the NLF estimates and the corresponding net mesoscale flux (NMF) estimates of CO_2 for six different runs from grid 16, with gradient flux for CO_2 resulting in negative flux. Graphs (b), (d) and (f) in Fig. 2 indicate the degree to which the mesoscale flux accounts for the changes in the local flux estimates. In the cases shown, a two-term truncation level of nonlinear detrending was selected for runs 5, 6, 8, 9 and 10, where the transport mode as well as the magnitudes of the mesoscale flux account for the changes in the local flux estimates as a result of filtering. Linear detrending was used for run 7.

2.3. Structural analysis

Following a similar procedure used by Mitic et al. (1995), based on Duncan and Schuepp (1992) and Caramori et al. (1994), a series of analytical steps were taken to identify the structures that dominate turbulent transport. These "coherent" structures are defined as a set of correlated flux signals (w and c excursions) in time and space which are distinctly different and interspersed between less coherent components.

In order to separate these structures from incoherent noise, a hyperbolic hole corresponding to 0.2 rms was imposed on the scatter plot of c' versus w' excursions, prior to structure definition. This is consistent with similar methods used by Antonia (1981); Shaw (1985), Grant et al. (1986), Caramori et al. (1994) and Mitic et al. (1995) to remove weak signals that may be positioned at the tails of structures.

Structures are identified by a series of eight or more consecutive pairs of w' and c' excursions (corresponding to ~ 30 m in spatial extent) within the same mode of transport (excess up/down, deficit up/down). This minimum spatial scale is consistent with cospectral analysis of Twin Otter data at the flight level, which suggest that scales less than 30 m do not contribute significantly to the flux (Saucier et al., 1991; Desjardins et al., 1992a,b). The potential fragmentation resulting from inclusion of unmixed parcels of air was corrected by a defragmentation procedure as used by Mitic et al. (1995). A threshold based on a quadratic measure of the flux contribution from each structure (for details, see Duncan and Schuepp, 1992; Caramori et al., 1994; Mitic et al., 1995), was then imposed to eliminated the weak structures and retained only the extreme events which generally occupy 20% of the time domain of the run but contribute about 80% of the overall flux. These may be expected to present the clearest picture of interactions among flux variables and the surface.

2.4. Coincidence analysis

Structural analysis defines the physical locations (positions along the flight track) of structures separately for each scalar. These separately defined structures, termed *substructures* for the purpose of discussion, may physically overlap. Coincidence analysis attempts to reconstruct the size (along the flight line) of these structures and define their composition in terms of what scalars they are simultaneously transporting.

According to our concept, overlapping substructures were considered part of a main structure whose dimensions are defined by the outer limits of the overlapping substructures, from the beginning of the first substructure to the end of the last substructure within the overlap, and whose composition is given by the combined composition of the substructures. If one or more substructure were embedded in a larger one, the same rule for composition applied, with the size of the resulting structure defined by the extent of the larger substructure. It was expected that linking these reconstructed structures to the underlying surface would give insight into the co-location of sources and sinks, the degree to which driving forces are partitioned between the surface and the atmosphere, and a qualitative appreciation of the degree of mixing that occurs within coherent structures.

Association between fluxes was defined in two ways: (a) as a ratio (or percentage) of the number of structures with a particular composition to the total number of structures transporting a particular scalar, and (b) as a ratio of the number of structures with a particular composition to the total number of structures defined across the grid site. This is an adaptation to the Jaccard coefficient used by Mitic et al. (1995), which defined flux associations based only on the coincidence of two scalars. The modifications applied in this study eliminate ambiguity of flux associations in cases where structures simultaneously transport more than two scalars. The flux associations for the various combination of scalars are mutually exclusive and expressed as

$$F_{\mathrm{A}} = \frac{C_{i,j,k,l}}{N_x - \Sigma\, mp} \tag{2}$$

where $C_{i,j,k,l}$ is the number of coherent structures with the composition of scalars i, j, k, l, or any combination of one, two or three of them as may be relevant; N_x is the total number of substructures for the scalar x (either i, j, k or l), or for the overall grid site; mp is the number of sub-structures for x in excess of one, that is incorporated in any one coherent structure, so that $N_x - \Sigma\, mp$ is the total number of reconstructed structures.

3. Results and discussion

In the combined grids (44 grid lines for each scalar), linear detrending was selected in 19% of the cases, based on the criteria outlined in Section 2.2. A second-term Fourier series truncation level accounted for 53%, third-order truncation for 24%, and fourth-order for 3% of the cases. In only four cases (2.2%) were there unresolved inconsistencies in the direction of change of the net local flux and the net transport mode of the mesoscale flux. The thresholding procedures outlined in Section 2.3 resulted in an average reduction of approximately 20% in the flux estimates, as expected, indicating that 80% of the flux is transported by the dominant coherent structures.

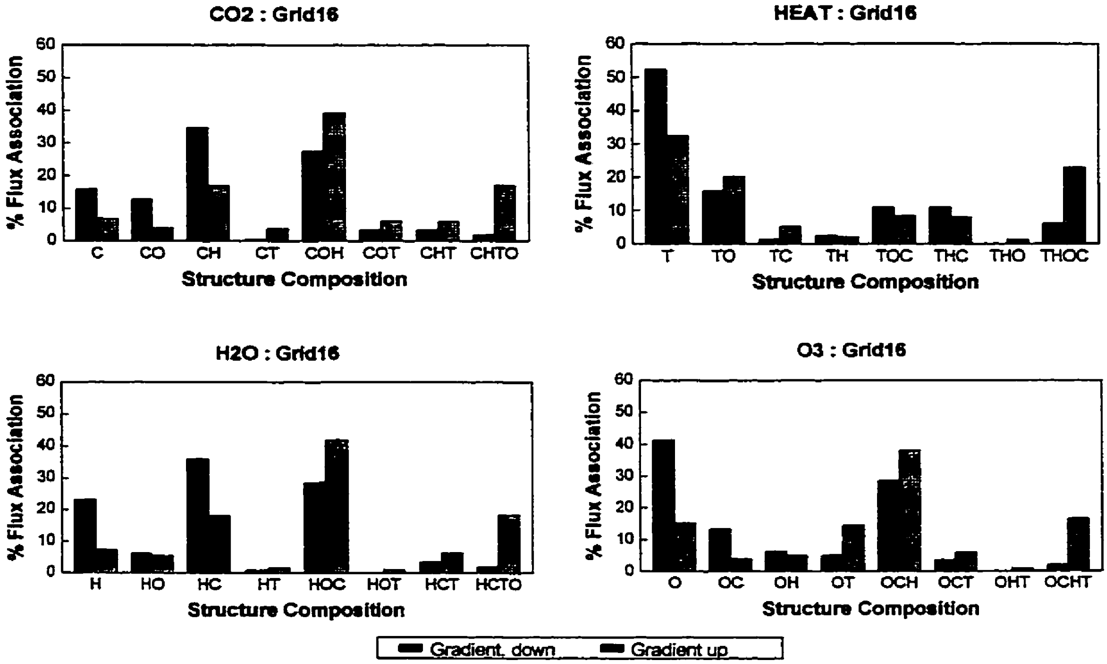

Fig. 3. Flux associations for grid 16, calculated as functions of the total number of structures that transport each variable. C, T, H and O denote CO_2, heat (temperature), H_2O and O_3, respectively, and combinations of these letters represent structures that contain the associated scalars.

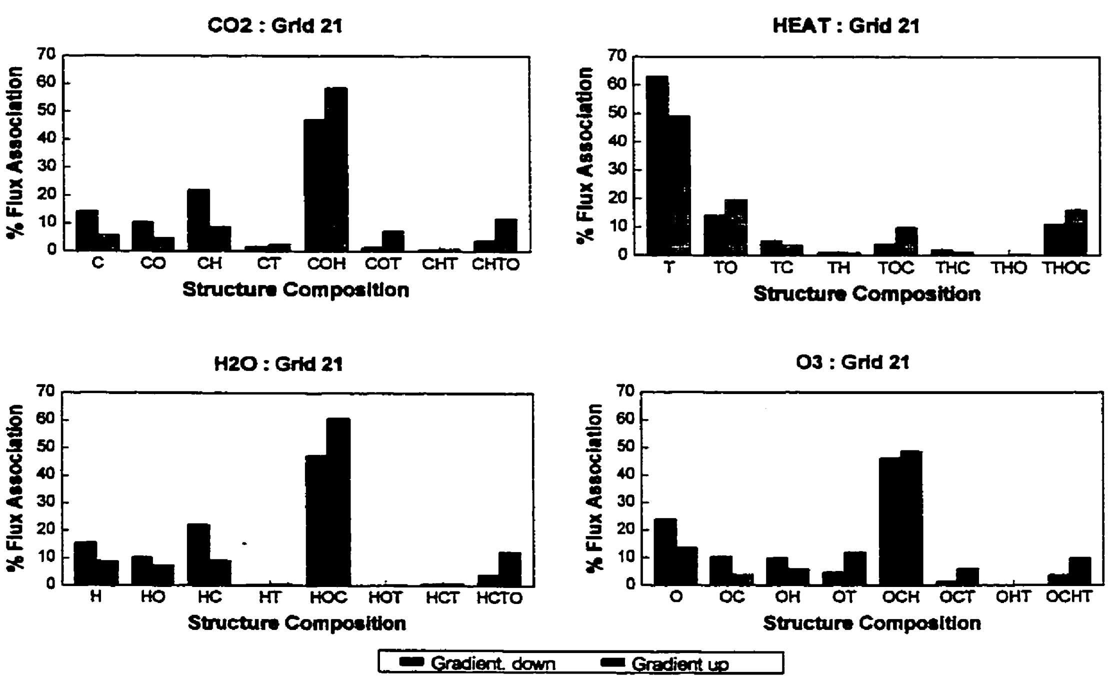

Fig. 4. Flux associations for grid 21, calculated as a function of the total number of structures which transport each variable.

3.1. Flux association in the gradient modes

Flux associations for the two gradient modes are shown in Figs. 3–5. Figs. 3 and 4 show the flux association calculated as a function of the total number of structures transporting the individual scalars (CO_2, H_2O, heat and O_3 are denoted by C, H, T and O, respectively, in the designation of combined structures) for grid flights 16 and 21. Fig. 5 shows the flux association as a function of the total number of structures identified within the grid. The following observations are apparent in Fig. 3 (Flt 16): Among the structures transporting CO_2, the dominant associations for structures moving toward the surface (gradient down) are with H_2O and with structures carrying both H_2O and ozone (H–O). For the gradient up mode, flux association of CO_2 with H–O dominates. In both gradient modes the majority of structures transporting heat are not associated with other fluxes. H_2O shows a similar pattern of flux association as CO_2, with dominant flux association to CO_2 as well as to the C–O combination, as expected. In the gradient down mode, the dominant proportion of ozone structures is not associated with other fluxes (41%) [1] with a 29% association to CO_2 and H_2O, while in the gradient up mode O_3 association to CO_2 and H_2O dominates (38%). The flux associations in Fig. 4 (Flt 21, flown two days after Flt 16), show similar relationships for both gradient down and gradient up modes, but the dominance of co-occurrence of CO_2, O_3 and H_2O in the same structure (C–O–H), and of single thermal structures, is more pronounced.

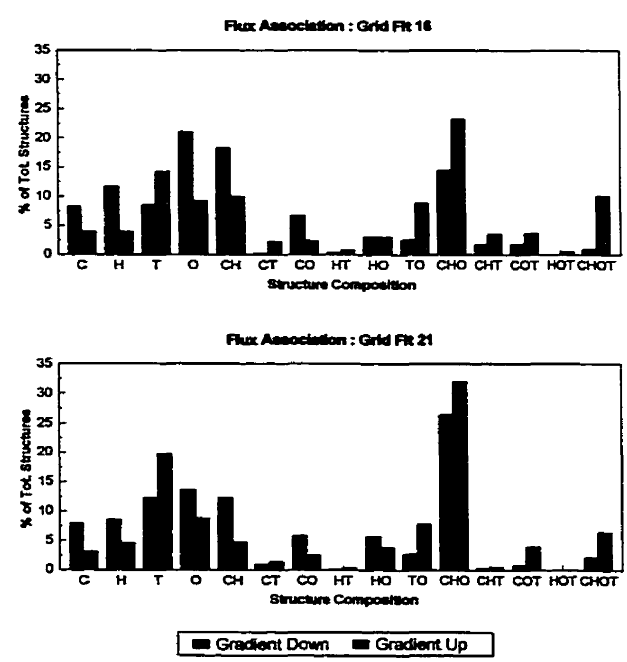

Fig. 5. Flux associations, calculated as a function of the total number of structures identified for each grid.

The relationships indicated for the individual fluxes are reflected in the flux associations calculated as functions of the total number of structures for each grid, as shown in Fig. 5. For grid 16, structures transporting only ozone, and associations of C–H–O and C–H, dominate in the gradient down mode, while the C–H–O combination dominates in the gradient up mode. For grid 21, the flux association in the gradient down mode is dominated by C–H–O, with single-component structures and C–H combinations also relatively frequent. For the gradient up mode, the dominant flux associations are with structures transporting only heat, and those transporting C–H–O. The percentage of the total number of structures without heat in its composition tends to be larger for the gradient down mode than for the gradient up mode, with the notable exception of C–H–O. This indicates that heat is more important as a driving force for transport away from the surface than towards the surface. The relative importance of structures with C–H–O composition in the gradient up mode reflects the significant role of stomatal exchange processes in vegetation for the net transport of all these scalars.

The total number of structures (by composition) for the two gradient modes for the two grids is given in Table 1. The overall ratio of structures in the gradient up mode to those in the gradient down mode is 1.34 and 1.41 for flights 16 and 21, respectively, for all scalars and combination of scalars across the grid. This indicates the importance of the surface in generating these structures. The important role of surface-generated buoyancy is shown by the fact that this ratio increases to around 2.7 for the heat

[1] Percentage figures are rounded to the nearest integer in this and the following discussion.

Table 1
Structures identified in the gradient up and gradient down modes, categorized by the fluxes they transport, for grids 16 and 21

Structure composition	Gradient down		Gradient up	
	Grid 16	Grid 21	Grid 16	Grid 21
Heat	43	63	113	171
O_3	106	70	73	76
CO_2	42	41	32	27
H_2O	59	44	32	40
O_3–heat	13	14	70	68
O_3–CO_2	34	30	19	22
O_3–H_2O	16	29	24	33
O_3–CO_2–H_2O	73	135	184	276
O_3–CO_2–H_2O–heat	5	11	80	56
Heat–CO_2	1	5	18	12
Heat–H_2O	2	1	7	3
Heat–H_2O–CO_2	9	2	28	4
Heat–H_2O–O_3	0	0	4	1
Heat–CO_2–O_3	9	4	29	34
CO_2–H_2O	92	63	79	41
Total	504	512	792	864

structures alone, and to 5.4 for all structures associated with heat. The number of structures transporting exclusively H_2O, CO_2 and O_3 (the latter in the case of Flt 16), and the number transporting C–O and C–H combinations, are larger for the gradient down mode than the gradient up mode. Structures with other compositions are larger in number for the gradient up mode.

A closer examination of the structures in the gradient up mode, i.e. away from the surface, may help to interpret the observed flux associations. Assuming that uptake of CO_2 by vegetation is the only daytime surface sink for CO_2 across the grid site, we may try to classify the surface in terms of vegetated and non-vegetated areas based on the presence or absence of CO_2 in the structure composition. We may then subdivide the vegetated areas into water-stressed and non-water stressed sub-categories based on the presence or absence of H_2O. The hierarchical classification of structures according to this scheme is shown in Fig. 6, and will be the focus of discussion in the next two paragraphs.

CO_2 flux is transported by 59% and 55% (Flts 16 and 21, respectively) of all structures in the gradient up mode. These figures are roughly comparable with the 60% land cover attributed to growing cotton within the grid area on the basis of remote sensing observations (Mitic et al., 1995). Of these structures, about 45% include either C–H or C–O combinations, while 36% include both C–O combinations and single H_2O structures. Structures with O_3 and H_2O account for 39%. Of the total CO_2 transporting structures, 21% are related to water-stressed vegetation for flight 16, and 20% for flight 21. This results in an approximate 4:1 ratio of unstressed to stressed vegetation for the overall grid. For flight 16, 49% of structures transporting CO_2 over the water-stressed portion of the canopy are associated with ozone and 71% over the unstressed portions, while the corresponding figures for flight 21 are 59% and 88%.

Grid areas that do not demonstrate the transport of CO_2 may be classified as non-vegetated (no active photosynthesis). These areas account for an average of 43% of all structures in the gradient up mode, of which 65% are associated with heat and 49% with ozone. As seen in Fig. 6, ozone is primarily associated with structures not transporting heat over these areas. For both grid flights, the vegetated areas account for the bulk of ozone uptake (43% of structures). One-quarter of structures, however, have ozone in their composition in the absence of CO_2, indicating an additional non-vegetated sink for ozone.

In the estimation of ozone uptake by vegetation, the degree of error associated with directly linking ozone uptake to stomatal conductance of moisture varies across the canopy (Massman et al., 1993). The flux associations given above, suggest variations across canopies in the simultaneous uptake of CO_2 and ozone, and the release of water vapour, and that such differences vary with variations of moisture within the canopy. This could have implications for the estimation of ozone deposition if the degree of differential water stressed conditions of the canopy, and therefore the degree of association between ozone and H_2O or ozone and CO_2 is not considered. Using stomatal conductances acquired over water-stressed portions of the canopy could underestimate ozone uptake for a canopy that is not uniformly water stressed. Our results indicate that it would be desirable to attach differential weights both to the relationship between ozone and CO_2 and ozone and H_2O in order to make more accurate estimates of ozone uptake by vegetation.

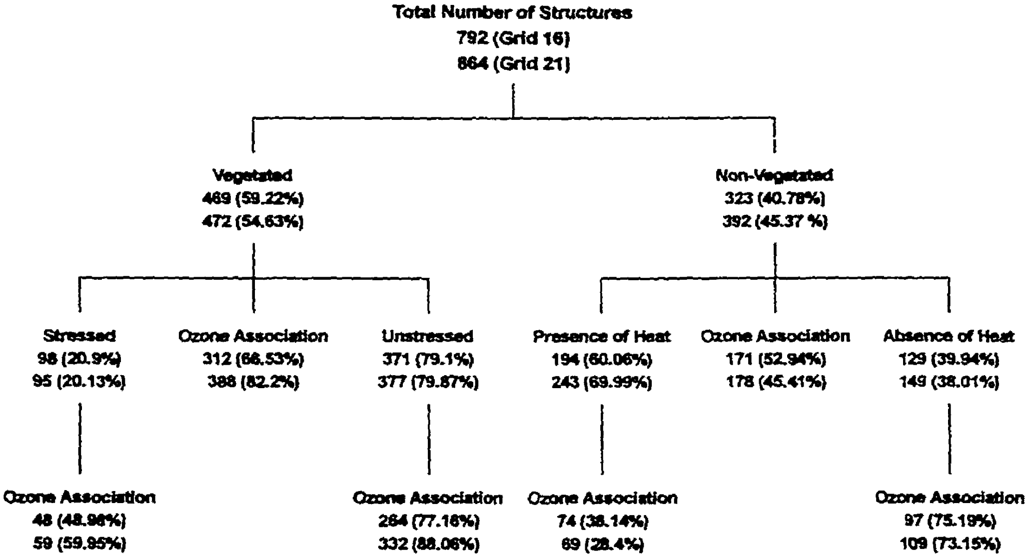

Fig. 6. Hierarchical breakdown of surface conditions based on the flux composition of structures: presence of CO_2 (vegetated); absence of H_2O in structure composition (stressed); presence of O_3 in structure composition (ozone association).

A tentative classification and interpretation of the driving forces affecting flux transport may be based on the presence/absence of H_2O and heat, i.e. on the relative importance of water vapour density gradients and thermal buoyancy. As shown in Fig. 7, water vapour as a driving force (defined as the presence of H_2O in the absence of heat) accounts for an average of 43% of the structures, which is about the same proportion (42%) as structures that contain heat. Structures transporting only ozone, CO_2, or both in association, for which shear may be assumed to be the dominant driving force, account for the remaining 15%. This distribution of the driving forces underlines the importance of the surface as the source for driving forces of vertical exchange at a height of 30 m.

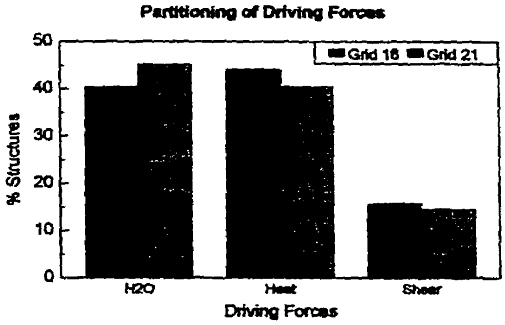

Fig. 7. Partitioning of the driving forces operating on surface fluxes, as deduced from the composition of the transporting structures.

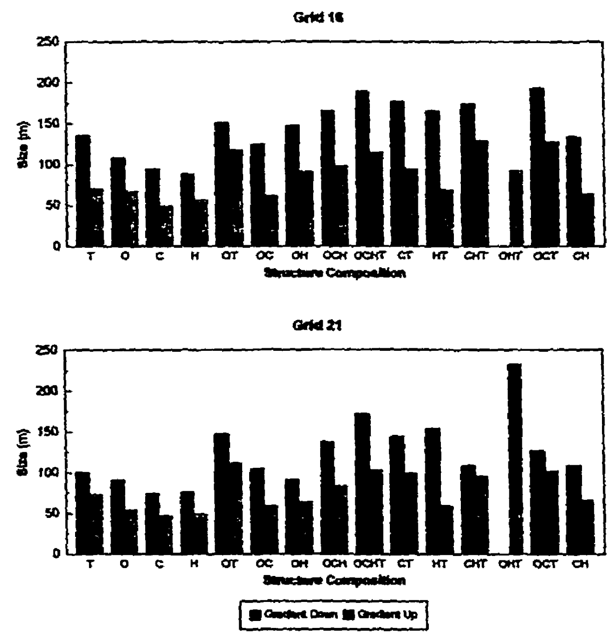

Fig. 8. Sampled horizontal dimension, as a measure of the size of structures moving towards the surface (gradient down) and away from the surface (gradient up).

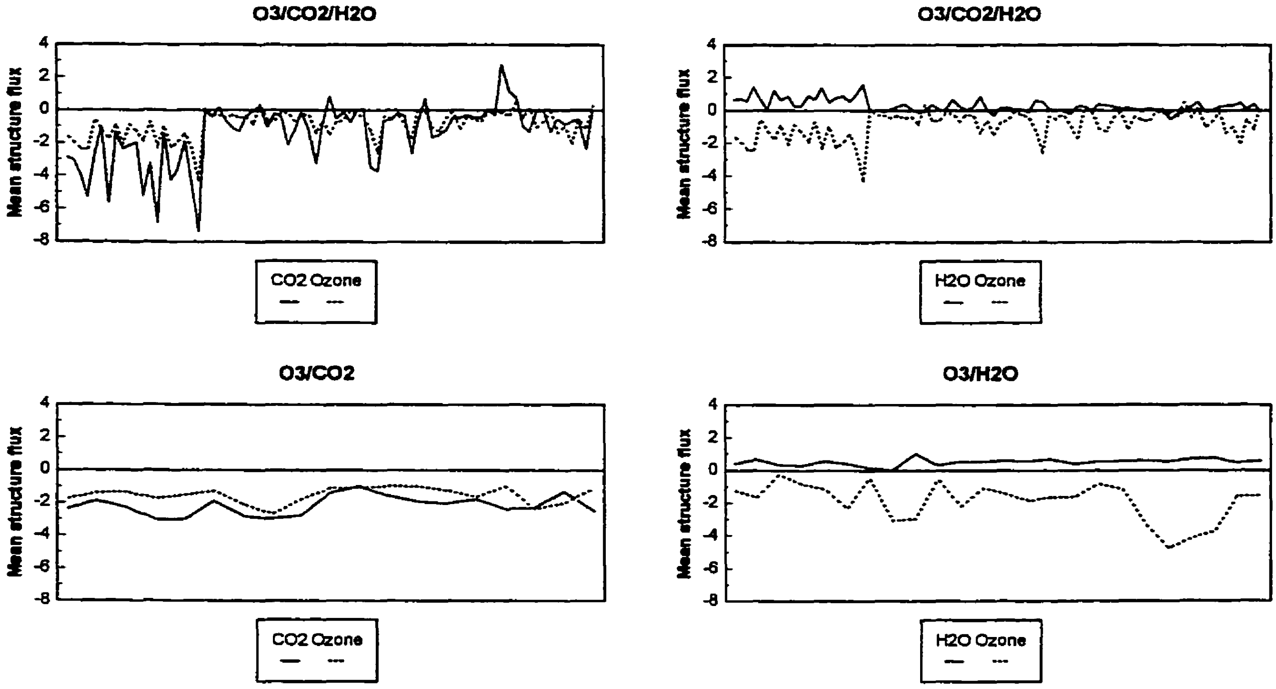

Fig. 9. Variations in the mean fluxes carried by structures of particular compositions. The x-axis represents the sequence of structures with that particular composition throughout the grid. Units of measurements are: CO_2 (mg m^{-2} s), H_2O (g m^{-2} s), O_3 (μg m^{-2} s).

3.2. Structure sizes and mean intensities

The average diameters of the structures defined by their flux composition, as determined from horizontal, one-dimensional transects, are given in Fig. 8. Not surprisingly, structures moving towards the surface (gradient down) are significantly larger than structures moving away from the surface, structures transporting a single flux variable are generally smaller than composite structures with multiple fluxes, and structures which contain heat are consistently bigger than those that do not.

The results of an examination of the flux densities carried by structures with associations of O–C–H, O–C and O–H from flight 16 are summarized in Fig. 9. For O–C–H structures, the fluxes of O_3 and CO_2 are correlated, with a low CO_2 flux corresponding to a low ozone flux, and vice versa. The same holds true for the relationship between flux densities of H_2O and O_3 in those structures, with inverse sign in the correlation, as expected. The corresponding R^2 values are 0.62 for O_3 and CO_2, 0.54 for O_3 and H_2O, and 0.89 for CO_2 and H_2O. For structures transporting only O_3 and CO_2, the relationship degrades, with an R^2 value of 0.21. Structures transporting only O_3 and H_2O have an even smaller R^2 value of 0.14. These results support the flux associations discussed earlier, where ozone, although highly associated to H_2O, has a higher association to CO_2.

4. Conclusions

The flux association of coherent structures has been shown to generate a large amount of information about the characteristics of these structures which dominate transport. Some findings from an earlier, more limited study (Mitic et al., 1995) have been confirmed, where ozone show differential degree of association to CO_2 and H_2O, indicating variations in the spatial distribution of sources and sinks within the vegetated portion of the site. The examination of the flux composition of the structures indicates that ozone is still taken up by the vegetation even under water stressed conditions. This was shown not only by the flux association values but also by the R^2 values calculated for the mean fluxes within each structure. The partitioning of ozone uptake between the vegetated and non-vegetated surface was also apparent, suggesting a second, non-physiological sink for ozone, possibly associated with destruction of ozone by NO emissions from soil (Guo et al., 1995b).

The study also showed that the driving forces for fluxes in the gradient up mode are dominated by surface forcing, through water vapour density gradients and thermal buoyancy, with a relatively much smaller percentage attributable only to shear forces. Transport in the gradient down mode is dominated by atmospheric driving forces, and structures are larger and fewer.

Although the magnitude of the mesoscale flux across the grids was quite small, the analytical scheme used to partition the local flux events from mesoscale flux was very effective. This procedure may be useful in cases where there are much larger and more dominant mesoscale motions contributing significantly to flux transport.

Further extension of this analysis, currently underway, includes ground-based tower data, both under stable and unstable conditions, over canopies with different characteristics. These studies are intended to add to our understanding of the degree of mixing that occurs as the turbulent transport structures move away from the surface, in terms of composition and size. Our analysis should be seen in the context of current attempts to define smaller-scale climate, energy and gas exchange models to be nested within boundary layer models, with increasingly realistic description of surface features, including vegetation. This raises questions as to the scales at which surface features should be parameterized, and the height above the surface where vertical transport loses its "signature" of distinct surface source and sink distributions. We hope that the study of flux associations at different heights help to link structure composition to spatial distribution patterns of surface source and sink distributions and the spectral and thematic characteristics of the surface. In this way, this study and those currently in progress may be useful to validate models of biosphere–atmosphere exchange processes, and of the mixing among scalars within near-surface structures, at increasingly finer scales.

Acknowledgements

The direct and indirect support of this project through the San Joaquin Valley Air Quality Study, the Natural Science and Engineering Research Council and the Eco Research Council of Canada, the National Research Council of Canada and the Atmospheric Environment Service of Canada, is gratefully appreciated.

References

Antonia, R.A., 1981. Conditional sampling in turbulence measurement. Ann. Rev. Fluid Mech. 13, 131–156.

Austin, L.B., Schuepp, P.H., Desjardins, R.L., 1987. The feasibility of using airborne flux measurements for the imaging of the rate of biomass production. Agric. For. Meteorol. 39, 13–23.

Caramori, P., Schuepp, P.H., Desjardins, R.L., MacPherson, J.I., 1994. Structural analysis of airborne flux measurements over a region. J. Climate 7, 627–640.

Desjardins, R.L., MacPherson, J.I., 1989. Aircraft-based measurements of trace gas fluxes. In: Andreae, M.O. and Schimel, D.S. (Eds.), Exchange of Trace Gases between Terrestrial Ecosystems and the Atmosphere. Wiley, New York, pp. 135–172.

Desjardins, R.L., Hart, R.L., MacPherson, J.I., Schuepp, P.H., Verma, S.B., 1992a. Aircraft and tower-based fluxes of carbon dioxide, latent, and sensible heat. J. Geophys. Res. 97(D17), 18477–18485.

Desjardins, R.L., Schuepp, P.H., MacPherson, J.I., 1992b. Spatial and temporal variations of the fluxes of carbon dioxide and sensible and latent heat over the FIFE site. J. Geophys. Res. 97(D17), 18, 467–18, 475.

Desjardins, R.L., MacPherson, J.I., Neumann, H., den Hartog, G., Schuepp, P.H., 1995. Flux estimates of latent and sensible heat, carbon dioxide, and ozone using an aircraft–tower combination. Atmos. Environ. 29(21), 3147–3158.

Duncan, M.R., Schuepp, P.H., 1992. A method to delineate extreme structures within airborne flux traces over the FIFE site. J. Geophys. Res. 97(D17), 18487–18498.

Eloranta, E.W., Forrest D.K., 1992. Volume imaging lidar observations of the convective structure surrounding the flight path of a flux-measuring aircraft, J. Geophys. Res. 97(D17), 18383–18498.

Grant, R.H., Bertolin, G.E., Herrington, L.P., 1986. The intermittent vertical heat flux over a spruce forest canopy. Boundary-Layer Meteorol. 35, 317–330.

Guo, Y., Desjardins, R.L., MacPherson, J.I., Schuepp, P.H., 1995. The correspondence of aircraft-measured fluxes of sensible heat, latent heat, CO_2, and ozone to the surface characteristics in the San Joaquin valley of California, Atmos. Environ. 29(21), 3159–3168.

Guo, Y., Desjardins, R.L., MacPherson, J.I., Schuepp, P.H., 1995b. A simple scheme for partitioning aircraft-measured ozone fluxes into surface uptake and chemical transformation. Atmos. Environ. 29(21), 3199–3207.

Lenschow, D.H, 1986. Aircraft measurements in the boundary layer. In: Lenschow, D.H. (Ed.), Probing the Atmospheric Boundary Layer, Am. Meteorol. Soc., Boston, pp. 29-55.

Mack, A.R., Desjardins, R.L., MacPherson, J.I., Schuepp, P.H., 1990. Relative photosynthetic activity of agricultural lands from airborne carbon dioxide and satellite data. Int. J. Remote Sensing 11(2), 237–251.

MacPherson, J.I., Desjardins, R.L., Schuepp, P.H., Pearson, Jr., R., 1995. Aircraft-measured ozone deposition in the San Joaquin valley of California. Atmos. Environ. 29(21), 3133–3145.

Mahrt, L., Sun, J., Vickers, D., MacPherson, J.I., Pederson, J.R., Desjardins, R.L., 1994. Observation of fluxes and inland breezes over a heterogeneous surface. J. Atmos. Sci. 51, 2484–2499.

Mahrt, H., Ek, M., 1993a. Mesoscale (subgrid) variability of turbulent fluxes in HAPEX and CODE, Proc. Conf. on Hydroclimatology, Amer. Meteorol. Soc., Anaheim, CA, Jan. 17–22, 1993, 130–131.

Mahrt, H., Ek, M., 1993b. Spatial variability of turbulent fluxes and roughness lengths in HAPEX-MOBILHY, Boundary Layer Meteorol. 65, 381–400.

Massman, W.J., Pederson, J., Delany, A., den Hartog, G., Neumann, H.H., Grantz, D., Pearson Jr., R., 1993. A comparison of independent determinations of the canopy conductance for carbon dioxide, water vapour and ozone exchange at selected sites in the San Joaquin valley of California. Proc. Conf. on Hydroclimatology, Am. Meteorol. Soc., Anaheim, CA, January 1993, pp. 112–117.

Mitic, C.M., Schuepp, P.H., Desjardins, R.L., MacPherson, J.I., 1995. Spatial distribution and co-occurrence of surface–atmosphere energy and gas exchange processes over the CODE grid site. Atmos. Environ., 29(21): 3,169–3,180.

Pederson, J.R., Massman, W.J., Mahrt, L., Delany, A., Oncley, S., Den Hartog, G., Neumann, H.H., Mickle, R.E., Shaw, R.H., Paw U, K.T., Grantz, D.A., MacPherson, J.I., Desjardins, R., Schuepp, P.H., Pearson R. Jr., Arcado, T.E., 1995. California Ozone Deposition Experiment: Methods, Results and Opportunities. Atmos. Environ. 29(21), 3115–3132.

Saucier, A., Duncan, M.R., Austin, G.L., 1991. Mean flux estimation and cospectra of airborne carbon dioxide and water vapour eddy flux measurements in the planetary boundary surface layer. Boundary-Layer Meteorol. 55, 227–254.

Schuepp, P.H., Desjardins, R.L., MacPherson, J.I., Boisvert, J., Austin, L.B., 1987. Airborne determination of regional water use efficiency and evapotranspiration: present capabilities and initial field tests. Agric. For. Meteorol. 41, 1–19.

Shaw, R.H., 1985. On diffusive and dispersive fluxes in forest canopies. In: The Forest–Atmosphere Interaction. Reidel, Dordrecht, pp. 407–419.

Wyngaard, J.C., 1983. Lectures on the planetary boundary layer. In: Lilly, D.K. and Gal-Chen, T. (Eds.), Mesoscale Meteorology Theories, Observations and Models. Reidel, Dordrecht, pp. 603–650; 216–224.

GENERAL INFORMATION

A detailed *Guide for Authors* is available upon request, and will also be printed in the first issue to appear in each year's subscription. The guide can also be found on the World Wide Web: URL address is http://www.elsevier.nl/locate/agrformet. You are kindly asked to consult this guide. Please pay special attention to the following notes.

Language

The official language of the journal is English. It is expected that, prior to submission, the manuscript will have been carefully reviewed for correctness and clarity of expression.

Preparation of the text

a) The manuscript should be typewritten with double spacing and wide margins and include at the beginning of the paper an abstract of not more than 500 words. Words to be printed in italics should be underlined. The metric system should be used throughout.
b) The title page should include: the title, the name(s) of the author(s) and their affiliations, an abstract and 4–6 keywords. For a list of suggested keywords see also Vol. 84/1–2 of the journal or http://www.elsevier.nl/locate/agrformet. Authors will be provided with a list of keywords by the editor/regional editor once the manuscript has been reviewed.

References

a) References in the text start with the name(s) of the author(s), followed by the publication date in parentheses.
b) The reference list should be in alphabetical order and on sheets separate from the text.

Tables

Tables should be compiled on separate sheets. A title should be provided for each table and they should be referred to in the text.

Illustrations

a) All illustrations should be numbered consecutively and referred to in the text.
b) Drawings should be completely lettered, the size of the lettering being appropriate to that of the drawings, but taking into account the possible need for reduction in size (preferably not more than 50%). The page format of *Agricultural and Forest Meteorology* should be considered in designing the drawings.
c) Photographs must be of good quality, printed on glossy paper.
d) Figure captions should be supplied on a separate sheet.

Proofs

One set of proofs will be sent to the author, to be checked for printer's errors. In the case of two or more authors please indicate to whom the proofs should be sent.

Submission of manuscripts

For North America: Dr. Kya Tha Paw U, LAWR, Atmospheric Sciences, Hoagland Hall, University of California, Davis, CA 95616, USA

For Europe, Africa and the Middle East: Dr. John Stewart, University of Southampton, Department of Geography, Highfield, Southampton SO17 1BJ, UK.

For Asia, Australia, New Zealand, Central and South America: Dr. Ray Leuning, Centre for Environmental Mechanics, G.P.O. Box 821, Canberra, A.C.T. 2601, Australia

A manuscript rejected for publication in *Agricultural and Forest Meteorology* may not be resubmitted.

Manuscript and illustrations should be submitted in triplicate. One set should be in a form ready for reproduction: the other two may be of lower quality. Submission of an article is understood to imply that the article is original and unpublished and is not being considered for publication elsewhere. Upon acceptance of an article by the journal, the author(s) will be asked to transfer the copyright of the article to the publishers. This transfer will ensure the widest possible dissemination of information.

Submission of electronic text

In order to publish the paper as quickly as possible after acceptance, authors are encouraged to submit the final text also on a 3.5" or 5.25" diskette. Both double density (DD) and high density (HD) diskettes are acceptable. Make sure, however, that the diskettes are formatted according to their capacity (HD or DD) before copying the files onto them. Similar to the requirements for manuscript submission, main text, list of references, tables and figure legends should be stored in separate text files with clearly identifiable file names. The format of these files depends on the word processor used. Texts made with DisplayWrite, MultiMate, Microsoft Word, Samna Word, Sprint, Volkswriter, Wang PC, WordMARC, WordPerfect, Wordstar, or supplied in DCA/RFT, or DEC/DX format can be readily processed. In all other cases the preferred format is DOS text or ASCII. It is essential that the name and version of the wordprocessing program, type of computer on which the text was prepared, and format of the text files are clearly indicated. Authors are encouraged to ensure that **the disk version and the hardcopy must be identical.** Discrepancies can lead to proofs of the wrong version being made.

0168-1923/97/$17.00

∞ The paper used in this publication meets the requirements of ANSI/NISO Z39.48-1992 (Permanence of Paper).

PRINTED IN THE NETHERLANDS

Pergamon

Atmospheric Environment Vol. 29, No. 21, pp. 3169–3180, 1995

1352-2310/95 $9.50 + 0.00

1352-2310(94)00331-9

SPATIAL DISTRIBUTION AND CO-OCCURRENCE OF SURFACE–ATMOSPHERE ENERGY AND GAS EXCHANGE PROCESSES OVER THE CODE GRID SITE

CONSTANCE M. MITIC,* PETER H. SCHUEPP,*
RAYMOND L. DESJARDINS† and IAN J. MACPHERSON‡

Department of Natural Resource Sciences, McGill University, Macdonald Campus, Ste-Anne-de-Bellevue H9X 3V9, Canada; †Center for Land and Biological Resources Research, Agriculture Canada, Ottawa, Canada; ‡Institute for Aerospace Research, National Research Council of Canada, Ottawa, Canada

(*First received* 30 *November* 1993 *and in final form* 2 *September* 1994)

Abstract—Grid-type flight patterns at an altitude of 30 m were executed in the summer of 1991 by the Canadian Twin Otter flux research aircraft over a 15 km × 16.1 km agricultural area, as part of the California ozone deposition experiment (CODE). This permitted the mapping, by eddy covariance techniques, of surface–atmosphere exchange for sensible heat, moisture, CO_2 and ozone, in the form of GIS-interpolated flux maps and in the discrete form of those coherent structures of the turbulent transfer process that dominate these exchange processes. The magnitude of surface-related mesoscale contributions to the flux was also quantified. Flux observations were compared against radiometrically observed surface temperatures and vegetation indices (NDVI and VI), observed from aircraft and satellite, and surface characteristics obtained from ground surveys. Flux maps showed the expected close correspondence between greenness, evapotranspiration (ET) and CO_2 exchange, but a weaker correspondence between these and ozone flux maps than would be expected if ozone uptake could consistently be scaled to stomatal conductance for moisture or CO_2. Examination of the spatial coincidence between transporting structures for the various scalars (heat, moisture, CO_2 and ozone), through the Jaccard coefficient of co-location, J, showed a lower overall value ($0.45 < J < 0.55$) for coincidence in transfer between ozone and moisture than between CO_2 and moisture ($0.6 < J < 0.7$), and analysis of coincidence for the various crop types within the grid permits quantitative assessment of the potential error made when scaling ozone uptake to stomatal conductance. In general, the findings suggest the existence of two sinks for ozone only one of which is tied to stomatal conductance, and indicates a possible relative advantage for estimates of ozone uptake based on CO_2 rather than moisture exchange.

Key word index: Micrometeorology, trace gas exchange, ozone uptake, flux mapping, turbulent transport.

1. INTRODUCTION

The intermittent nature of "coherent structures" that dominate the turbulent transfer of various scalars (sensible heat, moisture, CO_2 and trace gases) between the Earth and the atmosphere is well documented (e.g. Wyngaard, 1983; Austin *et al.*, 1987; Eloranta and Forrest, 1992; Mahrt and Ek, 1993a, b). Their spatial distributions, their coupling to the surface and their mutual spatial relationships are of particular interest for our understanding of surface–atmosphere interactions in general and of driving forces on gas exchange in particular.

In recent years, tropospheric ozone (O_3) has emerged as a topic of great concern (Simarski, 1992), in particular its distribution and deposition to vegetation (Prat *et al.*, 1983; Runeckles, 1992; Lefohn, 1992; Runeckles and Chevone, 1992). While its damaging effects on vegetation are relatively well known in principle, little is known about the association between O_3 uptake and other plant–atmosphere exchange processes such as transpiration and photosynthesis for different plant species under varying canopy and environmental conditions. This uncertainty may cause serious error if O_3 deposition is estimated indirectly on the basis of local plant physiological parameters such as stomatal resistance to H_2O and CO_2 (Massman *et al.*, 1993).

As part of the California ozone deposition experiment (CODE) in 1991, the Twin Otter aircraft of the National Research Council of Canada was used for regional estimation of near-surface fluxes of various scalars including O_3 (MacPherson *et al.*, 1995). Within these airborne observations, our paper addresses the following questions: What are the spatial distributions, relative importance and possible mutual interactions between the coherent structures responsible for the bulk of the transport of heat, moisture, CO_2 and O_3 within the surface boundary layer, over an agricultural surface with clearly differentiated surface characteristics? What is the relationship (spatial coincidence) between the structures transporting O_3 and those transporting other scalars over different types of surface cover? To what extent are the distributions and mutual relationships of such structures determined or affected by surface characteristics such as greenness and surface temperature? The examination of these questions should be seen as an extension of previous airborne observations, which have demonstrated their potential to relate flux estimate of heat, moisture and CO_2 to independently observed surface characteristics such as greenness and surface temperature excess (Desjardins *et al.*, 1992b), after correction for downwind displacement of diffusing plumes between the surface and the airborne sampling transect (Schuepp *et al.*, 1992).

2. SAMPLING SITE, DATA COLLECTION AND DATA ANALYSIS

2.1. *Site description and airborne data collection*

Our study analyses data obtained over a 15 km × 16.1 km area of irrigated and non-irrigated agricultural land in Kings County of the San Joaquin Valley, with diagonal corners defined at 36.083°N/119.696°W and 35.940°N/119.869°W (McPherson *et al.*, 1995). The flat terrain consisted of square and rectangular fields, with typical field size of 1.75 km^2, intersected by irrigation canals. Field boundaries and crops were mapped on the basis of a land-use/crop-type survey (State of Calif. Air Resource Board). Within the site, growing cotton and senescent safflower dominated, accounting for approximately 60 and 25% of the surface area, respectively. The remaining 15% of the site consisted mostly of pasture and alfalfa mix, grain and hay crops, idle fields and native vegetation (Fig. 1).

Airborne observations result from two Twin Otter grid flights, consisting of 22 runs each at 30 m altitude in an E–W direction (Flight 16: 26 July from 1136 to 1457 h PDT; Flight 21: 2 August from 1239 to 1553 PDT). Flight lines for each grid were offset by 0.75 km in the N–S direction, to give an effective spacing of 0.375 km between 44 lines for the combined grid flights (flight trajectories for Flight 16 only are shown in Fig. 1).

The aircraft was equipped to measure the three components of air motion, and the flux densities of momentum, heat, moisture, CO_2 and ozone, as well as radiative surface temperature and vegetation index (infrared-to-red ratio IR/R). Flux estimates were obtained by eddy correlation technique, i.e. from the covariance of fluctuations in vertical wind and scalars. Data were digitized at 16 Hz, for an effective data point separation of 3.8 m at a true airspeed of 60 m s^{-1}. Georeferencing of aircraft position was interpolated within the 2 s resolution of the Loran-c navigation system, extrapolated during the 4 s lag at the end of each sampling run, and the entire grid shifted 300 m SW to correct for a systematic offset noted in the navigation system. Adjustments were also made to compensate for the physical displacement between sensor positions on the aircraft. For details of instrumentation and primary data processing, see MacPherson (1992) and MacPherson *et al.* (1995).

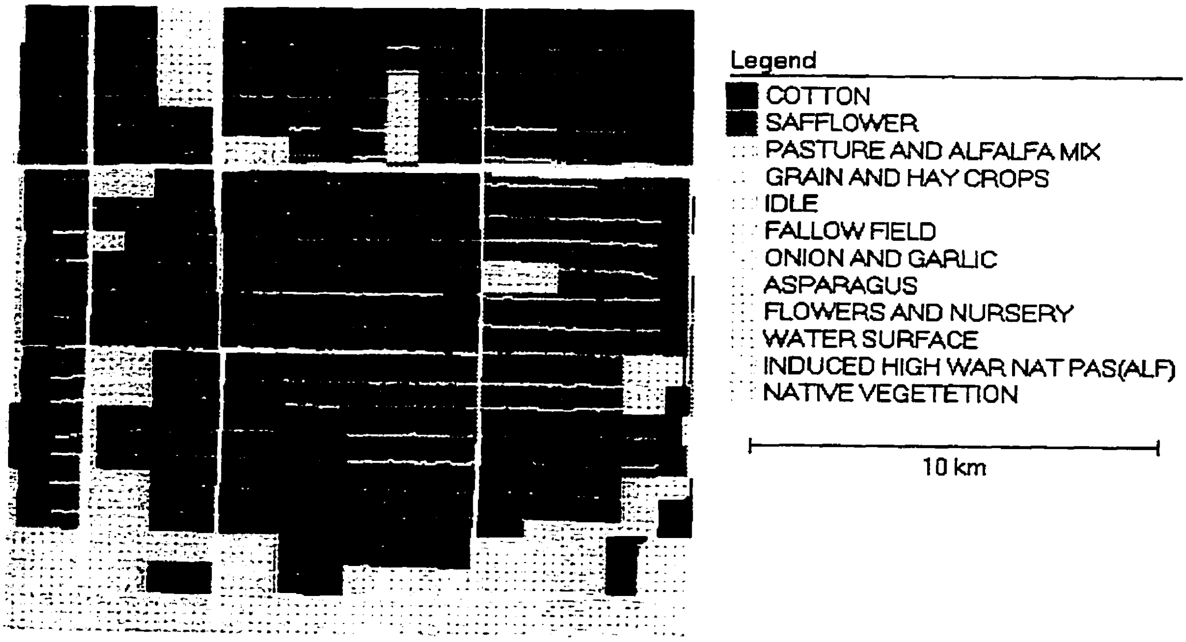

Fig. 1. Land use survey of the CODE grid site with the two dominant crops isolated for emphasis, and trajectories of Flight 16 (lines of Flight 21 were offset to intermediate positions between those of Flight 16).

Footprint corrections, i.e. corrections for advective displacement of wind and concentration fields between the surface source/sink area and the above-surface airborne sampling location were not deemed necessary, based on estimates derived from the stability-dependents, approximate solutions of the diffusion equation given by Horst and Weil (1992). Results suggested that between 84 and 90% of the information obtained along the flight path would come from the most immediate upwind 400 m. Exceptions were made for interpretation in areas where flight lines were closer than 400 m to field boundaries.

2.2. *Weather conditions and stability*

The weather conditions were clear for both days, with average incident shortwave radiation of 840 W m^{-2}. On 26 July, flight level winds were from NNW, at between 1.9 and 4 $m\,s^{-1}$, the convective boundary layer (CBL) top was at 549 m and temperature 31°C on landing. On 2 August, flight level winds were from the NNE, between 0.26 and 2.97 $m\,s^{-1}$, with CBL top at 701 m and temperature 32°C on landing. Thermal stratification was unstable, with z/L at flight level ≈ -3.3, based on an Obukhov length $L \approx -9$ m derived for the mean values of friction velocity $u^*(\approx 0.22\,m\,s^{-1})$ and sensible heat flux $(w'T' \approx 85\,W\,m^{-2})$.

2.3. *Definition of the mean flux mapping procedure*

Local estimates of flux by the eddy correlation technique are based on deviations of vertical wind and scalars from a mean established over a distance that should be large relative to the scale of those turbulent structures that dominate Earth–atmosphere transport processes. Problems of convergence of the mean in observations of the turbulent boundary layer have been well documented, in principle (Wyngaard *et al.*, 1978; Lenschow and Stankov, 1986; Wyngaard, 1986) and more or less empirically for Twin Otter flux estimates (Austin *et al.*, 1987; Schuepp *et al.*, 1989; Saucier *et al.*, 1991).

The definition of a local mean is complicated over spatially heterogeneous surface conditions by trends or discontinuities in traces of scalars and/or vertical wind, usually corrected by filtering or detrending techniques designed to remove dominant trends. Nonlinear detrending appeared to give a more reasonable definition of the mean (in terms of agreement of flux estimates with independently observed surface fluxes and distribution of turbulent structures along sampling runs) when compared to linear detrending for Twin Otter FIFE data (Caramori *et al.*, 1994). By contrast, Mahrt and Ek (1993), in their study of turbuent fluxes over a neighboring CODE site, used surface-related sectional averaging to define local means, with contributions from mesoscale variability to the flux estimated from deviations of sectional averages from overall run averages. In our study we used nonlinear detrending (based on a Fourier series truncated at the third term), unless inspection of the flight trace clearly suggested a linear trend, in which case linear detrending was substituted. For example, the latter was found to be adequate for vertical wind in all cases. Sectional averaging was employed as an alternative technique to test the sensitivity of results to the definition of the mean. It is clear that non-linear detrending and sectional averaging techniques tend to remove or separate out potential long wavelength contributions from the flux estimates. In this paper we will present some evidence that flux contributions from larger scales are not likely to be very significant over the given site, and concentrate on contributions from smaller scales which not only dominate the flux estimate but are most directly linked to surface characteristics. Figure 2 illustrates the different detrending routines applied to the data set.

Spatial flux maps were generated from interpolation by Geographic Information System (GIS) of 1 km-averaged flux, derived from deviation of flux variables from the detrended mean. Interpolation was based on a maximum of eight neighboring data points, with a linear decay rate. GIS-based maps of surface characteristics were constructed for greenness (vegetation index) and surface temperature from airborne observations and—for comparison purposes—from NOAA AVHRR normalized vegetation index (NDVI) with 1.1 km resolution. This allows for intercomparison of surface patterns generated from aricraft- and satellite-based observations. Classification of spatial maps is based on standard deviations from the mean of the detrended flux values for each scalar and the mean surface parameters (greenness and surface temperature excess) across the site: (1) > 1 rms below the mean, (2) < 1 below the mean, (3) < 1 rms above the mean, (4) > 1 rms above the mean.

2.4. *Thresholds and the definition of structures*

A coherent structure may be defined as a "connected turbulent fluid mass with instantaneous phase-correlated vorticity over its spatial extent" (Hussain, 1986), interspersed between less coherent components. Pragmatically, it may be defined as an "event" in time and space where variables involved in turbulent transport, such as vertical wind and admixture concentration, are correlated in such a way as to contribute significantly to the flux. This empirical definition is compatible with the imposition of threshold values on such parameters as temperature, humidity and turbulent intensity, as well as on the combination of moisture and vertical wind, which have been used to define convective cells (Lenschow and Stephens, 1980; Grossman, 1984). The result of structural analysis will appear as an intermittent sequence of those structures along the flight track which are responsible for most of the turbulent transport. Our present study will only report on structures representing the "dominant gradient

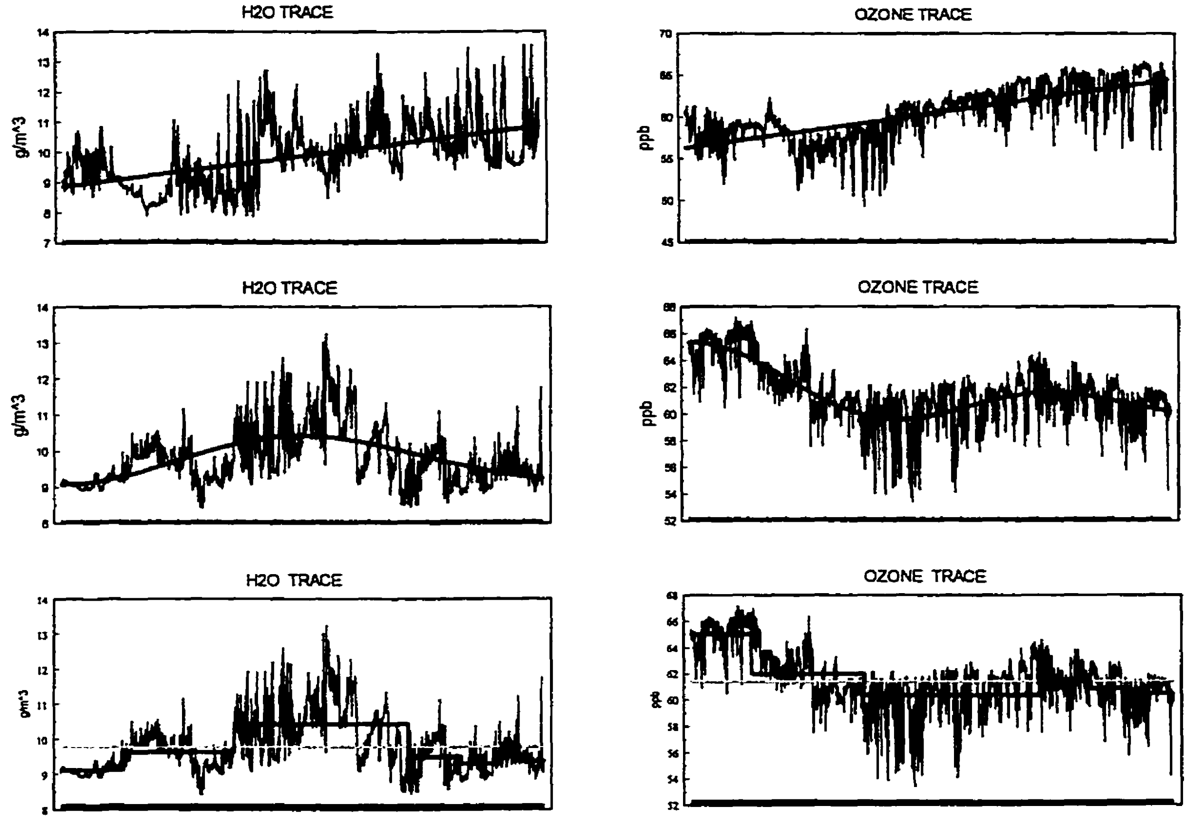

Fig. 2. Illustration of linear and nonlinear detrending, and sectional averaging, applied to H_2O and O_3 trace within the sampled grid.

mode" of transfer, i.e. those associating positive (upward directed) fluctuations in vertical wind with excess of moisture and heat, and deficit of CO_2 and ozone. This means that the underlying surface (plant canopy) is studied in its role as a source of moisture and heat and a sink for CO_2 and ozone.

The recognition of coherent structures in turbulent flow depends not only on the definition of the mean but also on thresholds used to separate "significant" flux event from those resulting from less coherent "noise". Thresholds may be imposed before or after signals are grouped into coherent structures. Thresholds applied prior to structure definition eliminate weakly correlated signals, corresponding to the application of a "hyperbolic hole" in quadrant analysis techniques, generally defined as multiples of the mean flux (Antonia, 1981; Shaw, 1985; Grant et al., 1986) or as fractions of the standard deviation (Lenschow and Stephens, 1980). Caramori et al. (1984) showed that the imposition of a hyperbolic hole corresponding to 0.2 rms eliminated weak signals that may represent the tails of coherent structures, and serves to clarify the external definition of dominant structures. A threshold of 1 rms retained only the signals associated with the core of the structures. In our study we applied both the 0.2 and 1 rms thresholds, in order to assess the sensitivity of coincidence analysis to the intensity level retained for the structure (main structure vs core).

Imposition of a threshold after coherent structures have being defined will eliminate weaker structures which occupy a significant time fraction of the run, but contribute relatively little to the flux, on the assumption that significant interactions may be most clearly seen in the dominant structures. As defined (and used) by Duncan and Schuepp (1992) and Caramori et al. (1994), this threshold based on the product of the mean flux density of each structure, (F_{st}), and its fractional contribution to the total flux, F, i.e. a quadratic measure of the flux contribution of each structure expressed as $\phi = F_{st}F$. The relationship between increasing threshold values ϕ and the cumulative flux fraction carried by structures within that threshold is highly nonlinear, so that subtraction of events with progressively larger ϕ values initially has a very small effect on reduction of the cumulative flux estimate. The criterion for separation of the "extreme events" is based on the point of maximum curvature in the plot of $\log(\phi)$ vs cumulative flux fraction, i.e. on ϕ values above which subtraction of events significantly reduces the cumulative flux estimate (Duncan and Schuepp, 1992). For the flight data obtained in

CODE, similar to those observed in FIFE, this generally occurs at the point where 70–80% of the cumulative flux estimates comes from events (structures) that occupy $\approx 20\%$ of the time fraction along the run. "Extreme" events were, therefore, arbitrarily identified as those which, in descending order of their ϕ value, cumulatively account for a 20% time fraction along the run. Due to the lack of consensus on an objective definition of significant turbulent structures, the above procedure is no more arbitrary than alternative definitions of "extreme events" such as a hyperbolic hole set at four times the value of $\langle w'c' \rangle$ used, e.g. by Grant *et al.* (1986).

2.5. *Defragmentation*

A coherent structure will be manifested as a set of consecutive data points along the data vector, where significant contribution towards the covariance of vertical wind (w) and concentration of the scalar (c) exists within the given mode of transport (excess-up for heat and moisture, deficit-up for CO_2 and ozone). These structures, however, may appear artificially fragmented into separate structures due to the inclusion of unmixed air parcels, causing brief excursions (usually in concentration) that are inconsistent with the main structure. This is corrected by a defragmentation procedure similar to that used by Duncan and Schuepp (1992) and Caramori *et al.* (1994), which re-establishes the continuity of artificially separated structures: a coherent structure is assume to occupy at least eight data point within a given quadrant of w and c excursions along the data vector (corresponding to a spatial scale of 30 m at the given flight speed and digitizing rate). This essentially arbitrary criterion is based on cospectral analysis of Twin Otter data (Saucier *et al.*, 1991; Desjardins *et al.*, 1992a, b), which showed that structures below this scale contribute negligibly to the flux estimate. Structures with less than eight data points are either eliminated from the data set (if the preceding and following dominant structures represent different modes of transport) or incorporated into the dominant structure (if they are embedded in preceding and following structures of the mode of transport).

2.6. *Association of structures*

Analysis of coincidence of structures which transport the various scalars, as a function of surface characteristics, might be expected to provide indirect information about the driving forces between the various fluxes, including co-location of sources and sinks. For example, a positive association (co-location) of structures transporting O_3 and those transporting H_2O and CO_2 would be expected if stomatal conductance is seen as the determining factor of O_3 uptake. The only previous investigations related to the association of O_3 with other atmospheric gases and air pollutants relate to the co-occurrence of excursions in concentration between O_3, NO_2 and SO_2 at several monitoring sites across the U.S. (Lefohn and Tingey, 1984; Lefohn *et al.*, 1987).

Association between transporting structures may be expressed through the probability that the center of a structure carrying one scalar is located within the structure defined for another scalar at the given threshold level. These two separately defined structures may then suggest a single structure carrying both flux variables. Following Cheethan and Hazel (1969) and Wheeler and Krystinik (1987), it is quantified by the *Jaccard coefficient*, J, defined by

$$J = \frac{C_{i,j}}{N_{\mathrm{TOT}}} = \frac{C_{i,j}}{N_i + N_j - C_{i,j}} \tag{1}$$

where $C_{i,j}$ is the number of coincident structures, in the sense defined above, between two parameters (scalars) indicated by subscripts i and j. N_i and N_j are the number of structures carrying flux parameters i and j, respectively, and N_{TOT} is the total number of structures present in both parameters (i and j), with each pair of coincident structures counted only once.

The value of J ranges from 0 to 1, in proportion to the degree of co-location. Co-location of structures is more likely for—but does not prove—co-location of sources and sinks for the scalars involved. J coefficients were calculated for the structures in the dominant gradient transfer mode, for the overall grid and for the dominant surface cover types within the grid.

2.7. *Sensitivity analyses*

The sensitivity of flux estimates and structure definition of the mean was tested by comparing results obtained from linear/nonlinear detrending to those obtained under sectional averaging. The mutual association of structures (J coefficient) also depends on thresholds used in the structure definition; the sensitivity of conclusions to threshold values may be inferred by comparing results obtained for the 0.2 and 1 rms thresholds applied to the covariance. In all cases, data for the two grid flights (26 July, 2 August) were analyzed separately before being combined into the full grid, so that the temporal reproducibility of findings can also be assessed. The sensitivity of structural analysis to potential errors in the assessment of advective displacement has also been investigated by repeating the analysis for an advective shift (beyond that calculated by the footprint function) observed in the spatial patterns of the coherent structures superimposed on crop type.

3. RESULTS AND DISCUSSION

3.1. *Flux and surface maps*

Satellite-observed (NOAA AVHRR, 2 August overpass) greenness (NDVI) map, the aircraft-observed interpolated map of greenness (VI), surface temperature excess and maps of airborne flux estimates of sensible heat, H_2O, CO_2 and O_3 are shown in Fig. 3.

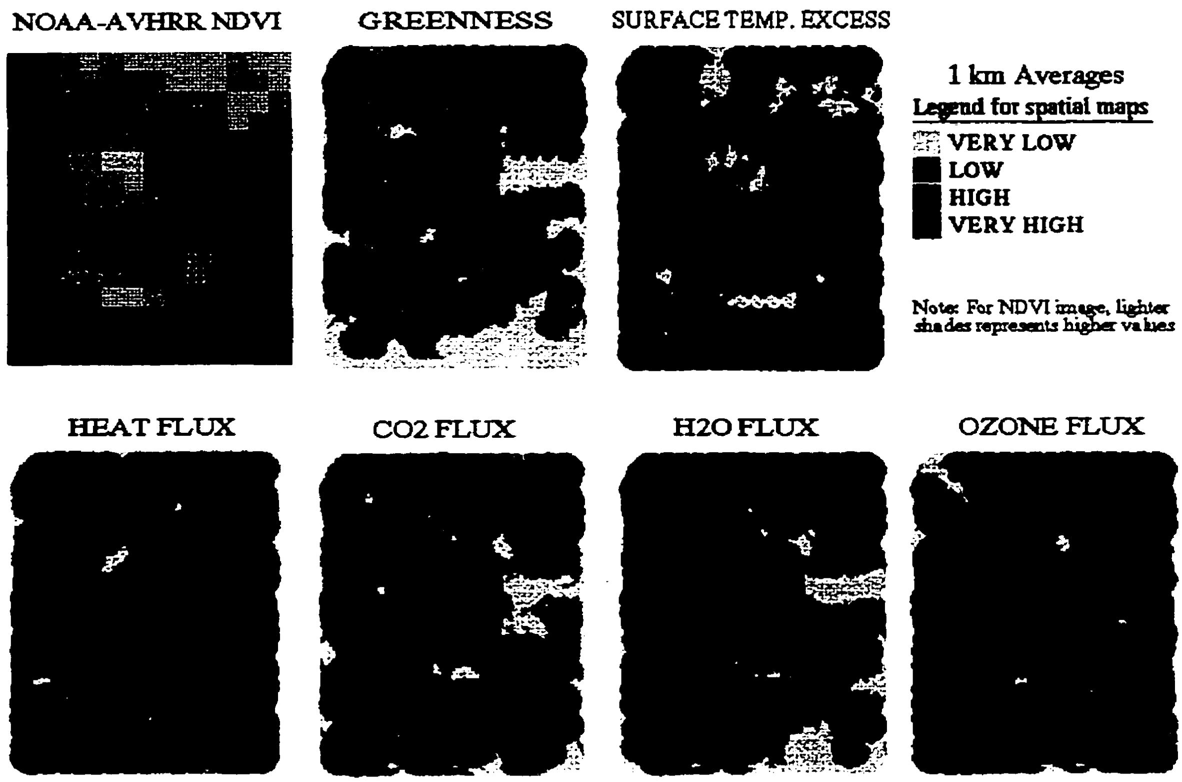

Fig. 3. NOAA-AVHRR data of greenness (NDVI, with high intensity areas in lighter shades), and maps of greenness and fluxes of sensible heat, moisture, CO_2 and ozone for the CODE grid site.

Clearly, the relationship between the distribution patterns of VI and those fluxes of H_2O and CO_2, with an inverse relationship to sensible heat flux and surface temperature, reflects the fact that (largely irrigated) vegetation generates the high photosynthetic and moisture fluxes, associated with low sensible heat fluxes and low surface temperature. The apparent southward shift of flux patterns, relative to those of VI, reflect on advective effect of wind from the north that appears somewhat stronger than that suggested by the analytical footprint prediction. By contrast, the spatial distribution of O_3 flux appears less obviously related to VI although some coincident areas of high flux levels are evident, suggesting that along with stomatal conductance, there are other processes involved in the regulation of O_3 uptake. It therefore calls into question the validity of linking O_3 sink strength to stomatal conductance of vegetation, and agrees in principle with surface observations (also in CODE) where relationships of O_3 uptake and stomatal exchange of H_2O and CO_2 were found to be complex and species-specific (Massman *et al.*, 1993). It is possible in those small isolated pockets where VI and O_3 are high but CO_2 and H_2O are low, that stomates may be partly closed, still maintaining a sizeable influx of O_3 but decreased CO_2 consumption due to increased internal CO_2 concentration as a result of reduced photosynthetic assimilation (Reich *et al.*, 1985; Aben *et al.*, 1990). This behavior would be more likely in C4 plants which are more sensitive to changes in the levels of CO_2 concentration. It is also possible that areas with significant O_3 flux in the face of lower VI and lower fluxes of H_2O and CO_2 may consist of vegetation at a mature stage where it does not (or no longer) require significant degree of photosynthesis in its maintenance, or represent O_3 sinks from non-transpiring portions of the canopy. Overall, the spatial patterns observed in the maps suggest that ozone may be regulated by a number of processes and call for further investigation of the association of ozone flux with exchange of CO_2 and moisture.

The high degree of correspondence between airborne flux maps and maps of surface temperature and vegetation illustrates the capability of low flying aircraft to document Earth–atmosphere exchange processes within the surface boundary layer, at scales relevant to satellite-based remote sensing, at least for this surface with well-defined, high contrast ("test pattern") surface source configurations. No surface observations were available within the grid site to test absolute flux values, but interpolated flux values over cotton within the grid, for CO_2 (0.46–0.8 $mg\,m^{-2}\,s^{-1}$ over 90% of the area), H_2O (300–490 $W\,m^{-2}$) heat (10–80 $W\,m^{-2}$) and ozone (0.4–1.2 $\mu g\,m^{-2}\,s^{-1}$) cover the range of surface fluxes measured over cotton elsewhere (lat. 36°49′; long. 120°41′) in the CODE area (MacPherson, 1992).

3.2. *Distribution of coherent structures*

Figure 4 shows the distribution of coherent structures in the dominant (excess-up for H_2O and heat, deficit-up for CO_2 and O_3) transfer mode for the combined grid flights, at the lower (0.2 rms) threshold level. Displayed structure size reflects its relative flux contribution. Comparison against maps of crop type, VI and surface temperature (Figs 1 and 3), shows the preponderance, in number and importance, of CO_2 and H_2O structures over cotton fields (high VI and low surface temperature), with much fewer structures over mature safflower, native vegetation and idle fields (low VI and high surface temperature). As expected, the distribution of dominant heat structures is complementary to that of H_2O and CO_2, predominantly located over hot dry safflower and idle fields. O_3 structures appear across all crop types, but structures with higher mean flux are more frequent over the cotton fields. Compared to the distribution patterns of heat, CO_2 and H_2O, no clearly defined distribution pattern is evident for ozone structures.

3.3. *Mutual association of coherent structures*

(a) *Across the grid*: The association between the structures transporting heat, H_2O, CO_2 and O_3 across the grid (Jaccard coefficient J) is sum-

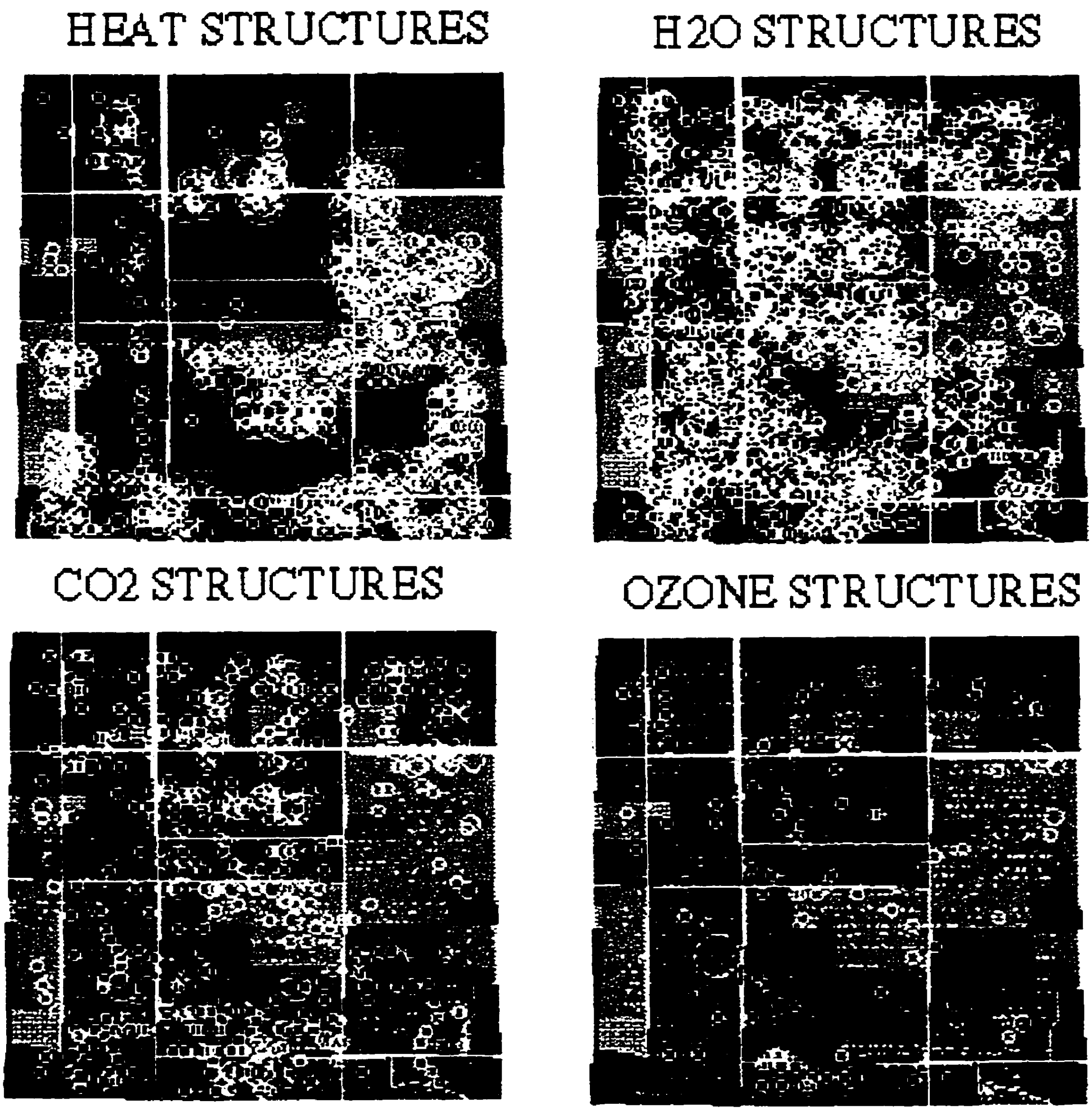

Fig. 4. Maps of coherent structures for sensible heat, moisture, CO_2 and ozone, sampled over the CODE grid site.

Table 1. Association of coherent structures across the grid, in terms of the Jaccard coefficients, J, for threshold levels of 0.2 and 1 rms

Coinciding structures	Flight 16, 26 July		Fight 21, 2 August		Combined grid	
	0.2	1	0.2	1	0.2	1
CO_2 on H_2O	0.634	0.507	0.711	0.586	0.670	0.544
H_2O on CO_2	0.570	0.476	0.675	0.570	0.619	0.520
O_3 on CO_2	0.472	0.377	0.568	0.421	0.519	0.398
CO_2 on O_3	0.480	0.345	0.541	0.402	0.510	0.372
O_3 on H_2O	0.452	0.364	0.570	0.421	0.509	0.391
H_2O on O_3	0.410	0.318	0.512	0.390	0.460	0.353
CO_2 on heat	0.281	0.161	0.175	0.117	0.227	0.139
Heat on CO_2	0.259	0.151	0.172	0.102	0.216	0.127
O_3 on heat	0.313	0.226	0.266	0.186	0.288	0.206
Heat on O_3	0.286	0.180	0.248	0.153	0.266	0.167
H_2O on heat	0.223	0.125	0.116	0.074	0.168	0.099
Heat on H_2O	0.237	0.139	0.123	0.066	0.179	0.102

Table 2. Association of coherent structures as a function of crop type, in terms of the Jaccard coefficient, J, for the threshold levels of 0.2 and 1 rms

Coinciding structures	Cotton		Pasture and Alfalfa mix		Native veg and idle fields		Safflower	
	0.2	1	0.2	1	0.2	1	0.2	1
CO_2 on H_2O	0.693	0.570	0.701	0.541	0.656	0.521	0.606	0.464
H_2O on CO_2	0.648	0.553	0.667	0.520	0.525	0.459	0.240	0.464
O_3 on CO_2	0.530	0.412	0.467	0.444	0.475	0.394	0.486	0.355
CO_2 on O_3	0.524	0.386	0.479	0.383	0.443	0.369	0.467	0.350
O_3 on H_2O	0.523	0.416	0.536	0.494	0.451	0.344	0.435	0.325
H_2O on O_3	0.481	0.376	0.483	0.413	0.390	0.319	0.167	0.159
CO_2 on heat	0.202	0.098	0.193	0.102	0.259	0.194	0.293	0.205
Heat on CO_2	0.032	0.035	0.022	0.032	0.055	0.035	0.082	0.037
O_3 on heat	0.252	0.156	0.221	0.141	0.328	0.267	0.402	0.311
Heat on O_3	0.042	0.048	0.021	0.066	0.057	0.057	0.091	0.062
H_2O on heat	0.152	0.070	0.164	0.090	0.143	0.125	0.052	0.159
Heat on H_2O	0.026	0.033	0.031	0.054	0.031	0.042	0.074	0.038

marized in Table 1 for the separate and combined grid flights, at both threshold levels. The similarity of observations between the two grid flights, and the relative consistency between threshold levels, is reassuring. As expected, the strongest flux association is observed between H_2O and CO_2, reflecting coincident transport and co-location for sources and sinks in stomatal exchange. The incidence of CO_2 on H_2O structures tends to be slightly higher than *vice versa*, since the likelihood for photosynthesis occurring in absence of some exchange of moisture is smaller than that for moisture exchange in the absence of photosynthesis (e.g. irrigation canals, irrigated new fields, etc.). O_3 structures have a higher coincidence on CO_2 and H_2O structures than might perhaps have been expected on the basis of the flux maps (Fig. 3), with a stronger association with heat exchange than that shown by CO_2 or H_2O.

(b) *As a function of crop type*: Associations between the various fluxes over the dominant crop types within the grid are summarized in Table 2. Over *cotton*, we observe the expected high association between H_2O, CO_2, slightly higher for CO_2 on H_2O than *vice versa*, for reasons already noted. Association of O_3 with these structures is slightly lower, but high enough to indicate that fluxes of CO_2, H_2O and O_3 over cotton are largely carried by the same structures, suggesting a significant probability for co-location of their respective sources or sinks in stomatal exchange. The low degree of association to heat is not surprising in view of the scarcity of heat structures over cotton fields (Fig. 4). The imbalance between association of scalars with thermals and *vice versa* illustrates a non-negligible driving force of thermals on gas exchange even in that relatively well-watered ecosystem. Over *pasture/alfalfa mix* and *native vegetation/idle fields* the associations between H_2O, CO_2 and O_3 are of similar magnitude. The association of O_3 with heat, however, is relatively higher over native vegetation and idle fields than over cotton, reflecting the enhanced role of thermals in the transport of O_3. The results for *senescent safflower* are more complex, especially in the difference exhibited between J coefficients determined for the low (0.2 rms) and high (1 rms) threshold levels. When defined by the lower threshold, a pronounced asymmetry between transport mechanism for CO_2 and H_2O is noted, with structures carrying H_2O much more likely to be transporting CO_2, than *vice versa*. However, the discrepancy disappears when association between the cores of structures (high threshold) is displayed. The association of CO_2 flux with heat (even higher than that over native vegetation and idle fields) suggests that over this dry crop, sink areas for CO_2 are more likely to coincide with those for heat than over the other crop types. O_3, also, shows higher association with heat than over other surface cover, with almost equal probability of finding O_3 associated with thermal structures as with those carrying H_2O and CO_2. There is a significant, symmetrical flux association between CO_2 and O_3. However, as observed between CO_2 and H_2O, the flux association between O_3 and H_2O for the low threshold case is asymmetrical, with the coincidence of O_3 on H_2O much higher than *vice versa*. This suggests the existence of two distinct sinks for O_3 in safflower: areas where structures are transporting H_2O, CO_2 and O_3, and others where structures are transporting CO_2, heat and O_3.

This flux association analysis suggest two major sinks for O_3 over the grid site, in the form of vegetation and of non-transpiring surface areas (most likely soil), respectively. Over crops with high levels of photosynthetic activity and moist conditions (such as well-watered cotton), transpiring vegetation is the major sink for O_3 therefore scaling ozone uptake to transpiration rates or stomatal conductance would very likely account for most of the ozone depletion at the surface. The potential error made in such estimates can be estimated from the difference between the association of CO_2 and H_2O on the one hand, and that between those two scalars and O_3 on the other, which is $\leqslant 20\%$. Over safflower, native vegetation and idle fields, which represent low photosynthetic activity and hot dry conditions, the non-transpiring portion of the canopy and surface may still constitute a non-negligible O_3 sink, with considerably higher potential error when scaled to transpiration rates or stomatal conductance. These results are compatible with findings of other researchers: Reich *et al.* (1985) found water stressed soybean displayed a more rapid stomatal closure in response to exposure to ozone than unstressed plants, while Temple (1986) observed no such effect in field cotton. Van Paul and Jacobs (1993), in their experiments on maize, also found that in wet soil conditions the non-transpiring portions of the crop and soil accounted for less than 20% of the total above-canopy ozone flux, while during dry conditions non-transpiring portions of the crop and the soil appeared to be responsible for up to 65% of the flux.

The most consistent observation across all the varying surface conditions is the significant flux association between CO_2 and ozone, and the comparable association with these two fluxes and the heat flux. Under most conditions, but particularly under hot and dry conditions, it would seem more advisable, therefore, to scale ozone uptake to CO_2 instead of H_2O.

3.4. *Sensitivity analysis*

(a) *Reproducibility in time*: Comparison of data obtained on two separate days over the same grid generally showed no significant differences, such as illustrated by the data given in Table 1.

(b) *Effect of threshold level on J coefficients*: As shown in Tables 1 and 2, changes in threshold levels from 0.2 rms (removal of weak tails of structures) to 1 rms (retention of structure cores) changed the absolute value, but rarely the relative order of importance, of association between the various flux pairs. The reduction of the J values with increasing threshold indicates that the most intense cores of transporting structures are less likely to be co-located than the overall structures. To what degree this may be the result of the natural complexity of turbulent mixing within these structures, or reflect subtle differences in surface source/sink distributions would have to be further investigated.

(c) *Effect of advective displacement*: Figure 4 suggests a consistent offset of structures relative to crop boundaries, more or less in the direction of prevailing wind, beyond the advective displacement estimated from analytical solutions of the diffusion equation. Flux associations were, therefore, recalculated for artificially drawn crop boundaries which reflect the observed offset. There were no significant differences in the crop-based flux association values calculated with the inclusion or exclusion of those structures which appeared to have been displaced across field boundaries.

(d) *Effect of alternative definition of the local mean*: Sectional averaging over subsections of runs judged to be relatively homogeneous in terms of surface characteristics, such as explored by Mahrt and Ek (1993a) on a set of 35 km runs immediately N of the grid site, served to evaluate the sensitivity of flux estimates to the definitions of the mean and to assess the potential presence of mesoscale flux contributions. Mesoscale variability could be associated with terrain or surface features, in cases where terrain slope or surface heterogeneity drives secondary circulation, superimposed on the general flow field (Pielke *et al.*, 1991). The procedure used by Mahrt and Ek (1993a) decomposes the flux variables (vertical wind w and scalar concentration c) into a "domain average" over the whole run $\langle c \rangle$, a mesoscale deviation of the sectional average $[c]$ from the domain average ($c^* = [c] - \langle c \rangle$), and superimposed transient turbulent fluctuations (c'), with the flux written in terms of the covariance between the mesoscale deviations ($\langle w^* c^* \rangle$) and the

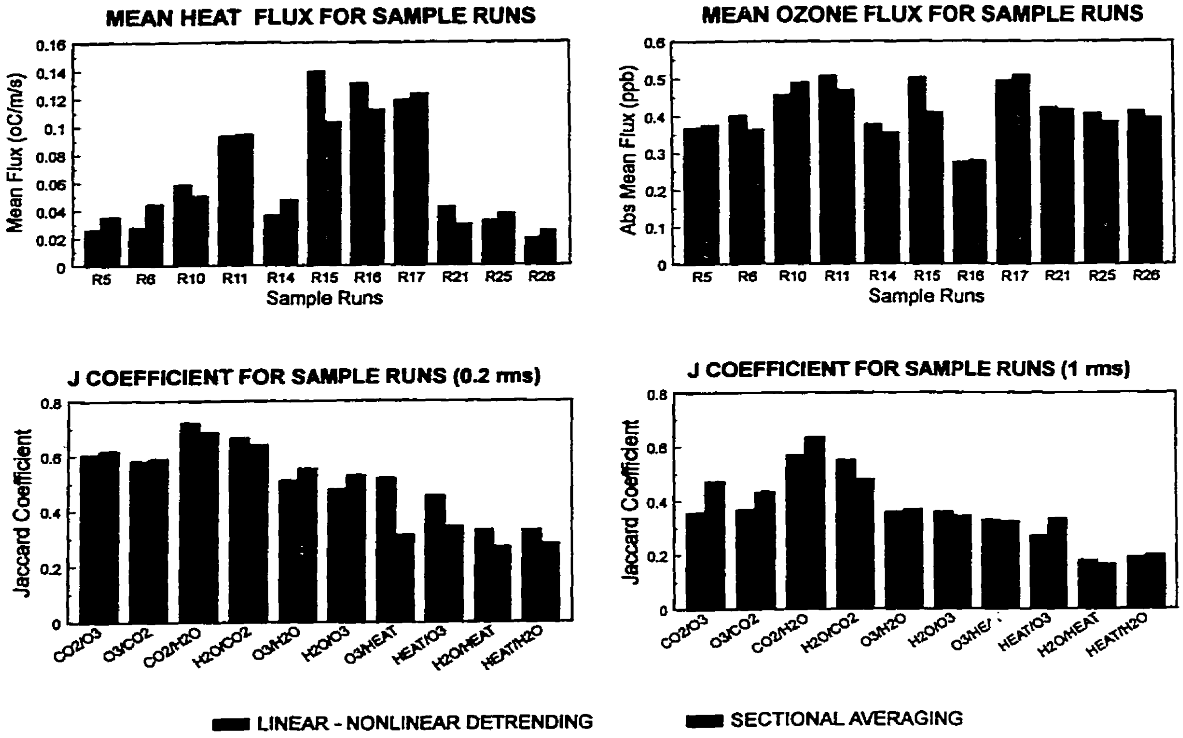

Fig. 5. Flux estimates for sensible heat and ozone (top) and J coefficients (bottom), for 11 sample runs across the grid site, for linear/nonlinear detrending and sectional averaging, respectively.

covariance of instantaneous fluctuations within the local subsections.

Figure 5 compares estimates for sensible heat flux (most likely to exhibit mesoscale components) and O_3 flux, based on linear/nonlinear detrending and sectional averaging. They were derived from 11 sample runs from northern, central and southern sections of the grid. As seen, flux estimates based on sectional averaging did not, in general, differ greatly between these two detrending techniques, with average difference $< 10\%$ for all four scalar fluxes. This suggests that surface-related mesoscale contributions to the flux are not significant, and that flux estimates may be considered to be fairly robust in terms of alternative definition of the mean.

(e) *Effect of sectional averaging on structural analysis*: Sectional averaging was also used to test the sensitivity of structure definition and flux association to the definition of the local mean along the run. Defragmentation and thresholding procedures, as previously used, were applied to fluctuations defined against the sectional average. The resulting structures show minor differences, but major structures are not significantly affected by this alternative definition of the local mean. This is summarized in Fig. 5 which, for the same 11 sample runs used above, compares the flux associations (J coefficients) obtained from sectional averaging against those based on linear/nonlinear detrending.

4. SUMMARY AND CONCLUSION

Flux maps (based on GIS-interpolated results from 1 km sampling segments of grid-type flight patterns) provide distribution patterns of source and sink strength for sensible heat, moisture and CO_2 that agree qualitatively with surface properties of vegetation index and surface temperature, in an ecosystem with discontinuous variations in source/sink strength at scales from one to several km. This degree of resolution is conditional to sampling within the surface boundary layer and a high number of repeated (or near-repeated) passes over the test area, very likely favored by flat terrain (which did not favor orographic mesoscale circulation) and high instability (with effective vertical surface–atmosphere coupling). Flux magnitudes agree with those observed by surface tower over similar crops. The spatial pattern of the ozone flux map showed no clearly defined relationship to those of CO_2, H_2O, heat, VI or surface temperature, requiring further analysis of the link of ozone uptake by vegetation to processes such as photosynthesis and evapotranspiration.

Dominant CO_2 and H_2O structures were found to be concentrated over the cool, moist cotton fields, and the dominant heat structures over hot, dry safflower, native vegetation and idle fields, as expected. Analysis of the spatial relationship (co-occurrence) between ozone uptake and transport processes of heat, H_2O

and CO_2 (at least for the dominant mode of gradient transfer) permit some quantitative assessment of the potential error to be expected when predictive models for ozone uptake are based on stomatal conductance for moisture exchange. It would be expected to be $\leqslant 20\%$ over well-watered crops such as cotton, but could be significantly higher over water-stressed or low-density vegetation. Over hot, dry surfaces the analysis of flux association of ozone to that of other scalars suggests that non-transpiring portions of the canopy are absorbing ozone at rates equal to—and sometimes greater than—the transpiring canopy sections. That a significant part of this non-physiologically based O_3 flux may result not so much from soil uptake than from O_3 destruction near the surface by interaction with NO emission from the soils strongly suggested by Guo *et al.* (1995). The consistently observed flux association between CO_2 and ozone, across all crop types, and the comparable association between these two fluxes and the heat flux, suggest that it would be more realistic to scale ozone uptake to CO_2 instead of H_2O, particularly under hot and dry conditions. In particular, linking ozone uptake to biochemical process models of the type developed for CO_2 assimilation in photosynthesis (e.g. Farquhar and von Caemerer, 1982) may reduce discrepancies associated with prediction of ozone uptake from stomatal conductance for moisture. While tests for sensitivity of results to changes in thresholding techniques and definition of local means demonstrated the essential robustness of these findings, their interpretation must consider that they are conditional to the time and place of observation and might have been different at other stages of crop development. Further work on airborne observation of trace gas exchange should include analysis of the three quadrants (non-dominant gradient transfer and countergradient transfer) of scalars not considered in the current study and include size and intensity criteria in the definition of *J*. It should also consider the possible effects of chemical reactions between ozone and nitrogen oxides (Guo *et al.*, 1995), leading to possible flux divergence between the surface and flight levels.

Acknowledgements—The direct and indirect support of this project through the San Jouquin Valley Air Quality Study, the Natural Science and Engineering Research Council of Canada, the National Research Council for Canada, the Atmospheric Environment Service of Canada and Agriculture Canada has been gratefully appreciated.

REFERENCES

Aben J. M., Janss-Jurkovicova M. and Adema E. H. (1990) Effects of low level ozone exposure under ambient conditions on photosynthesis and stomatal control of *Vicia faba* (*L*.). *Plant Cell Envir.* **13,** 463–469.

Antonia R. A. (1981) Conditional sampling in turbulence measurment. *Ann. Rev. Fluid Mech.* **13,** 131–156.

Austin L. B., Schuepp P. H. and Desjardins R. L. (1987) The feasibility of using airborne flux measurements for the imaging of the rate of biomass production. *Agric. Forest Meteor.* **39,** 13–23.

Caramori P., Schuepp P. H., Desjardins R. L. and MacPherson J. I. (1994) Structural analysis of airborne fluxes estimates over a region. *J. Climate* (in press).

Cheethan A. H. and Hazel J. E. (1969) Binary (presence–absence) similarity coefficients. *J. Paleontol.* **43,** 1130–1136.

Desjardins R. L., Hart R. L., MacPherson J. I., Schueppp P. H. and Verma S. B. (1992a) Aircraft and tower-based fluxes of carbon dioxide, latent and sensible heat. *J. geophys. Res.* **97** (D17), 18,477–18,485.

Desjardins R. L., Schuepp P. H., MacPherson J. I. and Buckley D. J. (1992b) Spatial and temporal variation of the fluxes of carbon dioxide and sensible and latent heat over the FIFE site. *J. geophys. Res.* **97**(D17), 18,467–18,475.

Duncan M. R. and Schuepp P. H. (1992) A method to delineate extreme structures within airborne flux traces over the FIFE site. *J. geophys. Res.* **97**(D17), 18,487–18,498.

Eloranta E. W. and Forrest D. K. (1992) Volume-imaging lidar observations of the convective structure surrounding the flight path of a flux-measuring aircraft. *J. geophys. Res.* **97**(D17), 18,383–18,393.

Farquhar G. D. and von Caemmerer S. (1982) Modelling of photosynthetic response to environmental conditions. In *Physiological Plant Ecology. II. Water Relations and Carbon Assimilation* (edited by Lange O. L., Nobel P. S., Osmond C. B. and Ziegler H.), pp. 549–588. Springer, Berlin.

Grant R. H., Bertolin G. E. and Herrington L. P. (1986) The intermittent vertical flux over a spruce forest canopy. *Boundary-Layer Met.* **35,** 317–330.

Grossman R. L. (1984) Bivariate conditional sampling of moisture flux over a tropical ocean. *J. atmos. Sci.* **41,** 3227–3253.

Guo Y., Desjardins R. L., MacPherson J. I. and Schuepp P. H. (1995) A simple scheme for partitioning the aircraft-measured ozone fluxes into the surface-uptake and atmospheric chemical rate. *Atmospheric Environment* **29,** 3201–3209.

Horst T. W. and Weil J. C. (1992) Footprint estimation for scalar flux measurements in the atmospheric surface layer. *Boundary-Layer Met.* **59,** 279–296.

Hussain A. K. M. F. (1986) Coherent structures and turbulence. *J. Fluid Mech.* **173,** 303–356.

Lefohn A. S. (1992) The characterization of ambient ozone exposure. In *Surface Layer Ozone Exposures and Their Effects on Vegetation* (edited by Lefohn A. S.), pp. 31–92. Lewis Publishers, Chelsea, MI.

Lefohn A. S. and Tingey D. T. (1984) The co-occurrence of potential phytotoxic concentrations of various gaseous air pollutants. *Atmospheric Environment* **18,** 2521–2526.

Lefohn A. S., Davis C. E., Jones C. K., Tingey D. T. and Hogsett W. E. (1987) Co-occurrence pattern of gaseous air pollutant pairs at different minimum concentrations in the United States. *Atmospheric Environment* **21,** 2435–2444.

Lenschow D. H. and Stankov B. B. (1986) Length scales in the convective boundary layer. *J. atmos. Sci.* **43,** 1198–1209.

Lenschow D. H. and Stephens P. L. (1980) The role of thermals in the convective boundary layer. *Boundary-Layer Met.* **19,** 507–532.

MacPherson J. I. (1992) NRC Twin Otter operations in the 1991 California ozone deposition experiment. National Research Council of Canada; Institute for Aerospace Research.

Mahrt H. and Ek M. (1993a) Mesoscale (subgrid) variability of turbulent fluxes in HARPEX and CODE. *Proc. Conf. on Hydroclimatoloy*, Amer. Meteorol. Soc., Anaheim, CA, 17–22 January 1993, pp. 130–131.

Mahrt H. and Ek M. (1993b) Spatial variability of turbulent fluxes and roughness lengths in HARPEX-MOBILHY. *Boundary-Layer Met.* **65**, 381–400.

Massman W. J., Pederson J., Delany A., den Hartog G., Neumann H. H., Grantz D. and Pearson R. Jr (1993) A comparison of independent determinations of the canopy conductance for carbon dioxide, water vapour and ozone exchange at selected sites in the San Joaquin Valley of California. *Proc. Conf. on Hydroclimatology*, Amer. Meteorol. Soc., Anahein, CA, 17–22 January 1993, pp. 112–117.

Pielke R. A., Dalu G. A., Snook J. S., Lee T. J. and Kittel G. F. (1991) Nonlinear influence of mesoscale land use on weather and climate. *J. Climate* **4**, 1053–1069.

Prat G. C., Hendrikson R. C., Chevone B. I., Christopherson D. A., O'Brien M. and Krupa S. V. (1983) Ozone and oxides of nitrogen in the rural upper midwestern U.S.A. *Atmospheric Environment* **10**, 2013–2033.

Reich P. B., Schoettle A. W. and Amundson R. G. (1985) Effect of low concentrations of O_3, leaf age and water stress on leaf diffusive conductance and water use efficiency in soybean. *Physiol. Plant* **63**, 58–64.

Runeckles V. C. (1992) Uptake of ozone by vegetation. In *Surface Level Ozone Exposures and Their Effects on Vegetation* (edited by Lefohn A. S.), pp. 157–188. Lewis Publishers, Chelsea, MI.

Runeckles V. C. and Chevone B. I. (1992) Crop response to ozone. In *Surface Level Ozone Exposures and Their Effects on Vegetation* (edited by Lefohn A. S.), pp. 189–270. Lewis Publishers, Chelsea, MI.

Saucier A., Duncan M. R. and Austin G. L. (1991) Mean flux estimation and cospectra of airborne carbon dioxide and water vapour eddy flux measurements in the planetary boundary surface layer. *Boundary-Layer Met.* **55**, 227–254.

Schuepp P. H., Desjardins R. L., MacPherson J. I., Boisvert J. B. and Austin L. B. (1989) Interpretation of airborne estimates of evapotranspiration. In *Estimation of Areal Evapotranspiration* (edited by Black T. A., Spittlehouse S. L. and Novak M. D.). Int'l. Assoc. of Hydrol. Sci. Press, Wallingford, Publ. no. 177, pp. 185–196.

Schuepp P. H., Leclerc M. Y., MacPherson J. I. and Desjardins R. L. (1990) Footprint prediction of scalar fluxes from analytical solutions of the diffusion equation. *Boundary-Layer Met.* **50**, 355–373.

Schuepp P. H., MacPherson J. I. and Desjardins R. L. (1992) Adjustment of footprint correction for airborne flux mapping over the FIFE site. *J. geophys. Res.* **97**(D17), 18,455–18,466.

Shaw R. H. (1985) On diffusive and dispersive fluxes in forest canopies. In *The Forest–Atmosphere Interaction* (edited by Hutchison B. A. and Hicks B. B.), pp. 407–419. Reidel, Dordrecht.

Simarski L. T. (1992) International meeting airs ozone studies. The trosphere: new hot spot for ozone research. *EOS, Trans. Amer. Geophys. Union* **73**(11), 273–276.

Temple P. J. (1986) Stomatal conductance and transpirational responses of field-growth cotton to ozone. *Plant Cell Environ.* **9**, 315–321.

Van Paul W. A. J. and Jacobs A. F. J. (1992) The conductance of a maize crop and the underlying soil to ozone under various environmental conditions. National Institute for Public Health and Environmental Protection, Bilthoven, The Netherlands.

Wheeler R. L. and Krystinik K. B. (1987) Evaluating coinciding anomalies along a fault trace or other traverse—simulations and statistical procedures. *U.S. Geological Survey Bull.* 1802.

Wyngaard J. C. (1983) Lectures on the planetary boundary layer. In *Mesoscale Meteorology Theories, Observations and Models* (edited by Lilly D. K. and Gal-Chen T.), pp. 603–650, 216–224. Reidel, Dordrecht.

Wyngaard J. C. (1986) Observational strategies. In *Probing the Atmospheric Boundary Layer* (edited by Lenschow D. H.), 269 pp. Amer. Meterol. Soc., Boston.

Wyngaard J. C., Pennell W. T., Lenschow D. H. and LeMone M. A. (1978) The temperature–humidity covariance budget in the convective boundary layer. *J. atmos. Sci.* **35**, 47–58.

PERGAMON

Atmospheric Environment 33 (1999) 1159–1173

ATMOSPHERIC ENVIRONMENT

Structural analysis and flux associations of CO_2, H_2O, heat and ozone over cotton and grape canopies

Constance M. Mitic[a,*], William J. Massman[b], Peter H. Schuepp[a], Jeffery L. Collett Jr[c]

[a]*Department Natural Resources Sciences, McGill University, Montreal, Canada*
[b]*US Department of Agriculture/Forest Service, Ft. Collins, CO, USA*
[c]*Department of Atmospheric Sciences, Colorado State University, Ft. Collins, CO, USA*

Received 17 December 1997; accepted 4 June 1998

Abstract

Micrometeorological tower data, collected over grape and cotton canopies as part of the California ozone deposition experiment (CODE) during the summer of 1991, are used to examine the temporal association between fluxes, and the physical characteristics of the coherent structures which dominate transport for both stable nighttime and unstable daytime conditions. Flux was calculated using the eddy covariance technique and the dominant modes of flux transport determined by quadrant analysis. The mean flux densities for both the cotton and grape site showed the surface acting as a sink for CO_2 and ozone and a source of heat and H_2O during the day, as would be expected, while during the night it became a source for CO_2 and a sink for heat, but remained a sink for ozone and a source of H_2O. The flux association results indicated a single vegetated ozone sink for the grape site, but a vegetated as well as a non-vegetated sink for the cotton site. For both sites, structures simultaneously transporting significant flux contributions of CO_2, H_2O, heat and ozone dominate during unstable conditions, but differed during stable conditions, where unmixed single flux structures dominated over cotton but not over grape. Structure sizes were less than 10 m during nighttime conditions and ranged from 3 to 69 m during the day. The results of this study contribute empirical evidence about the relationship between ozone uptake and the physical and physiological state of vegetation, as well as the limitations placed on eddy scales in simulation models.

Keywords: Coherent structures; Ozone uptake; Surface-atmosphere exchange; Surface flux

1. Introduction

The use of models for simulation and prediction of surface–atmosphere dynamics has become an integral part of research in the atmospheric/environmental sciences. Almost all forms of these models have to incorporate some form of parameterization of the surface characteristics (McGuire et al., 1991; Koster and Suarez, 1992; Sellers et al., 1992; Melillo et al., 1993; Bonan, 1993; Massman et al., 1994; Goetz and Prince, 1996; Ruimy et al., 1996). The fact that these models are sensitive to spatial variability of physical surface characteristics (Wollenweber, 1995; Klaassen and Claussen, 1995; Sud et al., 1988), and the uncertainty surrounding the relative influence of the various scales of such variability (Moore et al., 1993), highlight the need to improve our

* Corresponding author.

1352-2310/99/$ – see front matter
PII: S 1352-2310(98)00227-1

understanding of the atmosphere–ecosystem exchange processes. This need is reflected in the increasing number of studies that focus on the parameterization of surface characteristics (Hanan et al., 1995; Hall et al., 1995; Lee et al., 1996) and, in particular, the transport dynamics of various fluxes and their coupling to the underlying surface (Schuepp et al., 1987; Mack et al., 1990; Hollinger et al., 1994; Massman et al., 1993; Rochette et al., 1994; Baldocchi, 1994; Guo et al., 1995a; Mitic et al., 1997).

Some studies have specifically related the coherent motions of turbulence (as opposed to incoherent noise) in the surface layer to surface characteristics (Caramori et al., 1994; Mitic et al., 1995, 1997). These coherent "structures" are responsible for the bulk of turbulent transport in the surface layer and have been examined from various other perspectives (Wyngaard, 1983; Eloranta and Forrest, 1992; Mahrt and Ek, 1993a, b; Paw et al., 1995). A study of coherent turbulent structures allows for the improvement of our understanding of the processes operating on surface fluxes, and the associations of the various fluxes with each other and with the underlying surface. Identifying the physical extent of structures and their composition, will give some indication of the driving forces operating on flux transport as well as their partitioning between the surface and the atmosphere. This is of particular importance in the assessment of the potential for predicting fluxes from surface characteristics, in cases where some fluxes, like those of water vapour and CO_2, are more readily inferred from surface observation than others, such as ozone flux.

Our study uses tower data collected at the cotton and grape sites during the California Ozone Deposition Experiment (CODE) in the summer of 1991, to examine flux associations of CO_2, H_2O, heat and ozone. This is done for the two gradient modes of transport, where the surface acts as a sink for CO_2 and ozone, and a source of moisture and heat during the day, and a source of CO_2, and a sink for heat at night. The focus is on exchange processes at the "patch" scale (1 km^2), and the objective is to characterize the temporal evolution and characteristics of coherent structures during unstable (day) and stable (night) conditions over these two different crop canopies. Due to the importance of ozone deposition in the study area and the primary objective of CODE (part of the San Joaquin Valley Air Quality Study, Pederson et al., 1995), and given the fact that regional models for ozone deposition are based on a variety of physical and physiological surface characteristics at different scales (e.g. Massman et al., 1994), the emphasis is on the associations of ozone to the other flux variables. Such associations and the spatial scales involved are of interest as bases of reference for soil–vegetation–atmosphere transport (SVAT) models and to scaled-down large eddy simulation models, which are increasingly being used to describe canopy–atmosphere exchange.

2. Site and data description

The data were collected at two meteorological tower sites over a cotton and grape canopy located in the central valley of southern California at approximately 100 m above sea level (Pederson et al., 1995). The field observation period lasted from early July to early August, 1991. Five days were selected for study from each of the two data sets. For each of these days, two 20 min time segments were used for analysis, one during stable nighttime conditions and the other during unstable daytime conditions. The daytime segments were selected from periods between midday and mid-afternoon when the boundary layer was considered to be fully developed, with unstable thermal stratification (z/L significantly negative). The nighttime segments had zero solar radiation and stable stratification (positive z/L). The selection of days for analysis depended on data quality as well as on similarity in conditions such as mean wind speed and atmospheric stability. The data sets include eddy correlation observations, based on fast response sampling of the vertical wind component, air temperature, and the concentrations of CO_2, H_2O, and ozone. A detailed description of sites and sampling procedures is given below.

2.1. Cotton site

The tower at the cotton site was operated by the ASTER group from the US National Centre for Atmospheric Research (NCAR). The site was located at 36°48′50″N and 120°40′38″W, 80 km west of Fresno. The crop was planted in an E-W row orientation spaced 1 m apart. During the observation period, the average height of the cotton crop increased from 0.4 to 0.9 m, and the leaf area index from 1.8 to 2.5. Eddy correlation systems were located at 5 m above the surface to sample the three wind components, water vapour, CO_2 and air temperature at a frequency of 20 Hz. Data were collected continuously from 11 July to 7 August. The selected days and time segments used in this study are listed in Table 1. The mean wind direction was perpendicular to the rows. For the selected nighttime segments, the mean wind speed ranged from 1.7 to 2.2 m s^{-1}, z/L between 0.11 and 0.65, the mean surface temperature between 22 and 24.5°C, and dew was present in all cases. The daytime segments are characterized by mean wind speeds between 1.2 and 2.3 m s^{-1}, z/L between -0.19 and -2.0, mean surface temperature between 30 and 38.8°C and half hourly averaged incident solar radiation between 946 and 987 W m^{-2} with the exception of one day (August 5) where it was 750 W m^{-2}. The cotton fields were irrigated.

2.2. Grape site

The tower at the grape site was operated by the Air Quality Processes Research Division of the Atmospheric

4.1. Cotton site results

4.1.1. Flux associations

The FA for all 10 case studies are shown in Fig. 2. The pattern of flux associations is similar for structures in both the gradient down and gradient up modes. Under *stable nighttime conditions*, structures associated with transporting only one flux component (CO_2 (C), H_2O (H), O_3 (O) or heat (T), exclusively) dominate, cumulatively accounting for 35% to as high as 70% of the total number of structures. This may indicate the relative lack of mixing within the nighttime collapsed boundary layer as well as some decoupling of nocturnal surface processes. The association of ozone with non-CO_2 transporting structures (no sustained presence of coherent CO_2 flux) during the night indicates the existence of a non-vegetated sink for ozone. The non-vegetated ozone sink is indicated by the relative prominence of structures transporting H_2O–O_3-heat (HOT), which are also present during the day.

During *unstable daytime conditions*, structures simultaneously transporting CO_2–H_2O–O_3-heat (CHOT) dominate, with FA (in the gradient up mode) between 26 and 57%, associated with the dominant vegetated sink. This indicates not only a higher degree of mixing, compared to the nighttime cases, as would be expected, but presumably reflects also the co-located vegetated daytime source–sink for these variables. The association among structures transporting H_2O, O_3 and heat is the second consistently significant flux association. On DOY 213, however, structures transporting only CO_2, H_2O and ozone figure prominently at 19%. This corresponds to the low sensible heat flux during this time (Fig. 1) and is a direct result of the irrigation of the field. The association between the flux components of structures simultaneously transporting CHOT and HOT, indicating vegetated and non-vegetated source/sinks, respectively, were further documented by correlation analysis of the mean flux magnitudes within these structures, as shown in Figs. 3 and 4. The following discussion therefore deals with the correlation of the flux intensities within the dominant structure categories. For the CHOT structures, there is a consistent high correlation between H_2O and ozone flux intensities, ranging from 0.68 to 0.91. The correlation between CO_2 and ozone is more variable and reflects the correlation pattern between CO_2 and H_2O which ranges from 0.5 to 0.8. There is also a consistent moderate to high correlation between heat and ozone within these structures. The correlation plots for the combined CHOT structures from all five days (Fig. 4) show a positive relationship among all the flux components. The corresponding correlation coefficients show the highest overall correlation between H_2O and ozone, at 0.725. The mean structure flux intensities for the components of the CHOT structures may also be seen in Fig. 4, with approximate maximum values of -6.5 mg $m^{-2}s^{-1}$ for CO_2, -4.5 ppb m s^{-1} for ozone (where the negative sign indicates the surface as a sink), 2750 W m^{-2} for water vapour, and 750 W m^{-2} for heat. For structures transporting H_2O, O_3 and heat exclusively (HOT structures), the relationship between H_2O and ozone is even more pronounced with a correlation coefficient greater that 0.8 in all cases. The correlation between ozone and heat is more variable, but in all cases less than that of H_2O and ozone. The relationship for the individual DOY is also reflected in the correlation coefficient for the combined cases shown in Fig. 4, where the highest correlation is between H_2O and ozone at 0.7. In general, the correlation for all three fluxes is greater than 0.5. The above results suggest that under the well mixed daytime conditions over the cotton site, moisture and heat flux exert control over ozone flux with H_2O flux dominating in all cases.

4.1.2. Driving forces

The presence/absence of heat and H_2O in the structure composition is directly related to the buoyancy flux which incorporates terms corresponding to both the heat flux and the water vapour flux. The buoyancy flux ($w'\theta_v'$), i.e. the virtual temperature flux associated with the moisture content of the air, was not explicitly calculated, but in the absence of liquid water in the air it can be approximated by

$$\overline{w'\theta_v'} \cong (\overline{w'\theta'})[1 + 0.61\bar{r}] + 0.61\bar{\theta}(\overline{w'r'}) \quad (9)$$

where r is the water vapour mixing ratio (Stull, 1988). When $w'\theta'$ is negligible, the water vapour-related density effects dominate in buoyancy but even in the presence of significant heat flux the latter contribute to buoyancy, as shown by the ratios of virtual density flux to sensible heat flux which ranged from 1.1 to 1.4, representing considerable enhancement of total buoyancy over that associated with sensible heat flux only (1.0). In our analysis we differentiate between structures that have sensible heat and virtual temperature buoyancy effects from those that do not contain sensible heat flux, with a further category defined by the absence of buoyancy, presumably associated with shear forces. This partitioning of the driving forces operating at the cotton site during daytime conditions is shown in Fig. 5a. Heat is the dominant driving force in so far as 50–79% of the structures have coherent heat flux in their composition.

4.1.3. Structure sizes

Structure size refers to the one-dimensional horizontal extent (diameter) of the structure as intercepted by the tower and defined in Section 2. During stable nighttime conditions the majority of the structures are less than 10 m in diameter. During the day, the CHOT structure sizes range from 3 to 40 m, with a mean of 10.1 m. The sizes for HOT structures range from 2 to 32 m, with

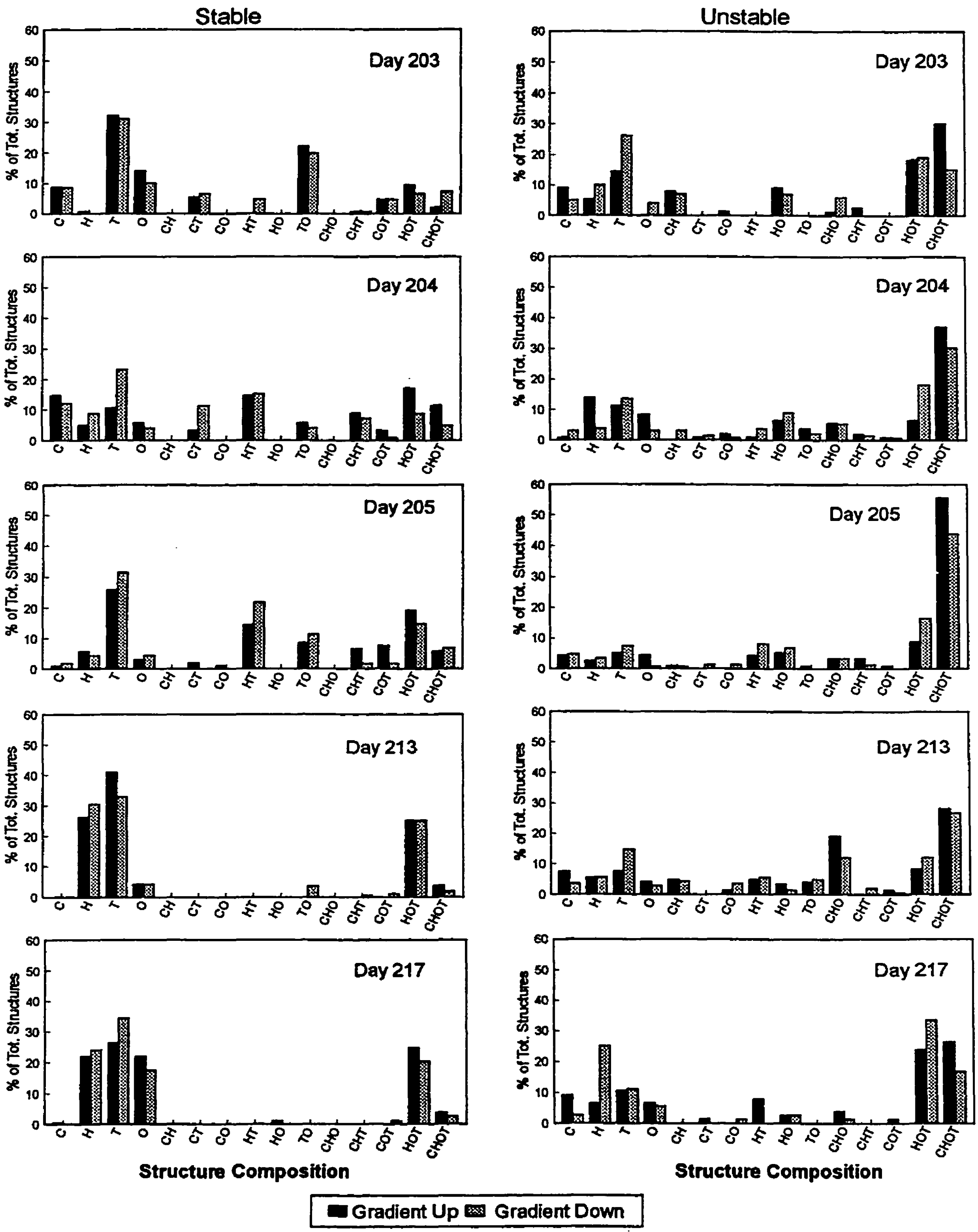

Fig. 2. Flux association at the cotton site for both stable and unstable conditions.

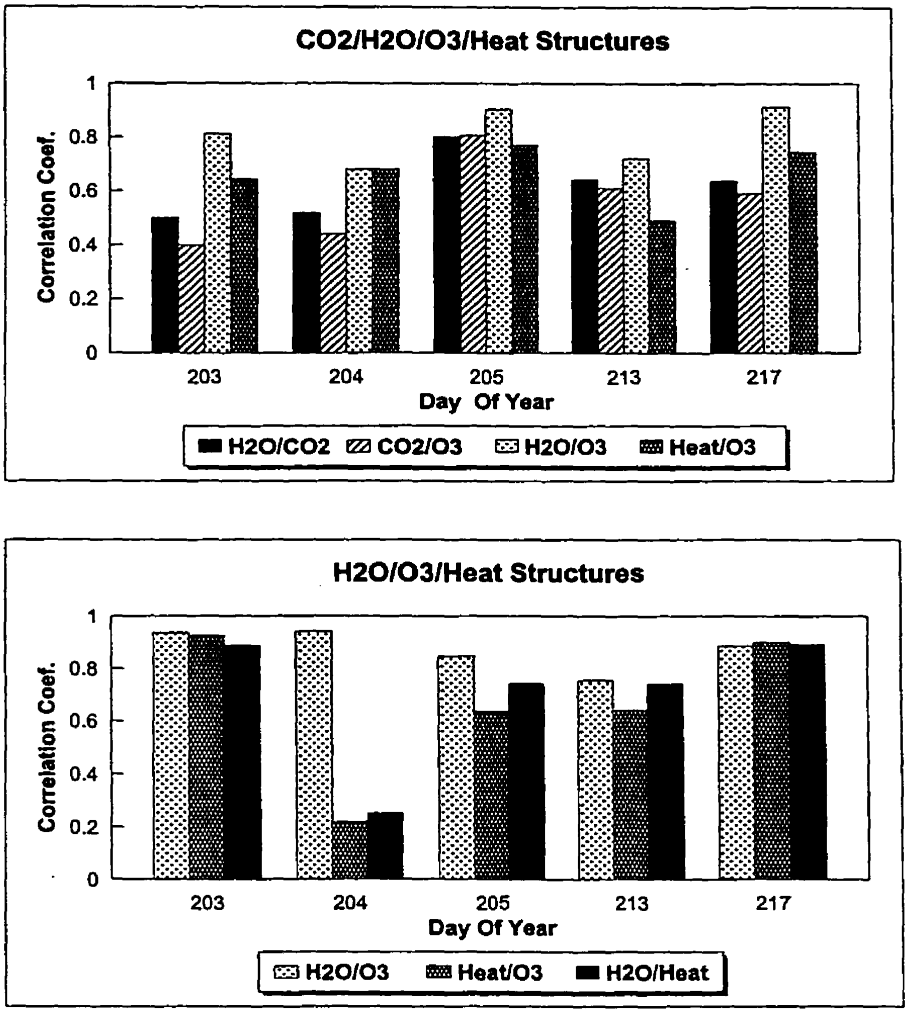

Fig. 3. Correlation analysis within the dominant gradient up structures for the cotton site during unstable conditions. All sample days shown.

a mean size of 6.1 m. Using Eqs. (4)–(8) in Section 3, with a λ range of 0.1–0.22 (from Fig. 5a), and the values for z and z/L from Section 2.1, l_M ranges from 2.8 to 4.8 m and l_H between 4.4 and 11.8 m. The mean mixing length (l) then ranges from 4.2 to 10.2 m. The mean CHOT structure sizes correspond closely to l_H, and fall within the range of the expected mean mixing length (l).

4.2. Grape site results

4.2.1. Flux associations

The results from the FA analysis on the grape data are shown in Fig. 6. The distribution of FA during *nighttime stable conditions* is very different from that of cotton. Here single component fluxes do not dominate, and ozone transport appears predominantly in the presence of CO_2 in CHOT structures. The distinctly low HOT structures in Fig. 6 suggests that a non-vegetated sink for ozone is not present. The consistently dominant structure compositions are CHOT with FA ranging from 16 to 29% and CHT with FA between 14 and 30%. This may reflect the much greater level of mixing during nighttime stable conditions over grape, linked to the greater measurement height (almost twice that of cotton), and possibly differences in the level of nocturnal metabolic activities such as respiration levels. The FA during the *daytime unstable conditions* is similar to that of cotton with the majority of structures transporting CO_2, H_2O, ozone and heat (CHOT) simultaneously, and FA between 25 and 48%. Structures with fluxes of CO_2, H_2O and ozone (CHO) are also prominent during two sample periods, with FA of 21 and 25%.

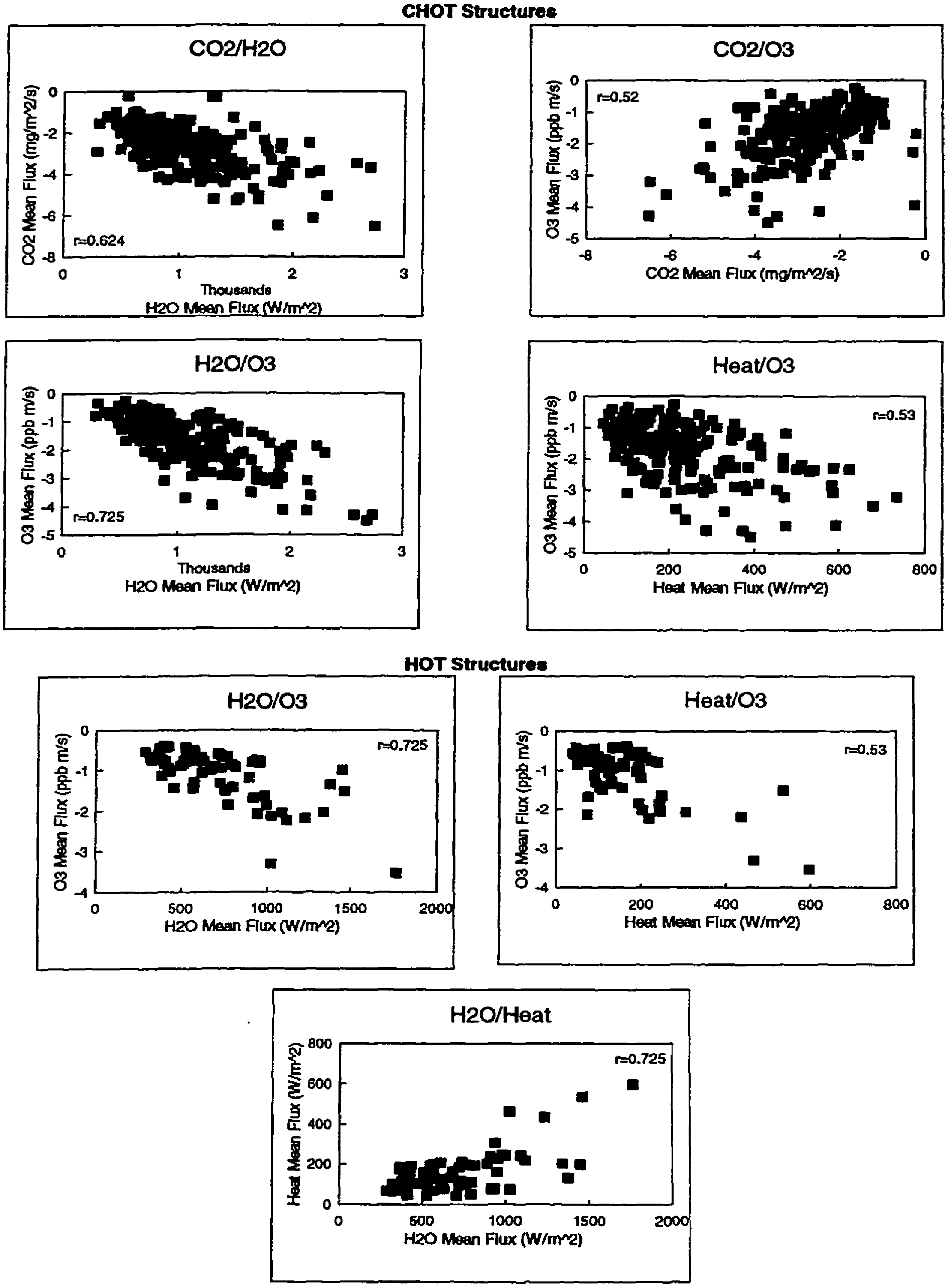

Fig. 4. Scatter diagram of the correlation analysis for the dominant structures over cotton during unstable conditions. Results from the five sample days are combined.

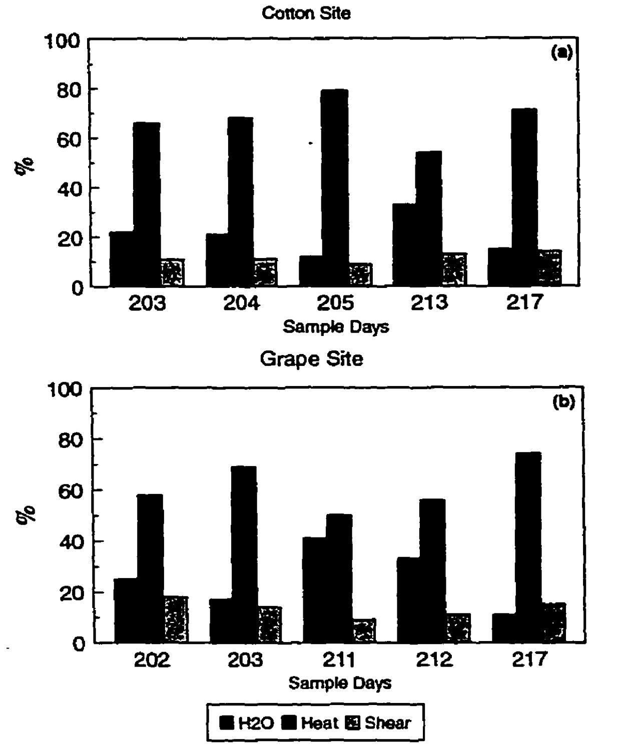

Fig. 5. Partitioning of driving forces over the cotton (a) and grape (b) sites during unstable conditions.

The indication of a single dominant ozone sink for grape, that is, the one associated with vegetation, represents a significant difference between the FA for grape and cotton. The non-vegetated ozone sink at the cotton site may be the result of deposition to the soil and photochemical reactions with NO, as suggested by Massman et al. (1995) from examining ozone flux divergence between tower and aircraft flux.

The correlations of flux intensities within the dominant CHOT structures for unstable daytime conditions (Fig. 7) are similar to those for cotton. There is a consistently high correlation between CO_2 and ozone (0.57–0.97), H_2O and ozone (0.64–0.96), and CO_2 and H_2O (0.67–0.96). The CO_2-ozone relationship, however, does not indicate a dependence on the correlation between the flux intensities of CO_2 and H_2O as appears to be the case over the cotton canopy. This difference may be due to the presence of the single ozone sink for the grape site. The flux intensity correlation for the combined CHOT structures for all five days are all very high with CO_2 and ozone at 0.88, H_2O and ozone at 0.86 and CO_2 and H_2O at 0.91. The correlation between heat and ozone, by contrast, is much lower at 0.49.

The scatter plot in Fig. 7 shows a positive relationship among all four fluxes within the CHOT structures. The mean flux intensities for the components of the CHOT structures (also shown in Fig. 7) indicate approximate maximum values (excluding a few outlier) of -4.5 mg $m^{-2} s^{-1}$ for CO_2, -3.5 ppb m s^{-1} for ozone, 3750 W m^{-2} for water vapour and 450 W m^{-2} for heat flux. Comparing the mean structure flux between grape and cotton, CHOT structures for cotton have a higher CO_2 flux, as may be expected given the actively growing stage of the cotton crop, as well as higher ozone and heat flux and lower H_2O flux. However, it should be considered that the partitioning of the energy fluxes at both sites depends on the dynamics of the rotating irrigation scheme. The findings on ozone flux correlate well with those of Massman et al. (1994, 1995), who found ozone flux to be higher at the cotton site than at the grape site. As suggested by Guo et al. (1995), the higher degree of wetness indicated by the higher H_2O flux and lower heat flux at the grape site would reduce the production of NO, accounting for the lower ozone flux as well as the absence of a dominant non-vegetated ozone sink.

4.2.2. Driving forces

The breakdown of the driving forces during unstable conditions, shown in Fig. 5b, indicates that although heat remains a principal driving force for the surface fluxes ($> 50\%$), water vapour density gradients play a more prominent role than was observed over cotton. This results in somewhat higher ratios of buoyancy flux to sensible heat flux (ranging up to 1.7 instead of 1.4), especially for days with significantly lower heat flux around the time of irrigation (211 and 212).

4.2.3. Structure sizes

The sizes for the dominant daytime CHOT structures are larger than those over cotton, ranging from 3 to 69 m with a mean of 15.7 m. Using Eqs. (4)–(8) in Section 3, with a λ range of 0.1–0.15 (Fig. 5b), and the values for z and z/L from Section 2.2, l_M ranges from 5.3 to 9.9 m and l_H between 8.4 and 26.9 m. The mean mixing length (l) then ranges from 8.1 to 24.3 m with the mean CHOT structure size falling comfortable within this range. The structure sizes for grape fall between those from the cotton site and those reported by Mitic et al. (1997) for aircraft data at 30 m over a partly irrigated grid area with cotton as the dominant crop. This indicates the increased mixing and subsequent coalescing of structures with increasing height (Caramori et al., 1994) and verifies to some degree the empirical definition of the physical extent of the coherent structures.

5. Conclusion

The association between fluxes of ozone and those of CO_2 and H_2O, within the turbulent structures that dominate exchange processes between cotton and grape

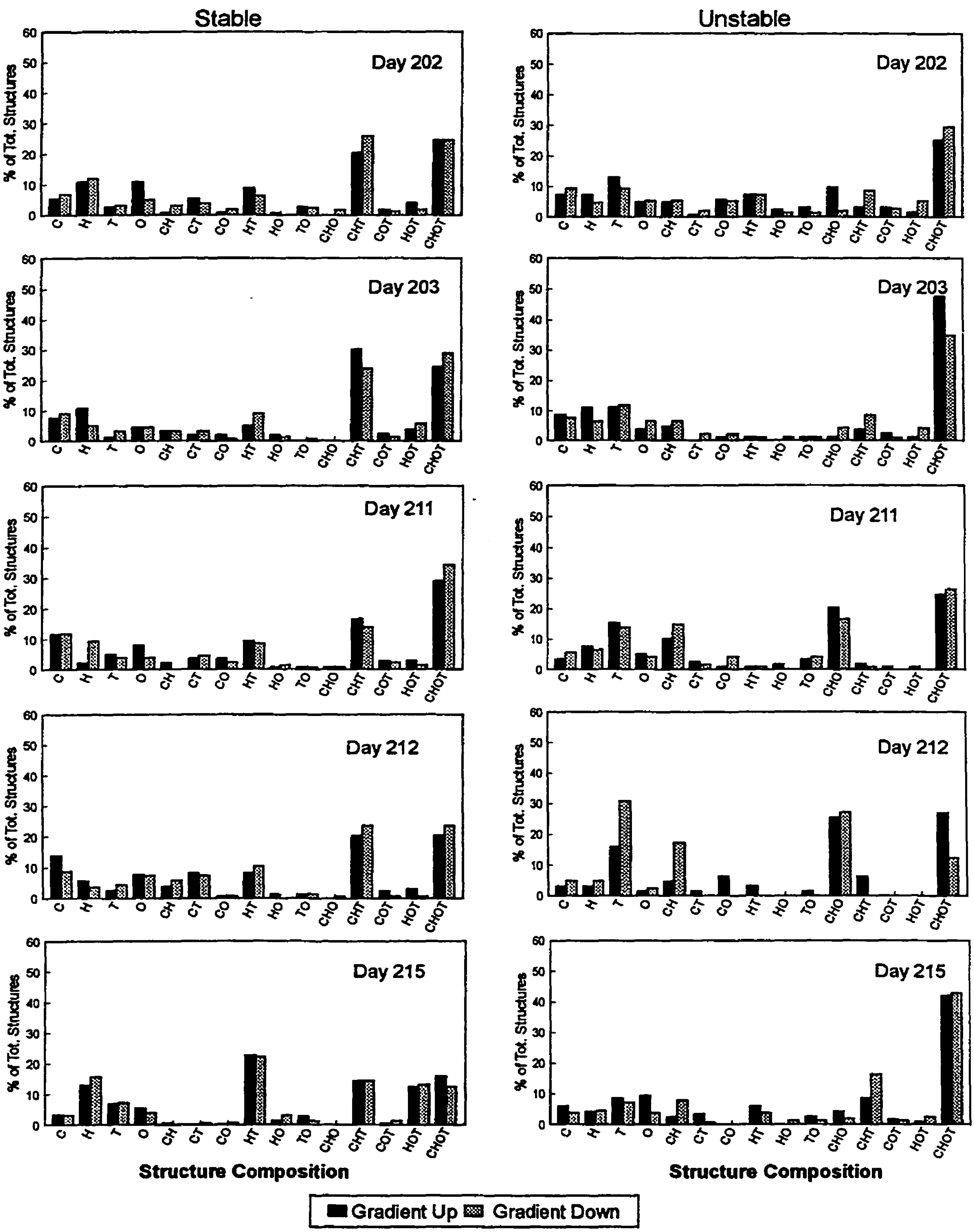

Fig. 6. Flux association at the grape site for both stable and unstable conditions.

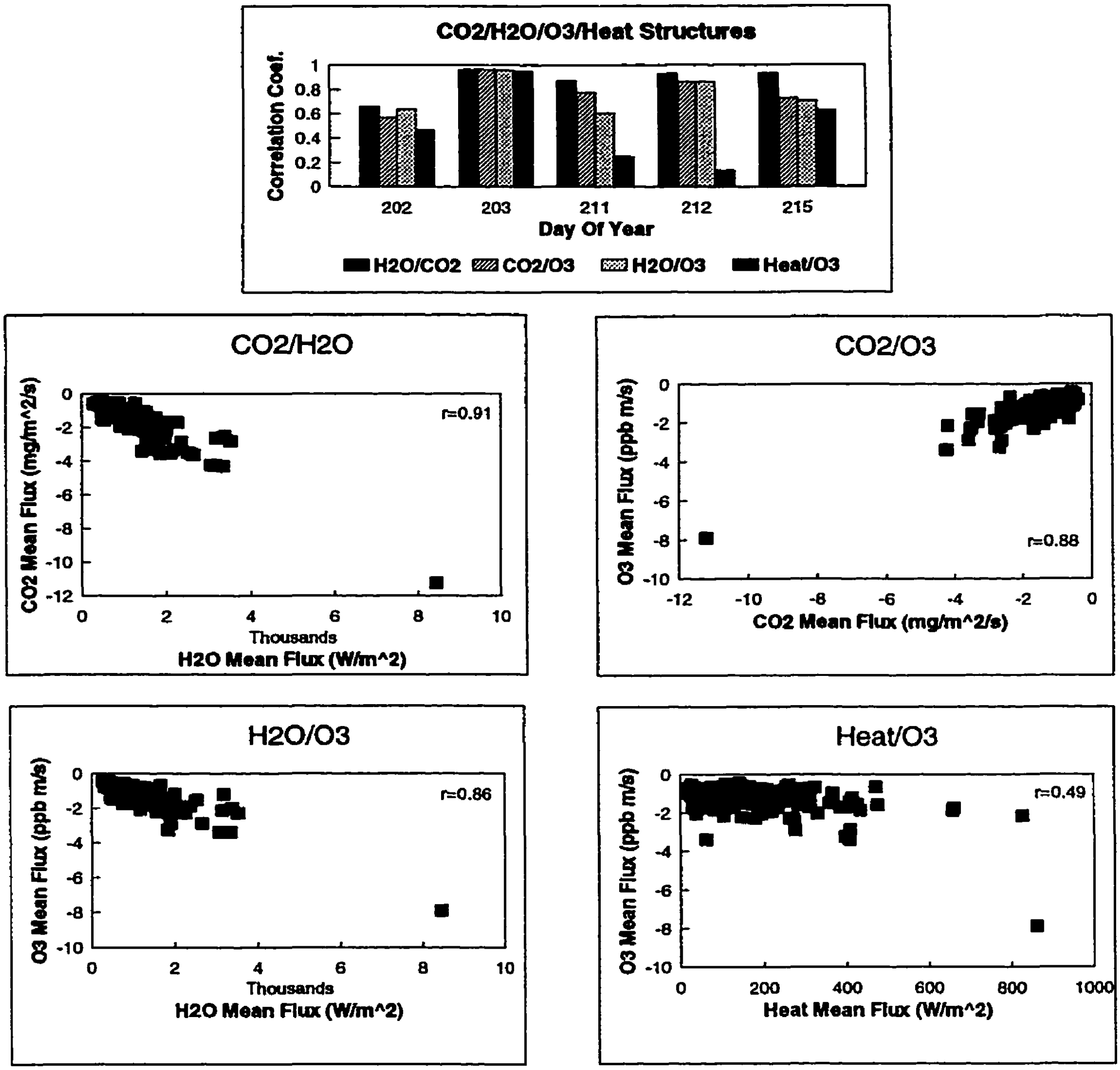

Fig. 7. Correlation analysis within the dominant gradient up structures for the grape site during unstable conditions.

canopies and the atmosphere under daytime conditions, is not affected by variations in the heat flux. Under unstable conditions, structures simultaneously transporting CO_2, H_2O, ozone and heat (CHOT) dominate for both the grape and cotton canopy. During stable conditions, the flux association differs between cotton and grape, with the cotton canopy having more dominant single component structures. The results for the stable conditions, however, must be interpreted with caution in light of the very small magnitude of the fluxes and the difficulties associated with sampling under nighttime stable conditions.

The separation of ozone deposition into vegetative and non-vegetative sinks may be inferred from the proportion of structures transporting ozone in the presence and absence of CO_2. For the cotton site, a vegetated ozone sink associated with CHOT structures and a non-vegetated sink associated with HOT structures were observed. The grape site indicated only a vegetated sink for ozone associated with the dominant CHOT structures. These results not only illustrate differences in the types of sinks for different vegetation types, but should help to quantify the link between ozone uptake by crops and their physical and physiological status. They may be compared with those of Mitic et al. (1997) for CODE aircraft data, where the dominant flux association was among CO_2, H_2O and ozone, without significant difference among the correlation of CO_2 and ozone, and H_2O and ozone. The aircraft data, however, were obtained at a height of 30 m above a 15×15 km grid with varying crop and surface conditions, i.e. at a height where considerable coalescence of structures has already occurred.

The structure sizes indicate that on average the dominant structures at the grape site are larger than those at the cotton site but considerably smaller than those reported by Mitic et al. (1997) for aircraft data from CODE. These structures sizes fall within range of the expected mean surface layer eddy scales and may be helpful as an empirical verification of eddy scale limitations within simulation models.

Acknowledgements

The authors extend their thanks to the members of the Air Quality Research Division of Atmospheric Environment Service, Canada, in particular, to G. den Hartog, R.E. Mickle, H.H. Neumann, J. Arnold, J. Deary and A. Beavan, for the use of the grape data. Our thanks also to Tony Delany, Steve Semmer, Tom Horst, Steve Oncley and Charlie Martin from the ASTER Facility at the National Centre for Atmospheric Research (NCAR) for the use of the cotton data. We especially express our appreciation to Jim Pederson and the California Air Research Board, and to the Natural Science and Engineering Research Council of Canada for funding this study.

References

Baldocchi, D.D., 1994. A comparison study of mass and energy exchange over a closed (wheat) and an open (corn) canopy. II: CO_2 exchange and water use efficiency. Agriculture and Forest Meterology 67, 291–321.

Bonan, G.D., 1993. Importance of leaf area index and forest type when estimating photosynthesis in boreal forest. Remote Sensing and Environment 43, 303–314.

Caramori, P., Schuepp, P.H., Desjardins, R.L., MacPherson, J.I., 1994. Structural analysis of airborne flux measurements over a region. Journal of Climate 7, 627–640.

Eloranta, E.W., Forrest D.K., 1992. Volume imaging lidar observations of the convective structure surrounding the flight path of a flux-measuring aircraft. Journal of Geophysical Research 97(D17), 18 383–18 498.

Goetz, S.J., Prince, S.D., 1996. Remote sensing of net primary production in boreal forest stands. Agriculture and Forest Meteorlogy 78, 149–179.

Guo, Y., Desjardins, R.L., MacPherson, J.I., Schuepp, P.H., 1995a. The correspondence of aircraft-measured fluxes of sensible heat, latent heat, CO_2, and ozone to the surface characteristics in the San Joaquin Valley of California. Atmospheric Environment 29 (21), 3159–3168.

Guo, Y., Desjardins, R.L., MacPherson, J.I., Schuepp, P.H., 1995b. A simple scheme for partitioning aircraft-measured ozone fluxes into surface uptake and chemical transformation. Atmospheric Environment 29(21), 3199–3207.

Hall, F.G., Shimabukuro, Y.E., Huemmrich, K.F., 1995. Remote sensing of forest biophysical structure using mixture decomposition and geometric reflectance model. Ecological Applications 5 (4), 993–1013.

Hanan, N.P., Prince, S.D., Begue, A., 1995. Estimation of absorbed photosynthetically active radiation and vegetation net production efficiency using satellite data. Agriculture and Forest Meteorolgy 76, 259–276.

Hollinger, D.Y., Kelliher, F.M., Byers, J.N., Hunt, J.E., McSeveny, T.M, Weir, P.L., 1994. Carbon dioxide exchange between an undisturbed old-growth temperate forest and the atmosphere. Ecology 75, 134–150.

Klaassen, W., Claussen, M., 1995. Landscape variability and surface flux parameterization in climate models. Agriculture and Forest Meteorology 73, 181–188.

Koster, R.D., Suarez, M.J., 1992. Modelling the land surface boundary in climate models as a composite of independent vegetation stands. Journal of Geophysical Research 97 (D3), 2697–2715.

Lee, X., Black, A.T., den Hartog, G., Nuemann, H.H., Nesic, Z., Janusz Olejnik, 1996. Carbon dioxide exchange and nocturnal processes over a mixed deciduous forest. Agriculture and Forest Meteorology 81, 13–29.

Mack, A.R., Desjardins, R.L., MacPherson, J.I., Schuepp, P.H., 1990. Relative photosynthetic activity of agricultural lands from airborne carbon dioxide and satellite data. International Journal of Remote Sensing 11 (2), 237–251.

Mahrt, H., Ek, M., 1993a. Mesoscale (subgrid) variability of turbulent fluxes in HAPEX and CODE. Proceedings of the Conference on Hydroclimatology, Americ. Meteorol. Soc., Anaheim, Calif., 17–22 January 1993, pp. 130–131.

Mahrt, H., Ek, M., 1993b. Spatial variability of Turbulent fluxes and roughness lengths in HAPEX-MOBILHY. Boundary Layer Meteorology 65, 381–400.

Massman, W.J., Pederson, J., Delany, A., den Hartog, G., Neumann, H.H., Grantz, D., Pearson Jr, R., 1993. A comparison of independent determinations of the canopy conductance for carbon dioxide, water vapour and ozone exchange at selected sites in the San Joaquin Valley of California. Proceedings of the Conference on Hydroclimatology, Americ. Meteorol. Soc., Anaheim, Calif., 17–22 January 1993, pp. 112–117.

Massman, W.J., Pederson, J., Delany, A., Grantz, D., den Hartog, G., Neumann, H.H., Oncley, S.P., Pearson Jr, R., Shaw, R.H., 1994. An evaluation of the regional acid deposition model surface module for ozone uptake at three sites in the San Joaquin Valley of California. Journal of Geophysics Research 99 (D4), 8281–8294.

Massman, W.J., MacPherson, J.I., Delany, A., den Hartog, G., Neumann, H.H., Oncley, S.P., Pearson Jr, R., Pederson, J., Shaw, R.H., 1995. Surface conductance for ozone uptake derived from aircraft eddy correlation data. Atmospheric Environment 29 (21), 3181–3188.

McGuire, A.D., Melillo, J.M., Joyce, L.A., Kicklighter, D.W., Grace, A.L., Moore, B., Vorosmarty, C.J., 1991. Interactions between carbon and nitrogen dynamics in estimating net primary productivity for potential vegetation in North America. Global Biogeochemical Cycles 6, 101–124.

Melillo, J.M., McGuire, D.A., Kicklighter, D.W., Moore III, Berrien, Vorosmarty C.J., Schloss, A.L., 1993. Global climate change and terrestrial net primary production. Nature 363, 234–240.

Mitic, C.M., Schuepp, P.H., Desjardins, R.L., MacPherson, I.J., 1995. Spatial distribution and co-occurrence of surface–atmosphere energy and gas exchange processes over the CODE grid site. Atmospheric Environment 29 (21), 3169–3180.

Mitic, C.M., Schuepp, P.H., Desjardins, R.L., MacPherson, I.J., 1997. Flux association in coherent structures transporting CO_2, H_2O, heat and ozone over the CODE grid site. Agriculture and Forest Meteorology (in press).

Moore, C.E., Fitzjarrald, D.R., Ritter, J.A., 1993. How well can regional fluxes be derived from smaller scale estimates?, Journal of Geophysics Research 98, 7177–7198.

Ogunjemiyo, S.O., Schuepp, P.H., MacPherson, J.I., Desjardins, R.L., 1997. Analysis of flux maps vs. Surface characteristics from Twin Otter grid flights in BOREAS 1994. Journal of Geophysical Research (in press).

Paw, U., Kyaw Tha, Qiu, Jie, Su, Hong-Bing, Watanabe, Tomonori, Yves Brunet, 1995. Surface renewal analysis: a new method to obtain scalar fluxes, Agriculture and Forest Meteorology 74, 119–137.

Pederson, J.R., Massman, W.J., Mahrt, L., Delany, A., Oncley, S., Den Hartog, G., Neumann, H.H., Mickle, R.E., Shaw, R.H., Paw, U., Grantz, K.T., MacPherson, D.A., Desjardins, J.I., Schuepp, R., Pearson Jr, R., P.H., Arcado, T.E., 1995. California ozone deposition experiment: methods, results and opportunities. Atmospheric Environment 29 (21), 3115–3132.

Powell, D.C., Elderkin, C.E., 1974. An investigation of the application of Taylor's hypothesis to atmosphere boundary layer turbulence. Journal of Atmospheric Science 31, 990–1002.

Rochette, P., Desjardins, R.L., Patty, E., Lessard, R., 1994. Measurement of crop net carbon dioxide exchange rate in soybean. 21st AFM Conference on Agricultural and Forest Meteorology. pp. 259–260. preprint.

Ruimy, A., Kergoat, L., Field, C., Bernard S., 1996. The use of CO_2 flux measurements in models of the global terrestrial carbon budget. Global Change Biology 2, 287–296.

Schuepp, P.H., Desjardins, R.L., MacPherson, J.I., Boisvert, J., Austin, L.B., 1987. Airborne determination of regional water use efficiency and evapotranspiration: present capabilities and initial field tests. Agriculture and Forest Meteorology 41, 1–19.

Schuepp, P.H., MacPherson, J.I., Desjardins, R.L., 1992. Adjustment of footprint correction for airborne flux mapping over the FIFE site. Journal of Geophysics Research 97 (D17), 18455–18466.

Stull, R.B., 1988. An Introduction to Boundary Layer Meteorology, Kluwer Academic Publishers Dordrecht, The Netherlands, 666 pp.

Sud, Y.C., Shukla, J., Mintz, Y., 1988. Influence of land surface roughness on atmospheric circulation and rainfall. A simulation with a general circulation model. Journal of Applied Meteorology 27, 1036–1054.

Taylor, G.I., 1938. The spectrum of turbulence. Proceedings of the Royal Society A164, 476–490.

Wollenweber, G.C., 1995. Influence of fine scale vegetation distribution on surface energy partition. Agriculture and Forest Meteorology 77, 225–240.

Wyngaard, J.C., 1983. Lectures on the planetary boundary layer. In: Lilly, D.K., Gal-Chen, T. (Eds.), Mesoscale Meteorology Theories, Observations and Models. Reidel, Dordrecht, pp. 603–650 and pp. 216–224.